AN ABSTRACT OF THE THESIS OF

Melanie C. Kelman for the degree of Master of Science in Geology presented on May 29, 1998. Title: Hydrothermal Alteration of a Supra-Subduction Zone Ophiolite Analog, Tonga, Southwest Pacific.

Abstract approved: Redacted for Privacy
Sherman Bloomer

The basement of the Tonga intraoceanic forearc comprises Eocene arc volcanic crust formed during the earliest phases of subduction. Volcanic rocks recovered from the forearc include boninites and arc tholeiites, apparently erupted into and upon older mid-oceanic ridge tholeiites. Rock assemblages suggest that the forearc basement is a likely analog for large supra-subduction zone (SSZ) ophiolites not only in structure and lithology, but also in the style of hydrothermal alteration.

Dredged volcanic samples from the central Tonga forearc (20-24° S) exhibit the effects of seafloor weathering, low (<200°C, principally <100°C) alteration, and high temperature (>200°C) alteration. Tholeiites and arc tholeiites are significantly more altered than boninites. Seafloor weathering is due to extensive interaction with cold oxidizing seawater, and is characterized by red-brown staining and the presence of Fe-oxyhydroxides. Low temperature alteration is due to circulation of evolving seawater-derived fluids through the volcanic section until fluid pathways were closed by secondary mineral precipitation. Low temperature alteration is characterized by smectites, celadonite, phillipsite, mixed-layer smectite/chlorite, carbonates, and silica. All phases fill veins and cavities; clay minerals and silica also replace the mesostasis and groundmass phases. Low temperature alteration enriches the bulk rock in K, Ba, and Na, and mobilizes other elements to varying extents. The few high temperature samples are characterized by

mobilizes other elements to varying extents. The few high temperature samples are characterized by epidote, chlorite, quartz, oxides, and fibrous amphibole, which replace groundmass and phenocrysts, and fill cavities, and are presumed to have originated in zones of concentrated hydrothermal upflow.These three alteration types are similar to those seen in many ophiolites such as Troodos, where low temperatures prevailed in the volcanic section except in localized upflow zones. Alteration mineral chemistries are also broadly similar to those observed for the Troodos Ophiolite. Tonga forearc alteration differs from mid-oceanic ridge alteration in the presence of Al-rich dioctahedral smectites (not common in mid-oceanic ridge crust), the high Al content of saponite, and the predominance of K as an interlayer cation in clays. Hydrothermal alteration of the Tonga forearc is likely the product of extensive interaction with compositionally evolving seawater-derived fluids beginning at the time of emplacement. The distribution and intensity of alteration in these crustal sections depend principally on the porosity and permeability of the crust during alteration, which are influenced by the primary porosity, igneous morphology, and the presence of faults and fractures which could affect fluid flow.

Hydrothermal Alteration of a Supra-Subduction Zone Ophiolite Analog, Tonga, Southwest Pacific

by

Melanie C. Kelman

A THESIS

submitted to

Oregon State University

in partial fulfillment of
the requirements for the
degree of

Master of Science

Presented May 29, 1998
Commencement June 1999

Master of Science thesis of Melanie C. Kelman presented on May 29, 1998

APPROVED:

Redacted for Privacy

Major Professor, representing Geology

Redacted for Privacy

Chair of Department of Geosciences

Redacted for Privacy

Dean of Graduate School

I understand that my thesis will become part of the permanent collection of Oregon State University libraries. My signature below authorizes release of my thesis to any reader upon request.

Redacted for Privacy

Melanie C. Kelman, Author

Table of Contents

Table of Contents (Continued)

Table of Contents (Continued)

Table of Contents (Continued)

List of Figures

List of Figures (Continued)

List of Figures (Continued)

List of Figures (Continued)

List of Figures (Continued)

List of Figures (Continued)

List of Tables

Hydrothermal Alteration of a Supra-Subduction Zone Ophiolite Analog, Tonga, Southwest Pacific

Chapter 1. Introduction

1.1 General introduction

The intraoceanic convergent margins of the western Pacific are typically extension-dominated and non-accretionary, with marginal basins. The forearc igneous basement of such convergent margins contains a record of the early development of the subduction zone, and study of these rocks is relevant to the question of the origin of ophiolites. Ophiolites are important because they mark ancient collision zones and have been interpreted as fragments of ancient seafloor. As such, they have been used as important pieces of many paleotectonic models and have been used to make inferences about processes at modern ocean ridges. Ophiolites formed in an extensional environment, indicated by the presence of sheeted dike complexes. However, mid-oceanic ridges primarily comprise tholeiitic basalts, whereas many ophiolites often contain not only basalts but boninites (high-Si, high-Mg, low-Ti basalts) and differentiated tholeiitic to calc-alkaline rocks (e.g. Rautenschlein et al., 1985; Bloomer and Hawkins, 1983; Serri, 1981). Several of the large, relatively intact Tethyan ophiolites such as the Troodos Ophiolite on Cyprus or the Semail Ophiolite in Oman have different geochemical signatures from mid-oceanic ridge crust, and must have formed above a subduction zone (e.g. Pearce et al., 1984; Rautenschlein et al., 1985; Bloomer et al., 1995). The most likely analog (in lithology, structure, and chemistry) for these supra-

1995). The most likely analog (in lithology, structure, and chemistry) for these supra-subduction zone (SSZ) ophiolites is forearc crust formed during the initial stages of subduction (Natland and Tarney, 1981; Ishii, 1985). The basement of the Tonga forearc comprises Eocene and younger arc volcanic crust, formed during the earliest phases of subduction in the region (Bloomer et al., 1994). If this is true of many of the large ophiolites, it may be necessary to reconsider how their presence in the geologic record is interpreted. There are numerous studies of the primary mineralogy and chemistry of ophiolites and of their possible analogs in oceanic crust and arcs. However, there are only a few detailed studies of hydrothermal alteration in oceanic crust, and almost none in sections of old forearc basement.

Hydrothermal alteration of mid-oceanic ridge crust and ophiolites is very similar, but there are some significant differences. Seawater to rock ratios for ophiolites are much greater than for other oceanic crust, as evidenced by O, Sr, and S isotope data, and by more extensive recrystallization of sheeted dikes in ophiolites (Schiffman et al., 1991; Alt et al., 1996a; Alt et al., 1998). The greater variety of lithologies, and the greater amounts of volatiles present in arc-derived rocks, plus tectonic effects (such as differences in stress regime, leading to different fracture pathways for fluid flow) also probably contribute to differences in hydrothermal alteration between ophiolites and mid-oceanic ridge crust (Schiffman et al., 1991; Bickle and Teagle, 1992; Alt et al., 1998). There have been few studies comparing modern arc basement to mid-oceanic ridge crust or ophiolites (Natland and Mahoney, 1981; Natland and Hekinian, 1981; Fryer et al, 1990; Taylor et al, 1990;

Schöps and Herzig, 1994; Alt et al., 1998); these have indicated both similarities and differences in the nature and extent of alteration.

The Tonga forearc (Figure 1) is a good place to study early arc development because it is a typical intraoceanic extension-dominated forearc; its subduction geometry is simple; it is undergoing tectonic erosion (therefore the basement is accessible) (von Huene and Scholl, 1991; Parson et al., 1992; MacLeod, 1994; Bloomer et al., 1996), and subduction has been semi-continuous since the middle Eocene (MacLeod et al., 1997).

This thesis has two objectives: to carefully characterize the hydrothermal alteration of volcanic rocks of the Tonga forearc, and to investigate the hypothesis that hydrothermal alteration patterns in intraoceanic forearcs more closely match those in ophiolites than those in mid-oceanic ridge crustal sections.

This study is based on samples dredged during the Scripps Institute of Oceanography's Boomerang Leg 8 cruise in 1996, and on samples collected from the Tongan island of 'Eua, the only site in Tonga at which forearc basement is exposed on land. The focus is primarily but not exclusively on samples from five dredges (D87, D88, D89, D90, D91, Figure 2) which represent a roughly perpendicular transect across the forearc in the 'Eua region.

The following specific questions are addressed:

(1) What alteration assemblages are present in Tonga forearc volcanic rocks? What were the physical conditions (particularly temperature, fluid composition, and water: rock ratio) under which alteration occurred? What sort of variations in the nature and extent of alteration are present, and what factors influence them?

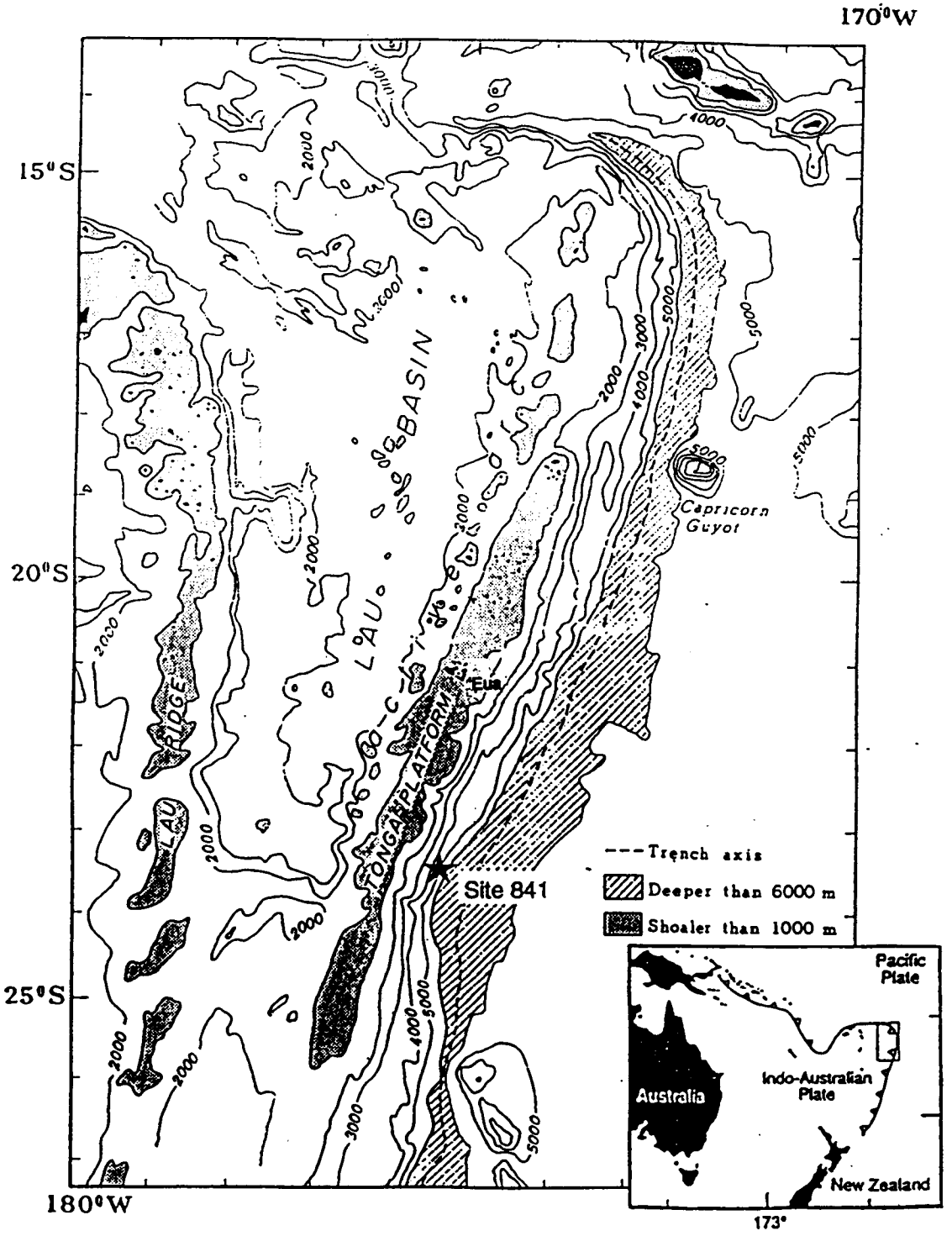

Figure 1. Location of Tonga trench and associated features, including ODP Site 841. After Bloomer et al. (1994).

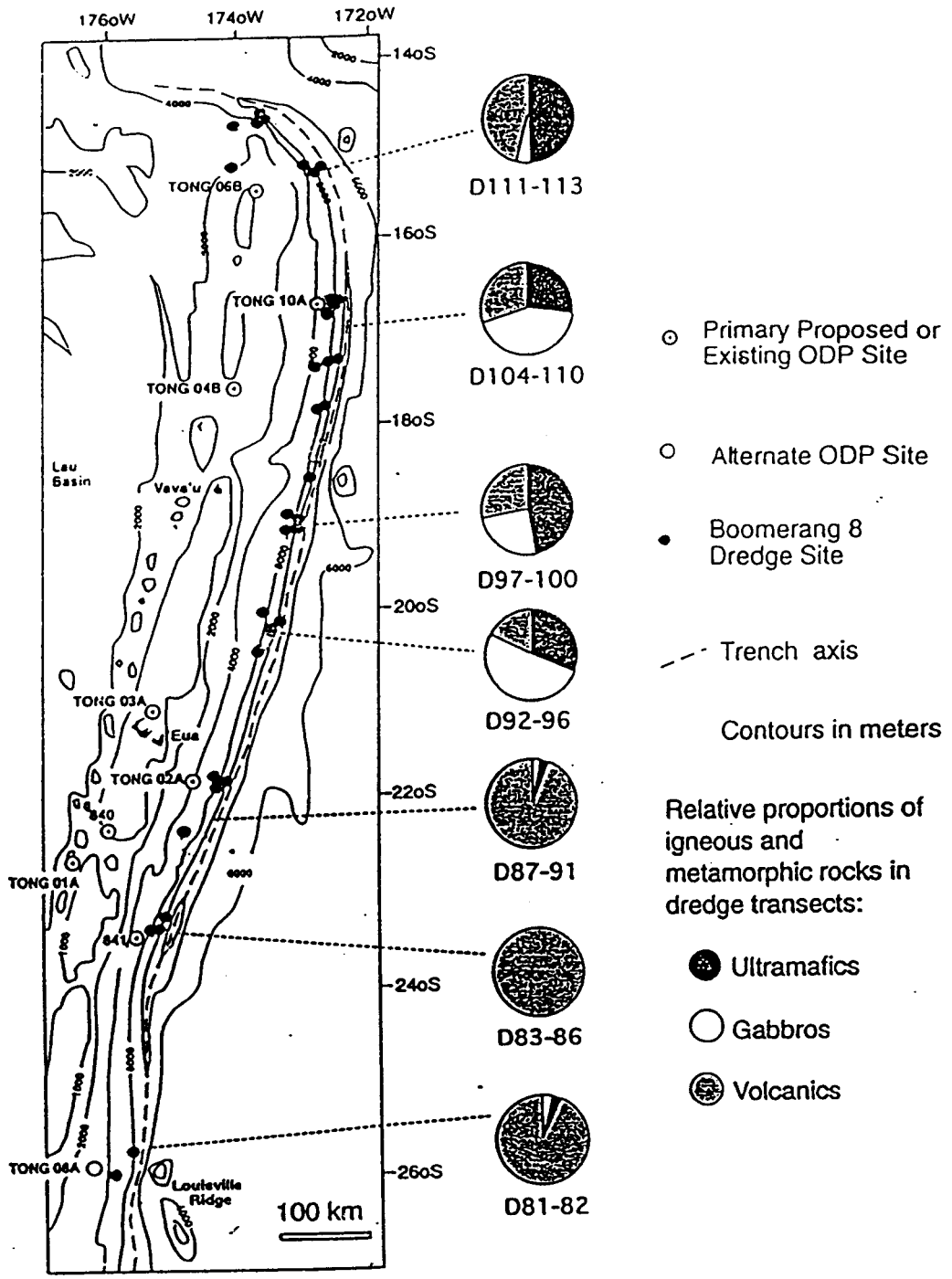

Figure 2. Summary of dredging results from Boomerang Leg 8 site survey cruise in May-June 1996. Dredge proportions (shown in pie charts) do not include sediments. Proposed drilling sites and ODP Site 841 are also shown. After MacLeod et al. (1997).

(2) How do the physical conditions for the hydrothermal alteration of Tonga forearc crust compare to those estimated for the hydrothermal alteration of ophiolites such as the Troodos Ophiolite, and for hydrothermally altered crust from mid-oceanic ridges?
(3) What geochemical fluxes result from hydrothermal alteration of the Tonga forearc volcanic sequence, and how do they compare to the elemental fluxes calculated for volcanic sequences from mid-oceanic ridges and supra-subduction zone ophiolites?
(4) What can be determined about the timing, duration, and spatial extent of hydrothermal alteration in Tonga forearc volcanic crust?

1.2 Previous Studies of Hydrothermal Alteration

1.2.1 Introduction

Heat flow values measured near mid-oceanic ridges fall beneath those which would be expected, based on conductive cooling plate models (Figure 3). This indicates that the oceanic crust is convectively cooled by the circulation of seawater (Lister, 1972; Williams et al, 1974; Anderson and Hobart, 1976; Stein and Stein, 1994). This circulation is important with respect to chemical and isotopic fluxes, heat fluxes, and the physical characteristics of oceanic crust (e.g. density). Subseafloor hydrothermal systems may be characterized as active or passive (Lister, 1982). Active systems occur along ridge axes and involve temperatures greater than 250°C, rapid circulation, and well-focused discharge at the seafloor (Fehn et al., 1983; Rosenberg et al., 1993). Passive convection

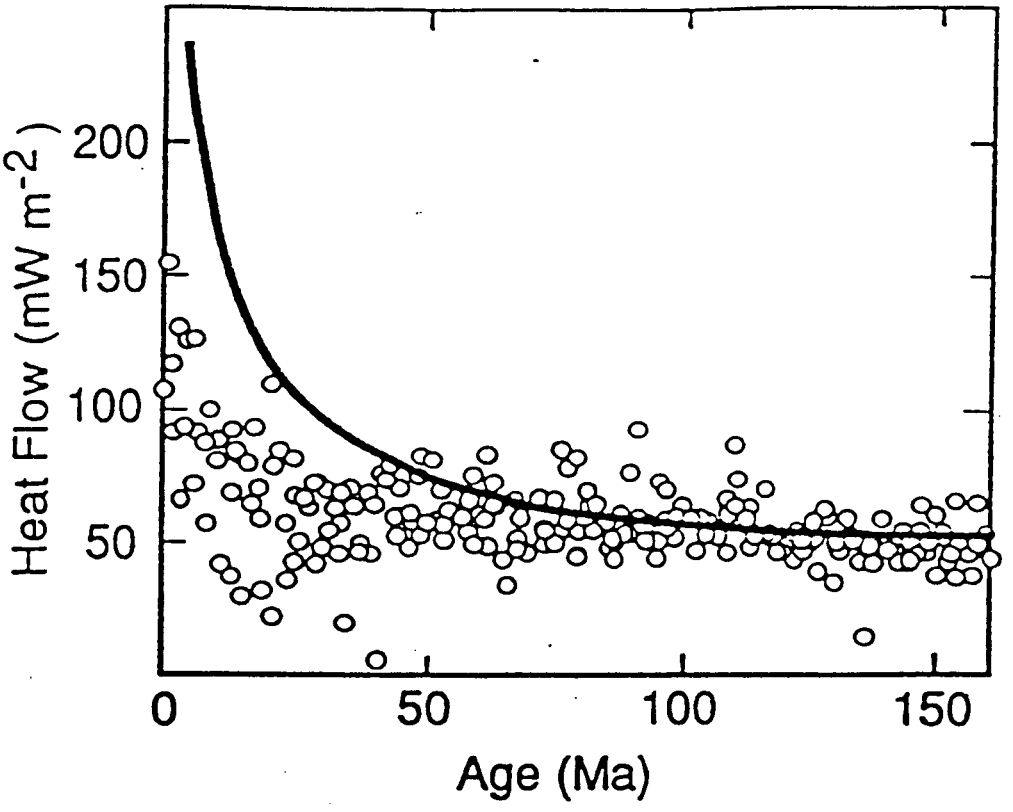

Figure 3. Heat flow versus age of oceanic crust. The open circles are measured values, which fall below the theoretical conductive cooling curve (heavy line) for oceanic crust, indicating that convective cooling by circulating seawater occurs. After Stein and Stein (1994).

systems occur away from ridge axes and involve temperatures less than 200°C and lesser circulation rates than those in on-axis systems (Lister, 1982; Fehn et al., 1983).

The geometry of a subseafloor hydrothermal convection system depends on its location, the lithologies involved, and age. The depth of fluid circulation on a ridge axis is limited by the top of the melt lens at fast-spreading ridges. Porosity and permeability, which are high in the upper volcanic section, permit greater rates of circulation, and flow may be three-dimensional. Massive lava flows may act as local barriers to flow, while brecciated zones may provide easy conduits for fluid flow (Pezard et al., 1992; Larson et al., 1993). Lower in the volcanic section and in the upper sheeted dikes, circulation is restricted due to lower porosity and permeability, and flow may be two-dimensional in the upper sheeted dikes due to igneous morphologies (Nehlig and Juteau, 1988; Haymon et al., 1991). Local topography and faulting may also influence convection system geometry. Off-axis, the depth of circulation is generally restricted to the upper several hundred meters of the permeable volcanic pile (Becker et al., 1989; Fisher et al., 1994). As crust progressively ages, clogging of fractures and pores by secondary minerals decreases both porosity and permeability, limiting or preventing fluid circulation. Circulation of seawater in the volcanic section can continue for tens of millions of years (Staudigel et al., 1981; Gallahan and Duncan, 1994; Stein and Stein, 1994). Heat flow measurements, however, eventually reach those expected for conductive cooling, indicating that hydrothermal circulation is no longer significant with respect to crustal heat loss. This is called the sealing age, which occurs at 65 ± 10 Ma for oceanic crust

(Stein and Stein, 1994). Variations in local sedimentation rate may influence this sealing age.

A submarine hydrothermal circulation system consists of recharge, reaction, and discharge zones (Figure 4). Recharge occurs where seawater enters the crust and migrates downward, and generally occurs by diffuse flow. Reaction zones may be defined as regions where high temperature (~350°C) fluids react with host rock to acquire their chemical characteristics. Discharge zones occur where fluids are expelled on the seafloor. They are generally characterized by focused flow along ridge axes and diffuse flow away from ridge axes.

The primary processes affecting oceanic crust at recharge zones are: fixation of alkalis (leading to nontronite and celadonite deposition in fractures), low temperature oxidation (leading to Fe-oxyhydroxide deposition), Mg fixation (as circulation becomes restricted, leading to smectite and chlorite formation [Alt and Honnorez, 1984; Bohlke et al., 1984; Alt et al., 1986a; Mottl and Wheat, 1994; Teagle et al., 1995]), anhydrite formation (depleting fluids in Ca and affecting their Sr contents [Seyfried, 1987; Berndt et al., 1988]), and alkali loss at higher temperatures (>150°C). The extent to which these processes are prevalent at ridge axes, however, is limited due to kinetic effects. In terms of vertical geometry, circulation is progressively restricted with depth due to porosity and permeability changes, resulting in a shift from oxidizing seawater-dominated conditions to reducing, rock-dominated conditions at deeper than 300-475 m in the volcanic pile (Alt and Honnorez, 1984; Alt et al., 1986a; Gillis and Robinson, 1988).

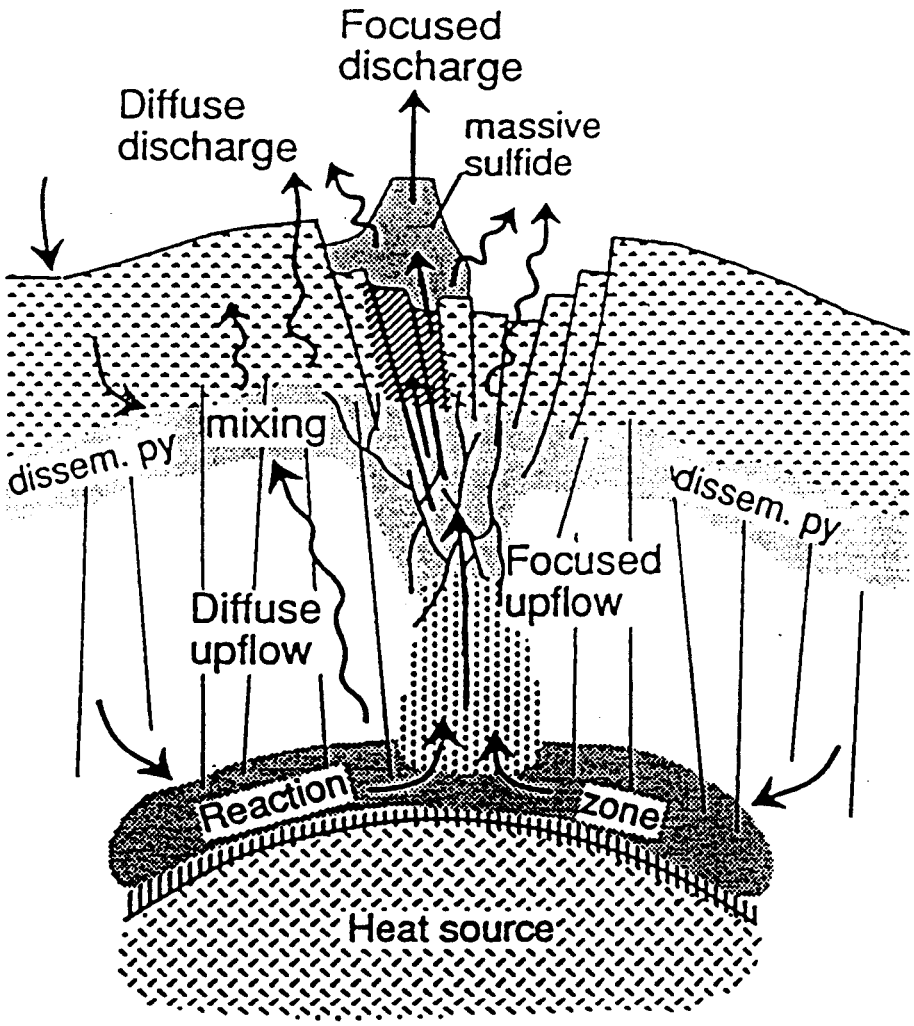

Figure 4. General anatomy of an axial hydrothermal system, showing recharge, discharge, and reaction zones. After Alt (1995).

Subsurface reaction zones are the places where metals and S are lost and fluids are heated; the link between specific mineral assemblages observed in dredged rocks and fluid compositions measured at vents, however, is unclear (Gillis et al., 1993). Models of mid-ocean ridge convection predict a steep temperature gradient as seawater (~200°C) approaches the magmatic heat source (Fehn et al., 1983; Sleep, 1991). Rapid temperature increases in the fluid (to 350-400°C) lead to chemical reactions with the lower part of the sheeted dike complex and upper gabbros. These hot, buoyant fluids then rise and are expelled at discharge zones. Where upflow is focused, high temperature fluids vent directly to the seafloor. Deep, focused upflow zones can be identified in ophiolites and are characterized by epidosite (Richardson et al., 1987; Schiffman et al.; 1987; Nehlig et al., 1995). Epidosite is a rock almost completely recrystallized to epidote, quartz, chlorite, and oxides. It has not been described in oceanic crust, which may be indicative of a fundamental difference between alteration in oceanic crust and in ophiolites. Schiffman et al. (1987) and Bettison-Varga et al. (1992) suggested that large amounts of extension (creating increased permeability) and late off-axis intrusions (providing heat) might have led to the deep vigorous hydrothermal circulation which produced epidosite in the Troodos Ophiolite.

Discharge zones may be manifested, not only as focused flows, but also as diffuse three-dimensional zones of upflow. In this case, the upwelling fluids may not even reach the seafloor but might mix with seawater in the substrate, resulting in precipitation and mineralization. An indication of this kind of flow might be the disseminated sulphide mineralization which commonly occurs near the top of the sheeted dike complex (e.g. Alt et al., 1986a).

1.2.2 Hole 504B and Hole 896A

Much of what is known about hydrothermal alteration in the oceanic crust comes from studies of ODP/DSDP Hole 504B located 200 km south of the Costa Rica Rift in the eastern equatorial Pacific (Figure 5). It is in the center of a 170 km long east-west spreading segment, bounded by fracture zones to the east and west. It is the first hole to be drilled to depths past the pillow basalts-sheeted dikes transition (to a maximum depth of 2111 mbsf; Alt et al., 1996a). The crust at this site is dated at 6.6-6.9 Ma (Cande and Kent, 1995), and the sedimentation rate is estimated at 50 m/Ma (Cann et al., 1983). Heat flow matches the regional average, and fluids are moving horizontally through the uppermost basement (Mottl, 1989).

The detailed stratigraphy and alteration of Hole 504B are presented in Alt et al. (1996a,b). The uppermost sedimentary part of Hole 504B comprises siliceous oozes, chert, limestone, and chalk. Below this lies the volcanic section, which is made up of 70% pillow basalts and breccias, 13% massive units, 13% thin flows, and 4% dikes (Pezard, 1990). Compositions are aphyric to highly phyric, moderately evolved tholeiitic basalts which are strongly depleted in incompatible elements. The upper 100-200 m of the volcanic section are highly porous and permeable; this is seismic Layer 2A (Newmark et al., 1985). Original porosity in the lower 500 m (seismic Layer 2B) has been mostly sealed by secondary mineralization (Becker, 1985; Pezard, 1990).

The transition zone and upper dike section consists primarily of hydrothermally altered and highly brecciated pillows and dikes. Dikes are fine to medium-grained diabase. Overall porosity and permeability decrease significantly across the transition

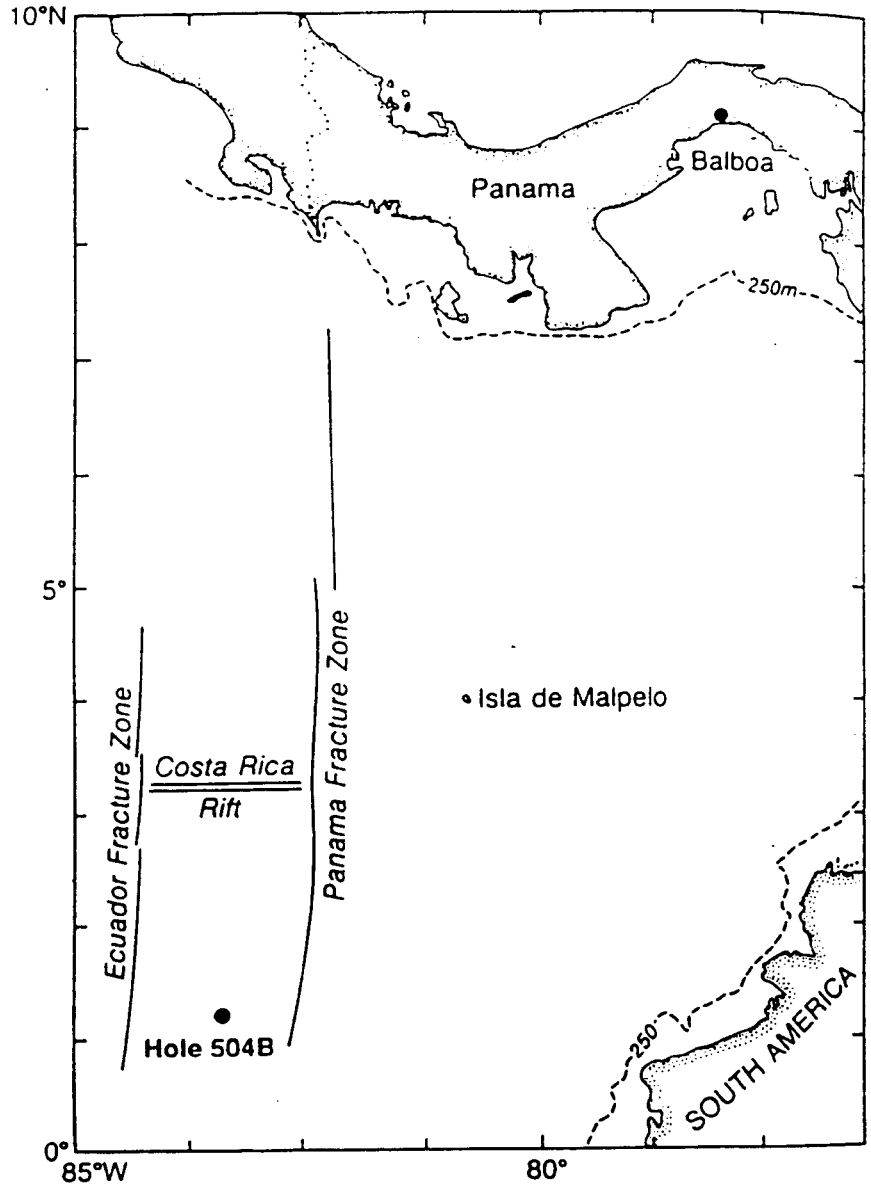

Figure 5. Location of DSDP/ODP Hole 504B in the eastern Pacific (Alt et al., 1986a).

zone. (Porosity changes from ~10% to ~2%; Anderson et al., 1982). The lower dikes are also fine to medium-grained diabase, similar in igneous composition to the upper dikes. General igneous stratigraphy and detailed alteration mineralogy with depth for Hole 504B are shown in Figure 6.

Alteration in the volcanic section is of three types (Alt et al., 1996a,b). A dark gray alteration occurs throughout the section. It is characterized by alteration of olivine to saponite ± talc and plagioclase to saponite. Saponite replaces glassy rinds, fills fractures and vesicles, and cements breccias. Minor pyrite, rare K-feldspar, and albite are also present. Veins contain carbonates and phillipsite. Fine veins high in the section contain celadonite, while veins lower in the section commonly contain minor quartz and anhydrite. The second type of alteration is characterized by the formation of red haloes along fractures in the uppermost volcanic section. This alteration is similar to the dark gray type except for the alteration of olivine to Fe-oxyhydroxides, and the presence of Fe-oxyhydroxides in the groundmass or staining saponite. The third alteration type produces black haloes alongside or within some red haloes. These black haloes consist of celadonite, saponite, and Fe-oxyhydroxides.

Bulk rock analyses of the upper volcanic section (100-200 m) show increases in K, Rb, B, CO_2, and H_2O due to alteration. Chemical changes are greatest in the red and black halos. The lower volcanic section shows similar bulk compositional changes of lesser magnitude.

In the volcanic section, black halo formation occurred due to rock interaction with low temperature Fe-rich hydrothermal fluids (Laverne et al., 1996; Teagle et al., 1996).

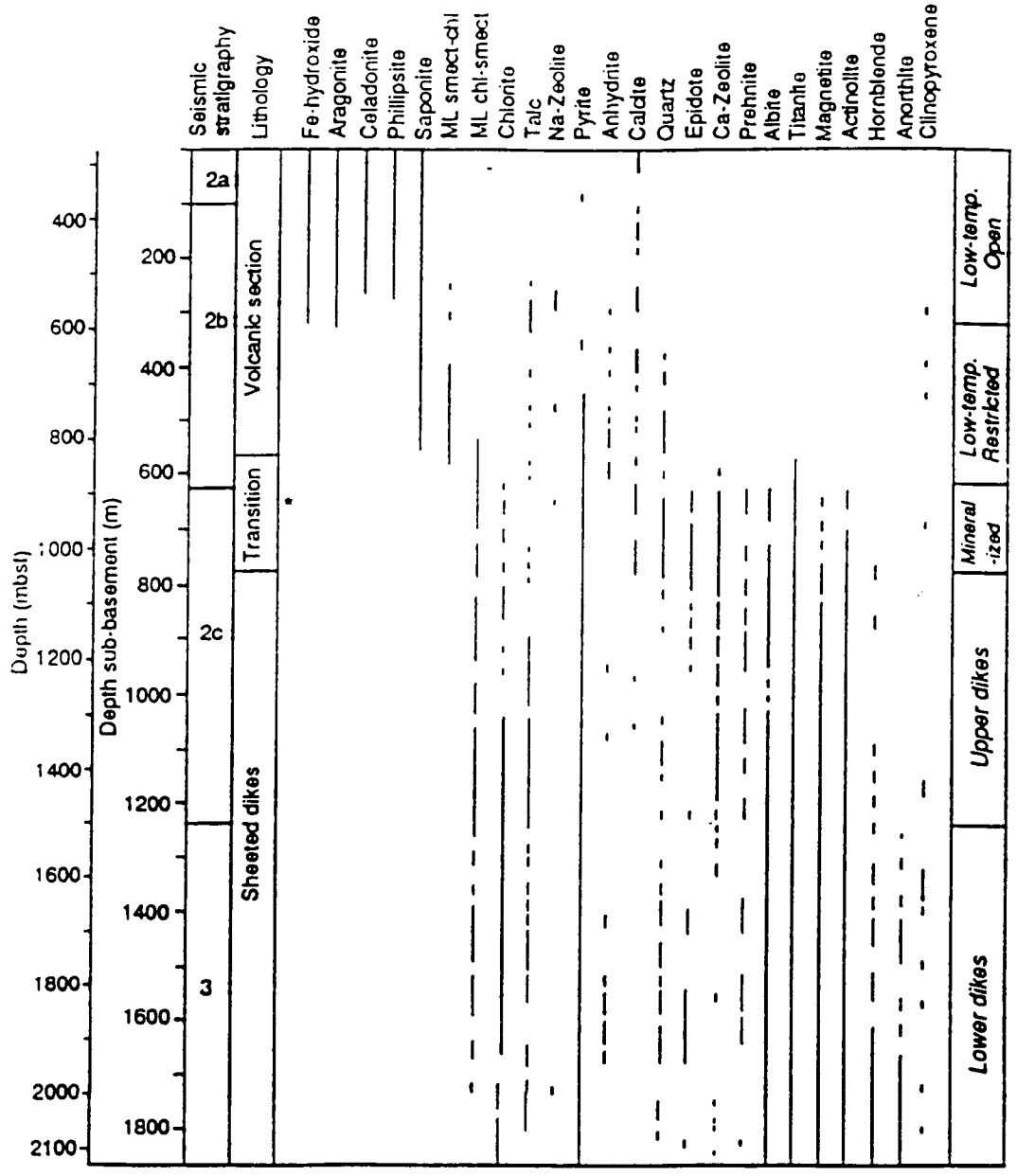

Figure 6. Lithostratigraphy and distribution of secondary minerals in Hole 504B. ML = mixed-layer, chl = chlorite, smec = smectite. After Alt et al. (1996a).

Such fluids could have originated from local breakdown of glass and titanomagnetite, from the lower volcanic section, or from the mixing of low temperature hydrothermal fluids with seawater. These black halos appeared in <10 000 years (Adamson and Richards, 1990) and thus the Fe-rich solutions may have been related to initial cooling of hot lavas or from water-rock interaction during dike emplacement events. These types of features are typical of DSDP/ODP volcanic drill cores in mid-oceanic ridge basalt crust (e.g. Alt, 1986a). Following black halo formation, the red Fe-oxyhydroxide-rich halos developed along fractures as a result of the reaction of rocks with large amounts of cold, oxidizing seawater moving through fractures. Estimates of the seawater:rock mass ratios needed to produce the observed K enrichments and oxidation range from 10-100 (Alt et al., 1996a,b). This indicates extensive seawater circulation in the upper volcanic pile; circulation in the lower volcanic section was more restricted. Such conditions would occur in a ridge flank circulation system near a spreading axis where there was little sedimentary cover. In Hole 504B, the conditions evolved from more open and oxidizing during red halo formation to more restricted, involving more evolved fluids, during late zeolite-carbonate formation.

Alteration in the upper transition zone is similar to that of the lower volcanic section but also includes sphene, mixed-layer smectite/chlorite, minor laumontite, and anhydrite. A change in the nature of alteration (to markedly higher temperature assemblages) appears sharply at 898 mbsf. Alteration products range from dark gray, slightly recrystallized rocks to light green and gray intensively recrystallized rocks. Plagioclase cores are altered to albite-oligoclase ± laumontite, heulandite, and chlorite.

Olivine is replaced by chlorite and quartz or mixed-layer smectite/chlorite. Pyroxene is partially replaced by actinolite and minor magnetite. Titanomagnetite is replaced by sphene. Glassy rinds are altered to chlorite. Disseminated pyrite also occurs. Veins and breccia cements consist of chlorite ± actinolite, quartz, epidote, laumontite, heulandite, albite, calcite, analcite, and pyrite. There is a stockwork-like zone (within the transition zone) which consists of abundant veins of quartz and sulphides in a highly brecciated pillow unit.

The upper dike section comprises light to dark gray, variably recrystallized rocks, with light gray, more intensively recrystallized alteration halos around chlorite and chlorite-actinolite veins. Secondary mineralogy is similar to that of the transition zone, with a few differences. There is no calcite, less heulandite, and more scolecite and prehnite in veins and after plagioclase (than in the transition zone). Olivine is replaced by mixed-layer smectite/chlorite or locally by talc and magnetite. Titanomagnetite is replaced by sphene which may contain ilmenite exsolution lamellae. There is a range of phyllosilicates from true chlorite to random or regularly interstratified chlorite/smectite to talc. Veins are less abundant than in the transition zone and decrease in abundance with depth. There are four vein types. Earliest veins contain chlorite ± actinolite ± sphene ± quartz-chlorite selvages. The next vein assemblage to have precipitated contains quartz ± epidote ± sulphides. The third vein type contains laumontite, scolecite, and prehnite ± calcite. Finally, some late anhydrite occurs in reopened chlorite-actinolite veins. Some coarser dike rocks have more intensively recrystallized light gray alteration patches which may contain amygdules of chlorite ± actinolite ± laumontite ± scolecite.

Bulk rock chemical changes due to alteration in the upper dikes and transition zone are more substantial than those of the lower volcanic section. There are enrichments in Cu, Zn, Mn, and S where sulphide mineralization and Mn-chlorite are present. H_2O increases dramatically with the extent of recrystallization. K_2O and Fe^{3+}/Fe^{total} show stepwise decreases with depth. CaO and Na_2O vary due to calcic plagioclase albitization and to zeolite occurrences. There is no consistent Mg enrichment. This is notable because, as temperatures increase, MgO is rapidly lost from solution during reaction of seawater with basalt (Seyfried, 1987) by forming Mg-OH complexes (i.e. clay minerals). As in the volcanic section, the greatest chemical changes occur in alteration halos.

Alt et al. (1986a, 1996a) distinguished four overlapping stages of alteration in the transition zone and upper dikes, which are also relevant to the history of the volcanic section. The first stage was that of axial hydrothermal alteration involving seawater-derived fluids. This led to the formation of chlorite-actinolite veins and greenschist mineral assemblages (chlorite, actinolite, albite-oligoclase, shene, and talc). Temperatures were 200->300°C (Alt et al., 1996a). Secondly, evolved fluids (depleted in Mg and enriched in Ca, ^{18}O, and metals) upwelling from the dikes mixed with seawater-derived fluids in the transition zone. This caused the stockwork-like sulphide zone to form (at 250-380°C; Alt et al., 1996a). There was a steep temperature gradient at this time, ranging from 100-150°C in the lowermost volcanic section to as high as 380°C in the transition zone, over a 70 m vertical distance. The steep temperature gradient may have been the result of a sharp permeability contrast (which today occurs within the volcanic section at 200 m into the basement; Becker, 1996). The third stage occurred when the

crust moved off-axis and was faulted and fractured. This allowed cool seawater to penetrate into the warm crust, leading to anhydrite (having $\delta^{34}S$ values identical to seawater) precipitation in fractures and as a replacement of plagioclase. The final stage consisted of off-axis low-temperature alteration involving evolved (increased pH and Ca/Mg) hydrothermal fluids. Temperatures ranged from 100-250°C (Alt, 1986b). Unlike the volcanic section, which was cooled after emplacement and then reheated variably during axial hydrothermal alteration, the transition zone and upper dikes likely never cooled below their present temperatures (at least 110°C at the top of the transition zone; Becker, Foss, et al., 1992).

Hydrothermal alteration of the lower dikes is superficially similar to that of the upper dikes, although there are chemical and mineralogical differences. In addition to most of the alteration minerals occurring in the upper dikes, there is secondary calcic plagioclase and clinopyroxene, more amphibole, common magnesiohornblende, more abundant ilmenite exsolution lamellae in titanomagnetite, and anhydrite outside of veins. Recrystallization is much more intense, with the least altered rocks still 10-40% recrystallized.

In the lower dikes, Cu, Zn, and S have been lost; mass balance calculations indicate that the amounts of Zn and Cu lost from the lower dikes balance the Cu and Zn increases in the mineralized transition zone (Zuleger et al., 1995). Generally, bulk chemical changes in the lower dikes are small. As for the upper dikes and transition zone, CaO and Na_2O show small increases and decreases, there are slight losses of K_2O, and

TiO_2 and P_2O_5 scatter due to limited mobilization. As in the upper dikes, there is no consistent Mg enrichment.

Alteration processes in the lower dike section somewhat paralleled those in the upper dikes and transition zone. They are summarized by Alt et al. (1996a). The first stage was an early high temperature (>400°C) stage preceding the first stage of alteration that occurred in the upper dikes. Next was a period of pervasive alteration at temperatures up to 350-400°C. The third stage involved the deposition of quartz-epidote veins due to upwelling fluids at temperatures of 310-350°C. Fourth was local formation of anhydrite due to the incorporation of oxidized basaltic sulphide into sulphate-bearing hydrothermal fluids under oxidizing conditions (Seyfried and Ding, 1993; Alt, 1995). Lastly, after the crust had moved off-axis, was the local formation of laumontite and prehnite at temperatures less than 250°C. Conditions were the same as for the deposition of similar veins in the last stage of upper dike alteration, but these late veins are less abundant with increasing depth, indicating restricted permeability and off-axis circulation for the lower dikes when compared with the upper dikes and transition zone.

Hole 896A, which penetrated 290 m into basement, is located 1 km southeast of Hole 504B, across a fault and on the inferred footwall. It is on a small bathymetric high. The crust is of similar age to Hole 504B (Cande and Kent, 1995). The site, unlike Hole 504B, is on a local heat flow maximum, and basement fluids are upwelling. For this reason, it is probably not representative of most mid-oceanic ridge crust.

Hole 896A stratigraphy and alteration details are summarized in Teagle et al. (1996). It passes through sediments which consist of siliceous oozes, chalk, limestone,

and chert. The volcanic section beneath comprises 51% pillows, 40% massive units, and 9% breccias. Lithologies are strongly depleted, moderately evolved, sparsely to highly phyric tholeiitic basalts (Alt et al., 1993) similar to those in Hole 504B, although there is no direct lithologic or geochemical correlation between the two holes.

Alteration characteristics in Hole 896A are similar to those in Hole 504B, with a few major differences. There is a greater abundance and thickness of smectite and carbonate veins, more breccias, no celadonite-bearing black halos, and greater sealing of the basement by secondary minerals in 896A. Bulk rock chemical changes are also similar, and the greatest changes are present in haloes and breccias. Alteration conditions were similar to those in the upper volcanic section of Hole 504B; there was open and intensive seawater circulation. In Hole 896A, temperatures of vein carbonates indicate that they formed under two different thermal regimes, further documenting the evolution of the system from cooler, more open circulation to warmer, more restricted circulation. The variable distribution of the two temperature groups of carbonates is interpreted to reflect permeability heterogeneities and the sealing of fractures by progressive deposition of carbonates (Teagle et al., 1996).

1.2.2 Troodos Ophiolite

The Troodos Ophiolite (Figure 7), located on south central Cyprus, is at the northwestern end of a belt of Cretaceous ophiolites that are exposed discontinuously along the margin of the Arabian plate (Moores et al., 1984). Its age is 88.5-91.5 Ma

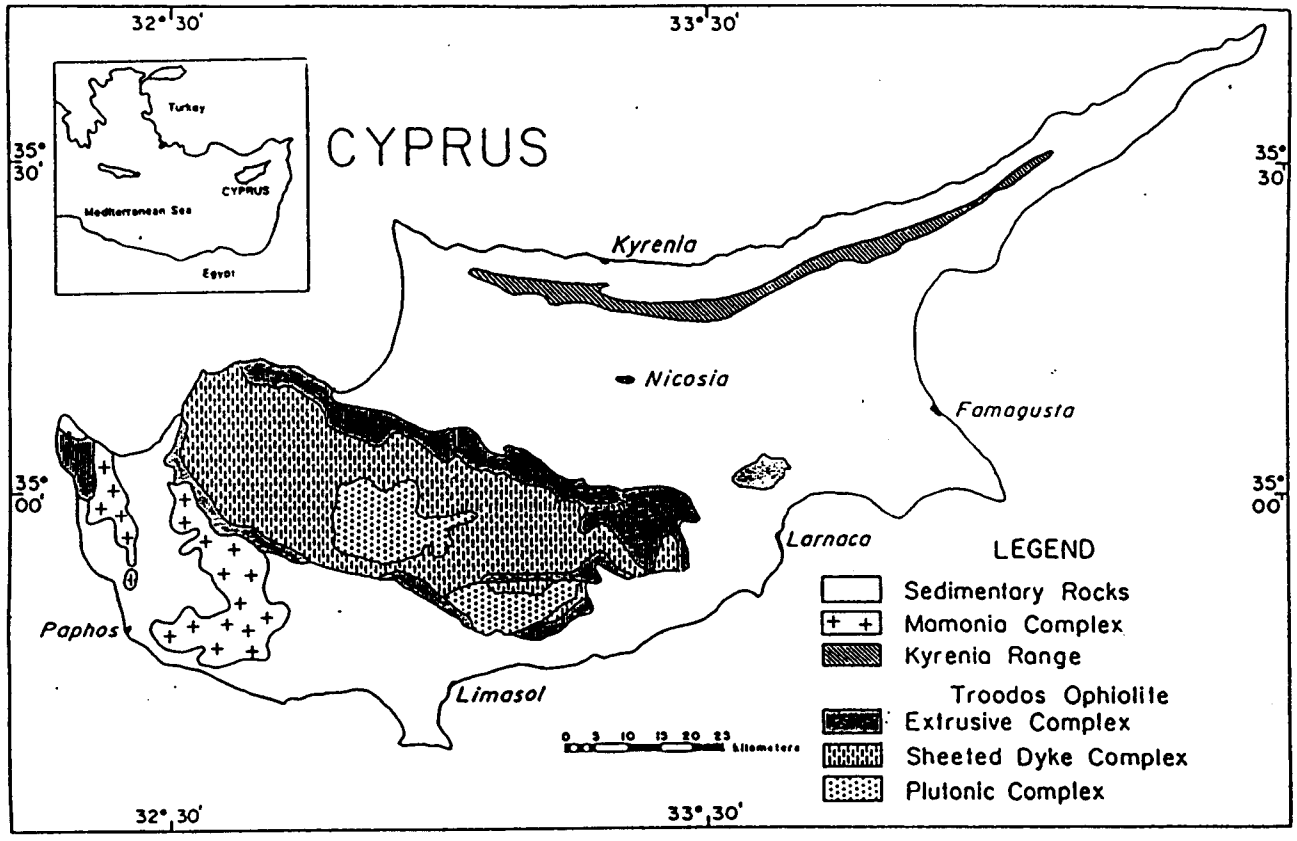

Figure 7. Location and general geology of the Troodos Ophiolite. After Gillis (1987).

(Hartland et al., 1982). Uplift and erosion have exposed all levels, which include an extrusive sequence, sheeted dike complex, and plutonic complex.

The volcanic section comprises pillows, massive and sheet flows, breccias, and hyaloclastites. There are two lava geochemical suites on the ophiolite's northern flank, a high MgO-high SiO_2 suite and an arc tholeiite suite (Robinson et al., 1983). The high MgO-high SiO_2 suite is uppermost and consists of picritic and andesitic depleted arc tholeiite. The lower arc tholeiite suite consists of andesite, dacite, and rhyodacite. On the ophiolite's south flank is a strongly depleted boninitic suite (Mehegan and Robinson, 1985). The sheeted dike complex is aphyric to sparsely phyric.

Traditionally, regional metamorphic zones were used to describe the alteration patterns seen in many ophiolites (e.g. Gass and Smewing, 1973). However, work by Baragar et al. (1987), Gillis (1987), Gillis and Robinson (1987), Richardson et al. (1987), and Schiffman et al. (1987) indicated that this was not appropriate, and that ophiolite alteration has many similarities to that of in situ oceanic crust.

Based on field appearance and secondary mineral assemblages (from field mapping and drill cores, particularly the CY-1 and CY-1A cores), Gillis and Robinson (1987) and Gillis (1987) defined five alteration zones for the Troodos Ophiolite. However, there is significant spatial variability in both intensity and style of alteration on scales of tens to hundreds of meters. The CY-1 and CY-1A drillcores are both located in the extrusive sequence of the Akaki River Canyon (Figure 7). The CY-1 drillcore penetrates 475 m of lavas and consists of phyric to sparsely olivine-phyric and picritic pillows and breccias, grading downwards into aphyric to sparsely olivine-phyric pillows

and flows. The CY-1A drillcore shares 50-75 m of stratigraphic overlap with the drilled core of CY-1, and penetrates 702 m of volcanic material; its lithologies are similar to those of the lower half of the CY-1 drillcore (Gillis, 1987). Stratigraphy and alteration mineralogy of the CY-1 and CY-1A drillcores are summarized in Figure 8. The spatial variability of alteration zones is shown in Figure 9.

The Seafloor Weathering Zone (SWZ) has a red, oxidized appearance and is pervasively altered. Interpillow sediment is locally abundant. Olivine is altered to goethite and calcite and clinopyroxene to smectite. Groundmass minerals are altered to K-feldspar, smectite, and maghemite, and mesostasis to smectite and calcite. Glassy rinds are altered to smectite ± phillipsite. The Low Temperature Zone (LTZ) is the most dominant zone in the extrusive section, and shows a greater spatial variability in its intensity of alteration. For example, there may be fresh glass next to highly altered rock. Olivine is altered to goethite and calcite or serpentine, clinopyroxene to smectite, plagioclase to smectite, calcite, and celadonite, and titanomagnetite to maghemite. Groundmass minerals are altered to smectite, calcite, celadonite, and maghemite, and mesostasis to smectite, celadonite, and calcite. Glassy margins are altered to smectite ± phillipsite ± analcite ± celadonite ± heulandite, depending on whether the glassy rind belongs to a pillow, flow, or hyaloclastite. The Transition Zone (TZ) has attributes of the zones above and below it. Clinopyroxene is altered to smectite or smectite/chlorite and plagioclase to albite. Groundmass minerals are replaced by smectite, smectite/chlorite, albite, K-feldspar, and mesostasis by quartz and pyrite. Glassy rinds are altered to smectite ± smectite/chlorite ± laumontite. The Upper Dike Zone (UDZ) is pervasively altered and may contain rocks

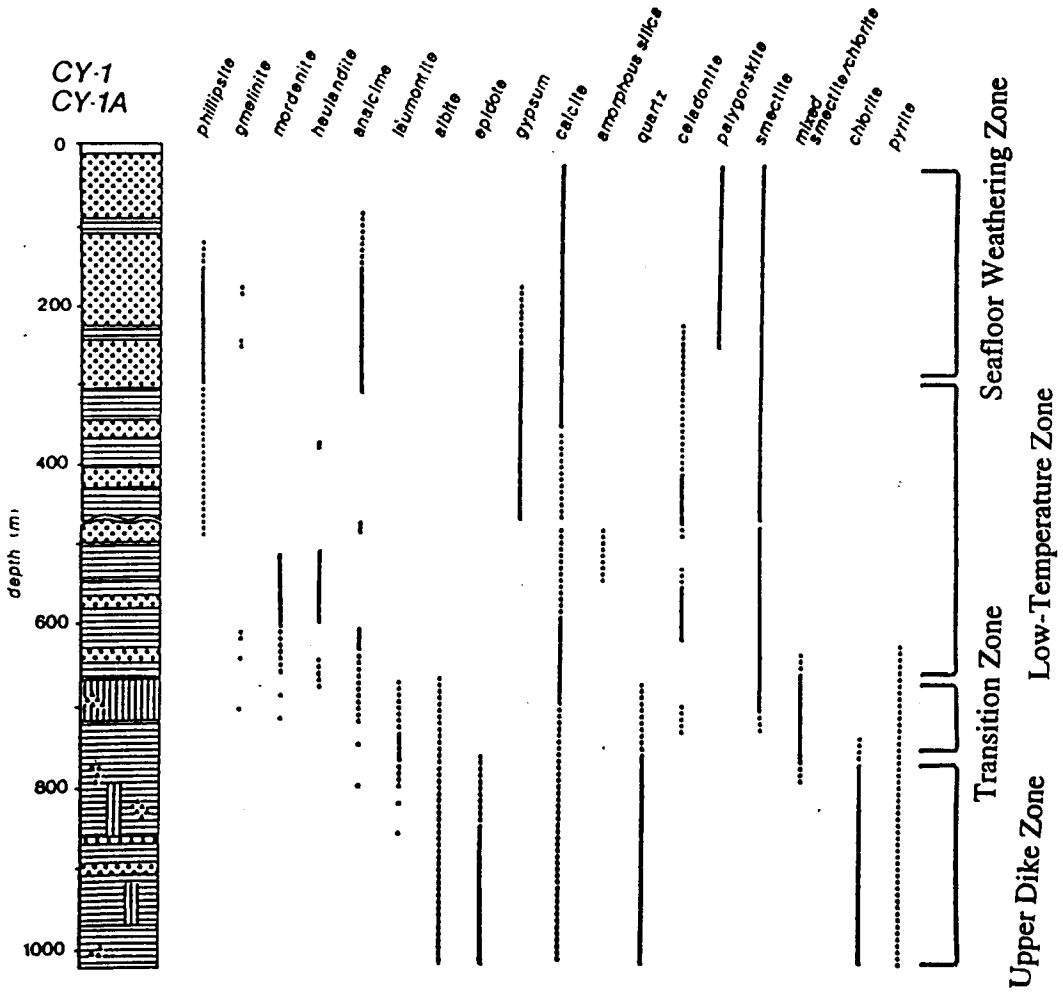

Figure 8. Distribution of secondary minerals in the CY-1 and CY-1A drillcores in the Troodos Ophiolite. Vertical lines represent dike-dominated units. Triangles represent units dominated by breccias or hyaloclastites. After Gillis (1987).

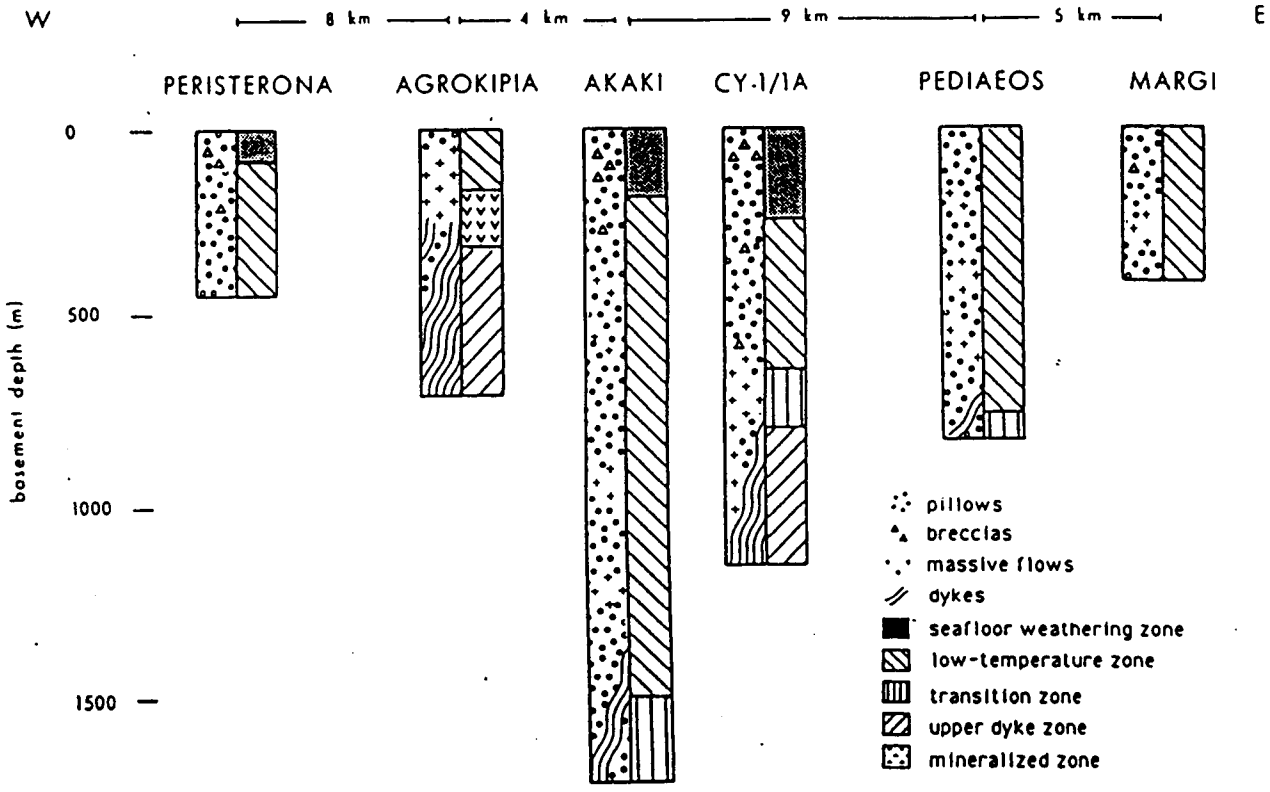

Figure 9. Spatial variability of alteration zones along the northern flank of the Troodos Ophiolite. The top of the extrusive sequence is the datum. Stratigraphic columns show the igneous morphologies on the left and the alteration zones on the right. Gillis and Robinson (1991).

recrystallized to epidosite. It occurs principally within the upper sheeted dikes although it extends into the lower lavas at some locations. Clinopyroxene is altered to chlorite and plagioclase to albite, calcite, epidote, and chlorite. Groundmass minerals are replaced by chlorite, albite, epidote, and sphene, and mesostasis by chlorite, quartz, epidote, and pyrite. Glassy margins are altered to chlorite and quartz ± epidote. The Mineralized Zone (MZ) contains massive sulphide deposits and is restricted spatially, but occurs at all stratigraphic levels within the volcanic sequence. There are significant lateral and vertical variations in the thickness and distribution of all of these zones, and some boundaries, notably the lower boundary of the SWZ, are gradational.

Trends in bulk rock chemistry are relatively consistent with the defined alteration zones. Analyses of the CY-1 drillcore (Gillis, 1987) indicate variations in some elements with depth, although some show no consistent patterns. Fe^{3+}/Fe^{total} consistently decreases with depth, indicating that the upper lavas are more oxidized. In the upper 200 m of the CY-1 core, K_2O, Na_2O, and Rb are gained. This portion primarily consists of SWZ. From 200-350 m in depth, K_2O, Na_2O, MnO, Ba, Rb, and Zn are gained, and CaO and Sr are lost. From 350-700 m, SiO_2, MnO, Na_2O, Cu, and Zn are gained, and MgO, K_2O, CaO, Rb, V, Ba, and Sr are lost. Rocks below 200 m belong principally to the LTZ.

The distribution of alteration mineral assemblages demonstrates that different physical and chemical conditions existed at different depths in the volcanic section at different times. Gillis (1987) divided alteration into four stages. The first occurred during and just after emplacement (referring to lava eruption, not ophiolite obduction), and involved the circulation of cool seawater in the upper, permeable volcanic section at

temperatures <100°C. Permeability decreased progressively as minerals were deposited in fractures. Cold seawater depressed the thermal gradient high in the volcanic section, but in the TZ there was a sharp temperature increase, due to decreased permeability preventing the influx of cool seawater. Downwelling seawater may also have mixed with more evolved deeper fluids to deposit minerals in parts of the TZ and UDZ where there was hydrothermal upwelling. The second stage still involved cool seawater circulation, but due to decreased permeability from previous mineralization, deposition of further minerals occurred only in open fractures. Lessened circulation led to fluids that were more alkaline and oxygen-poor compared to those of the first stage. The distribution of zeolites in the permeable layer and TZ suggests that there were preferred fluid paths; lateral variations in permeability due to cooling unit distribution may have controlled the flow of seawater. The third alteration stage involved a general change in conditions. The stepped temperature gradient which prevailed during the first two stages was decreased, and calcite was deposited from Mg-depleted seawater at all levels. However, fluid flow direction is unknown. The final stage applies only to the upper several hundred meters. It involved deposition of minerals in reopened fractures, and its effects greatly decrease with depth, since the fluid involved was seawater. In general, the composition of the reacting fluids and the extent to which they interacted with the rock depended on temperature, permeability, and the associated water:rock ratio, and bulk chemical trends and spatial variability in alteration reflect this.

1.2.3 Izu-Bonin-Mariana Forearc

Site 786 is located 70 km west of the axis of the Bonin trench, in the outer Izu-Bonin-Mariana forearc (Figure 10). The IBM forearc formed in the middle to late Eocene (similar in age to the Tonga forearc) during the initiation of subduction in the western Pacific, with initial crustal production rates that may have been similar to slow-spreading ridges (Bloomer et al., 1995). Hole 786B represents a volcanic edifice that formed in an extensional setting. It has been drilled to a maximum depth of 828 mbsf. The principal igneous units are dated at 41.3 Ma. There was later minor intrusive activity at 34.6 Ma and 17 Ma (Mitchell et al., 1992).

Hole 786B penetrates 104 m of marls and clays, followed by 22 m of volcanic breccias, followed by 665 m of massive and brecciated flows, ash flows, and intercalated vitric siltstones and sandstones (in the upper part of the core), and pillow lavas and dikes (in the lower core) (Arculus et al., 1992). In the upper section, compositions are intermediate-Ca boninite and its fractionation products (intermediate-Ca bronzite andesite, andesite, dacite, and rhyolite). In the lower section, compositions are low-Ca boninite and low-Ca bronzite andesite. The late intrusions are dikes or sills of intermediate-Ca or high-Ca boninite.

Stratigraphy and alteration mineralogies are shown in Figure 11. Details of alteration are summarized by Alt et al. (1998). All igneous rocks in Hole 786B are altered to some degree. Secondary mineralogy varies with depth. Even the freshest rocks contain 5-25% secondary minerals. In typical, least altered rocks, olivine and orthopyroxene are partially altered to smectite, vesicles are filled with smectite, and the rock has a gray

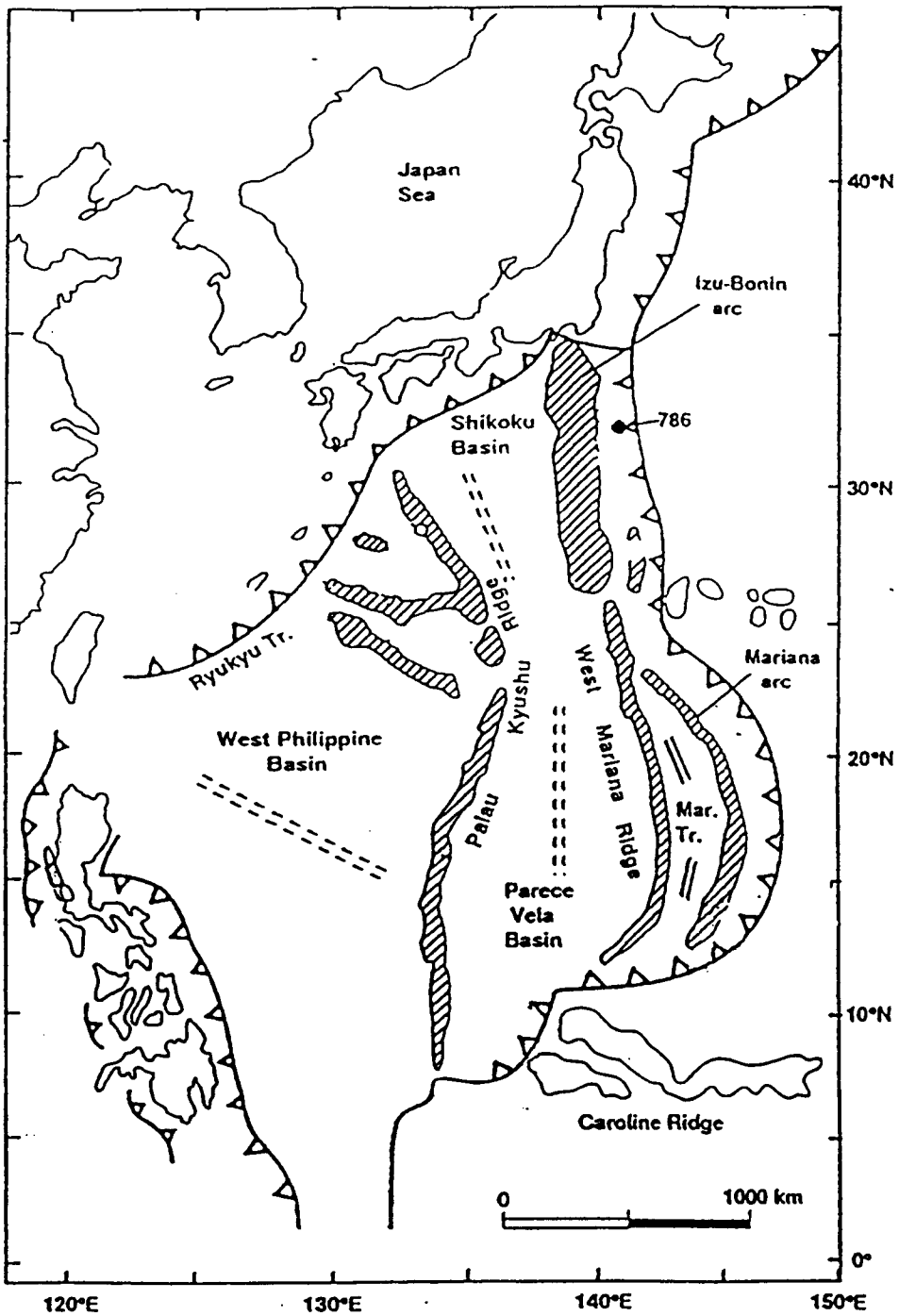

Figure 10. Map of the Philippine Sea, showing the Izu-Bonin-Mariana forearc and other major tectonic features of the region. Site 786 is shown with a black circle. After Bloomer et al. (1995).

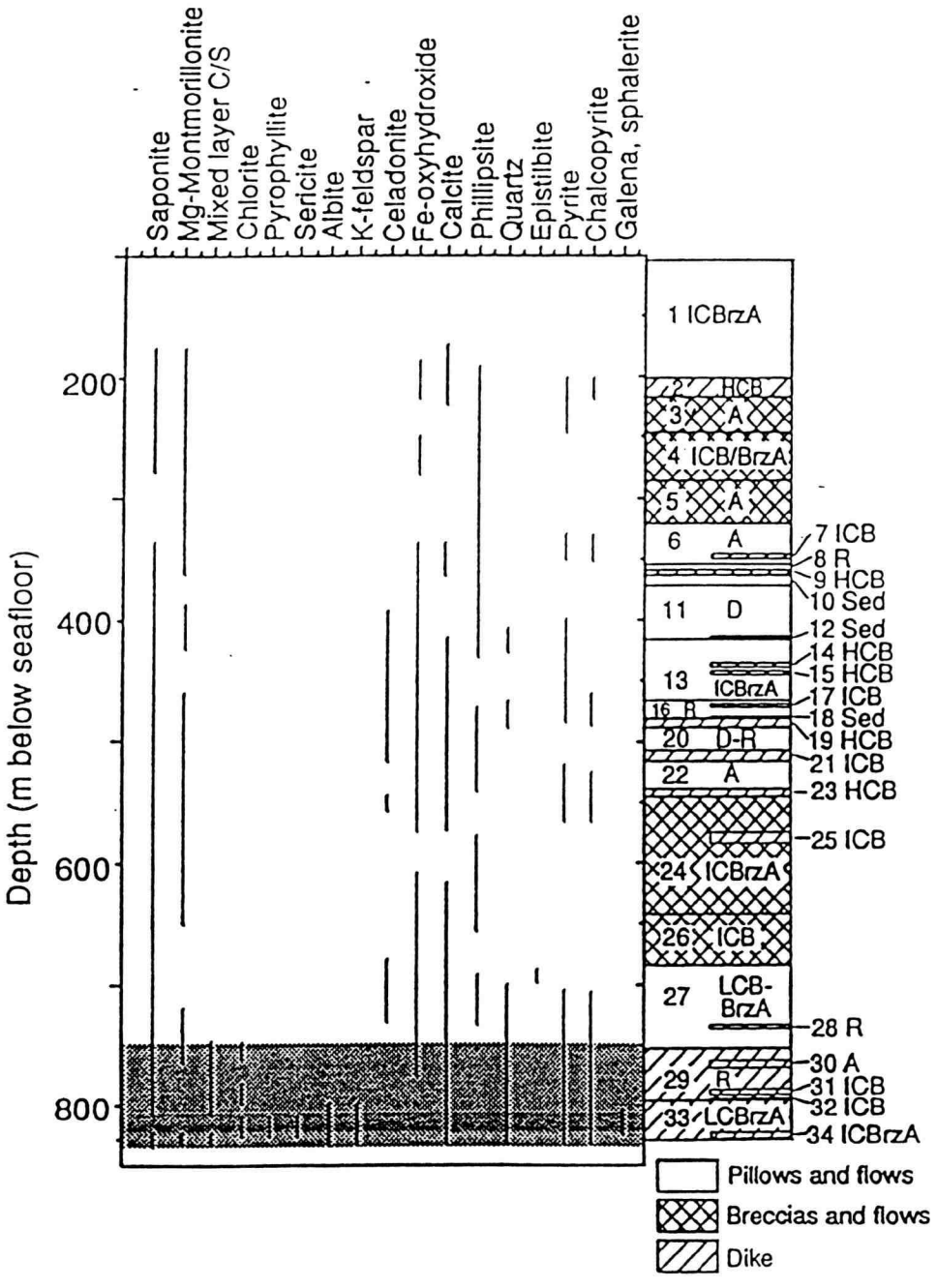

Figure 11. Stratigraphic column showing igneous morphologies and alteration mineralogies for Hole 786B. Alt (1997).

color. The most altered rocks contain >60% secondary minerals. In typical most altered rocks (which include low-Ca boninite and bronzite andesite), olivine and orthopyroxene are completely replaced by smectite, celadonite, chalcedony, and quartz, and plagioclase is slightly altered to smectite. Fractures and voids are filled with smectite, phillipsite, carbonates, and quartz ± analcite. The most altered rocks are light gray to green or brown to red. Rocks brecciated in place have glassy groundmass altered to smectite, and fractures filled with smectite, phillipsite, and carbonates ± celadonite. Veins contain smectite, Fe-oxyhydroxides, celadonite, phillipsite, and carbonate in various combinations or alone. The general precipitation sequence in veins is smectite ± celadonite ± Fe-oxyhydroxides, followed by phillipsite, followed by carbonate. Veins containing smectite may have brown oxidation halos. Sulphide mineralization occurs at several depths. There are disseminated pyrite and chalcopyrite, veins of quartz and pyrite ± other sulphides, and traces of various sulphides in the low-Ca bronzite andesite dikes near the base of the section. There is also a 5 m thick interval of very altered and pyrite-rich rocks in the same part of the section. Here rocks are totally altered to either a pale green assemblage of chlorite, quartz, albite, and K-feldspar, ± smectite and magnetite, or to a bleached assemblage (occurring adjacent to quartz veins) of sericite, quartz, K-feldspar, albite, and minor chlorite. Both assemblages also contain abundant disseminated pyrite. There is also a 7.5 m interval in rhyolite (Unit 16) with rocks 40-80% replaced by Mg-montmorillonite and minor calcite, and containing abundant pyrite, plus veins of quartz, phillipsite, pyrite, calcite, and analcite.

Most chemical changes in Hole 786B are typical for low temperature (<150°C) alteration of mid-oceanic ridge basalt (MORB) and ophiolite volcanic sections (Alt et al., 1986a).Geochemical trends are generally consistent throughout all rock types (Alt et al., 1998). K, Rb, P, Y, and Loss-On-Ignition (LOI) are enriched in the altered rock. Si, Na, Ca, Mg, Fe, and Sr show various gains and losses, indicating that they were mobilized during alteration. Sulphide zones show enrichments in S, Cu, Zn, As, and Mo. In the sericite-rich zones low in the section, Ca, Na, and Sr have been locally lost, and K and Rb have been locally gained, due to feldspar replacement by K-feldspar and sericite. Si has been gained in the sericitized zones due to silicification, but lost from the nearby chlorite-rich zones, which have gained Fe and Mg that was lost from the sericitized zones.

In general, alteration temperature appears to have increased steadily with depth in the section, with a sharp increase at the volcanic-dike transition, based on mineralogic and isotopic data (Alt et al., 1998). This is reflected by more intensive recrystallization, increasing sulphide abundance, the disappearance of phillipsite and Fe-oxyhydroxides, and the appearance of albite, K-feldspar, mixed-layer smectite/chlorite, and chlorite as depth increases. Crosscutting relationships indicate that early phyllosilicates and oxidation preceded deposition of phillipsite and then carbonates. This is supported by the lower temperatures calculated for carbonate formation, reflecting progressive cooling with time. The change from phyllosilicate to zeolite and carbonate deposition also reflects decreasing Mg and increasing Ca in solution, and increasing pH. The bulk gains of Mg in the chloritized rocks required a Mg-bearing fluid; since Mg is quickly lost from solution during the reaction of seawater with basalt (Seyfried, 1987), the solution must have been

only partially-reacted seawater or a mixture of seawater and Mg-depleted fluid. If the increase in MgO of the chloritized rocks came from the uptake of all the available Mg from seawater (53 millimolal Mg), water: rock ratios would have been 16-32. If the MgO increase came from a mixture of seawater and a Mg-poor fluid, water:rock ratios would have been even higher (Alt et al., 1998). The evolution of fluid composition with time is also seen in MORBs (e.g. Alt and Honnorez, 1984; Alt et al., 1986b; Teagle et al., 1996).

1.2.4 Summary

Site 504, Site 896, the Troodos Ophiolite, and Site 786 share many similarities in the nature of alteration of their volcanic rocks. Site 504 and the Troodos Ophiolite both display the effects of interaction with relatively unmodified seawater, seen in the red, oxidized, pervasively altered Seafloor Weathering Zone at Troodos, and in the red haloes along fractures at Site 504. However, K-feldspar is abundant at Troodos but rare at Site 504. Low temperature alteration effects at all of these locations are broadly similar; celadonite, smectites, Fe-oxyhydroxides, carbonates, and low temperature zeolites occur, and there is enrichment of K and Rb in the upper volcanic section (other elements behave more variably from one location to another). Even at a single location, there may be great spatial variability. This is most apparent in the Low Temperature Zone at Troodos because more spatial information is available (the other places are drillsites in the ocean). At all of these localities, high temperature phases (e.g. sphene, mixed-layer smectite/chlorite, chlorite, albite, quartz, actinolite, epidote, and sulphides) increase in abundance with increasing depth; at Site 786 in the IBM forearc, there is higher

temperature mineralization at several stratigraphic levels. Bulk chemical changes (such as decreases in Fe^{3+}/Fe^{total}) are also commonly more significant as depth increases.

Certain broad alteration features are common to all of these settings. The temperatures at which alteration occurred generally increase with depth, with (where evident) a sharp increase at the volcanic-dike transition, reflected by more intensive recrystallization, greater sulphide abundance, and higher temperature mineral assemblages. The thermal regime at each locality changed progressively with time, reflecting a general transition from more open and intensive seawater circulation, especially close to the seawater:rock interface, to more restricted circulation involving more evolved fluids. Overall, there are trends of cooling with time, visible in crosscutting relationships between low and high temperature alteration phases. Temporal and spatial changes in fluid composition also influenced mineralization, and were strongly related to temperature, permeability, and water:rock ratio.

Chapter 2. Regional Background

2.1 Regional tectonics and geology

The Kingdom of Tonga comprises two linear island chains lying west of, and parallel to, the Tonga Trench, which marks the nearly perpendicular westward subduction of the Pacific Plate beneath the Indo-Australian Plate (Figure 1), and contains the deepest point in the southern hemisphere, Horizon Deep (10,866 m). The trench and associated forearc are one of many in a series of western Pacific arcs that have developed since the middle Eocene (Herzer and Exon, 1985). Instantaneous convergence across the northern Tonga Trench occurs at a rate of 24 ± 1 cm/year (Bevis et al., 1995), the greatest plate velocity on the planet.

There are a number of structural units defined across the strike of the Tonga arc (Figure 12). The late Miocene-Recent Lau backarc basin (Figure 1) is bounded to its west by the Lau ridge, an inactive remnant arc (Cole et al., 1990). The eastern Lau basin is bounded by two ridges, which form the islands of Tonga. The western ridge is the Tofua arc, the presently active island arc; its subaerial and submarine volcanoes erupt basalt, basaltic andesite, and minor dacite. The eastern ridge lies on the inactive frontal arc, the shallow, 60-80 km wide Tonga platform, whose Eocene to Miocene volcanic rocks are overlain by younger carbonate sediments. The two island chains are separated by the Tofua trough. The northern Tofua arc is closer to the trench axis and overlies Tonga platform sediments (Scholl et al., 1985; Chase, 1985; Tappin, 1994). The morphological axis of the trench is at some points along the trench actually part of the Pacific Plate

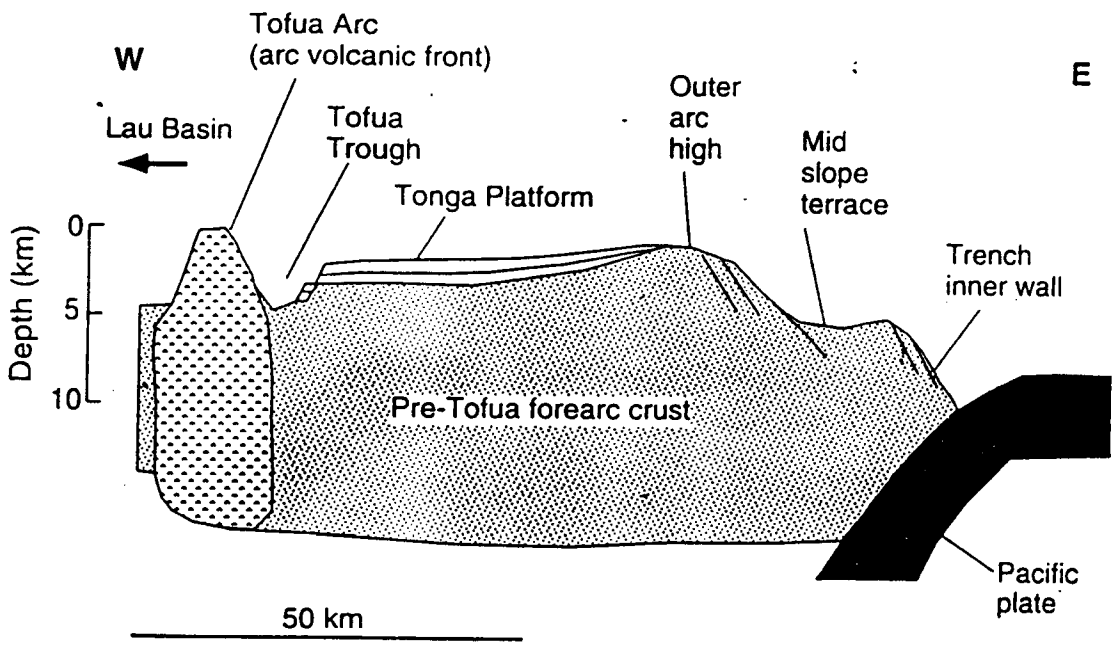

Figure 12. Simplified cross-section of the Tonga arc and forearc, showing major structural features. Clift et al. (1998).

(middle to late Mesozoic in age; Burns et al., 1973), as there is a graben along the lowest part of the trench (Hilde and Fisher, 1979; Hilde, 1983; Lonsdale, 1986). There are also a number of large trenchward-dipping normal faults on the trench slope, and some minor arcward-dipping faults (MacLeod and Lothian, 1994). Seamounts are present at 18°30' S (Capricorn Guyot) and further south (26°S) where the Louisville Ridge (a hotspot-related Upper Cretaceous seamount chain; Lonsdale, 1988; Watts et al., 1988) is being obliquely subducted at the intersection of the Tonga and Kermadec trenches (Figure 1). The collision of the Tonga arc and Louisville Ridge has been cited as a cause of uplift and faulting of the southern Tonga ridge, hiatuses in volcanism along the arc, and seismic gaps along the collision zone (Dupont and Herzer, 1985; Packham, 1985; Lonsdale, 1986; Tagudin and Scholl, 1994).

Three major units have been proposed as along-axis subdivisions of the forearc, based upon structure, morphology, and sedimentary geometry (Tappin, 1994). The southern unit (Figure 13a) lies south of 21.5°S and is submarine with shallow water depths. Its sedimentary units dip westward and abut against the Tofua arc. The central unit (Figure 13b) lies between 22.5-18.25°S and consists of many small islands and an eastward-dipping sedimentary section, which is separated from the Tofua arc by the submarine Tofua trough. The northern unit (Figure 13c) lies north of 18.25°S, in deeper water. Small islands of the Tofua arc penetrate the sedimentary section, which is relatively thin and lacks a preferential regional dip. Transect 87-91, the focus of this thesis, lies across the central unit in the Tongatapu-'Eua region (Figure 1).

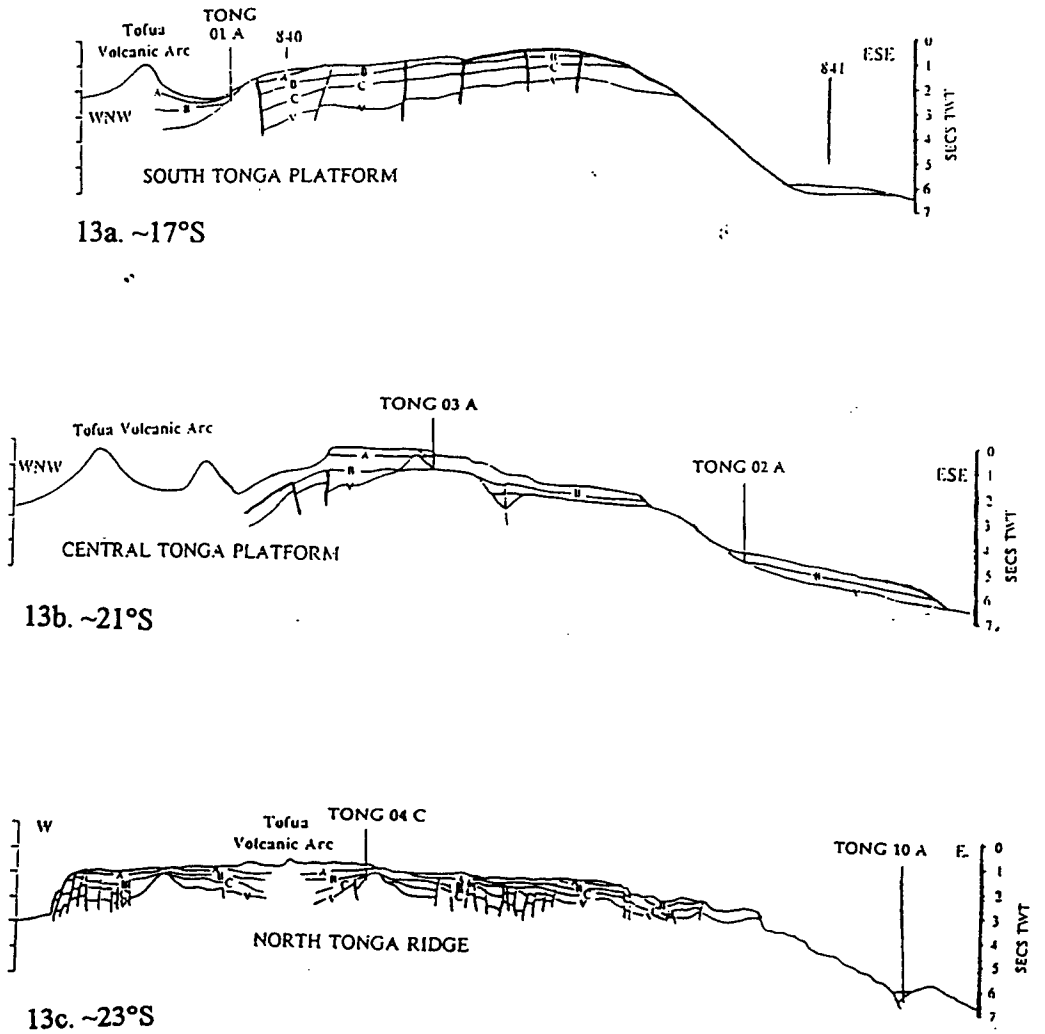

Figure 13. Line drawing interpretation of structures and seismostratigraphy for the southern (13a), central (13b), and northern (13c) portions of the Tonga forearc. After MacLeod et al. (1997).

The Tonga forearc and trench developed during the middle Eocene as part of the westward-subducting Melanesian arc, which no longer exists except as fragments of several modern arcs (Burns et al., 1973). This timing is supported by the oldest ages determined for igneous rocks in the region; rhyolite from ODP Site 841, on the middle trench slope in the southern forearc, was dated as middle Eocene (44+/-2 Ma; McDougall, 1994), and gabbro from the northern Tonga trench was dated as early-middle Eocene (50+/-9 Ma; Acland et al., 1992). Sediments of middle Eocene age in Hole 841 (Shipboard Party, 1992), on the island of 'Eua (Ewart and Bryan, 1972; Tappin, 1994), and in boreholes on Tongatapu (Cunningham and Anscombe, 1985) also support this age for the forearc. Early in the Melanesian arc's history (during the middle Oligocene), there was rifting and spreading in the South Fiji Basin (Malahoff et al., 1982) . Late in the Miocene, rifting of the Lau basin occurred (Hawkins, 1974; Parson et al., 1992), and the New Hebrides arc separated from the Lau-Fiji-Tonga arc by the initiation of east-dipping subduction beneath it (Herzer and Exon, 1985). Throughout the Miocene, volcanism continued along the Lau Ridge, shedding volcaniclastic sediment to form the Tonga platform to its east (Herzer and Exon, 1985). There was also some intrusive activity beneath the Tonga platform in the form of Miocene dikes and sills (Cunningham and Anscombe, 1985). About 6 m.y.a. (late Miocene), spreading began in the Lau Basin (Parson et al., 1992), resulting in regional uplift of the Tonga platform (Herzer and Exon, 1985), eastward movement of the Tonga platform (away from the Lau Ridge), and clockwise rotation of the whole forearc (Sager and MacLeod, 1995); the present active

arc now lies west of the Tonga platform. Lau Ridge volcanism didn't cease until 2.4 m.y.a. (Pleistocene) (Cole et al., 1985). Spreading in the Lau Basin continues today.

Since the 1960's, dredging in the Tonga Trench has yielded a variety of igneous and sedimentary rocks. Petelin (1964) recovered tuffs, agglomerates and basalt from depths of 8000-500 m at 20°20'S (the region just north of 'Eua). Abdenko et al. (1972) and Udintsev et al. (1974) dredged basalts and andesites from 5700 m at 19°19'S. Later dredges continued to recover a variety of igneous and volcaniclastic rocks (Fisher and Engel, 1969; Fisher, 1974; Anosov et al., 1983; Sharaskin et al., 1984; Vallier et al., 1985). Fisher (1974) described a crude stratification of the nearshore trench flank: the uppermost stratum (<5500 m) contains siltstone, calcareous rocks, and debris, and silicic to intermediate volcaniclastic rocks, pumice, and occasional diabase. Further downslope, there is alkali olivine basalt and gabbro. The deepest levels of the trench yield harzburgite, dunite, and serpentinized lherzolites overlying vesicular alkali basalts and variolitic low-alkali basalts. Fisher and Engel (1969) interpreted these rocks as an arc construction exposed by faulting. Hilde and Fisher (1979) suggested that the lowermost basalts came from the subducting plate. Vallier et al. (1985) proposed that these forearc rocks were the subsided early foundation of the arc.

Most of the Tonga forearc basement is presently submarine or unconformably overlain by calcareous sediments; it is exposed subaerially only on the island of 'Eua. Ewart et al. (1977) and Duncan et al. (1985) dated this basement radiometrically at 46-40 Ma (middle to late Eocene). It consists of depleted island-arc tholeiitic basalts, andesites, and dacites (Ewart and Bryan, 1972; Hawkins and Falvey, 1985; Cunningham and

Anscombe, 1985). This basement has been observed on seismic reflection profiles to continue eastward across the forearc (Greene and Wong, 1983; Gnibidenko et al., 1985). Dredging (throughout the forearc) and drilling at Site 841 support the seismic reflection evidence that the Eocene basement is exposed on the landward trench slope. Drilling of basement at ODP Site 841 recovered mid-Eocene arc volcanic rocks, and dredged samples from nearby include arc tholeiites. Dredges from elsewhere in the forearc include arc tholeiite, andesite, boninite, highly depleted serpentinite, and gabbro. All of this evidence supports the hypothesis that the entire arc is underlain by arc-derived crust (as opposed to older oceanic crust; Fisher and Engel, 1969; Vallier et al., 1985; Bloomer and Fisher, 1987). The presence of arc-derived rocks far from where they probably formed (since there would not be volcanism immediately adjacent to a trench) also supports the theory that the forearc is undergoing subduction erosion (Bloomer and Fisher, 1987; Vallier et al., 1985). Additional evidence for this includes the significant subsidence of the forearc (greater than the expected thermal subsidence) during the breakup of the Melanesian arc (9 Ma) and the opening of the Lau Basin (Clift, 1995), the trenchward tilting of sedimentary beds (as occurs in the central unit of the forearc, described above and shown in Figure 13b) at a relatively constant rate since the Eocene (MacLeod, 1994), and the continued subsidence of the forearc; all of these require the removal of material from the underside of the forearc lithosphere by subduction erosion (Ballance et al., 1989).

The Tonga and Izu-Bonin-Mariana forearcs have had similar histories, but there are some differences in their geology. There is no evidence for widespread serpentine

diapirism in the Tonga forearc, whereas it does occur in the IBM forearc (Bloomer et al., 1995). The Tonga forearc is undergoing subduction erosion (e.g. Lonsdale, 1986; Bloomer and Fisher, 1987), whereas the IBM forearc has probably been undergoing minor accretion since the Oligocene (Taylor, 1992). There is active extension in the Tonga forearc, but not in the IBM forearc. These differences notwithstanding, it has been proposed that the Tonga forearc may be used to test hypotheses about the evolution of intraoceanic convergent margins which were originally derived from studies of the IBM forearc (Bloomer and Wright, 1995).

The only site at which alteration of the Eocene basement has been examined at all is at ODP Site 841 (Figure 1), which was drilled just west of the outer trench-slope break, 48 km inboard of the axis of the Tonga trench, and about 70 km outboard of the eastern edge of the Tonga platform (equivalent to the position of 'Eua further north). Hole 841B was drilled to 834 mbsf in 4810 m of water, penetrating 211 m of igneous basement overlain by 623 m of sediments.

Igneous rocks recovered from Hole 841B consist of low-K rhyolite, rhyolite tuffs, breccias, and welded and unwelded lapilli tuffs. Due to the presence of welding, the lack of interbedded marine sediment or fauna, and the lack of density sorting in pumice breccias, these rocks are interpreted to have originated in a subaerial environment (Hawkins, 1994). Sedimentary and igneous stratigraphy for Hole 841B are shown in Figure 14. This rhyolite complex was hypothesized to be either an Eocene sequence or a rifted fragment of Cretaceous crust similar to the Lord Howe Rise (van der Lingen, 1973) which also consists of high-silica tuffs and rhyolite (Parson et al., 1992), and was

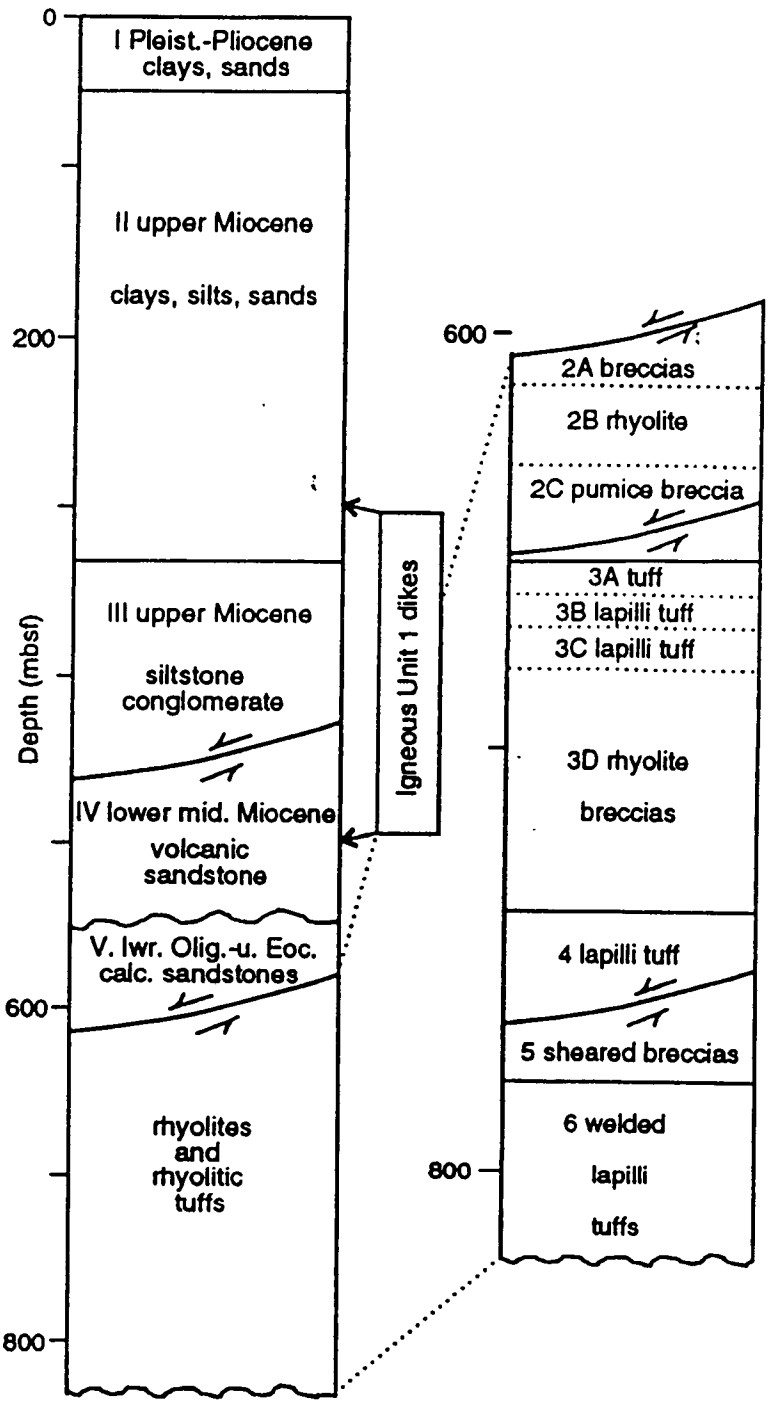

Figure 14. Sedimentary and igneous stratigraphy for Hole 841B. Bloomer et al. (1994).

dispersed during the original breakup of the southwest Pacific (Burns et al., 1973). Rhyolite from Hole 841B has been dated at 44±2 Ma (Eocene) (McDougall, 1994), illite dates from the rhyolite tuffs cluster in the Eocene (Schöps, 1993), and trace element signatures at Hole 841B differ from those at the Lord Howe Rise (Bloomer et al., 1994). Thus, the first hypothesis seems more probable.

Sedimentary rocks in Hole 841B include 55 m of Eocene and lower Oligocene calcareous volcanic sandstones whose basal age is 41.3 Ma (Parson et al., 1992) faulted over the igneous basement by a north-northeast striking, east-dipping (10-30°) normal fault (MacLeod, 1994). Photic zone fauna indicate that these units were deposited in shallow water, which is consistent with the subaerial nature of the basement rhyolite. Since the Eocene, the basement must have subsided more than 5000 m. Eocene-Oligocene sediments are overlain by 91 m of middle Miocene turbiditic sandstones and siltstones which are unconformably overlain by 125 m of upper Miocene siltstones, sandstones, and volcanic conglomerates, and 277 m of upper Miocene vitric siltstones and sandstones. Several plagioclase-orthopyroxene-clinopyroxene-phyric basalt dikes and sills intrude this Miocene section. Their chemistry suggests derivation (via larger feeder dikes) from the active arc, even though Site 841 would have been 70-100 km away during the Miocene (Bloomer et al., 1994). All of this is overlain by 56 m of Pleistocene-Pliocene clays, sands, and ashes. Numerous normal microfaults and a few small reverse faults cut the section (MacLeod, 1994). Two larger normal faults also cut the section, the first being that which separates the igneous basement from the sediments, and the second

at 449-458 mbsf, dipping at 60°, possibly having accommodated more than 1 km of movement (MacLeod, 1994).

Sedimentary materials deposited in the Tonga forearc are predominantly volcaniclastic debris from the current active arc (presently the Tofua arc). Lesser quantities of sediment may come from erosion of older forearc sediment or igneous basement, or collision with subducting seamounts such as the Louisville Ridge (Cawood, 1994). Sedimentation processes in the Tonga forearc are principally controlled by the structural development of the arc and forearc, which is strongly related to its collision with seamounts (Capricorn Guyot and the Louisville Ridge). The usual processes of tectonic erosion, subsidence, and accumulation of volcaniclastic material, and the typical extensional stress regimes which dominate forearc history for long time periods are interrupted by these collisional events, which cause local compression and uplift in the outer forearc. This leads to the development of major angular unconformities within sedimentary basins on the midslope, to downcutting by canyons along the trenchward edge of the Tonga platform, to steepening of the trench slope, and to development or reactivation of across-arc faults which are then exploited as canyons by mobilized sediments (Clift et al., 1998). Thus sedimentary material that would normally accumulate in midslope basins is carried deeper into the trench. After seamount collision, the trench slope eventually becomes more gradual again, as evidenced by the changes in trench morphology progressively northward from the current Louisville Ridge collision zone (Clift et al., 1998).

The sedimentary successions at ODP Site 840 (Figure 1), which did not penetrate the igneous basement, and at ODP Site 841 (Figure 1) record the subsidence and sedimentation history of the forearc. At Site 841, three major depositional episodes are represented (Clift et al., 1994). The first occurred at 37 Ma, contemporaneous with rifting in the South Fiji basin. At approximately this time (recorded at 605 mbsf in the Hole 841B drillcore), sedimentation rate is estimated to have been 160 mm/k.y. (Parson et al., 1992). A second sedimentation episode occurred before 16 Ma. The third episode occurred at 10 Ma. Around this time (recorded at 449-458 mbsf in the Hole 841B drillcore), sedimentation rate is estimated to have been 142 mm/k.y. (Parson et al., 1992). High energy mass flow sedimentation in the Site 841 region began at approximately 16 Ma. At Site 840, a decrease in volcanic activity (indicated by a decrease in the volume of volcaniclastic debris) occurred after rifting of the Lau basin (at 3.25 Ma) (Clift et al., 1998). Thus, major tectonic events may have a large influence on the rate and distribution of sedimentation in the forearc. Since the study of dredge samples does not provide precise knowledge of where they originated, however, it may be difficult to relate sedimentation rates and volumes with their effects on alteration of igneous rocks.

2.2 Hydrothermal alteration at Site 841

Few studies of hydrothermal alteration of Tonga forearc rocks have been conducted. The most detailed study was conducted by Schöps and Herzig (1994a) on altered felsic rocks from Site 841.

The Miocene basaltic dikes and sills at Site 841 have been altered at low temperature. Groundmass is typically 5-50% replaced by clays, chlorite, and zeolites, and there are commonly veins of quartz, carbonate, K-feldspar, and thaumasite +/- sulphides (Bloomer et al., 1994). Thaumasite, $[Ca_3Si(OH)_6\ H_2O](SO_4)(CO_3)$, is likely indicative of low temperature (<60°C) alteration by seawater-derived fluids rich in $CaCl_2$, nearly identical to those currently circulating on the seafloor (Schöps and Herzig, 1994b). The Eocene felsic volcanic rocks in the lower part of Hole 841B have also all been subjected to some degree of hydrothermal alteration (Schöps and Herzig, 1994a). The distribution and relative abundances of alteration minerals vary with depth (Figure 15). Quartz and plagioclase are the major constituents of most altered rocks, except for the upper 5 m of the section, where feldspar is totally altered to illite and chlorite. Secondary minerals include kaolinite, vermiculite, chlorite, calcite, albite, and quartz. Disseminated pyrite is abundant and may be up to 10% of the rock. It may occur as fine (<0.2 mm) veins in fresher samples. Rare amphibole may be replaced by rutile (common in the alteration of felsic rocks). Local veins of quartz and Mn-calcite may contain marcasite. In the upper section, secondary Fe-hydroxides (hematite) are common.

The upper part of the Site 841 volcanic section shows the greatest elemental gains and losses during alteration (Schöps and Herzig, 1994a). The upper 70 m are strongly depleted in SiO_2, slightly depleted in Na_2O, and enriched in Al_2O_3, Fe_2O_3, MgO, and K_2O. Deeper rocks are richer in SiO_2, slightly depleted in K_2O, and Fe and Mg appear not to be significantly affected by alteration. CaO varies, reflecting some degree of

Core, section	Depth (mbsf)	Quartz	Feldspar	Kaolinite	Illite	Vermiculite	Chlorite	Calcite	Pyrite
135-841B-									
47R-2[a]	605.34	+++++	—	+++++	+	—	+++	—	+
47R-2[b]	605.34	+++++	—	+	+	—	+	—	+
47R-CC	607.18	+++++	—	+	+	—	+	—	+++
51R-3	644.41	+++	++++	—	—	+	—	+	—
52R-2	652.84	+++	+++	+++	—	+	—	+	+
53R-2	662.79	+++++	+++++	+++	—	+	+	+	+
54R-1	670.88	+++++	+++++	+	—	+	—	+	+
55R-1, 9 cm	679.89	+++++	+++++	+	—	—	—	—	+
55R-1, 17 cm	679.97	+++++	+++++	+	—	—	—	+	+
57R-1	699.14	+++++	+++++	++++	—	—	—	+	—
57R-CC	700.68	+++++	+++++	+++	—	—	—	+++	+
58R-1	709.14	++++	++++	+	—	—	—	+	+
59R-1	718.11	+++++	+++++	+	—	—	—	—	+
60R-1	727.86	+++++	+++++	+	—	—	—	+	+
61R-1	737.54	+++++	+++++	+	—	—	—	+	+
62R-CC	750.28	+++++	+++++	+	—	—	—	+	+
64R-CC	766.50	+++++	+++++	+	—	—	—	—	+
70R-CC	824.60	++++	++++	—	—	—	++++	+	+

Notes: Dash (—) = not detectable, + = rare, ++ = few, +++ = common, ++++ = abundant, and +++++ = major component.

[a]Hematitic.

[b]Silicified.

Figure 15. Distribution and relative abundances of mineral phases detected by XRD in felsic rocks of Hole 841B. Schöps and Herzig (1994).

mobilization during alteration. Mn varies, but is highest in the most altered samples (greatest Loss-On-Ignition [LOI]) (Schöps and Herzig, 1994a).

Sulphur isotope values in Site 841 pyrite are greater than those observed in mid-oceanic ridge sulphides, and are similar to those of Kuroko massive sulphides, Ryukyu island arc volcanic rocks, and Okinawa Trough massive sulphides. This is probably due to an arc sulphur component mixed with seawater (Schöps and Herzig, 1994a). The most intense alteration occurred closest to faults, under oxidizing conditions, and the fluid involved in this was probably modified seawater. Distant from faults and deeper in the volcanic pile, lower oxygen and sulphur fugacity indicate reducing conditions. Additionally, the occurrence of clinochlore (Mg-rich chlorite) and hematite high in the section requires an oxidizing environment, while the formation of pycnochlorite (Fe-rich chlorite) lower in the section requires a more reducing environment. Water:rock ratios appear to have decreased with depth, based on the decreased mobilization of many elements, and on the change from Mg-rich chlorite (clinochlore) to Fe-rich chlorite (pycnochlorite), whose formation would require more evolved fluids. Temperatures for chlorite formation (265-290°C) are consistent with minimum temperatures of fluid inclusions in secondary quartz, giving a range of 270-297°C. Lower temperature, late-stage minerals (e.g. illite at the top of the volcanic series, formed at <<200°C) are also present. The higher temperatures suggest a zone of localized hydrothermal upflow (a discharge zone), since cold seawater alteration would not produce these mineral assemblages. The fluid chemistry implied by the mineralization indicates that the alteration fluids were derived from seawater, rather than from the subducting slab

(MacLeod, 1994; Schöps and Herzig, 1994a). Schöps and Herzig (1994a) described four successive alteration stages. First, there was recrystallization of amphibole to rutile and biotite to vermiculite, and formation of symplectitic quartz-feldspar intergrowths. Then, there was mobilization, transport and redeposition of silica, and Mg fixation in chlorite at ~30°C. This was followed by the formation of pyrite and marcasite in quartz-calcite veins at ~250°C, and finally, by late fixation of K (by illite formation) and formation of kaolinite, at temperatures much less than 200°C.

2.3 Description of dredge locations and procedures

Samples were collected by dredging during the May-June 1996 Boomerang Leg 8 cruise on the Scripps Institute of Oceanography R/V Melville. Cruise objectives were to test hypotheses about the origin and structure of the Tonga forearc, and to perform detailed site surveys of potential future drilling sites (swath bathymetry, gravity, magnetics, seismics, sidescan sonar). The dredge sites represent a number of transects of the forearc, each comprising two or more dredge sites. Locations and the proportions of various rock types collected are shown in Figure 2.

This study of hydrothermal alteration focuses on a dredge transect across the central forearc (approximately 22°S, Figure 16) associated with potential drilling site TONG 02A. The site was selected for the purpose of constraining Tofua Arc volcanic history, subsidence history of the southern part of the outer forearc, and the age, chemistry, and structure of volcanic basement on the outer side of the platform (Tappin et al., 1998). Precise dredge sites were selected based on their likelihood of yielding

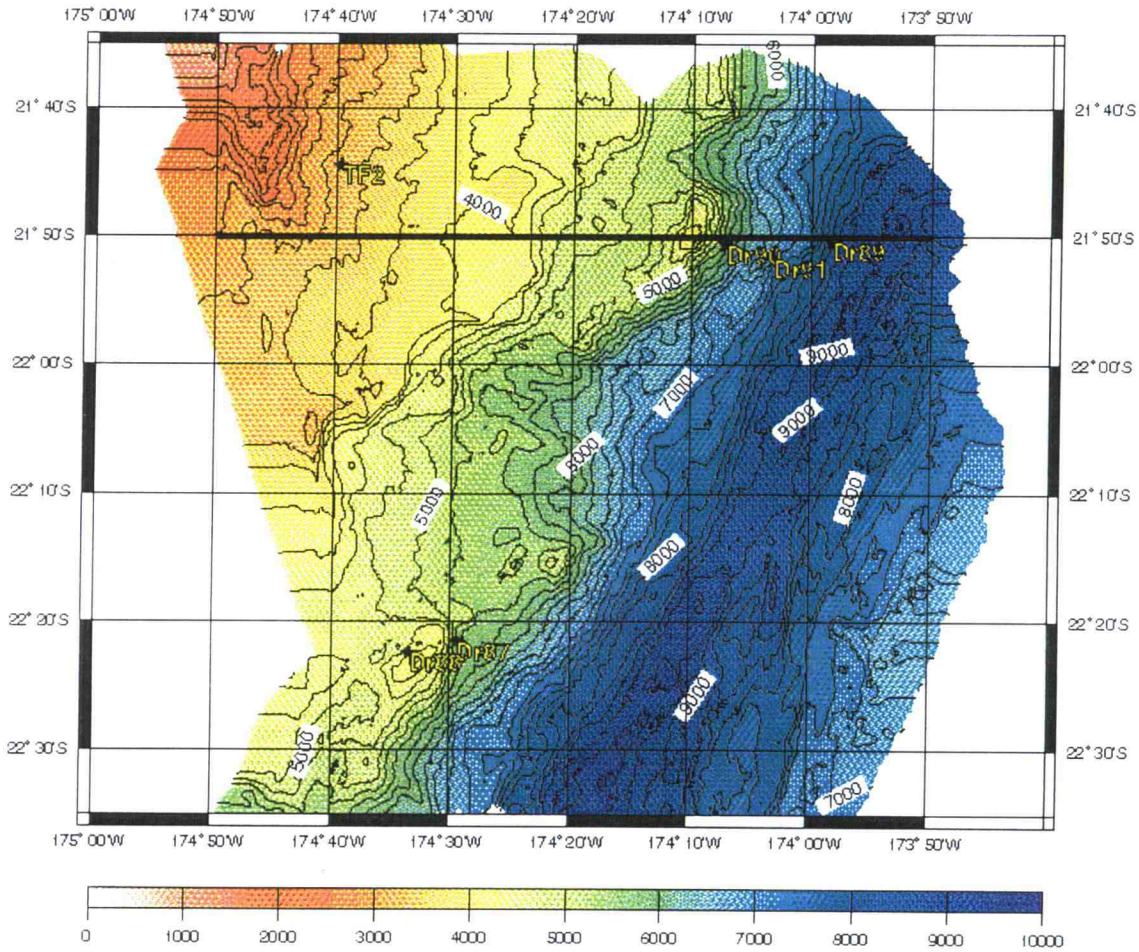

Figure 16. Detail map of the central Tonga forearc showing locations of dredges 87-91.

dredgeable igneous rock fragments. D87, D88, and D90 were located on the upper landward slope. D87 yielded pillow volcanic rocks and diabases. D88 yielded altered pillow volcanic rocks and volcaniclastic sediments. D90 yielded volcanic fragments, hyaloclastite breccias, gabbros, diorites, and assorted sediments. D91 was located on the middle landward slope, and yielded breccias, siltstones, volcanic fragments, and one ultramafic sample. D89 was located on the lower landward slope, and yielded volcaniclastic sediments and minor serpentinite and volcanic samples.

2.4 Igneous lithologies

2.4.1 Introduction

Primary lithologies of volcanic rocks collected during Boomerang Leg 8 include tholeiites, arc tholeiites, boninites, rhyolites, and tholeiite-derived rhyolites. The transect on which this study focuses includes only tholeiites, arc tholeiites, and boninites. Samples were assigned to compositional groups based on differences in Ti, Zr, and Mg; all other elements were considered suspect due to the altered nature of the rocks (Falloon, personal communication).

2.4.2 Tholeiites

Tholeiites are typically light gray to brown gray, very fine-grained, and aphyric to sparsely (<3%) plagioclase and clinopyroxene phyric. Phenocrysts are usually less than

0.5 mm. Primary porosity (equivalent to vesicularity) is 0-1%. Hand samples have a relatively fresh appearance.

Tholeiites appear in two dredges from transect 87-91, D89 (2 samples) and D90 (3 samples). They contain >0.9 weight % TiO_2, 6-9 weight % MgO, and >55 ppm Zr. These characteristics distinguish them clearly from arc tholeiites and boninites on plots of TiO_2 versus Zr (Figure 17) and TiO_2 versus MgO (Figure 18). Tholeiites from all Boomerang Leg 8 dredges may be further subdivided into four groups based on variations in Ti, Zr, and Nb (Falloon, personal communication). However, only two of these subgroups appear in transect 87-91, and Nb was not analyzed when examining alteration, so these subdivisions will not be considered further for the purposes of this thesis. Tholeiites analyzed from transect 87-91 define a fractionation trend in Ti-Zr space (Figure 17).

2.4.3 Arc Tholeiites

Arc tholeiites are typically brown to gray, fine to very fine-grained, and sparsely to abundantly phyric (Figure 19). Phenocrysts commonly include up to 20% euhedral zoned plagioclase (<0.5-3 mm), 2-10% euhedral clinopyroxene (0.1-1 mm), up to 3% euhedral olivine (<1-2 mm), up to 5% anhedral to subhedral opaque oxides, and rare spinel. Plagioclase and clinopyroxene are commonly glomeroporphyritic. Glass and spherulites (<0.5 mm across) are abundant in many samples. One sample (89-3-6, Figure 20) differs petrographically from the others in that it contains two distinct groups of plagioclase, one group having a sievelike texture and many glass inclusions, the second group inclusionless and distinctly polysynthetically twinned. These two groups may

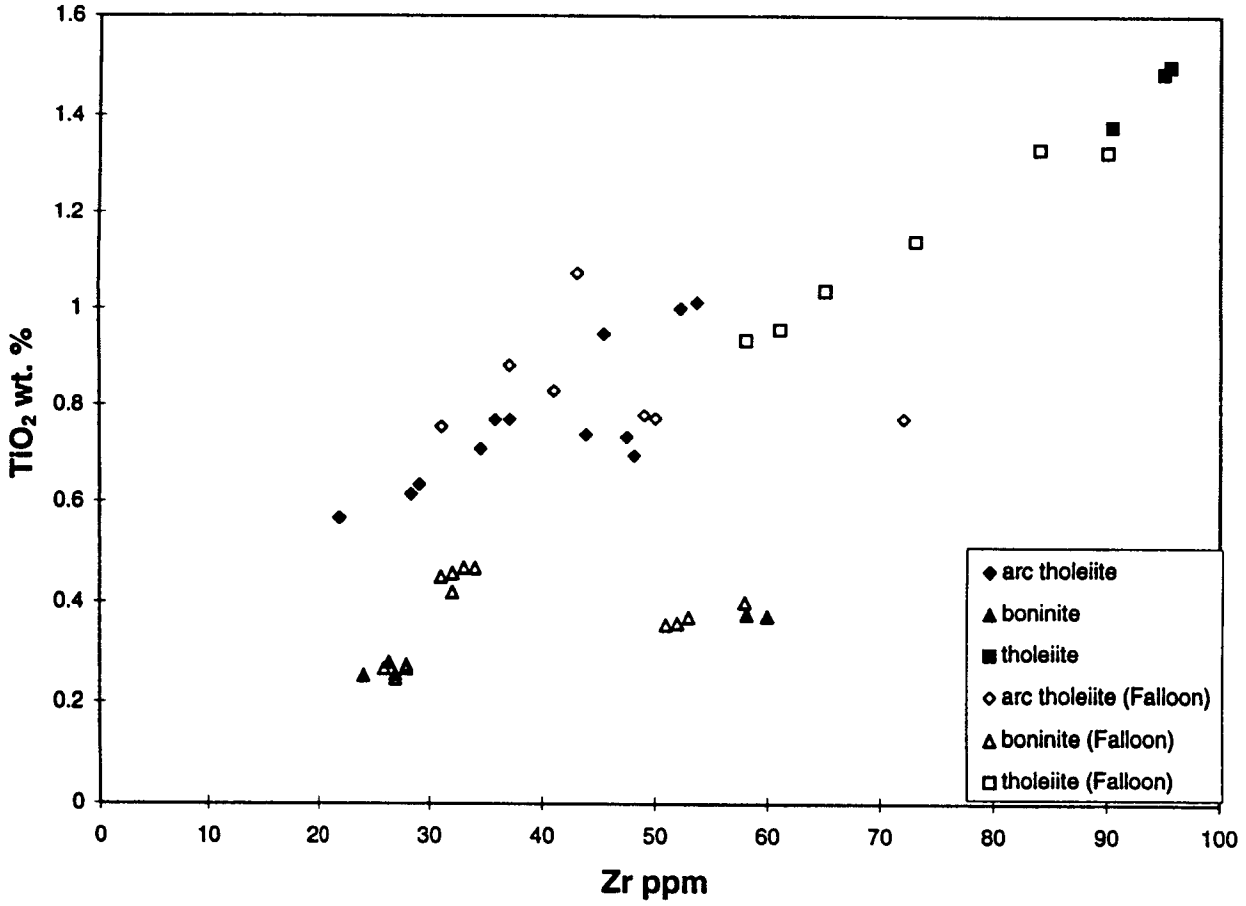

Figure 17. TiO_2 versus Zr content for arc tholeiite, tholeiite, and boninite samples from transect 87-91. Open symbols represent data from Falloon, which includes samples from dredges 88-91 (unpublished data).

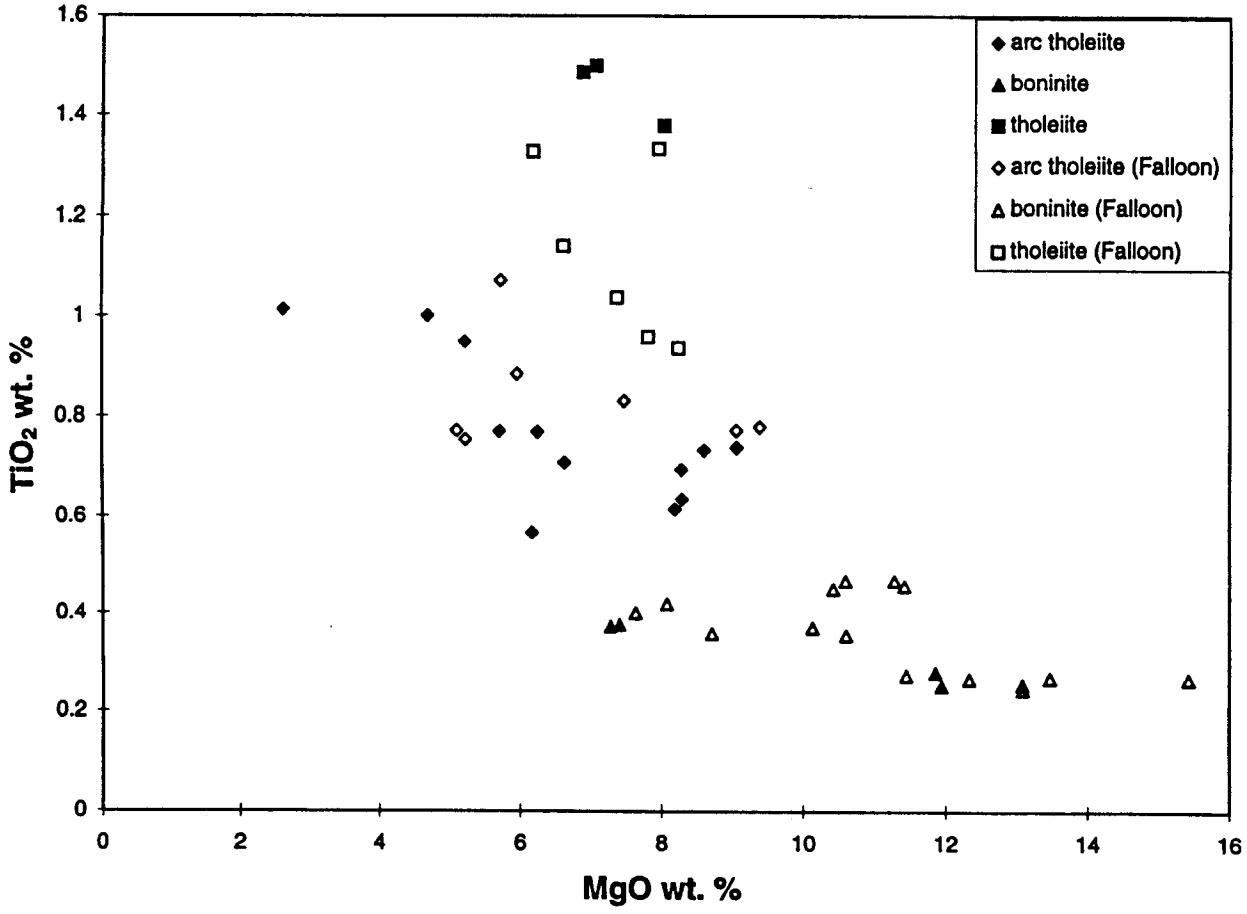

Figure 18. TiO_2 versus MgO content for arc tholeiite, tholeiite, and boninite samples from transect 87-91. Open symbols represent data from Falloon, which includes samples from dredges 88-91 (unpublished data).

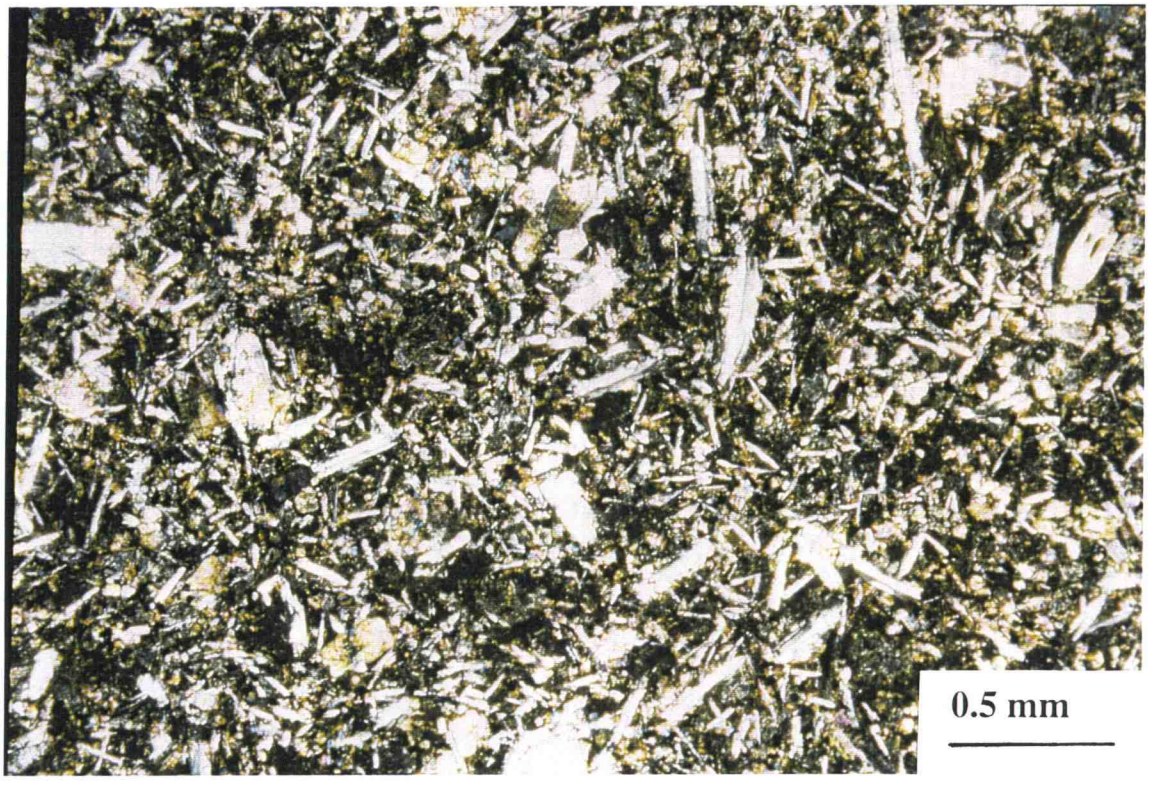

Figure 19. Sample 91-3-4, a typical arc tholeiite. Crossed polars.

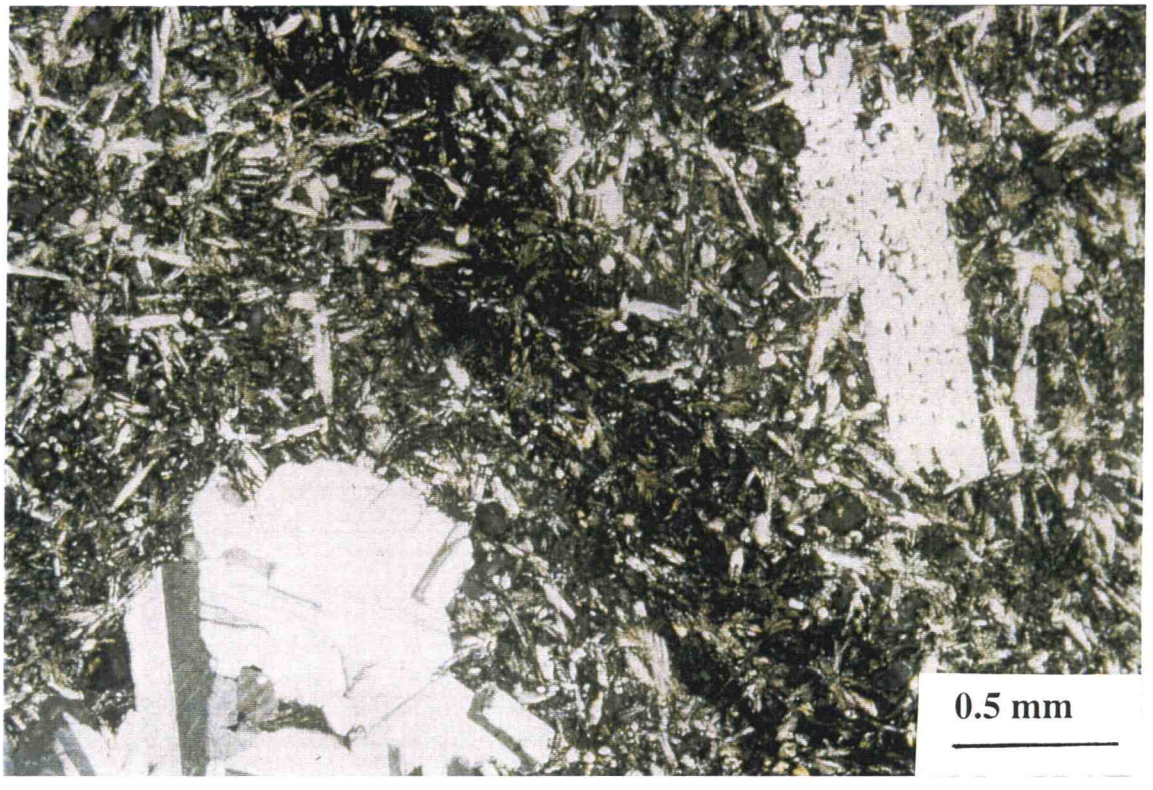

Figure 20. Sample 89-3-6, an arc tholeiite, showing the two groups of plagioclase therein. The dark line across the center of the slide is an ink line used for reference. Crossed polars.

indicate a mixing of two separate magmas. 'Eua arc tholeiites are petrographically distinct from other arc tholeiites (Figure 21). They contain slightly greater proportions of oxides, may have oxide segregations, and may include sedimentary fragments that appear to have been incorporated into the lavas and then thermally metamorphosed. Primary porosity in all the arc tholeiites varies from 0-5%, usually <2%. Hand samples show varying degrees of freshness.

All dredges analyzed from transect 87-91 contained arc tholeiites: D87 (5 samples), D88 (1 sample), D89 (2 samples), D90 (4 samples), and D91 (2 samples). Arc tholeiites contain TiO_2=0.5-1.1 weight percent, MgO=4-10 weight percent, and Zr=20-55 ppm (Figure 17, Figure 18). The two 'Eua samples analyzed were arc tholeiites.

2.4.4 Boninites

Boninites are light to dark gray or green-gray, fine to very fine-grained, and aphyric to abundantly phyric (Figure 22). Phenocrysts commonly include up to 15% euhedral olivine (1-4 mm), up to 15% euhedral to subhedral zoned orthopyroxene (1-4 mm), and rarely, zoned plagioclase (<1 mm). Orthopyroxene and olivine may form glomeroporphyrocrysts up to 1.5 mm across. Glass (± spherulites up to 0.5 mm) is common. Sample 88-1-31 (the boninite fractionate) is similar petrographically to boninites. Primary porosity is 0-3%. Samples show varying degrees of freshness. Hand samples commonly have a very weathered appearance.

Boninites were found only in D88 (16 samples) from this transect. Boninites contain <0.5 weight % TiO_2, >7 weight % MgO, and 20-65 ppm Zr (Figure 17, Figure

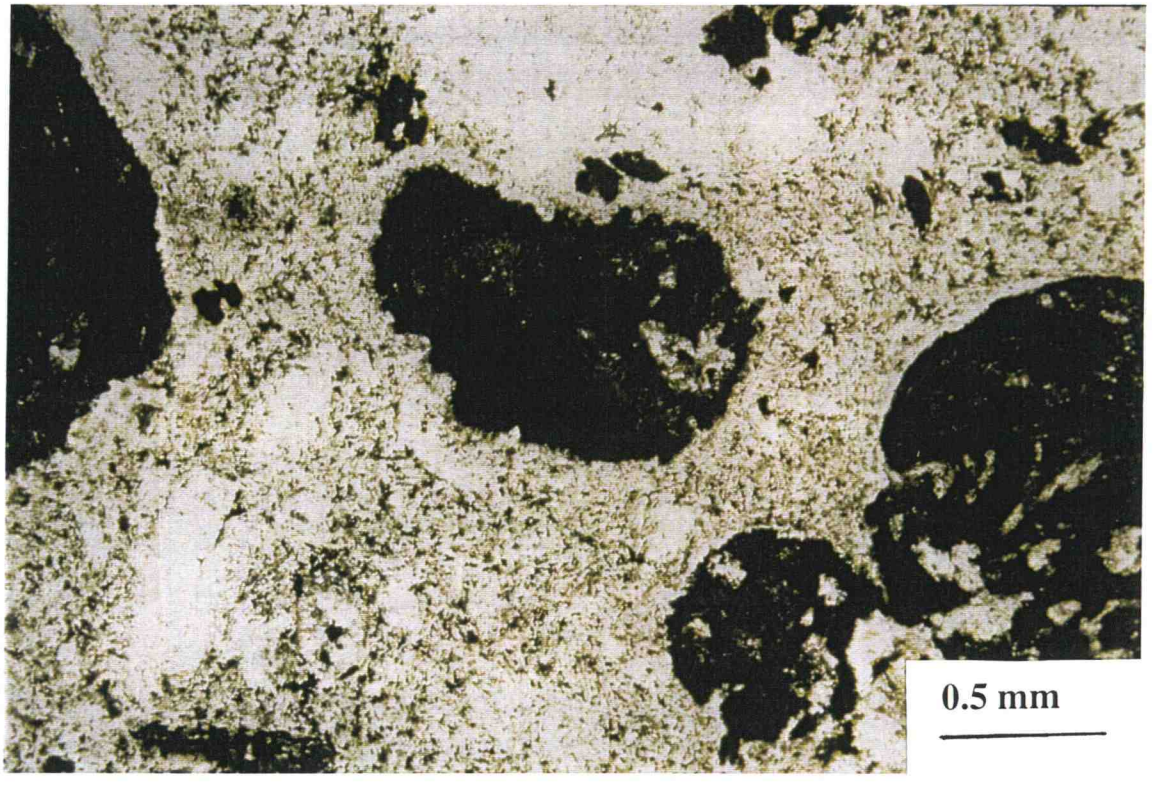

Figure 21. 'Eua sample, E96-1-2, an arc tholeiite. Black clumps are segregations of opaque oxides, which appear in several 'Eua samples. Uncrossed polars.

Figure 22. Sample 88-1-9, a typical boninite. Crossed polars.

18). Boninites from the entire forearc may be further subdivided into five groups based on Zr and Ti content (Falloon, personal communication). Three of these groups are represented in this transect (Figure 23). One sample (88-1-31), not considered to be a boninite, is probably a boninite fractionate (Bloomer, personal communication) (Figure 23).

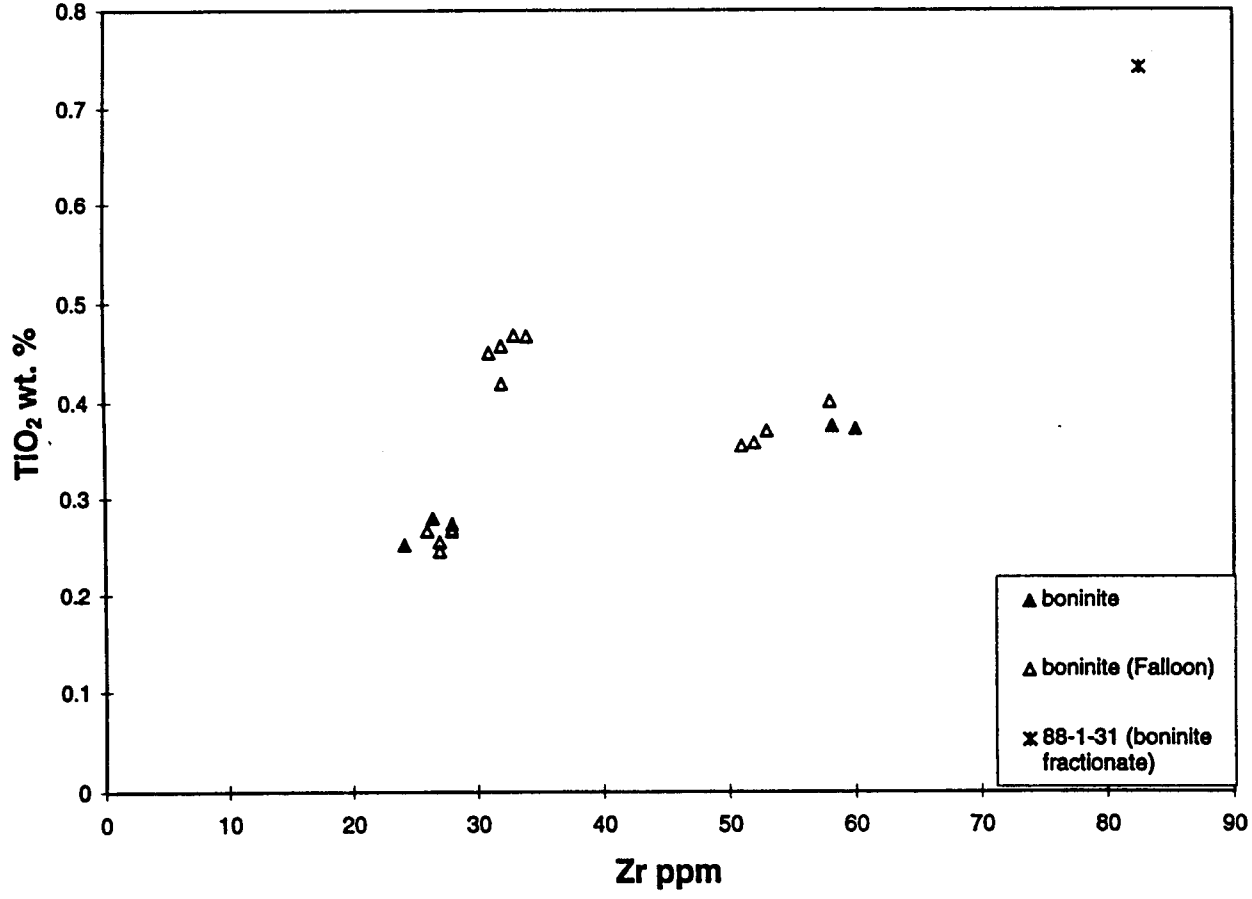

Figure 23. TiO_2 versus Zr content for boninites, showing the three boninite groups occurring in dredge 88. Sample 88-1-31, hypothesized to be a product of boninite fractionation, is also shown. Open symbols represent data from Falloon, which includes samples from dredges 88-91 (unpublished data).

Chapter 3. Alteration Mineralogy and Mineral Chemistry

3.1 Introduction

Hand samples and thin sections of volcanic rocks from the five dredges in transect 87-91 were examined. Selection of samples for thin sections and geochemical analyses was influenced by the availability of samples, since some dredges contained more volcanic material and larger fragments than others. As many samples as possible were selected for thin sections in order to obtain a general picture of the nature and extent of alteration within and between dredges. Forty-two volcanic samples from transect 87-91 and 11 from 'Eua were examined in thin section. This was supplemented by the examination (for comparison) of 10 volcanic samples from outside the transect, and 10 altered plutonic or ultramafic samples. After petrographic study, 16 thin sections containing abundant alteration phases (in veins/vesicles, or after groundmass/phenocrysts) were polished for analysis using the electron microprobe. Microprobe analyses were complicated by the difficulty in obtaining a high-quality polish on altered portions of rocks; in many cases, soft vein and vesicle-filling materials were plucked out during polishing. General details on electron microprobe procedures are given in Appendix I. Specific details relevant to the analysis of various phases (e.g. clays) are given in the sections of this chapter in which those phases are discussed. X-ray diffraction (XRD) analyses were performed on 14 unoriented bulk powder mounts, 13 oriented mounts of <2 μm clay separates, and 13 glycolated mounts of <2 μm clay separates. Sample selection was influenced by the distribution of altered volcanic rocks

between dredges; for some samples, alteration was so slight that the <2 μm clay fraction was too small to make an oriented mount. Thus, XRD analyses are restricted to samples from D87, D88, and D90, and one sample (from D84) outside transect 87-91. Details on XRD sample preparation and procedures are given in Appendix I.

There are three general types of alteration in transect 87-91. High temperature alteration (>200°C) occurs only in one sample (88-1-7), although samples of similar alteration from dredges 83, 84, and 85 were also studied for comparison. Low temperature alteration (<200°C, commonly <100°C) occurs in samples from all five dredges, and in all three rock types (boninites, tholeiites, and arc tholeiites). Seafloor weathering is a type of low temperature alteration characterized by red staining, particularly of the groundmass. The term "weathering" is used to indicate interaction with relatively unmodified seawater and should not be confused with "weathering" as a subaerial phenomenon. It may occur together with low temperature alteration in the same sample. It occurs in all three rock types but is less extensive in boninites (which are generally the least altered of the three rock types), although a few boninite samples display significant surface staining.

Seafloor weathering (Figure 24) is characterized by a red-brown staining that is pervasive throughout the affected portion of the rock, although the affected portions of a sample may only be patches or vein haloes. Affected portions of samples are commonly 40-80% replaced by secondary phases. Groundmass may also be replaced by smectite and Fe-oxyhydroxides. All olivine is totally replaced by Fe-oxyhydroxides. Plagioclase and pyroxene may be slightly to moderately altered to smectite and may be stained red or red-

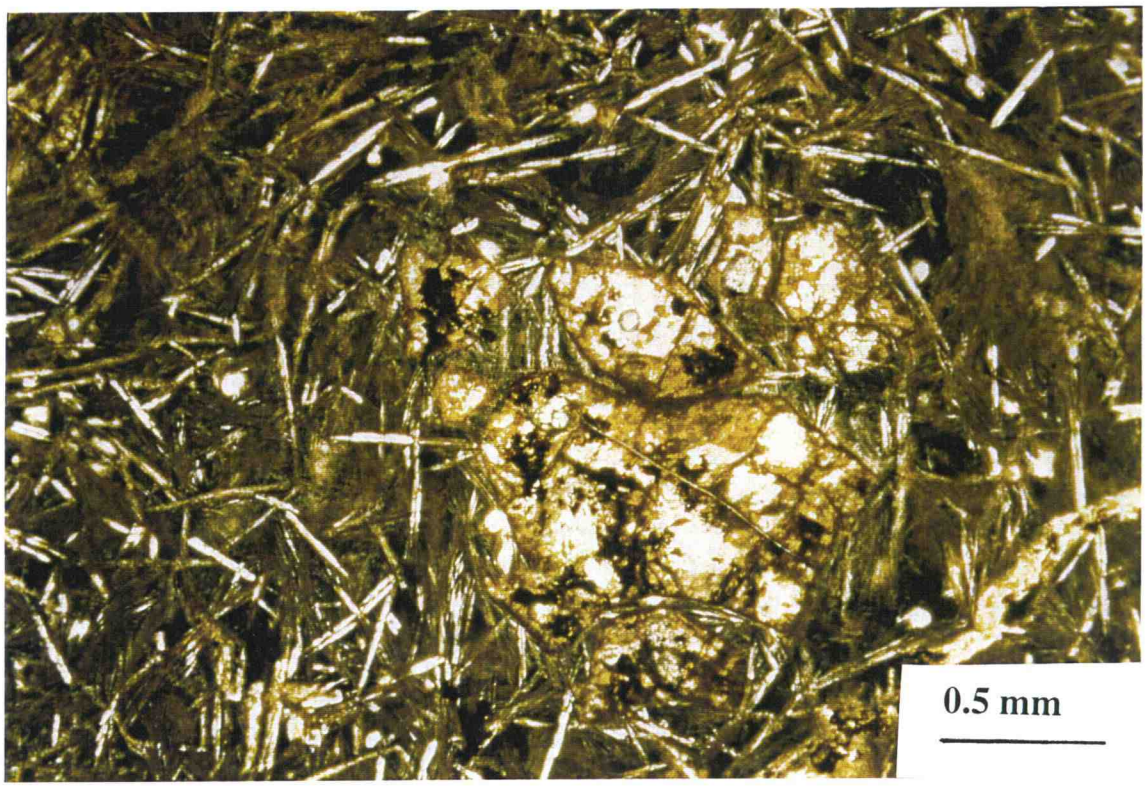

Figure 24. Sample 87-3-3, an arc tholeiite, showing typical seafloor weathering. Uncrossed polars.

brown. There are commonly smectite and Fe-oxyhydroxide veins (<1-2 mm), and the adjacent phenocrysts and groundmass may be stained red-brown. This weathering may accompany the low temperature alteration, but does not occur in all samples altered at low temperature. Petrography indicates that seafloor weathering generally preceded the low temperature alteration (in cases where the two appear together). Brecciated rocks tend to be more pervasively weathered.

In low temperature alteration, there is typically 0-50% replacement by secondary phases; a few samples are even more extensively altered. Olivine is partially to totally replaced by goethite ± calcite (Figure 25), or (less commonly) by smectite. Plagioclase phenocrysts are partially replaced by K-feldspar or are slightly to partially replaced by smectite ± celadonite. Clinopyroxene phenocrysts are commonly fresh but may be slightly to partially replaced by smectite. Orthopyroxene (only occurring in boninites) is either fresh or slightly replaced by smectite. Groundmass plagioclase and pyroxene may be fresh to moderately altered to smectite, depending on the extent of alteration of the whole rock. The mesostasis is slightly to extensively altered to smectite ± celadonite. ("Celadonite" is used in this introduction for bright green or blue-green clay minerals, although most of these clays are actually saponite-celadonite mixtures, to be discussed below.) The general sequence of minerals deposited in veins is (e.g. Figure 26) (less common occurrences are in parentheses):

smectite or smectite/chlorite---> (celadonite)---> zeolites---> carbonates---> silica

Figure 25. Sample 88-1-5, a boninite, showing low temperature alteration. Olivine is replaced by goethite, smectite, and calcite. Crossed polars.

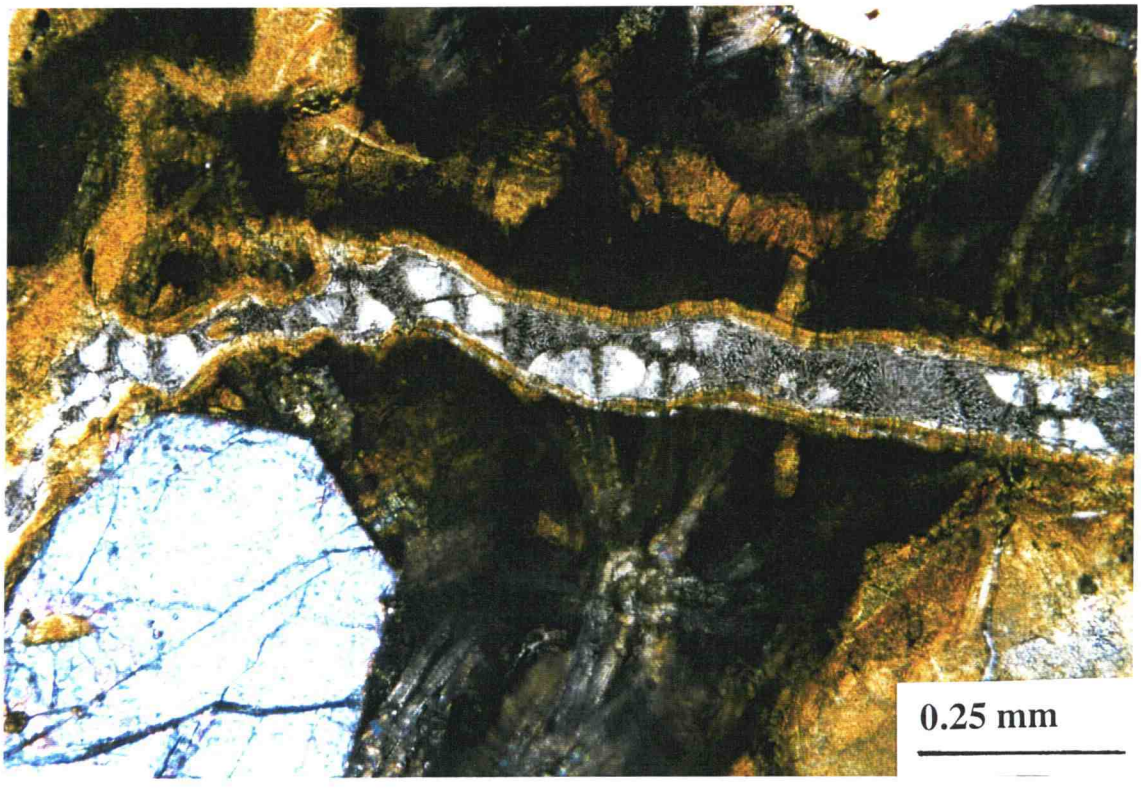

Figure 26. Sample 88-1-1, a boninite, showing low temperature alteration. The vein contains smectite followed by a zeolite, probably phillipsite. Crossed polars.

Not all of these minerals may be present. For example, many veins contain only smectite followed by silica (Figure 27). Rare adularia veins and filled vesicles also occur (they may be followed by silica, although their sequential relationship to other vein minerals is unknown). Silica may occur anywhere in the sequence, but is usually last. Smectite is most commonly first but may occur elsewhere in the sequence. There are commonly several cycles of smectite and silica deposition. Veins range in width up to 2-3 mm, but most are <0.5 mm. On those samples where a glassy rind is present, it is partially to totally altered to assemblages of silica, smectite, K-feldspar, and carbonates ± celadonite, zeolites, chlorite/smectite, and serpentine (Figure 28). Low temperature alteration is distinguished from seafloor weathering by the red-brown staining of seafloor weathering, and the presence of celadonite (or celadonite-saponite mixtures) in low temperature alteration. Where weathering effects are very slight, they may be difficult to distinguish.

High temperature alteration is characterized by the alteration of groundmass to the assemblage chlorite + quartz + epidote + oxides (Figure 29). (Its description here is based on samples 83-3-2, 84-1-3, 85-3-2, and 88-1-7.) The alteration may be patchy or pervasive. Affected portions of the rock are 80-100% replaced by secondary minerals. There are commonly zones of more intense recrystallization, in which epidote crystals may be up to 2 mm in length, surrounded by zones of lesser recrystallization. Plagioclase is partially to completely replaced by epidote, chlorite, and quartz, or may be altered partially to albite. Pyroxene may be partially replaced by fibrous amphibole. In sample 88-1-7 (the only high temperature sample from transect 87-91), there is also partial alteration of some plagioclase to clay and zeolites and rare vein celadonite and smectite

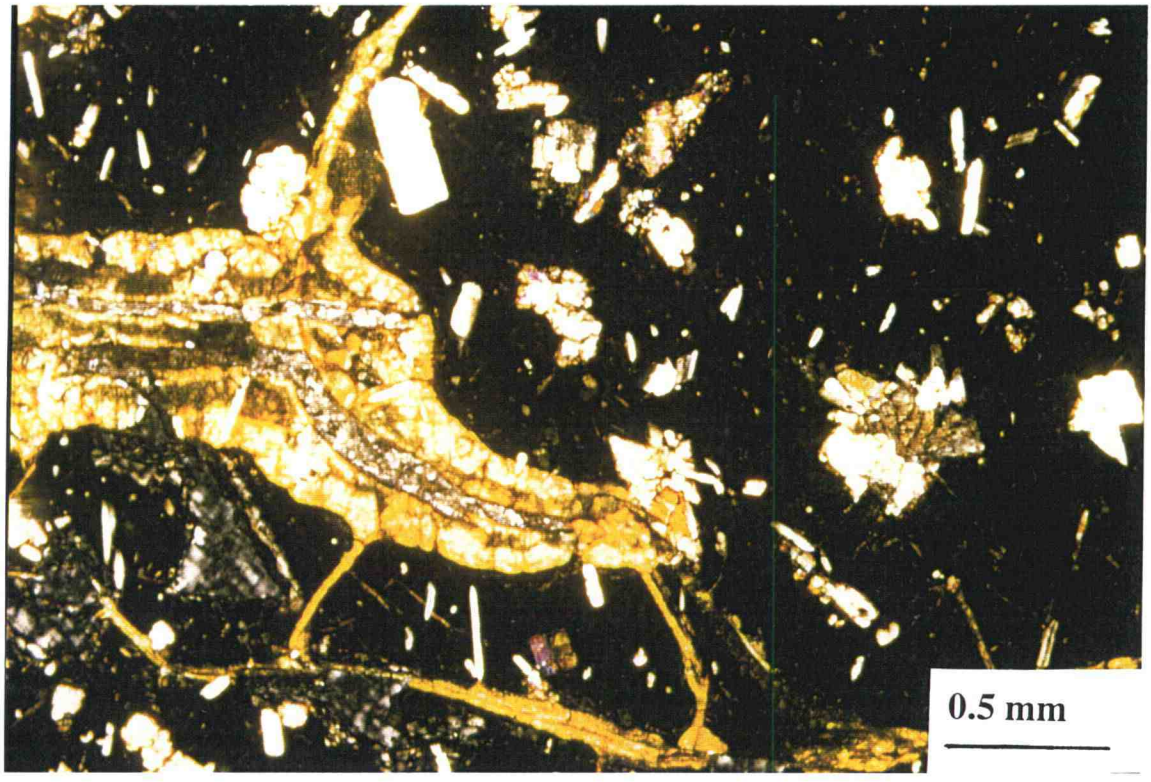

Figure 27. Sample 91-3-5, an arc tholeiite, showing low temperature alteration. The vein contains saponite followed by silica. Crossed polars.

Figure 28. Sample 87-2-1, an arc tholeiite, showing alteration of its glassy rind. Crossed polars.

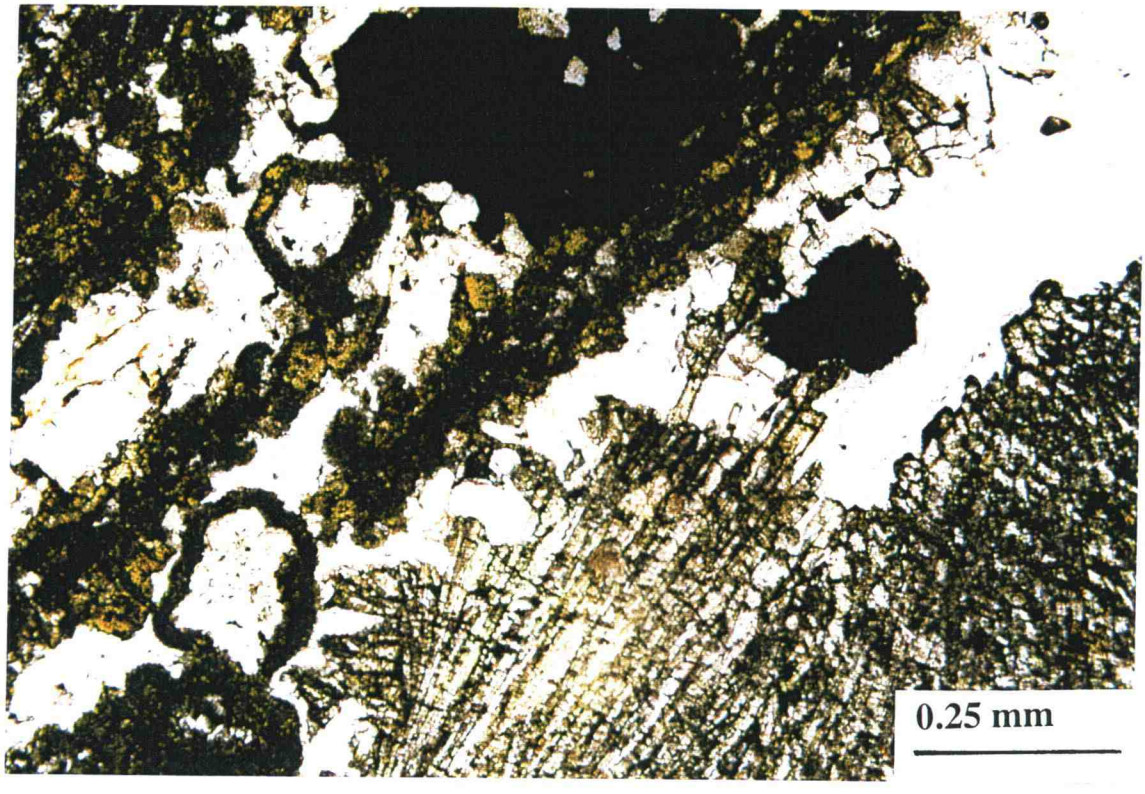

Figure 29. Sample 85-3-2, showing typical high temperature alteration (epidote + chlorite + quartz + oxides). Crossed polars.

(<1% of the rock's volume) (Figure 30). These features indicate low temperature alteration, which may have overprinted the high temperature alteration (which is localized near fractured zones), although petrographic relationships do not make this clear.

The degree of alteration is more variable between rock types than between dredges. Boninites exhibit relatively minor alteration compared to tholeiites and arc tholeiites. However, seafloor weathering (not to be confused with subaerial weathering) appears to be more variable between dredges (dredge 87 contains the most weathered samples).

Dredge 87 consists of brown or red-brown arc tholeiites which are slightly to moderately affected by low temperature alteration. All samples are affected by seafloor weathering to some degree; many are extensively weathered. Mn crusts are uncommon. Primary phases are 40-90% replaced. Samples contain <<1-3% vesicles, which are 80-100% filled.

Dredge 88 consists of gray or yellow-gray boninites (some samples have brown-gray rinds) which are fresh or slightly to moderately affected by low temperature alteration. One sample is affected by high temperature alteration. Seafloor weathering is slight and uncommon. Some samples have Mn crusts. <10-40% of primary phases are replaced. Samples contain <1-3% vesicles, which are 40-80% filled.

Dredge 89 comprises gray tholeiites and arc tholeiites which are slightly to moderately affected by low temperature alteration. Seafloor weathering is slight. Few samples have Mn crusts. Less than 5-20% of primary phases are replaced. Samples contain <1-5% vesicles (commonly <2%), which are 20-90% filled.

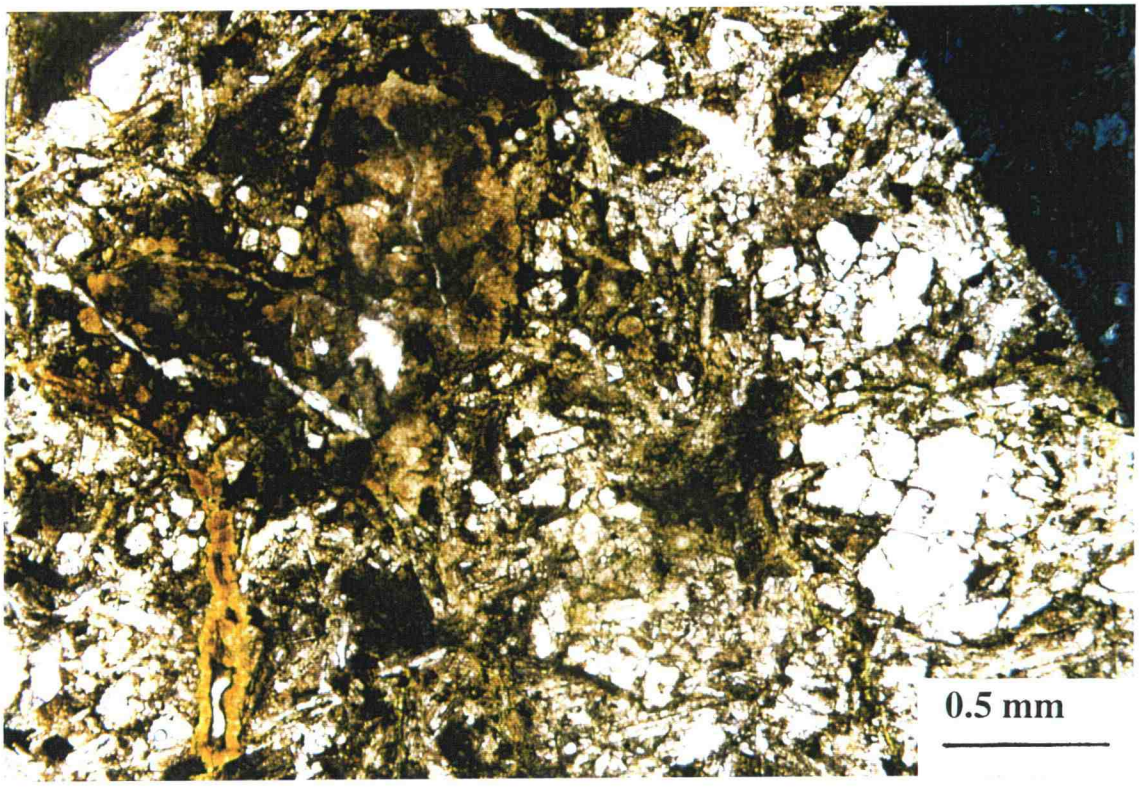

Figure 30. Sample 88-1-7, showing low temperature mineralization (this sample also contains high temperature assemblages [epidote + chlorite + quartz] in patches). The wide yellow vein at the left is smectite. The dark blue line at the right is an ink line drawn for reference. Uncrossed polars.

Dredge 90 consists of gray, yellow-gray, or brown-gray tholeiites and arc tholeiites which are slightly to moderately affected by low temperature alteration. One sample (90-2-31) is totally replaced by secondary minerals (to such an extent that its primary lithology is uncertain), but such pervasive alteration is rare. Samples may be unaffected or slightly to moderately affected by seafloor weathering. There are no Mn crusts. <10-40% of primary phases are replaced. Samples contain <1-3% vesicles, which are 20-100% filled.

Dredge 91 consists of brown-gray or green-gray arc tholeiites which are slightly to moderately affected by low temperature alteration. Seafloor weathering is slight to moderate. Some samples have Mn crusts. <10-30% of primary phases are replaced. Samples contain <3% vesicles, which are 20-100% filled.

'Eua samples (those analyzed geochemically) are gray or dark gray arc tholeiites, most with a rust-colored subaerial weathering concentrated along fractures and exposed surfaces. Seafloor weathering is slight to moderate. Low temperature alteration is slight. There is no evidence for high temperature alteration. Less than 10-40% of primary phases are replaced. Samples contain <2% vesicles, which are 40-100% filled.

3.2 Clay Minerals

3.2.1 Introduction

Minerals were identified as probable clays based on petrography. Analysis of <2 μm clay separates by XRD (details in Appendix I) revealed that the clays were smectites,

based upon peaks in d-spacing spectra at 15.5-16 Å, expandable to 18 Å upon glycolation. Smectites may have either a di- or trioctahedral structure. However, this cannot be distinguished based on XRD spectra, because most analyses were of oriented mounts. Hence, electron microprobe analyses (detailed in Appendix I) of clay phases were used to assign clays to specific compositional and structural groups. The total number of cations in octahedral positions is important for determining whether a clay's structure is di- or trioctahedral. These were determined by recalculating mineral formulas (using weight percent oxides provided by the electron microprobe) based on 22 oxygen (essentially using the procedure in Deer et al. [1992]). The numbers of Al in the tetrahedral positions were calculated by adding all Si and sufficient Al (the tetrahedral Al) to equal 8. Remaining Al was then assigned to the octahedral position. Octahedral totals were calculated by adding Mg + Fe + Ti + octahedral Al cations. If an octahedral total is less than 4.5, the clay is assumed to be dioctahedral. If octahedral total is 5.5-6, the clay is assumed to be trioctahedral. Octahedral totals between 4.5-5.5 are assumed to be mixtures of di- and trioctahedral smectites. For clays with a suspected chlorite component, cations were calculated based on 28 O. Unless otherwise noted in the text, octahedral totals may be assumed to have been calculated based on 22 O. Di- and trioctahedral smectites are further subdivided based on MgO and K_2O content. A trend from ~2-20% MgO (Figure 31) is thus defined, with dioctahedral smectites on the low MgO end, and trioctahedral smectites on the high end. K_2O is used to discriminate between analyses of dioctahedral smectite, and celadonite (a K-rich mica which is fairly common in altered oceanic basalts, but not abundant, except in ophiolites). Clay

octahedral totals and MgO and K_2O contents cover ranges of values, since most clays are mixtures of one or more types. Based on vein and vesicle traverses with the electron microprobe, most clays are compositionally variable on a very small scale.

Since the oxidation state of Fe is not determined in electron microprobe analyses, Fe could be assumed to be all in the 2+ oxidation state, all as 3+, or as a mixture of both. For this thesis, Fe is assumed to be either all Fe^{2+} or Fe^{3+}, depending on what clay type is thought to be predominant for that analysis (further details are given below).

3.2.2 Saponite

Saponite is a trioctahedral smectite $[Si_{7.34}Al_{0.66}Mg_6(1/2Ca, Na)_{0.66}]$ (Deer et al., 1962), with a structure similar to that of talc. Any iron will probably be present as Fe^{2+} (although small amounts of trivalent Fe may also be present in octahedral sites) (Andrews, 1980). For the purposes of this thesis, saponite includes all clay minerals with octahedral totals between 5.5-6 (Figure 31).

Saponite was identified positively by microprobe in several samples. It replaces the groundmass (often appearing to be mixed with Fe-oxyhydroxides, leading to a brown color) as a yellow-brown or green-yellow fine-grained material. In veins and filled vesicles, it is commonly the first clay phase. As a vein phase, saponite appears as a pale yellow, yellow-brown, or yellow-green fibrous mineral, growing perpendicularly inwards from the vein or void walls (Figure 32). Saponite may partially replace olivine (although olivine is principally replaced by Fe-oxyhydroxides). It may form along cracks in plagioclase and pyroxene. Saponite is difficult to distinguish petrographically from other

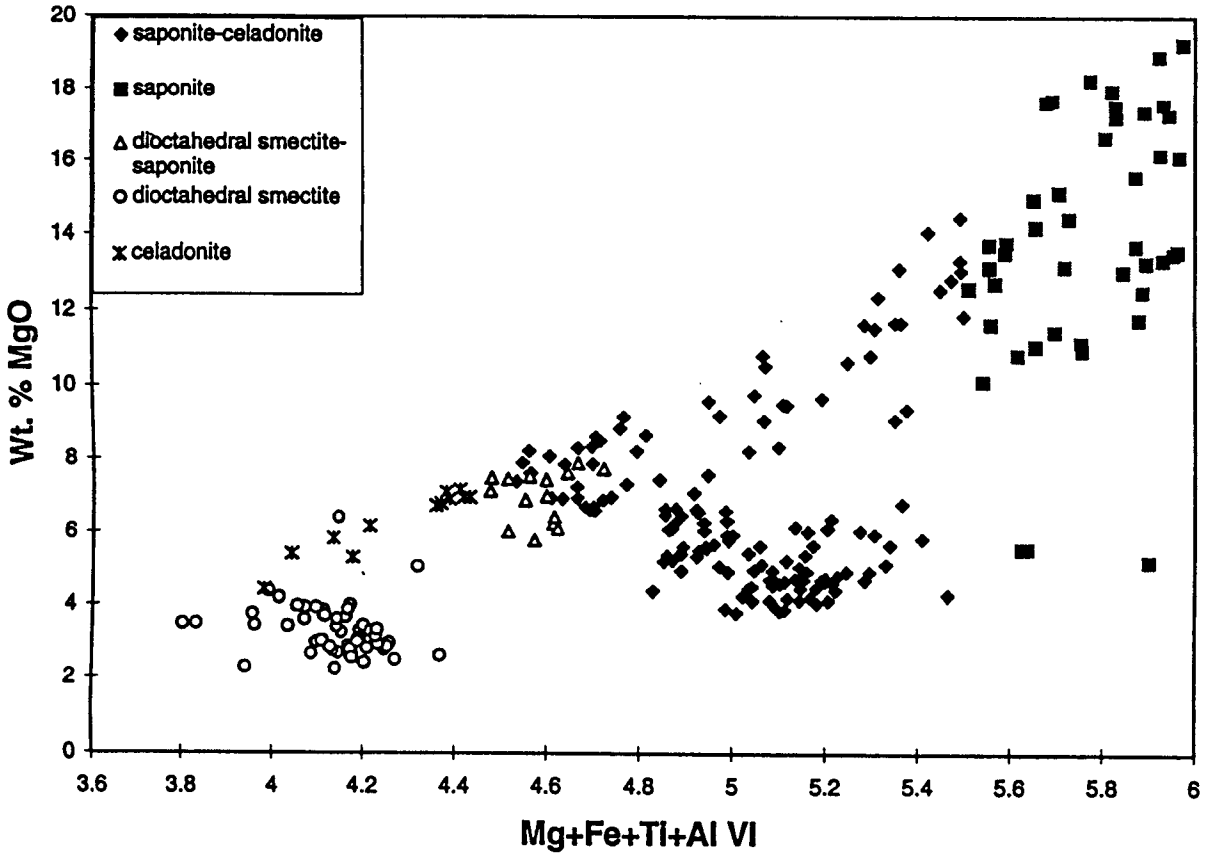

Figure 31. MgO versus octahedral total for Tonga forearc clays (excluding chlorite-smectite and chlorite).

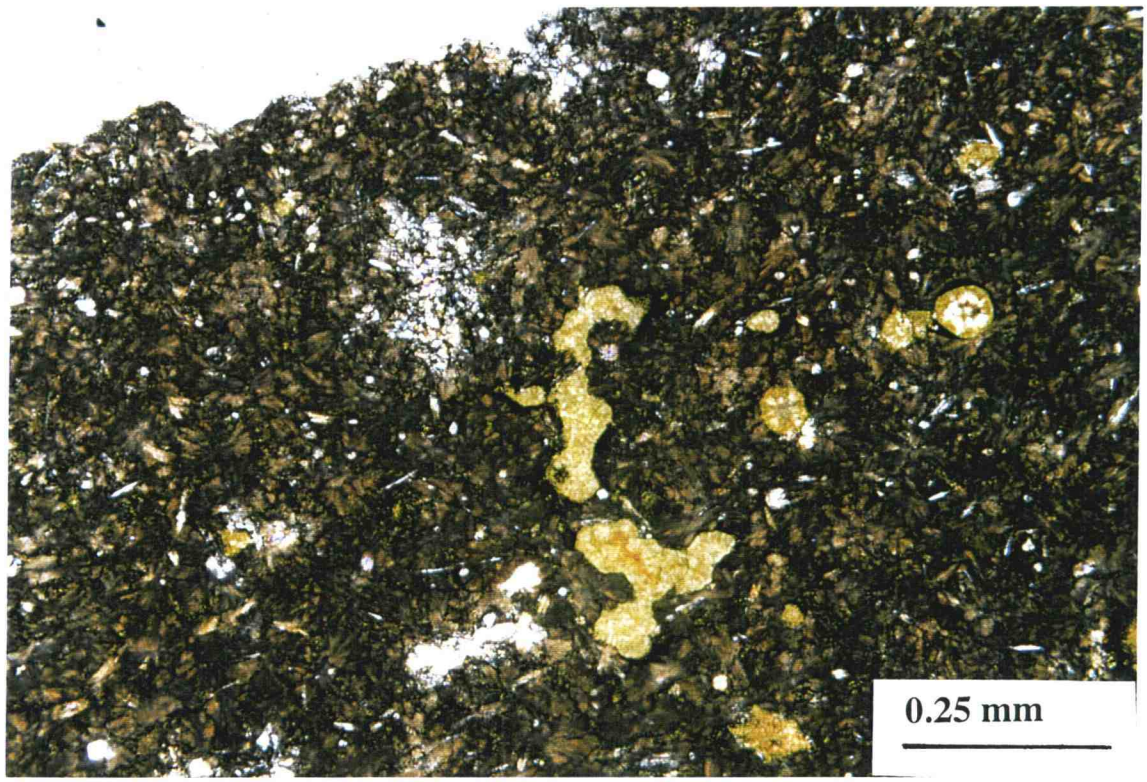

Figure 32. Sample 90-2-16, an arc tholeiite, showing vesicles filled with saponite. Uncrossed polars.

clays, so it cannot be positively identified without microprobe analysis. However, the abundance of similar-looking clays in many samples not analyzed with the microprobe suggests that saponite is a common phase.

Chemically, saponite is not pure end member saponite. While pure saponite should contain only Mg in octahedral positions (Deer et al., 1962), some saponite grains had higher than expected Al contents, indicating that some octahedral positions are occupied by Al; these are similar to high-Al saponites analyzed from the Troodos Ophiolite (Figure 33). Representative IBM and Site 896 saponites tend to be significantly lower in Al (Figure 34). Site 504B saponites are also Fe-rich with respect to ideal saponite compositions, particularly in the uppermost pillow section (Alt et al., 1986a). As with saponites from other settings, Tonga saponites are commonly mixed with dioctahedral smectites or celadonite, leading to lower octahedral totals. At all locations, however, as MgO increases, octahedral totals increase (Figure 35).

Saponite from Tonga forearc samples ranges more widely in composition (similar to Troodos ophiolite samples) than the more magnesian saponites typical of Site 896 and the IBM forearc (Figure 36). As with Site 896 saponites (Teagle et al., 1996), Tonga saponites show no consistent chemical differences based on mode of occurrence (e.g. vein versus groundmass).

The major interlayer cation present in Tonga forearc saponites is K (Figure 37), unlike Site 896 and the IBM forearc, where saponites commonly have Ca as the dominant cation (Teagle et al., 1996; Alt et al., 1998). Representative electron microprobe analyses of saponite are shown in Table 1.

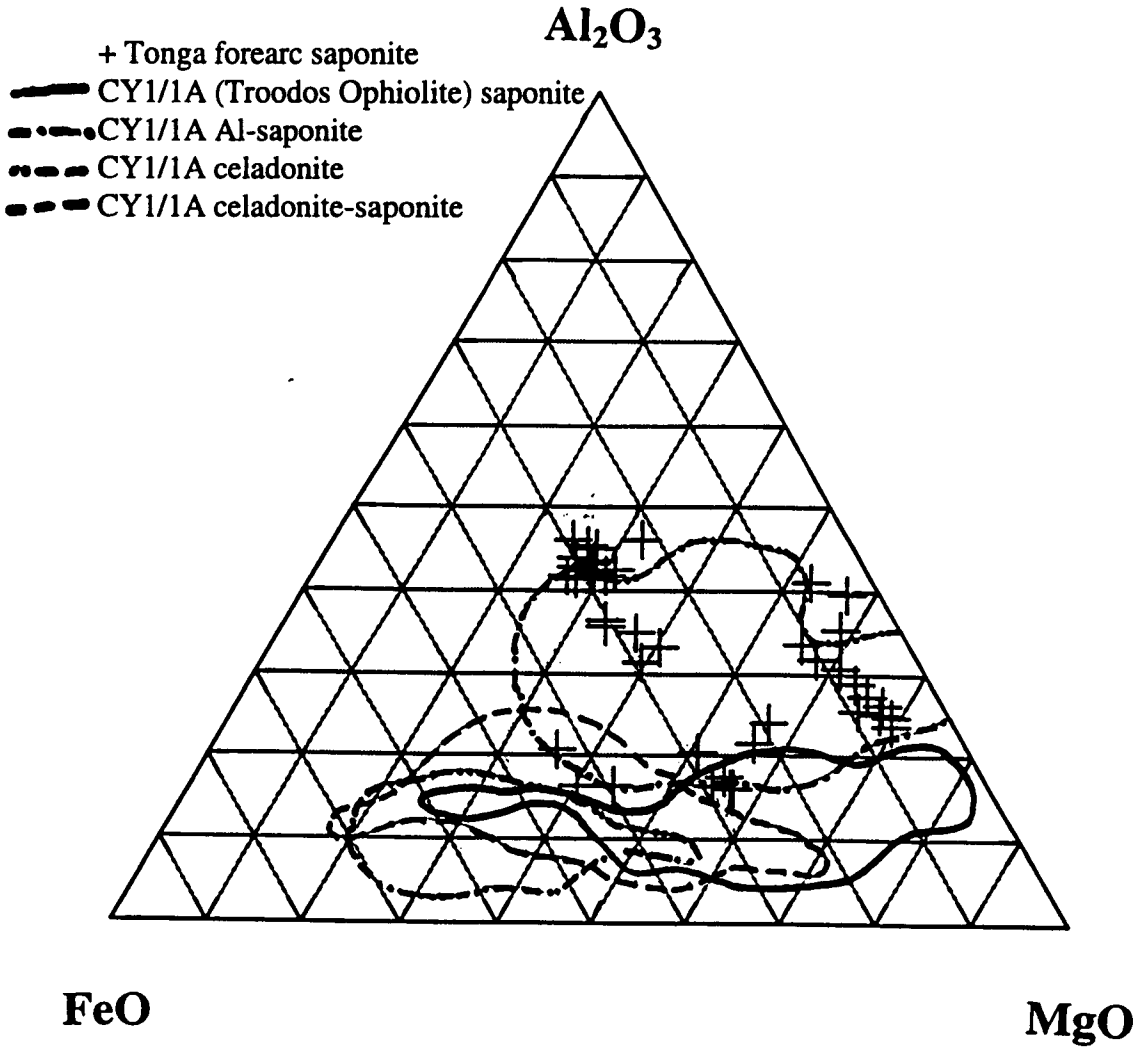

Figure 33. FeO-Al_2O_3-MgO ternary plot for Tonga forearc saponites (shown with + symbols) and Troodos Ophiolite saponites, celadonites, and celadonite-saponite mixtures. Troodos Ophiolite data from Gillis and Robinson (1990).

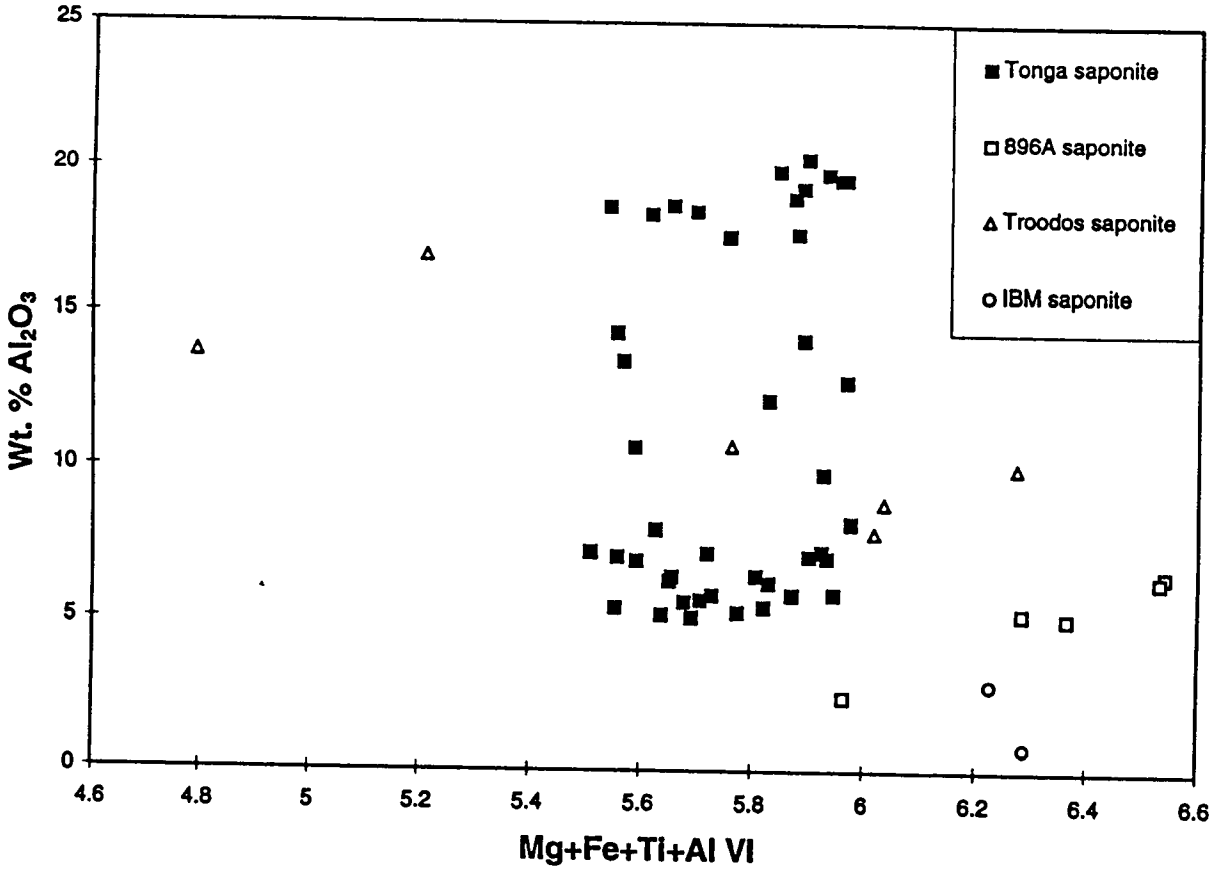

Figure 34. Al_2O_3 versus octahedral total for saponites from the Tonga forearc, Site 896, the Troodos Ophiolite, and Site 786 (IBM forearc). Site 896 data from Teagle et al. (1996). Troodos Ophiolite data from Gillis (1987). IBM data from Alt et al. (1998).

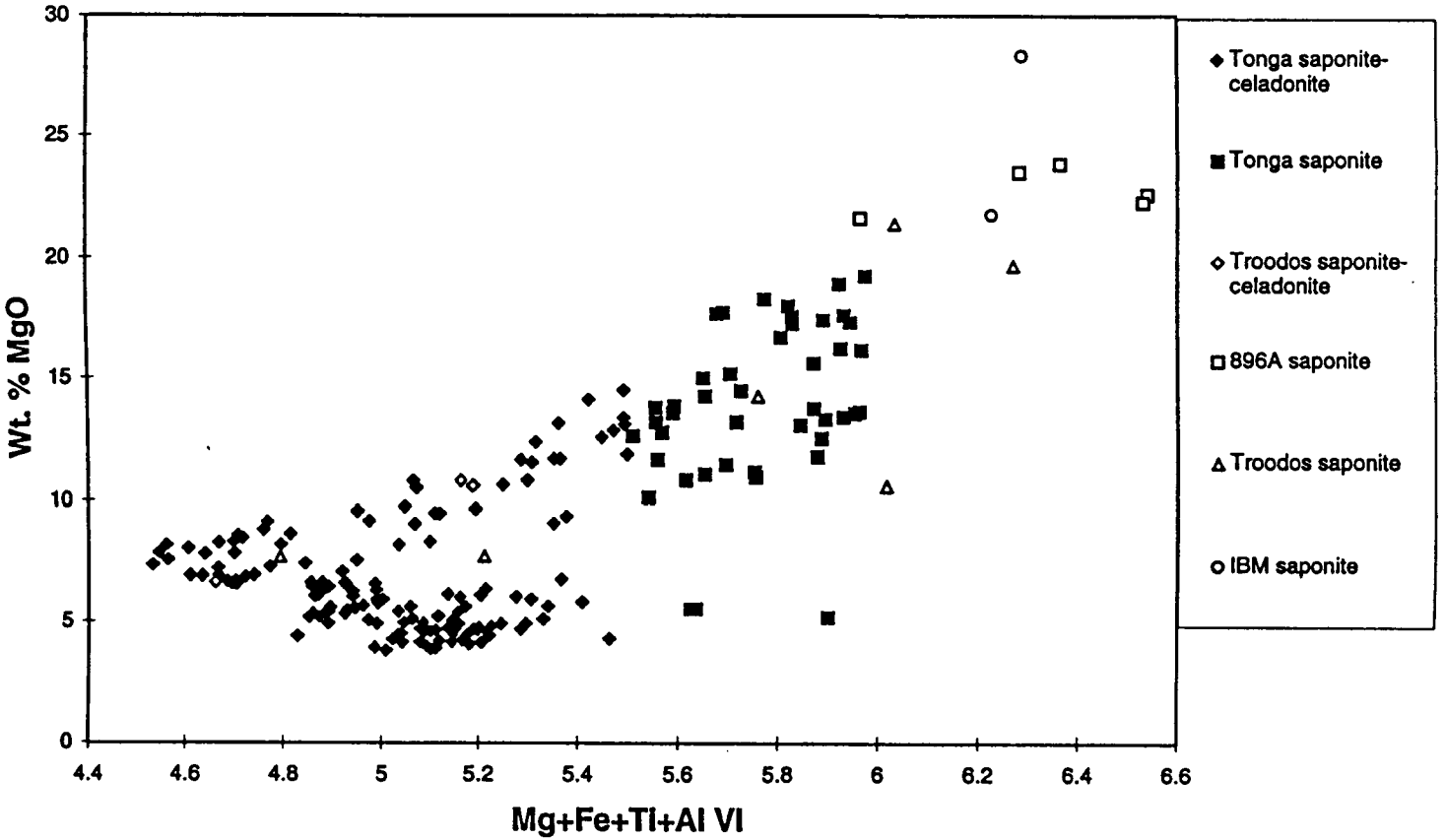

Figure 35. MgO versus octahedral total for saponites from the Tonga forearc, Site 896, the Troodos Ophiolite, and Site 786 (IBM forearc). Site 896 data from Teagle et al. (1996). Troodos Ophiolite data from Gillis (1987). IBM data from Alt et al. (1998).

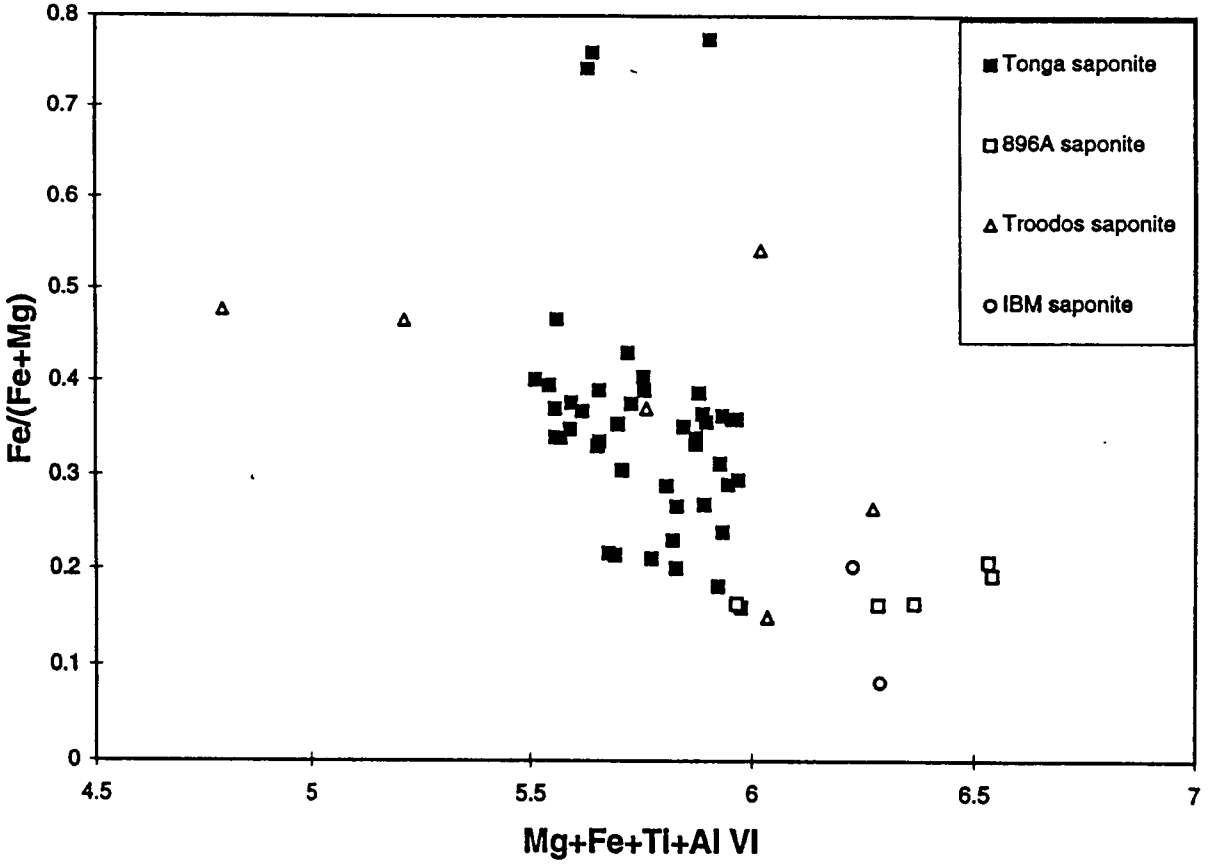

Figure 36. Fe/(Fe+Mg) versus octahedral total for saponites from the Tonga forearc, Site 896, the Troodos Ophiolite, and Site 786 (IBM forearc). Site 896 data from Teagle et al. (1996). Troodos Ophiolite data from Gillis (1987). IBM data from Alt et al. (1998).

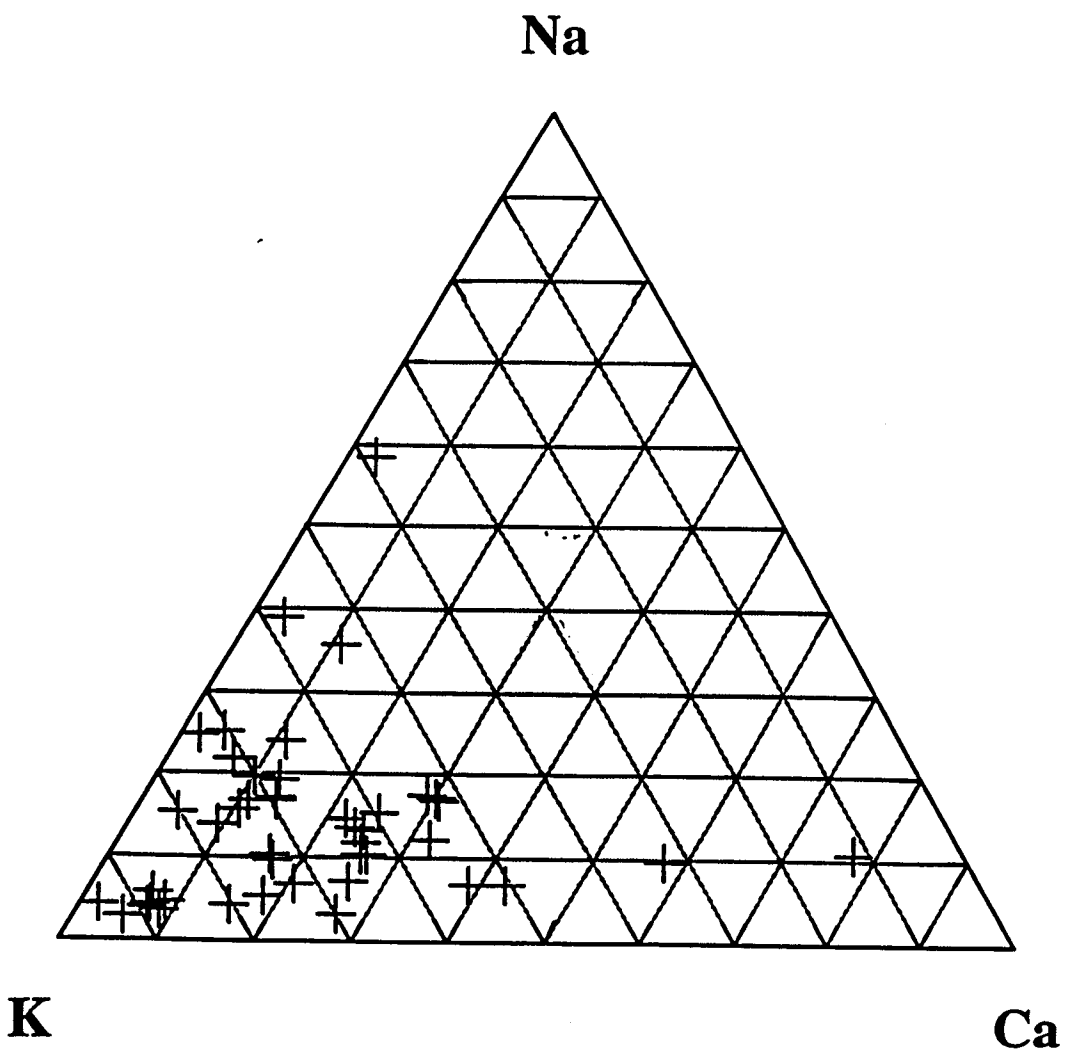

Figure 37. K-Na-Ca ternary plot for Tonga forearc saponites (shown with + symbols). K is usually the major interlayer cation.

sample	88-1-20	90-2-16	90-1-5	88-1-7
mineral	saponite	saponite	saponite	saponite
occurrence	vein	vesicle	vesicle	gm
SiO_2	46.14	40.27	40.90	43.66
TiO_2	0.60	0.07	0.00	0.00
Al_2O_3	5.11	19.31	7.13	8.22
FeO	8.61	12.73	31.63	6.53
MnO	0.05	0.31	0.23	0.03
MgO	17.71	12.50	5.17	19.25
CaO	0.32	0.91	0.41	1.40
Na_2O	0.57	0.19	0.13	0.11
K_2O	2.81	1.32	4.35	0.18
Total	**82.30**	**87.70**	**89.99**	**79.63**

Table 1. Representative electron microprobe analyses of saponites. "gm" = groundmass.

3.2.3 Celadonite

Celadonite [$KMgFe^{3+}Si_4O_{10}(OH)_2$] is a dioctahedral mica with a structure similar to that of biotite (Deer et al., 1962). It was identified in a number of samples by its 9.8-10 Å non-expandable peak in d-spacing XRD spectra. Relatively pure celadonite was not discernible in most microprobe analyses, however, suggesting that it is commonly physically mixed with other minerals on a scale too small for the resolution of the microprobe beam (<5 μm). Analyses were classified as celadonite on the basis of octahedral total between 4-4.5, and >5 weight % K_2O. These analyses thus mark the uppermost end of a compositional trend defined by analyses of saponite and saponite-celadonite mixtures (Figure 38). Increases in total Fe and K_2O characterize the transition from saponite through celadonite-saponite to celadonite. Fe in celadonite is dominated by Fe^{3+} (Wise and Eugster, 1964; Andrews, 1980).

Petrographically, celadonite is green or bright blue-green and fine-grained, commonly occurring in veins and vesicles. It may replace plagioclase and pyroxene along fractures.

The composition is similar to that of Troodos Ophiolite celadonites (Figure 39, Figure 40). Troodos celadonites (as above) have been described as mixtures of celadonite, saponite, and nontronite (Gallahan and Duncan, 1994); most celadonites that are not pure end members could also be described in this way. Tonga forearc celadonites, in comparison, do not appear to contain any appreciable nontronite component (Fe is too low, K too high). Troodos Ophiolite celadonites may have excess Si in the tetrahedral site due to the close association of celadonite with fine-grained silica (Gillis, 1987). This is

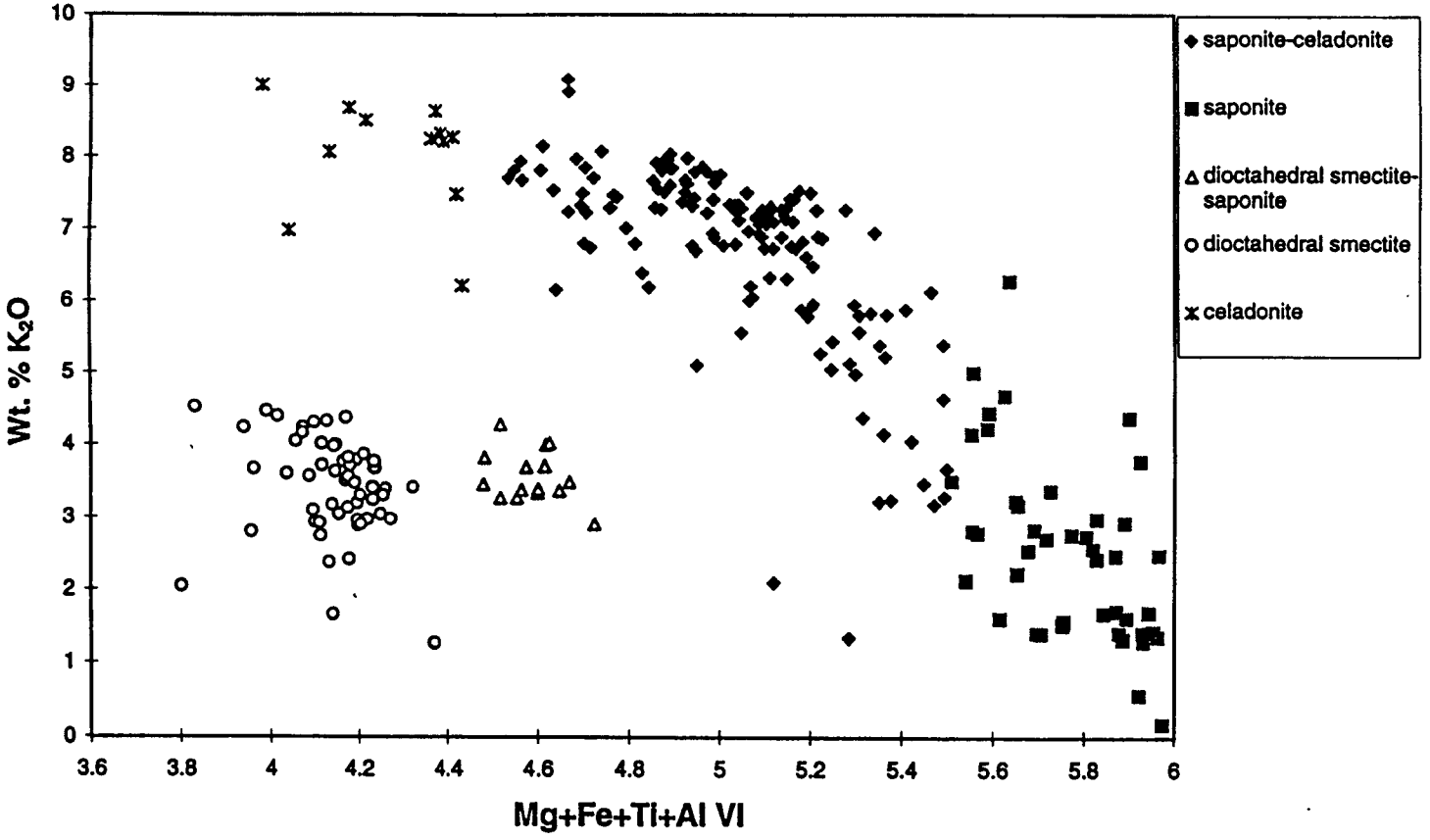

Figure 38. K_2O versus octahedral total for Tonga forearc clays. All Fe is calculated as Fe^{2+} for this diagram.

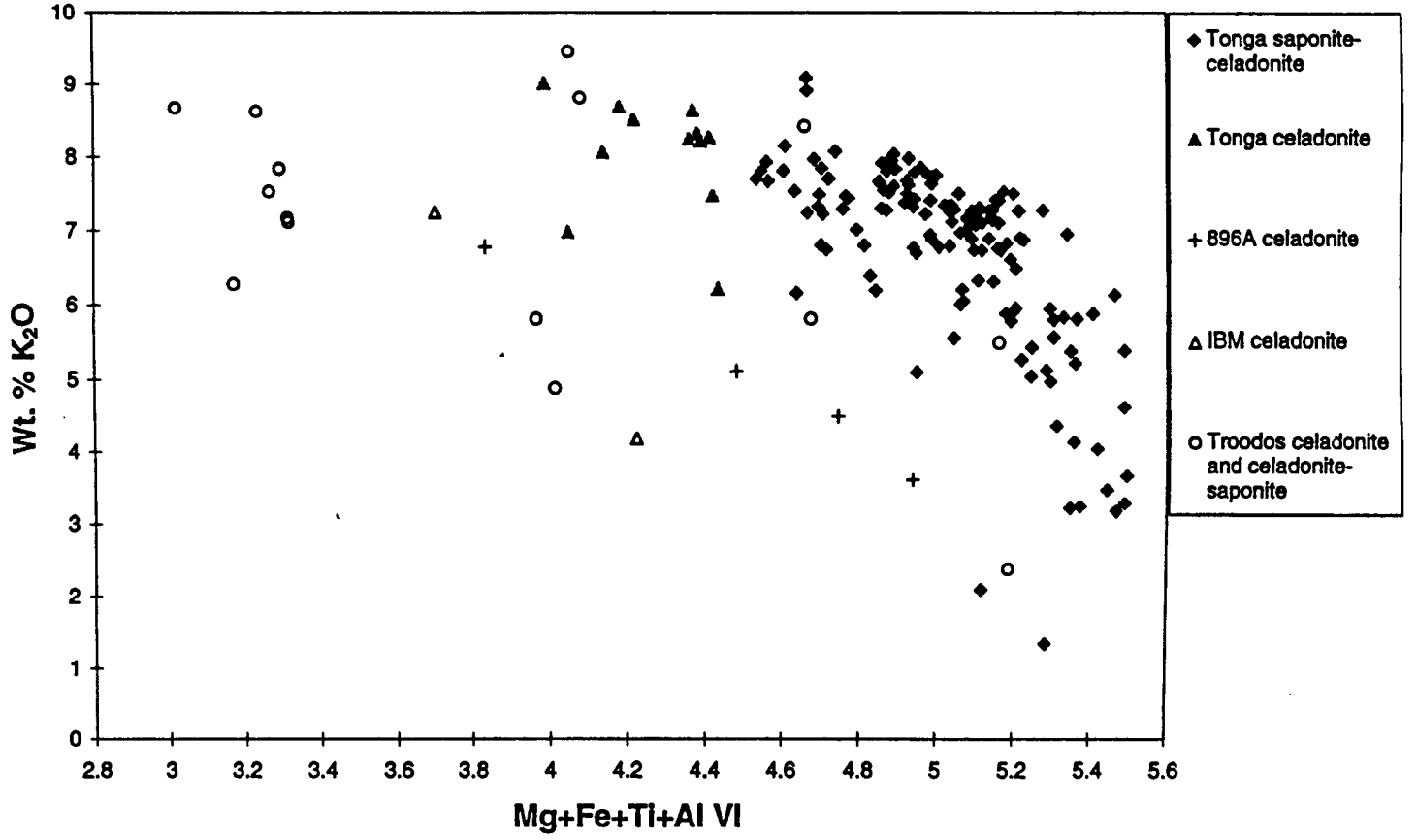

Figure 39. K_2O versus octahedral total for Tonga forearc saponite-celadonite mixtures and celadonites, and for celadonite and celadonite-saponite from Site 896, the Troodos Ophiolite, and Site 786 (IBM forearc). Site 896 data from Teagle et al. (1996). Troodos Ophiolite data from Gillis (1987). IBM data from Alt et al. (1998).

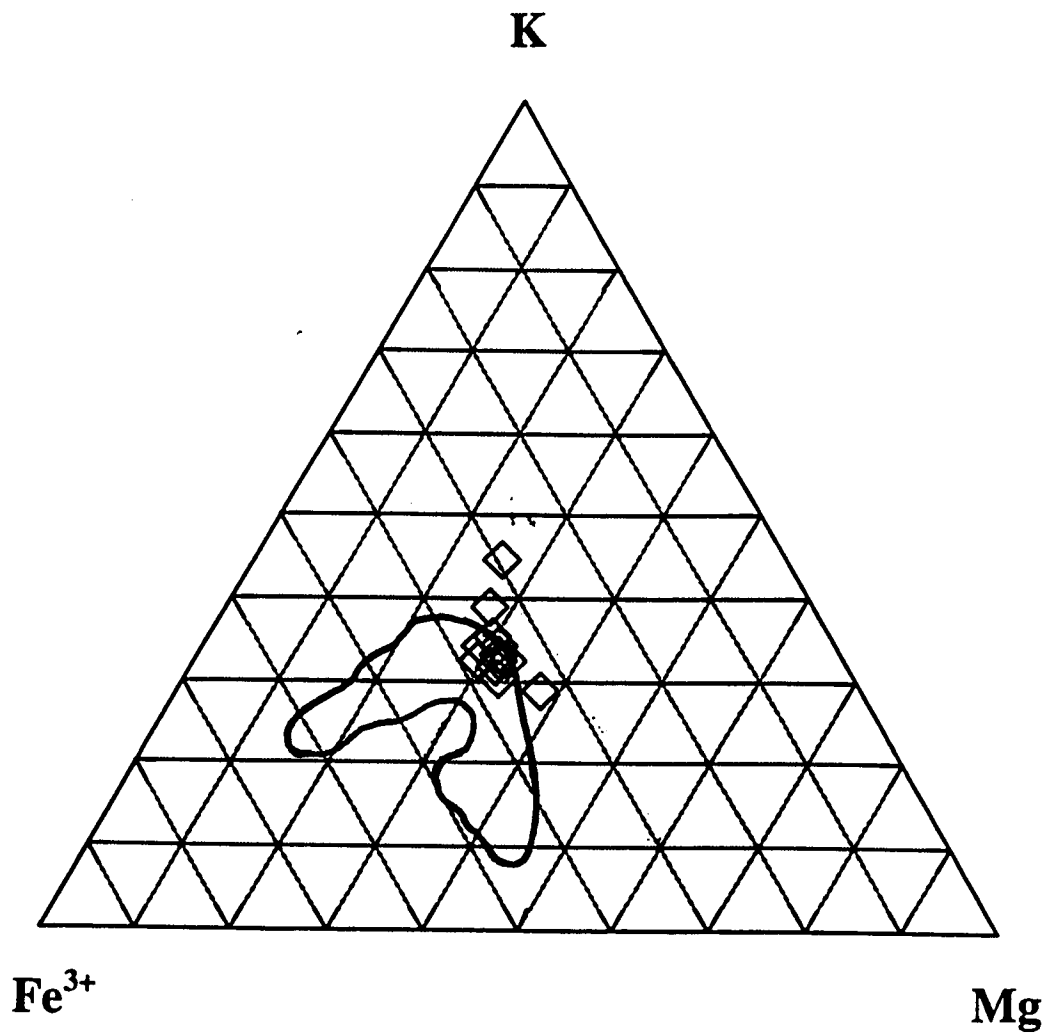

Figure 40. Fe^{3+}-K-Mg ternary plot for Tonga forearc celadonites (diamonds) and Troodos Ophiolite celadonites (solid line) (Gallahan and Duncan, 1994).

also true for Tonga forearc celadonites. Additionally, microprobe analyses may be high in silica due to this close association, even if the silica is not actually part of the celadonite structure. Troodos Ophiolite celadonites are closer to a pure celadonite composition (having lower octahedral totals associated with a particular K content) than Tonga samples, since Tonga samples generally contain a greater saponite component (Figure 39). Site 896 celadonites are also closer to end member celadonite compositions than most Tonga forearc celadonites (Teagle et al., 1996). True celadonite was analyzed in only one Site 786 sample (K is its dominant interlayer cation); others are mixtures of celadonite and smectite or glauconite (Alt et al., 1998). Representative microprobe analyses of celadonite are shown in Table 2.

3.2.4 Saponite-celadonite mixtures

A number of analyses of trioctahedral smectites have high K_2O (>3 weight %), as well as a significant dioctahedral component (octahedral total is 4.5-5.5). These are probably mixtures of saponite and celadonite. Although Fe in saponite is present as Fe^{2+} (Andrews, 1980), for the sake of simplicity, all Fe in these mixtures is treated as Fe^{3+}, which would be expected to predominate in pure celadonite (Wise and Eugster, 1964; Andrews, 1980). These analyses fall directly between pure celadonite and pure saponite (Figure 38).

Saponite-celadonite mixtures were identified by microprobe in seven samples from three dredges. Petrographically, saponite-celadonite mixtures are bright green, green-yellow, yellow-brown, or reddish brown fibrous or finely crystalline material,

sample	88-1-31	88-1-46	88-1-20	88-1-20	88-1-20
mineral	sap-cel	sap-cel	sap-cel	celadonite	celadonite
occurrence	vein	vein	after plag	vein	after plag
SiO_2	46.61	44.49	47.84	50.66	49.70
TiO_2	1.00	0.11	0.26	0.39	0.23
Al_2O_3	11.22	5.81	4.39	3.45	2.87
FeO	10.87	16.56	17.45	14.61	17.12
MnO	0.07	0.06	0.06	0.04	0.00
MgO	9.47	11.86	6.68	7.08	6.77
CaO	0.61	0.53	0.20	0.10	0.24
Na_2O	0.11	0.46	0.08	0.10	0.07
K_2O	2.09	3.65	7.96	8.31	8.63
Total	**82.06**	**83.52**	**84.92**	**84.80**	**85.72**

Table 2. Representative electron microprobe analyses of saponite-celadonite mixtures and celadonites. "sap-cel" = saponite-celadonite mixture. "plag" = plagioclase.

occurring in veins and vesicles (Figure 41), and groundmass. Where it can be positively determined, saponite-celadonite appears to precipitate before saponite. It may replace plagioclase and pyroxene along fractures.

Octahedral totals of celadonites from Site 896 vary, with higher totals indicating a significant smectite component. Increasing octahedral totals at Site 896 correlate with higher Mg and lower K, indicating that they are mixtures of celadonite and saponite rather than celadonite and nontronite (nontronite, being a dioctahedral smectite, would not show increasing octahedral totals) (Teagle et al., 1996). Mixtures of celadonite and nontronite, however, do occur at Site 896 (Laverne et al., 1996). Site 504B has mixtures of celadonite and saponite in the pillow section (Alt et al., 1996a). Chemically, the Tonga celadonite-saponite mixture falls along the celadonite-saponite trend defined by Gallahan and Duncan (1994) for Troodos Ophiolite samples (Figure 42). A comparison of the compositions of Tonga, IBM forearc, Site 896, and Troodos ophiolite celadonite-saponite mixtures is shown in Figure 39. For Tonga saponite-celadonite mixtures, the major interlayer cation is K (Figure 43). Representative microprobe analyses of saponite-celadonite mixtures are shown in Table 2.

3.2.5 Dioctahedral smectite (beidellite-nontronite mixtures)

Dioctahedral smectites, identified by octahedral totals <4.5, are mixtures of nontronite and beidellite. Nontronite is an Fe-rich smectite with the ideal composition $Si_{7.34}Al_{0.66}Fe_4^{3+}(1/2Ca, Na)_{0.66}$ (Deer et al., 1962). Beidellite has the same structure, but Al substitutes for Fe^{3+} in the octahedral positions. Tonga dioctahedral smectite-saponite

Figure 41. Sample 88-1-31, showing vesicles filled with saponite-celadonite mixture (green) and another clay (brown). Uncrossed polars.

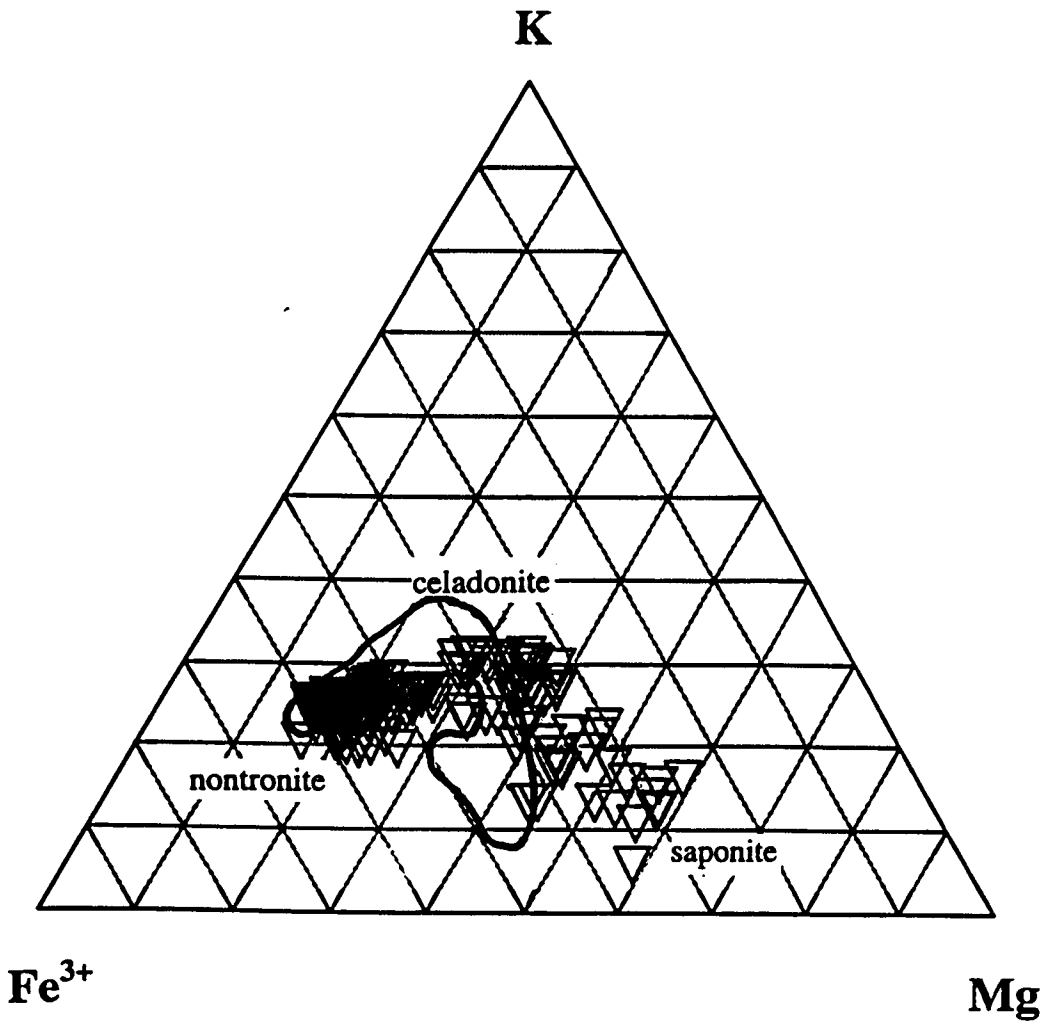

Figure 42. Fe^{3+}-K-Mg ternary plot for Tonga forearc saponite-celadonite mixtures (triangles), and Troodos Ophiolite celadonites (solid line) (Gallahan and Duncan, 1994). Locations of end member nontronite, celadonite, and saponite are shown.

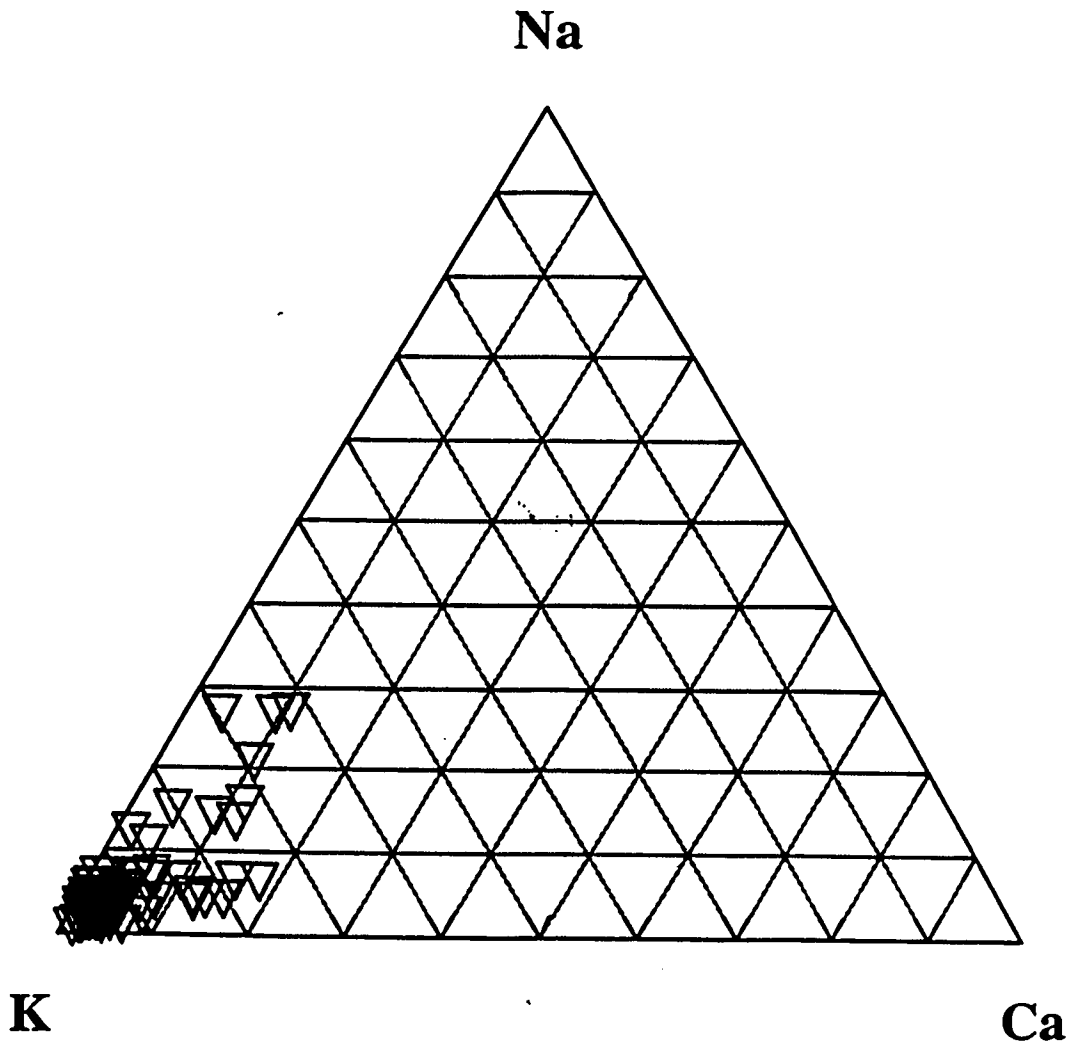

Figure 43. K-Na-Ca ternary plot for Tonga forearc saponite-celadonite mixtures (triangles). K is the major interlayer cation.

mixtures and dioctahedral smectites fall between nontronite and beidellite compositions (Figure 44). $K_2O<5$ weight percent distinguishes dioctahedral smectite from celadonite (Figure 38).

Dioctahedral smectite was identified in three samples from two dredges, one of which comprised more Fe-rich compositions whereas the other two were more Al-rich. It occurs principally as a fibrous or fine-grained material lining veins and vesicles, and as a finely crystalline groundmass material. Both vein-filling and groundmass types are green-brown or green-yellow in color. Dioctahedral smectite may also mix with Fe-oxyhydroxides, replace olivine (along with saponite and Fe-oxyhydroxides), or slightly replace plagioclase, clinopyroxene, and orthopyroxene along fractures.

Chemically, there is a continuum between more Fe-rich and more Al-rich types (Figure 45), although neither end member nontronite nor beidellite is present. The primary interlayer cation is K (Figure 46). Pure dioctahedral smectites have rarely been documented in altered oceanic rocks. Mixtures of celadonite and nontronite were identified at Site 896 (Laverne et al., 1996). Pure beidellite has been identified in very altered MORB and alkalic submarine basalts (Alt and Honnorez, 1984; Alt et al., 1992; Alt, 1993). Beidellite replaces olivine and orthopyroxene at Site 786 (the IBM forearc) (Alt et al., 1998). Representative microprobe analyses of dioctahedral smectites are shown in Table 3.

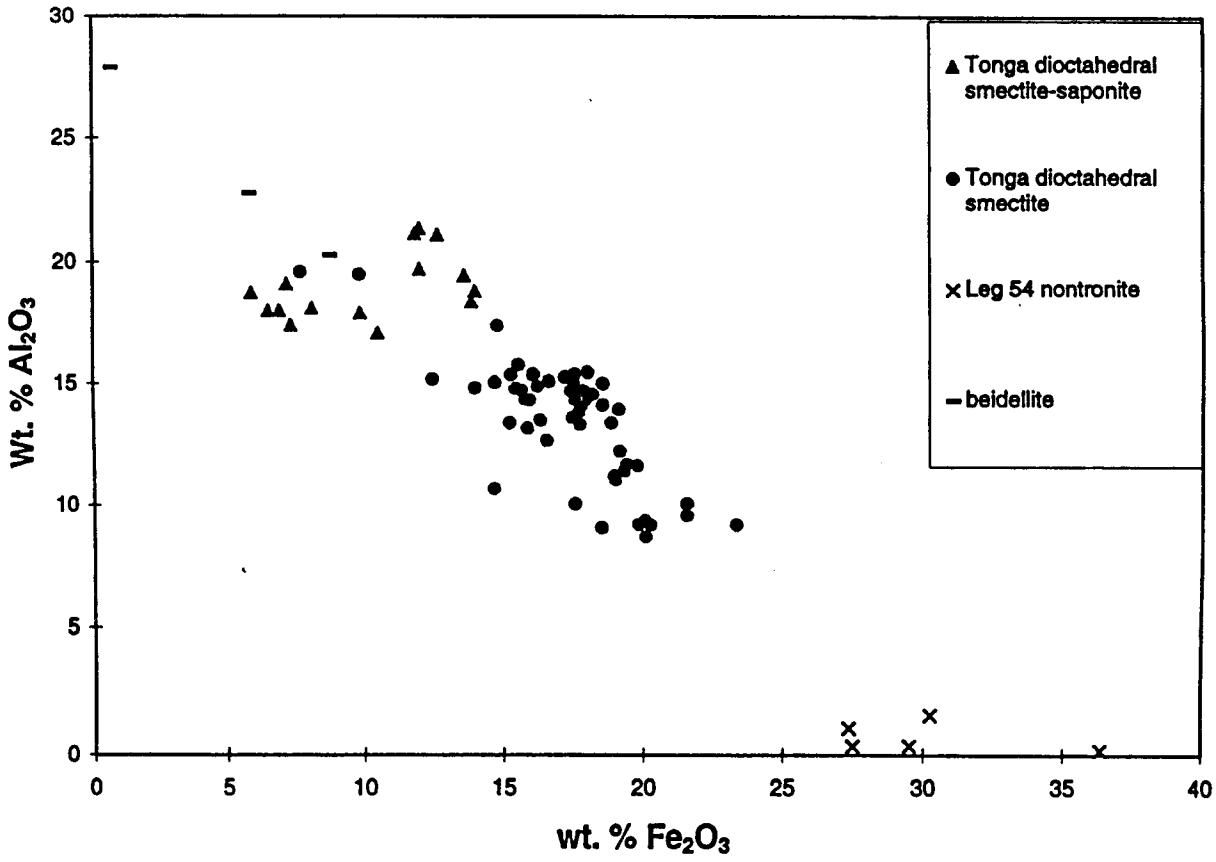

Figure 44. Al_2O_3 versus Fe_2O_3 for Tonga forearc dioctahedral smectites and dioctahedral smectite-saponite mixtures, and Leg 54 nontronites (Galapagos hydrothermal mounds) (McMurtry et al., 1983) and beidellites from several locations (Deer et al., 1962).

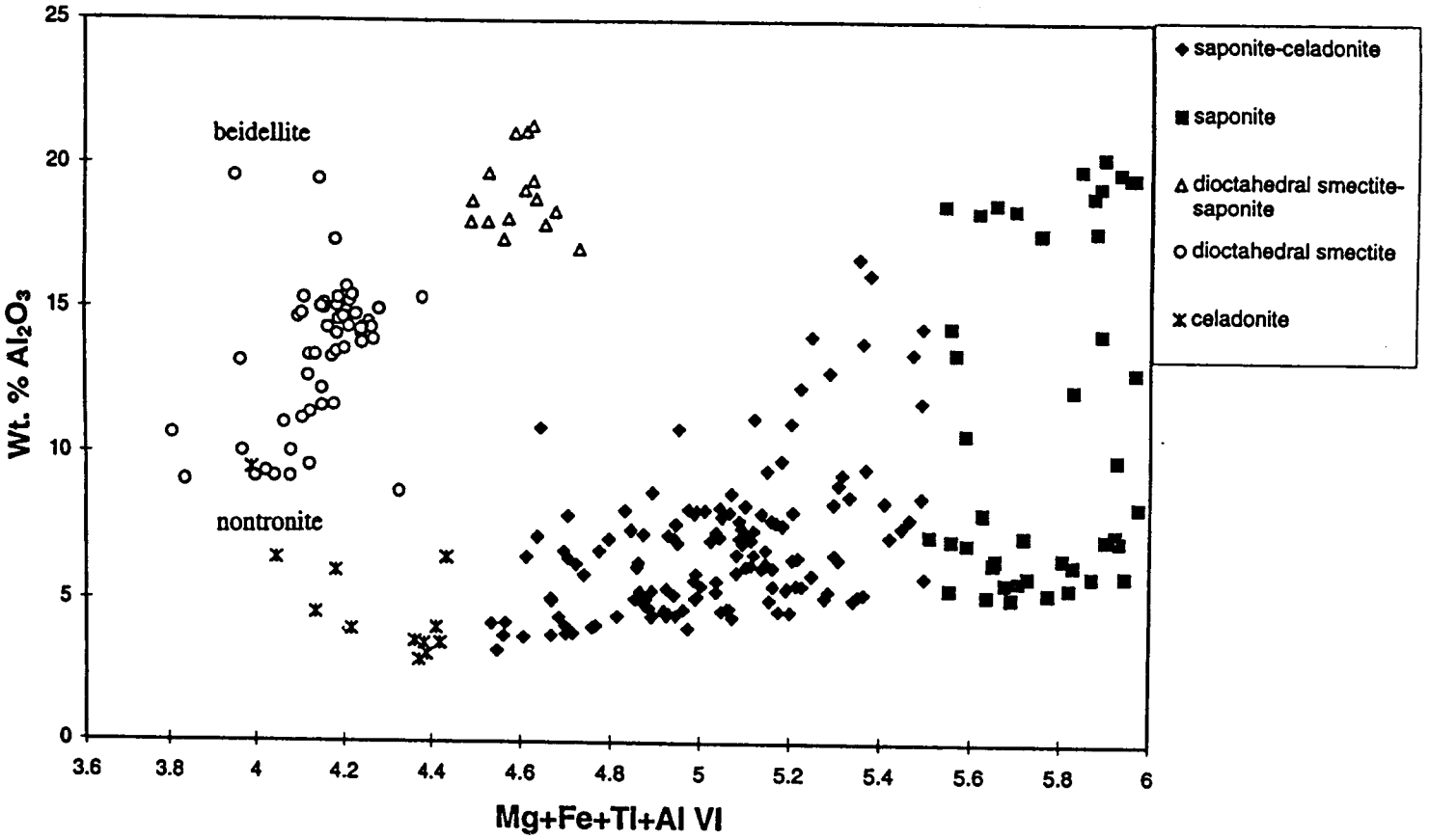

Figure 45. Al_2O_3 versus octahedral total for Tonga clays (excluding chlorite and chlorite-smectite). All Fe is calculated as Fe^{2+} for this diagram. Locations of beidellite and nontronite end members are shown.

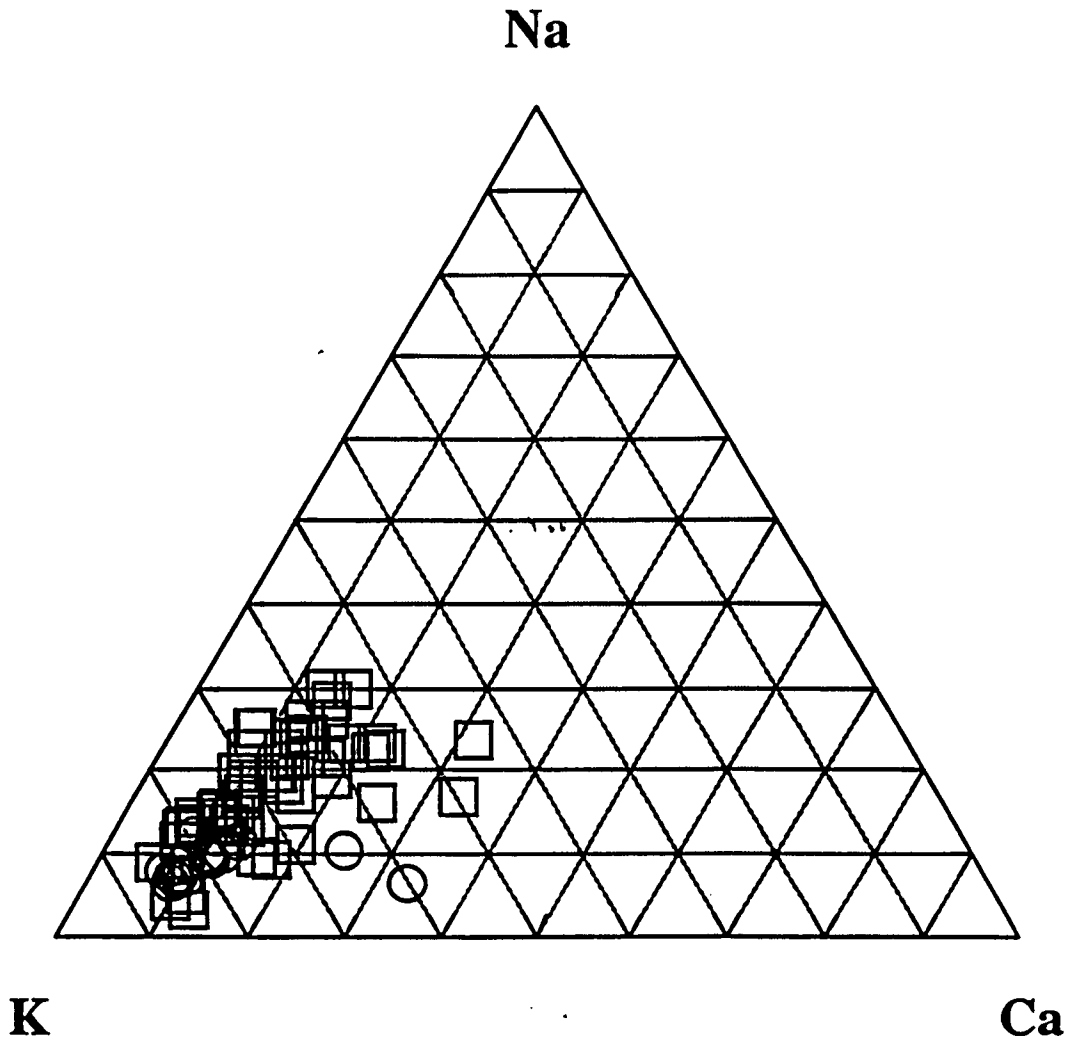

Figure 46. K-Na-Ca ternary plot for Tonga forearc dioctahedral smectites (squares) and dioctahedral smectite-saponite mixtures (circles). K is the dominant interlayer cation.

sample	90-2-16	90-2-16	90-2-16	91-3-5
mineral	ds-sap	ds-sap	di smec	di smec
occurrence	vein	vein	vein	vein
SiO_2	51.97	47.39	51.67	48.45
TiO_2	0.36	0.32	0.18	0.77
Al_2O_3	17.98	17.04	19.56	8.69
FeO	6.38	10.36	7.56	20.05
MnO	0.11	0.19	0.14	0.07
MgO	7.44	7.72	2.28	5.04
CaO	0.58	0.60	1.09	0.53
Na_2O	0.26	0.29	1.06	0.62
K_2O	3.26	2.89	4.23	3.41
Total	**88.48**	**86.96**	**87.82**	**87.74**

Table 3. Representative electron microprobe analyses of dioctahedral smectites and dioctahedral smectite-saponite mixtures. "ds-sap" = dioctahedral smectite-saponite mixture. "di smec" = dioctahedral smectite.

3.2.6 Dioctahedral smectite-saponite mixtures

Mixtures of di- and trioctahedral smectite were identified in one sample (90-2-16) on the basis of octahedral totals between 4.5-5.5, and $K_2O<5$ weight percent (Figure 38). These clays are compositionally distinct from saponite and beidellite-nontronite and are believed to be physical mixtures between the two (Figure 44).

Dioctahedral smectite-saponite mixtures occur as green or green-yellow, fine-grained materials in veins, vesicles, and groundmass, generally secondary to yellow clays, before quartz and zeolites, and before or contemporaneous with Fe-oxyhydroxides. They do not appear to replace any phenocryst phases, although the amount of clay positively identified as dioctahedral smectite-saponite mixtures may simply be too small to show all types of occurrence. Troodos Ophiolite "celadonites" have been described as mixtures of celadonite, nontronite, and saponite (Gallahan and Duncan, 1994). At Site 786, saponites with lower octahedral occupancies have been analyzed (Alt et al., 1998); these could be mixtures of saponite and dioctahedral smectite, or they could be mixed with celadonite. As with saponite, K is the major interlayer cation (Figure 46). Representative microprobe analyses of dioctahedral smectite-saponite mixtures are shown in Table 3.

3.2.7 Chlorite

Chlorite, $(Mg, Fe^{2+}, Fe^{3+}, Mn, Al)_{12}[(Si, Al)_8O_{20}](OH)_{16}$ (Deer et al., 1962), is a common hydrothermal alteration product of ferromagnesian minerals with a layered structure similar to that of micas. Chlorite was identified based on electron microprobe

analyses and petrography. Identification was also aided by non-expandable XRD peaks occurring on d-spacing spectra at 14.2 and 7.1 Å. Pure chlorite was positively identified by microprobe in only one sample (85-3-2), which is not from the main transect. Chlorite is inferred (based on petrography) to occur in other samples, and was simply not successfully analyzed due to its fine-grained nature and close association with other minerals. Pure chlorite is uncommon in this suite of samples. Identification as chlorite (as opposed to a mixture of chlorite and smectite) was based on the sum of the major non-interlayer cations and the total Al content (both calculated based on 28 O) (Figure 47), since the number of non-interlayer cations should increase with increasing chlorite content (Schiffman and Fridleifsson, 1991).

Chlorite occurs in vesicles, in close association with epidote and quartz and sometimes opaque oxides, as pale green, fine-grained, fibrous aggregates with somewhat anomalous interference colors. It also occurs sparsely in the groundmass, and occasionally in small amounts in veins, associated with quartz.

Chemically, the chlorite is pycnochlorite (Figure 48) and shares a similar composition to many chlorite samples analyzed from plutonic Tonga samples, although the plutonic samples show a broader range of compositions (Banerjee, 1998, unpublished data); this may be due to the comparatively large number of sites from which the plutonic analyses originated, as well as their broad range of lithologies. Chlorite from Hole 504B ranges from ripidolite to pycnochlorite in composition (Alt et al., 1996a) (ripidolite being a less siliceous chlorite). As with Tonga chlorite, as the proportion of smectite layers increases, chlorite-smectite mixtures show increasing Si and Mg and decreasing Al and

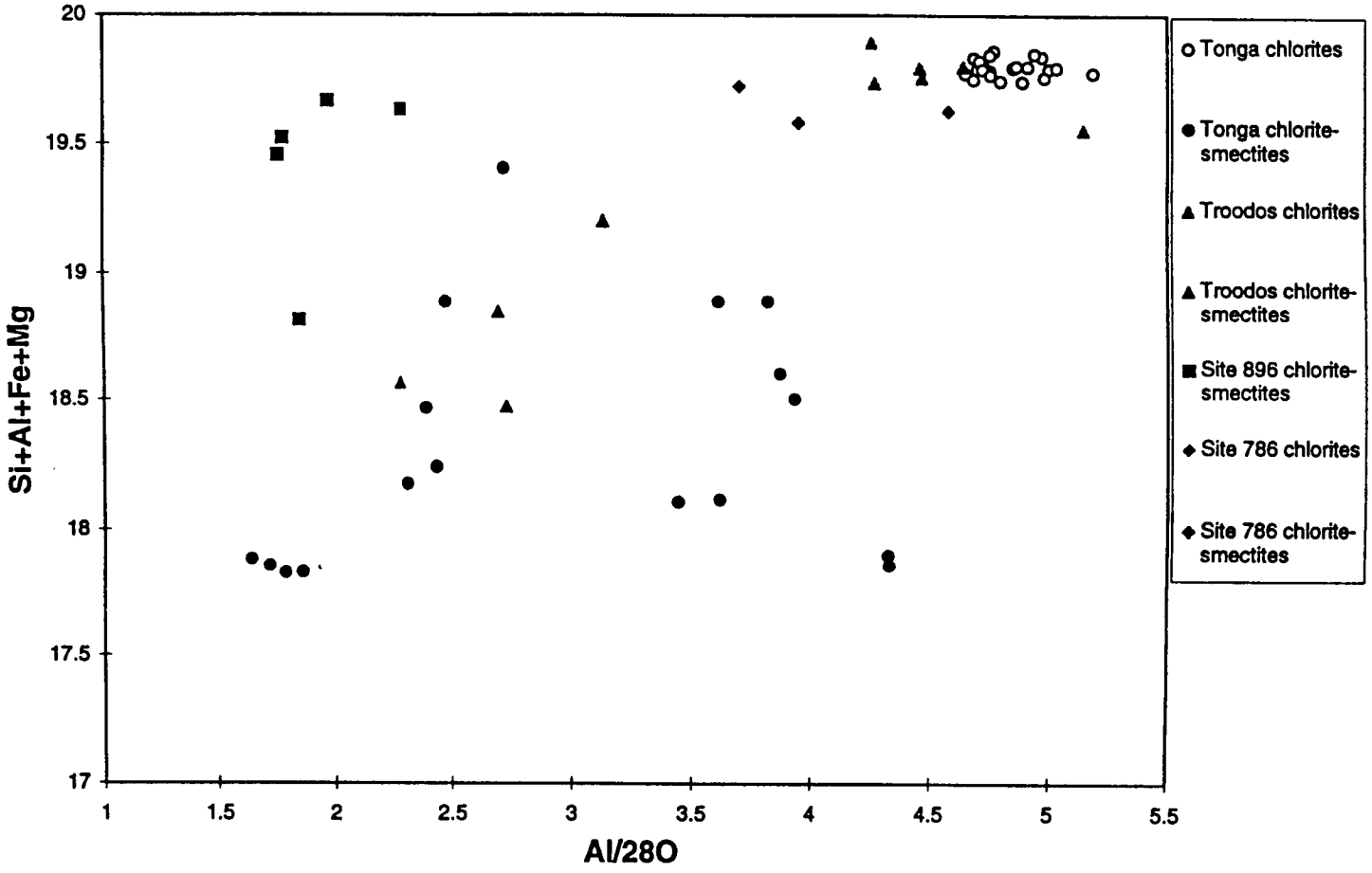

Figure 47. Total of major non-interlayer cations versus Al (calculated for 28 O) for chlorites and chlorite-smectites from the Tonga forearc, Site 896, the Troodos Ophiolite, and Site 786 (IBM forearc). Site 896 data from Teagle et al. (1996). Troodos Ophiolite data from Gillis (1987). IBM data from Alt et al. (1998).

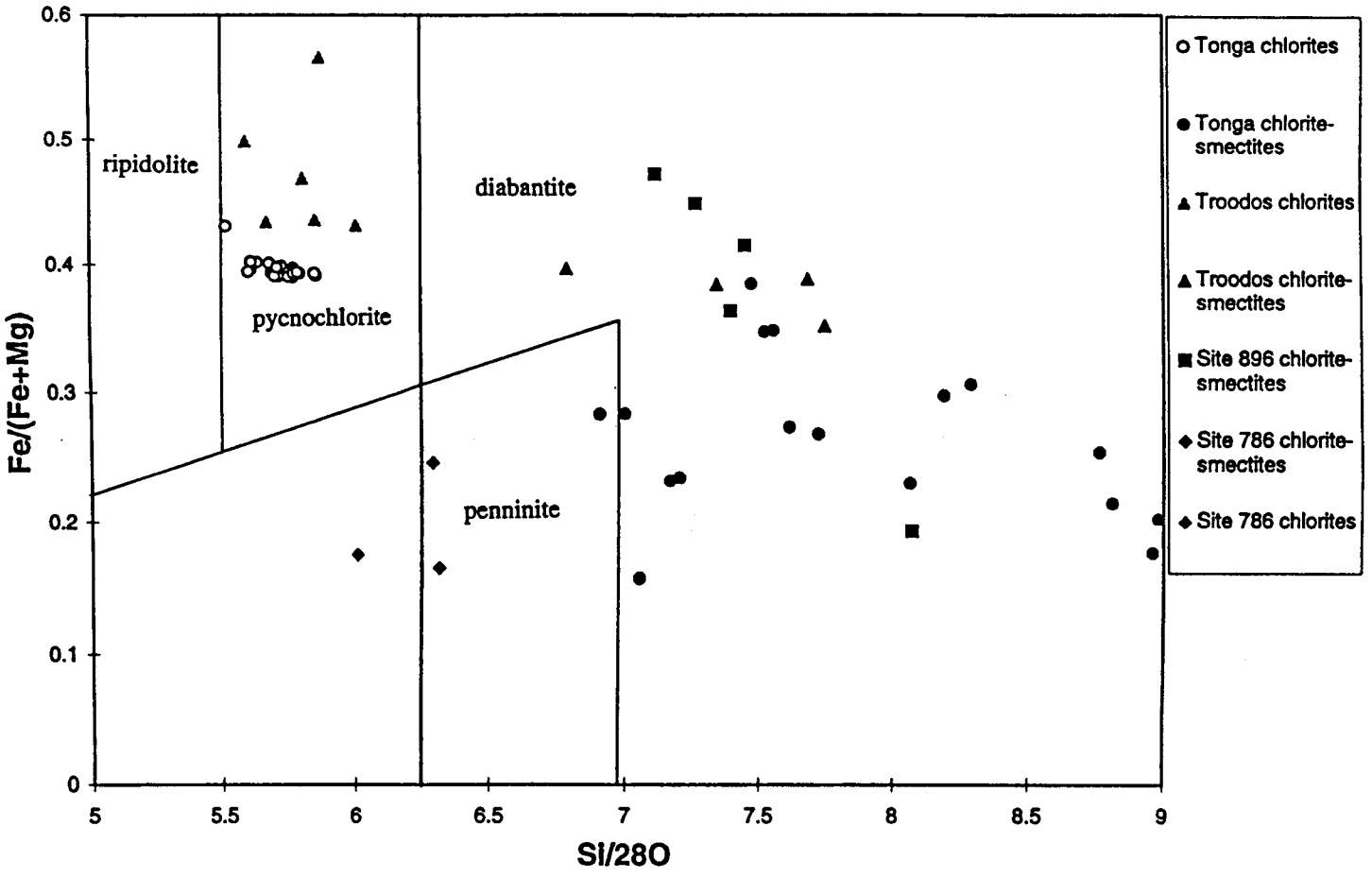

Figure 48. Fe/(Fe+Mg) versus Si (calculated for 28 O) for chlorites and chlorite-smectites from the Tonga forearc, Site 896, the Troodos Ophiolite, and Site 786 (IBM forearc). Site 896 data from Teagle et al. (1996). Troodos Ophiolite data from Gillis (1987). IBM data from Alt et al. (1998). Chlorite nomenclature after Hey (1954).

Fe. Chlorites from Site 504 show a similar range of compositions to the Troodos Ophiolite (Alt et al., 1996a). In the Troodos ophiolite, Fe increases slightly with depth, and chlorite may contain up to 1.5 weight percent MnO (Gillis, 1987). Both chlorite and chlorite/smectite at Site 786 are Mg-rich, with Fe/(Fe+Mg) = 0.15-0.25 (Alt et al., 1997) (typical chlorite from altered MORB and ophiolites has Fe/(Fe+Mg) = 0.25-0.8 (Evarts and Schiffman, 1983; Alt et al., 1986a; Gillis and Robinson, 1990; Pflumio, 1991; Gillis and Thompson, 1995). Tonga forearc chlorite and chlorite/smectite Al, Fe, and Mg contents are compared with other locations in Figure 49. Representative chlorite analyses are shown in Table 4.

3.2.8 Chlorite/smectite

Mixtures of chlorite and smectite were identified in several samples using microprobe analyses, based on octahedral totals (for 22 O) >5.5 and Al intermediate between saponite and chlorite (Figure 50). Additionally, the number of total non-interlayer cations also increases with increasing chlorite content due to the change in structure from smectite to chlorite (Figure 47). Based on XRD d-spacing spectra, which showed discrete non-expandable peaks for chlorite at 14.2 and 7.1 Å, and discrete (expandable to 18 Å) smectite peaks at 15.5-16 Å, some mixtures are assumed to be physical, not structural. However, for other samples, in which mixed-layer chlorite/smectite was identified based on microprobe data, distinct chlorite and smectite peaks could not be identified by XRD, indicating that the mixtures are structural.

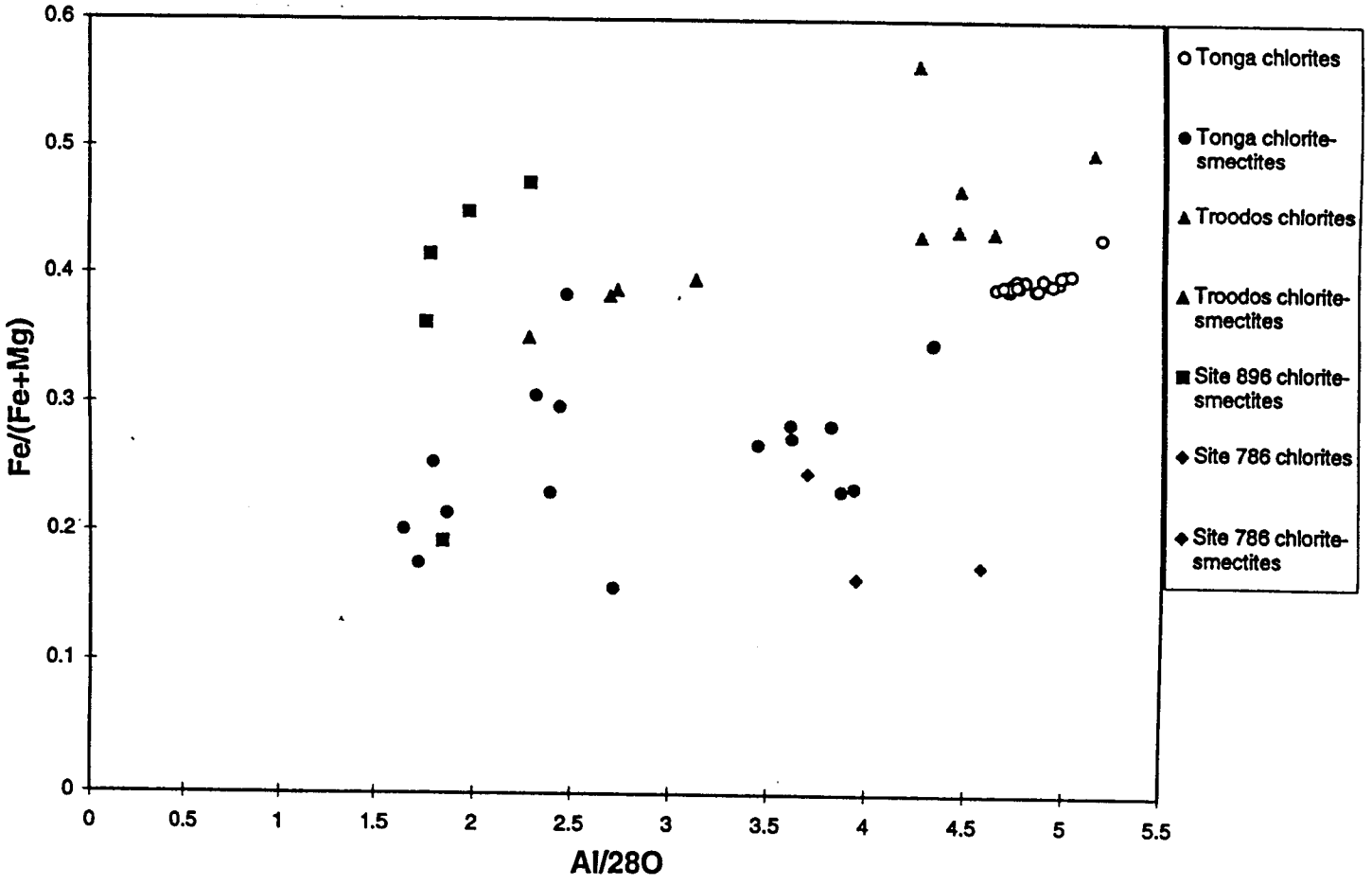

Figure 49. Fe/(Fe+Mg) versus Al (calculated for 28 O) for chlorites and chlorite-smectites from the Tonga forearc, Site 896, the Troodos Ophiolite, and Site 786 (IBM forearc). Site 896 data from Teagle et al. (1996). Troodos Ophiolite data from Gillis (1987). IBM data from Alt et al. (1998).

sample	90-2-16	88-1-7	88-1-7	88-1-7	85-3-2
mineral	chlor/smec	chlor/smec	chlor/smec	chlor/smec	chlorite
occurrence	vesicle	gm	gm	gm	gm
SiO_2	35.17	45.00	35.64	36.31	27.20
TiO_2	0.06	0.01	0.06	0.19	0.03
Al_2O_3	16.48	6.95	11.61	10.14	20.37
FeO	14.06	8.78	9.12	20.01	21.35
MnO	0.58	0.01	0.26	0.23	0.40
MgO	20.00	19.49	27.56	17.96	18.42
CaO	0.44	1.28	0.31	0.71	0.03
Na_2O	0.18	0.13	0.14	0.12	0.01
K_2O	0.44	0.12	0.26	0.99	0.01
Cr_2O_4	0.01	0.00	0.00	0.00	0.00
Total	**87.46**	**81.97**	**85.02**	**86.72**	**87.84**

Table 4. Representative electron microprobe analyses of chlorites and chlorite/smectites. "chlor/smec" = mixed chlorite/smectite. "gm" = groundmass.

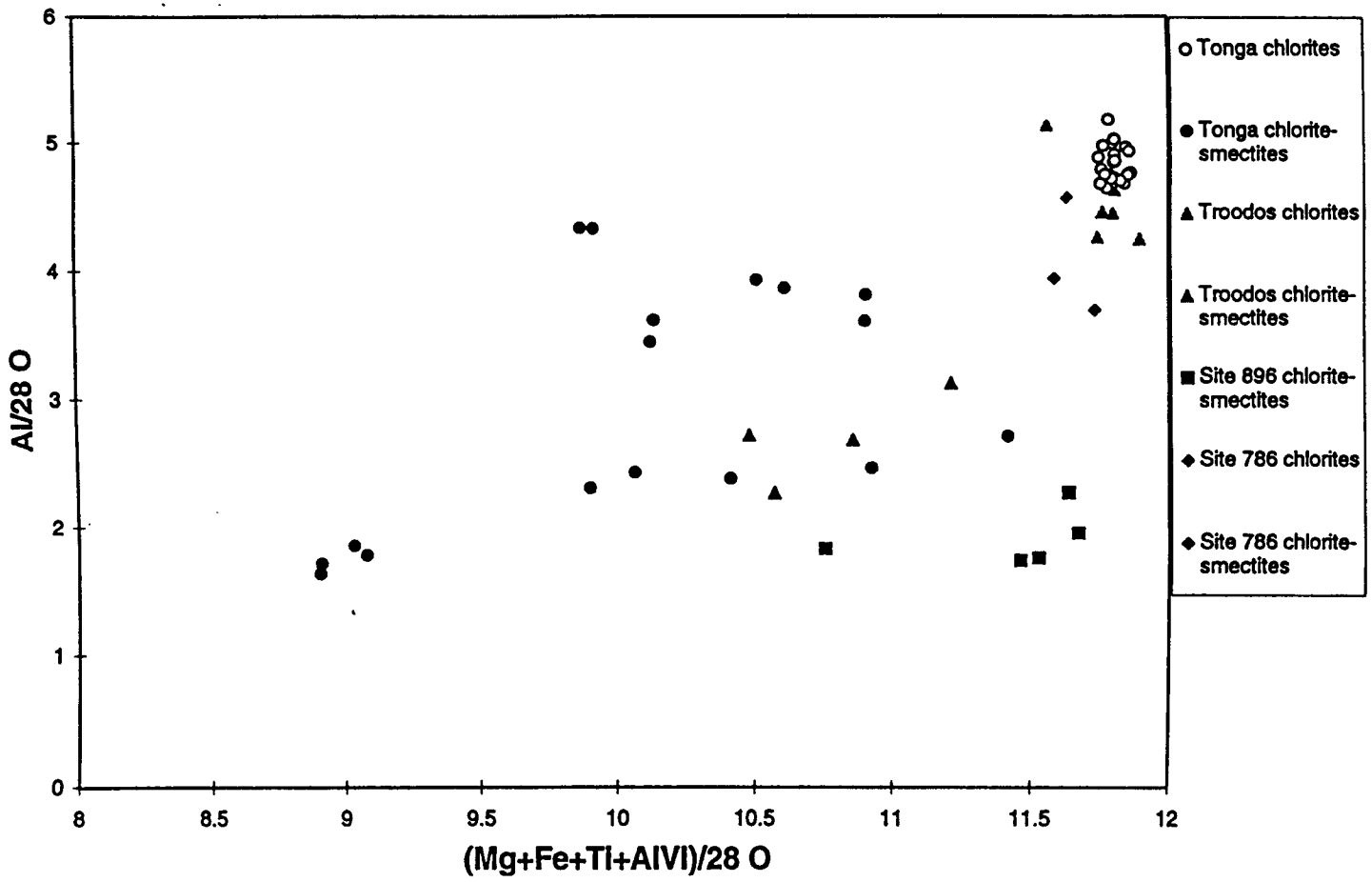

Figure 50. Total Al versus octahedral total (calculated for 28 O) for chlorites and chlorite-smectites from the Tonga forearc, Site 896, the Troodos Ophiolite, and Site 786 (IBM forearc). Site 896 data from Teagle et al. (1996). Troodos Ophiolite data from Gillis (1987). IBM data from Alt et al. (1998).

Chlorite/smectite mixtures, both physical and structural, occur in veins and vesicles and occasionally in groundmass as fine-grained brown-green or brown material which is difficult or impossible to distinguish petrographically from smectite. Its position in the depositional sequence varies.

Chemically, throughout the transition from pure smectite to pure chlorite, tetrahedral Al increases (Figure 51), total of interlayer cations decreases (Figure 52), and Fe/Fe+Mg increases (Figure 53).

Tonga forearc chlorite/smectite mixtures have similar Mg contents to typical altered oceanic crust (Fe/Fe+Mg=0.15-0.8). Pure Tonga forearc chlorite has similar Mg contents (Fe/Fe+Mg=0.4-0.5), but a smaller range of compositions. Representative microprobe analyses of chlorite/smectite are shown in Table 4.

3.2.9 Clay zoning in veins and vesicles

Due to the fine-grained nature of most clay minerals and to the wide range of colors observed for each clay type, it is difficult or impossible to distinguish the clay types petrographically; moreover, boundaries between clay types are often gradational. Based on microprobe data, however, clay depositional sequences and clay zonation have been identified. In general, dioctahedral smectite and dioctahedral smectite-saponite mixtures are not common but if present, they appear in this sequence (earliest to latest):

dioctahedral smectite---> dioctahedral smectite-saponite or saponite-celadonite

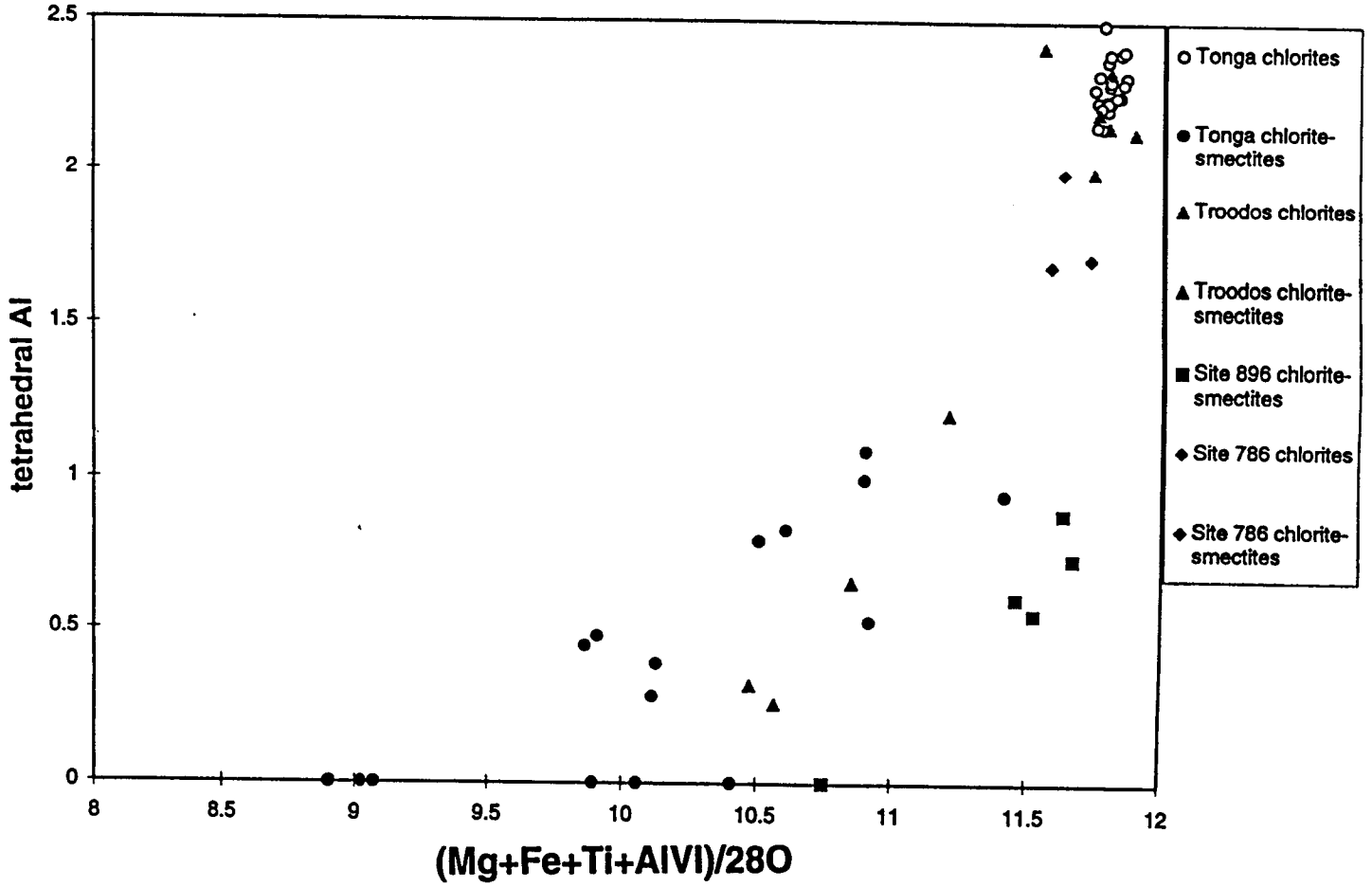

Figure 51. Tetrahedral Al versus octahedral total (calculated for 28 O) for chlorites and chlorite-smectites from the Tonga forearc, Site 896, the Troodos Ophiolite, and Site 786 (IBM forearc). Site 896 data from Teagle et al. (1996). Troodos Ophiolite data from Gillis (1987). IBM data from Alt et al. (1998).

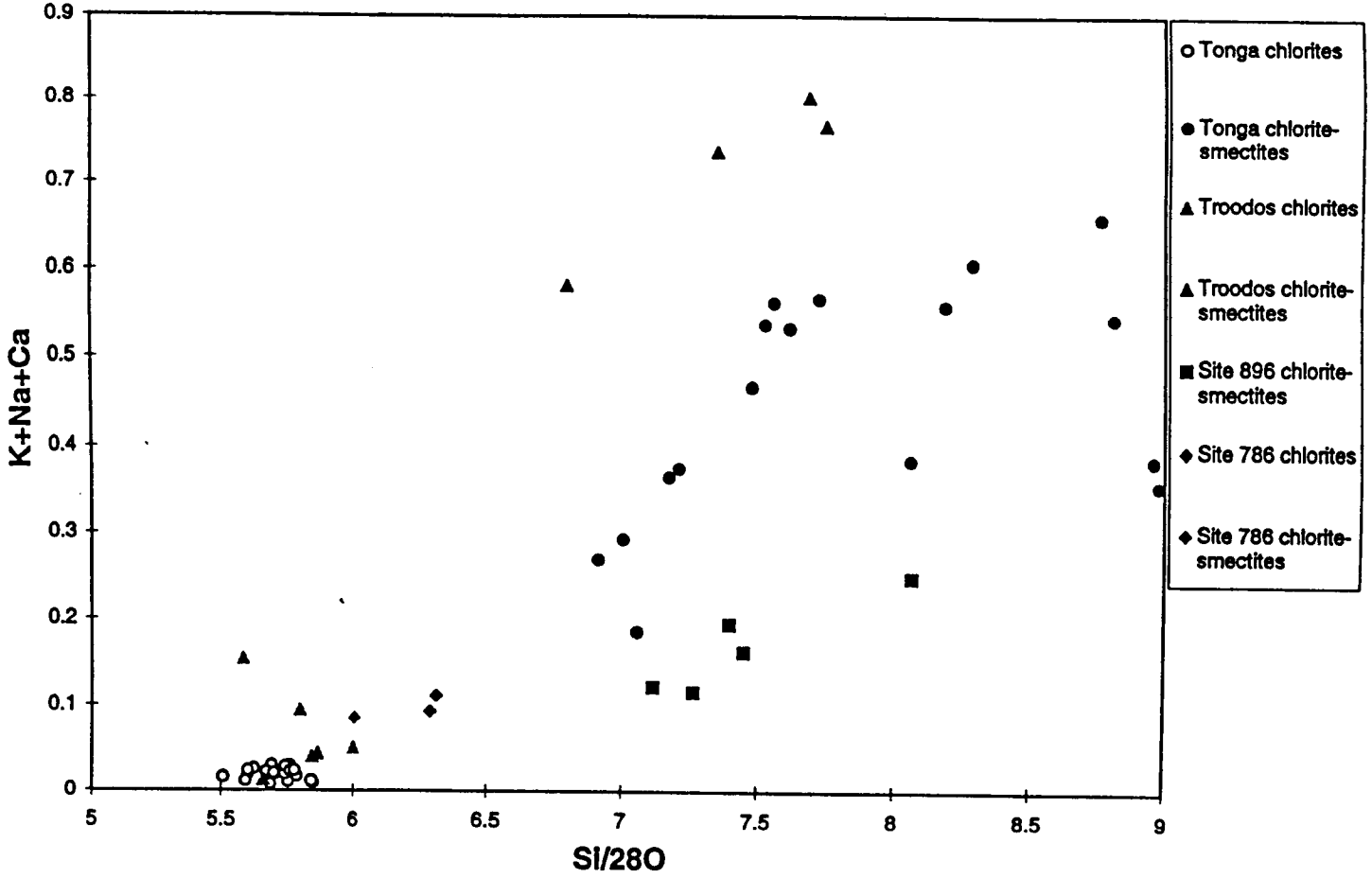

Figure 52. Total interlayer cations versus Si (calculated for 28 O) for chlorites and chlorite-smectites from the Tonga forearc, Site 896, the Troodos Ophiolite, and Site 786 (IBM forearc). Site 896 data from Teagle et al. (1996). Troodos Ophiolite data from Gillis (1987). IBM data from Alt et al. (1998).

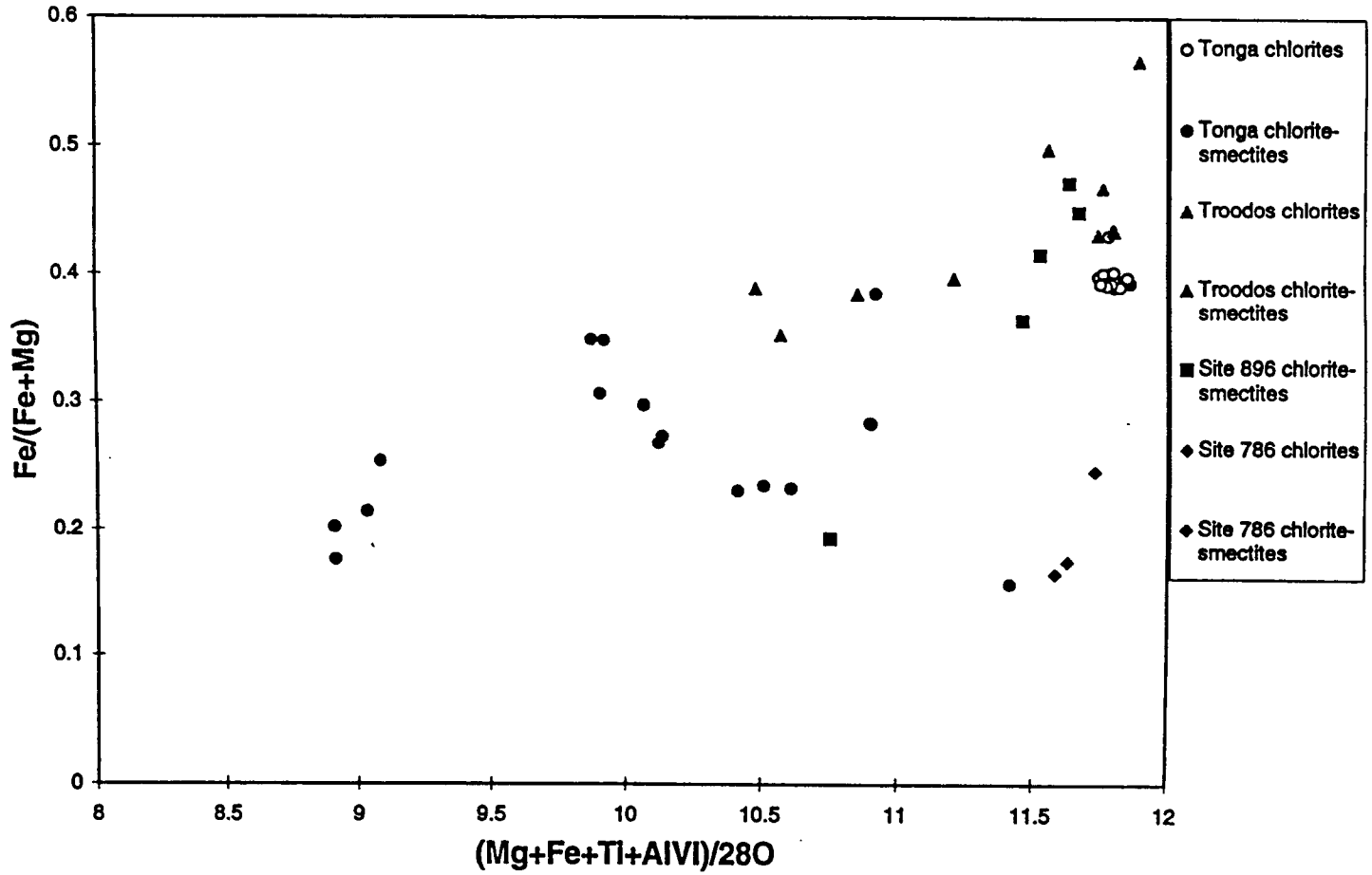

Figure 53. Fe/(Fe+Mg) versus octahedral total (calculated for 28 O) for chlorites and chlorite-smectites from the Tonga forearc, Site 896, the Troodos Ophiolite, and Site 786 (IBM forearc). Site 896 data from Teagle et al. (1996). Troodos Ophiolite data from Gillis (1987). IBM data from Alt et al. (1998).

Celadonite has not been found in conjunction with dioctahedral smectite but where celadonite or saponite-celadonite is present, the sequence of precipitation is:

celadonite---> saponite-celadonite---> saponite

This sequence may repeat several times within a single vein and may be reversed. Thus, a general trend of increasing saponite content with time is seen in veins and vesicles.

The trend of increasing saponite content with time correlates fairly well with chemical zonation of some elements within the clay minerals themselves. Mg in clays tends to increase towards the centers of veins, just as Mg content increases with increasing saponite component (Figure 31). Si either decreases slightly with time, or stays the same. Other elements vary less definitively across transects within the same clay mineral.

3.3 Zeolites

Zeolite structures are generally identified based on Al:Si ratio and then further classified based on Ca + Mg, Na, and K content (Deer et al., 1962). In the Tonga forearc samples, phillipsite, $(1/2Ca, Na, K)_3(Al_3Si_5O_{16})\cdot 6H_2O$ (Deer et al., 1962), is common and was identified based on petrography (which was used to determine only that it was a zeolite) and electron microprobe analyses which indicated, based on Al:Si ratio and K content, which zeolite was present (Figure 54). Phillipsite was also identified in some

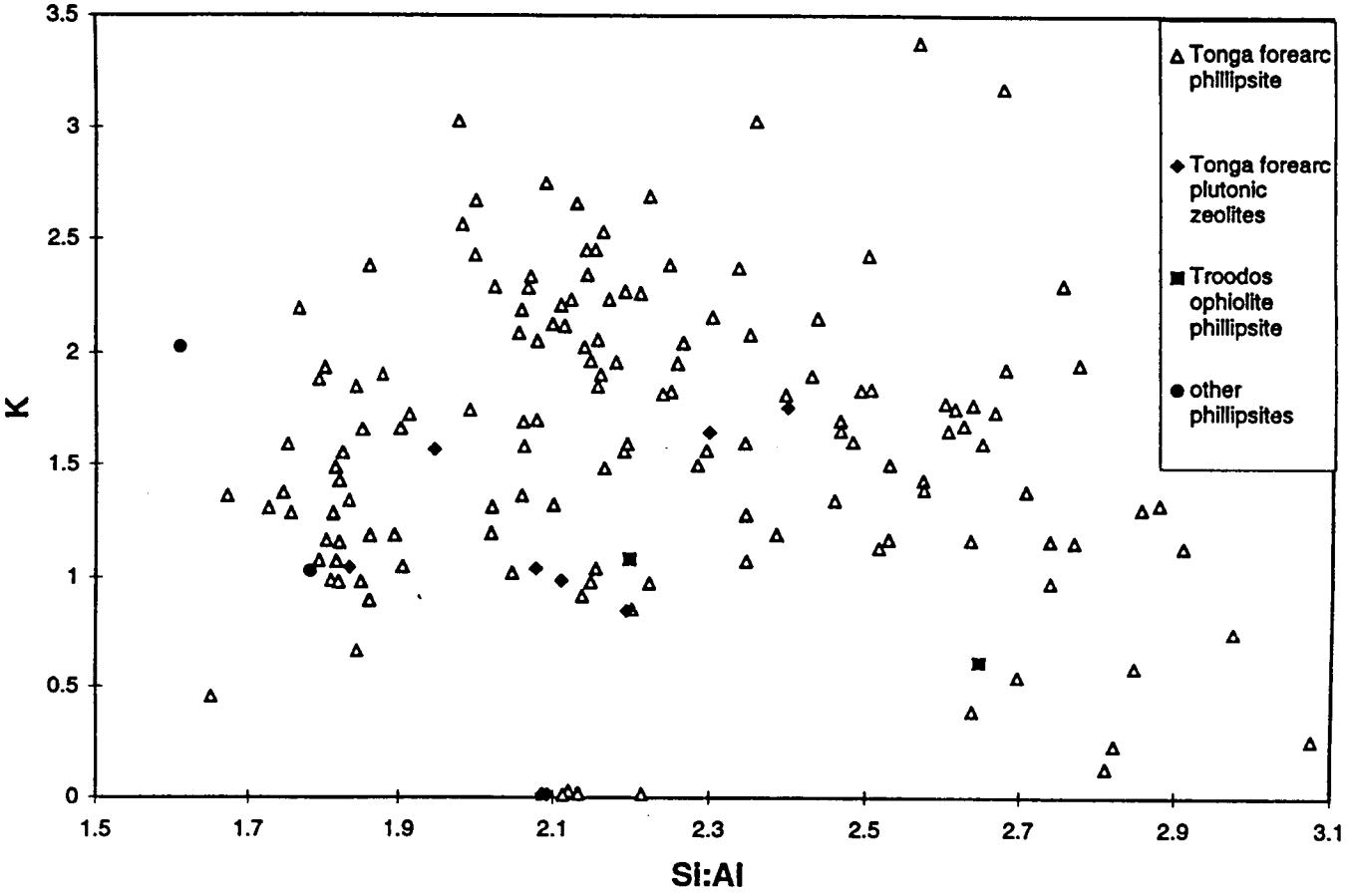

Figure 54. K versus Si:Al ratio for Tonga forearc zeolites and other zeolites. Tonga forearc plutonic zeolite data from Neil Banerjee (unpublished data). Troodos Ophiolite phillipsites are from Gillis (1987). "Other" phillipsites are from basalts from Hawaii and Sicily (Deer et al., 1962).

samples using XRD d-spacing spectra, from the peaks at 10, 7.2, and 3.2 Å (Brindley and Brown, 1980).

Phillipsite occurs as radiating aggregates of acicular crystals lining veins and voids (Figure 26). It generally follows clay minerals and precedes carbonates. Quartz may occur as an earlier, later, or contemporaneous phase (in this case, sometimes intimately mixed as fine grains).

A few zeolite grains were tentatively identified petrographically as chabazite (based on their rhombohedral crystal habit), although no microprobe analyses or XRD spectra confirmed this. Since chabazite is similar in Al:Si ratio to phillipsite and commonly occurs in association with it in altered basalts (e.g. Alt and Honnorez, 1984; Gillis, 1987), its presence would be plausible.

Phillipsite is a low-Ca zeolite, which forms in basaltic rocks altered at low temperatures (Deer et al., 1962). Phillipsite in the Tonga samples has a wide range in Na and K contents but contains little Ca (Figure 55). High Si content may be due to compositional variations or to fine-scale mixing with silica. Representative microprobe analyses of phillipsite are shown in Table 5.

3.4 Epidote

Epidote, Ca_2Al_2O (Al, Fe^{3+})$OH[Si_2O_7][SiO_4]$ (Deer et al., 1992), occurs as well-developed prismatic radiating sprays of yellow crystals (Figure 29) in samples affected by high temperature alteration. In pervasively altered zones it is intimately associated with

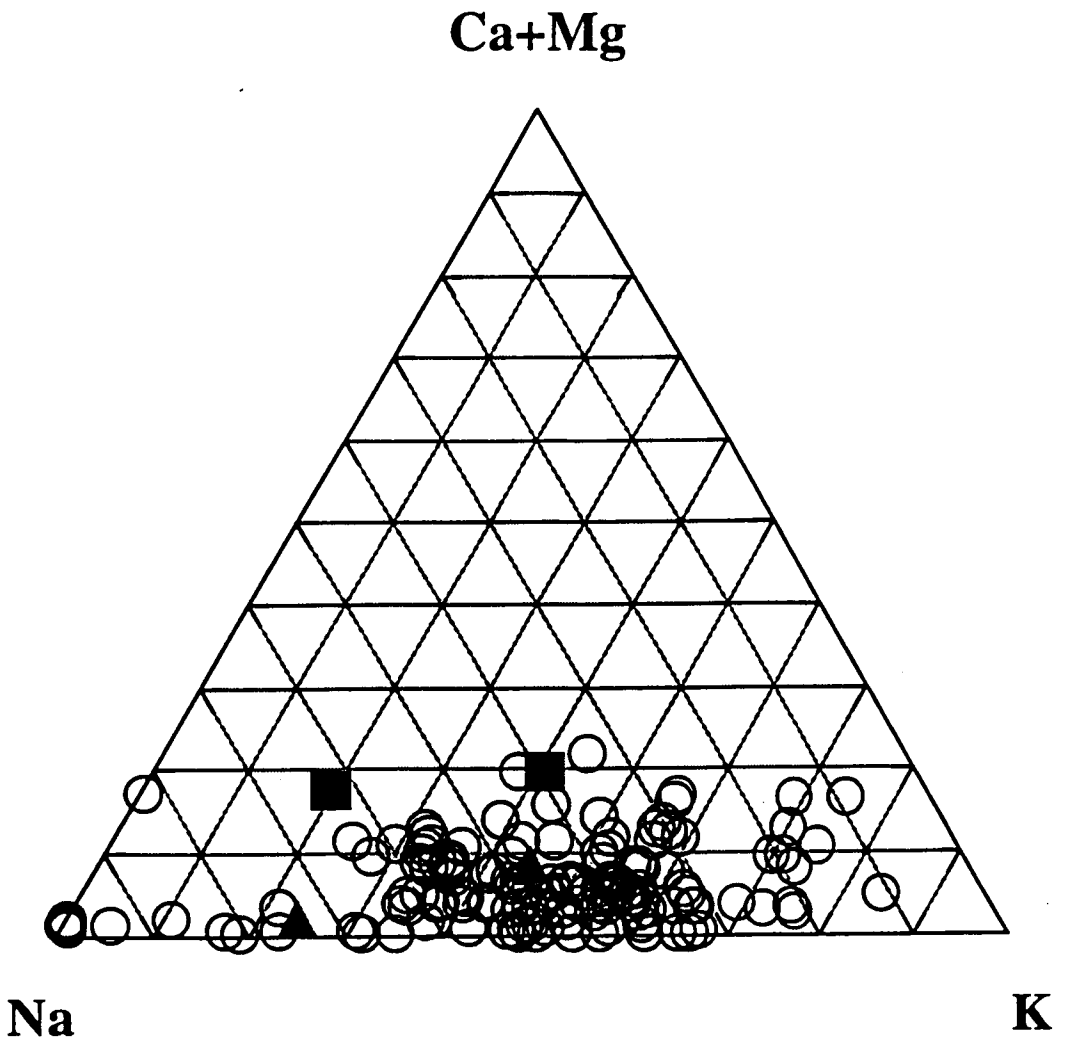

Figure 55. Na-Ca+Mg-K ternary plot for Tonga forearc phillipsites and other zeolites. Triangles are Troodos Ophiolite phillipsites (Gillis, 1987). Squares are phillipsites from basalts from Hawaii and Sicily (Deer et al., 1962).

sample	90-2-10	90-2-10	90-1-5	90-2-10
mineral	phillipsite	phillipsite	phillipsite	phillipsite
occurrence	vein	vein	vein	vein
SiO_2	68.63	59.11	54.20	48.81
TiO_2	0.01	0.00	0.02	0.54
Al_2O_3	20.63	23.73	23.26	22.71
FeO	0.06	0.11	0.18	1.33
MnO	0.01	0.00	0.01	1.37
MgO	0.00	0.02	0.09	1.03
CaO	0.03	0.38	0.69	2.18
Na_2O	3.14	11.05	3.11	4.26
K_2O	1.01	0.04	11.96	5.80
Cr_2O_4	0.00	0.01	0.01	0.00
Total	93.54	94.47	93.59	88.09

Table 5. Representative electron microprobe analyses of phillipsites.

chlorite, quartz, and opaque minerals. In less pervasively altered parts of samples it occurs as occasional small crystals, often associated with cryptocrystalline chlorite and/or quartz.

3.5 Other Secondary Minerals

3.5.1 Potassium Feldspar

K-feldspar, (K, Na)[$AlSi_3O_8$] (Deer et al., 1962), was identified in several samples based on electron microprobe analyses and petrography. Analyses show a K-rich phase which commonly replaces other feldspars, although it has a higher Na content than typical K-feldspars occurring in altered oceanic crust (e.g. Alt and Honnorez, 1984; Gillis et al., 1992). This same phase fills veins rarely. Although microprobe analyses cannot confirm its presence in all low temperature samples, petrography and the number of bulk chemical analyses high in K (to be discussed in Chapter 4) suggest that it is common. (Secondary K-feldspar forms at <50-140°C [Bohlke et al., 1984; Munha et al., 1980].) Representative microprobe analyses of K-feldspar are shown in Table 6.

3.5.2 Fe-oxyhydroxides

Fe-oxyhydroxides (probably goethite) were identified petrographically in almost all samples subjected to low-temperature alteration and seafloor weathering. Fe-oxyhydroxides tend to replace groundmass material, may form slight haloes around veins,

sample	87-2-2	87-2-2	87-2-2	87-2-2
mineral	K-feldspar	K-feldspar	K-feldspar	K-feldspar
occurrence	after plag	after plag	vein	after plag
SiO_2	65.65	63.67	59.14	62.47
TiO_2	0.00	0.00	0.00	0.00
Al_2O_3	21.59	20.30	19.54	19.82
FeO	0.03	0.07	0.17	0.04
MgO	0.01	0.00	0.02	0.01
CaO	0.01	0.06	0.00	0.01
Na_2O	4.21	3.47	6.93	3.83
K_2O	9.35	13.98	14.07	14.12
Total	**100.85**	**101.56**	**99.88**	**100.29**

Table 6. Representative electron microprobe analyses of K-feldspars.

and may be mixed with smectites. Fe-oxyhydroxides tend to be amorphous. A common occurrence is as the first material lining a vesicle (usually followed by some mixture of smectite minerals). Hematite (identified petrographically) also occurs in the groundmass of several samples.

3.5.3 Carbonates

Carbonates (probably calcite) were identified petrographically in several samples. They commonly fill fractures, generally as the last phase (other than possibly silica) to be deposited. Such carbonate-filled fractures are most common in heavily brecciated zones, especially brecciated glassy rinds. Carbonates are common as one of the last vein phases to precipitate in most hydrothermally altered oceanic basalts.

3.5.4 Silica

Silica veins, probably chalcedony (based on petrography and on the low alteration temperatures determined from other secondary minerals), occur in most samples, except for those showing only minimal alteration. Silica veins generally occur late during alteration and may be the last veins to form. Fine-grained silica may also be intimately mixed with zeolites or clay minerals. Groundmass quartz appears in samples containing high temperature assemblages.

3.5.5 Amphibole

A few samples affected by high temperature alteration contain fibrous greenish hydrothermal amphibole, probably actinolite, replacing pyroxene. Its presence was not verified by microprobe analyses.

3.6 Alteration of glass

Few samples analyzed by microprobe have significant glassy rinds. For those where such a rind is present, it is usually fractured and altered with assemblages similar to those of veins and vesicles, particularly saponite, saponite-celadonite, dioctahedral smectite, K-feldspar, phillipsite, calcite, and silica (Figure 28). Groundmass glass is altered to saponite-celadonite and saponite in low temperature samples, and to chlorite + epidote + quartz ± opaques in high temperature samples.

3.7 Summary

Secondary mineralogies for samples altered at high and low temperatures are summarized in Table 7. Alteration minerals versus temperature are shown in Figure 56. Alteration mineralogies of Tonga forearc volcanic rocks are relatively similar to those in the Troodos Ophiolite. Seafloor weathering, as defined for the Tonga forearc, is similar to the Seafloor Weathering Zone defined for the Troodos Ophiolite in its red, oxidized appearance (Gillis, 1987; Gillis and Robinson, 1990).

Table 7. (Following page) Summary of characteristics of seafloor weathering, low temperature alteration, and high temperature alteration.

Alteration Type	Phenocrysts	Groundmass	Glassy Margins	Vesicles/Veins	Extent of Alteration
Seafloor Weathering	olivine---> Fe-oxyhydroxides plagioclase---> smectite pyroxene---> smectite	plagioclase---> smectite + Fe-oxyhydroxides mesostasis---> smectite + Fe-oxyhydroxides (red or red-brown staining)	(red or red-brown staining)	Fe-oxyhydroxides +/- smectite	slight to pervasive
Low Temperature (<200 degrees C)	plagioclase---> K-feldspar + saponite + saponite-celadonite + dioctahedral smectite +/- silica +/- sericite	plagioclase---> smectite clinopyroxene---> smectite mesostasis---> saponite + saponite-celadonite + chlorite-smectite	saponite + saponite-celadonite + dioctahedral smectite + phillipsite + silica	saponite + saponite-celadonite + celadonite + dioctahedral smectite + dioctahedral smectite-saponite + chlorite-smectite + (Fe-oxyhydroxides) + phillipsite + silica + calcite	slight to pervasive
	olivine---> goethite + saponite + saponite-celadonite + dioctahedral smectite + calcite			Order of deposition: (1. Fe-oxyhydroxides) 2. smectite or chlorite/smectite (3. celadonite) 4. phillipsite and/or calcite 5. silica	
	clino- or orthopyroxene (mostly fresh)---> dioctahedral smectite + saponite				
High Temperature (>200 degrees C)	plagioclase---> epidote + chlorite + quartz +/- albite +/- sericite clinopyroxene---> actinolite +/- smectite	mesostasis---> chlorite + epidote + quartz +/- opaques	chlorite + quartz + smectite	quartz + chlorite + epidote +/- opaques	slight to pervasive

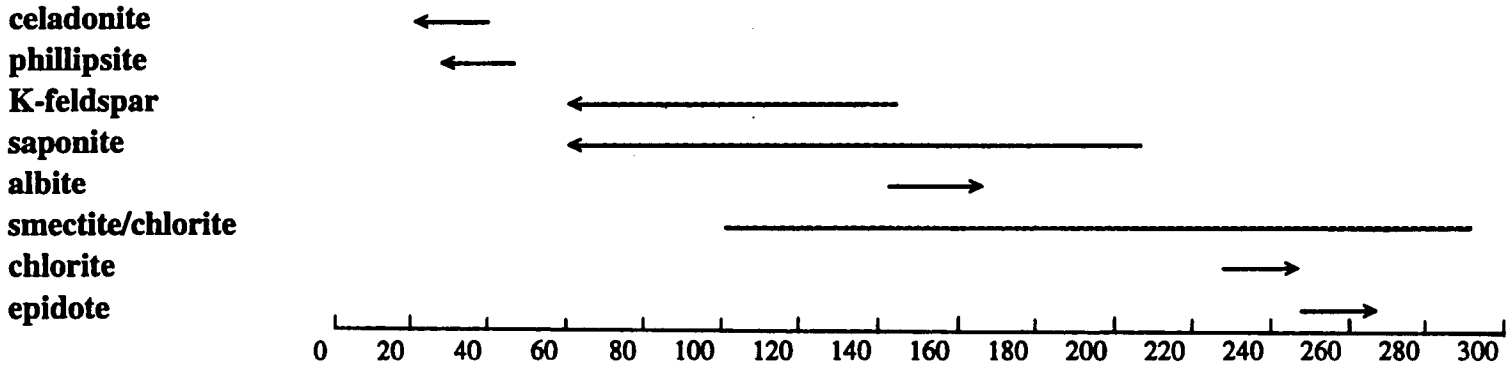

Figure 56. Alteration mineralogy versus temperature. Temperature data are from Kristmannsdottir (1975), Bohlke et al. (1984), Kastner and Gieskes (1976), Stakes and O'Neil (1982), Iijima and Utada (1971), Munha et al. (1980), Honnorez et al. (1983), Seyfried et al. (1978), Friedrichsen (1985), Honnorez (1978), and Liou et al. (1985).

The low temperature alteration defined for the Tonga forearc is broadly similar to the Low Temperature Zone defined for the Troodos Ophiolite (Gillis, 1987; Gillis and Robinson, 1990) in its alteration assemblages, although the variety of zeolites observed in the Troodos Ophiolite is much greater. This may be due in part to the larger number of zeolites analyzed in the Troodos Ophiolite, although there are probably chemical differences between the two locations which could be better understood if stratigraphic information were available for Tonga. Low temperature Tonga forearc alteration is somewhat similar to the dark gray alteration described by Alt et al. (1996a,b) for Site 504, and to that described for Site 896 (Teagle et al., 1996), although Site 896 lacks celadonite. Some differences between Site 896 and other locations may be due to its location on a local heat flow maximum, where basement fluids are upwelling (Teagle et al., 1996). Tonga forearc low temperature alteration is also very similar to the secondary mineralization at Site 786 in the IBM forearc, except for the absence of analcite in Tonga (Alt et al., 1998).

The high temperature alteration seen in the Tonga forearc isn't clearly analogous to a specific alteration zone defined for the Troodos Ophiolite, but the assemblage of epidote + chlorite + quartz is seen in epidotized rocks in the Upper Dike Zone of the Troodos Ophiolite (Gillis and Robinson, 1990), and these minerals are also seen in breccia zones in the upper transition zone at Site 504 (Alt et al., 1996a,b).

The relative timing of alteration processes in the Tonga forearc is broadly similar to what has been observed in the Troodos Ophiolite. In the Troodos Ophiolite, there was circulation of cool seawater (<100°C) in the volcanic section during and shortly after

emplacement (Gillis, 1987). In Tonga, similar events could have produced the seafloor weathering seen in many samples and, as seawater evolved (becoming more oxygen-poor and alkaline) as it passed deeper into the volcanic section, the low temperature alteration could also have developed. Zeolites in the Tonga forearc, which generally followed clays, are restricted to fractures and voids, meaning that they must have precipitated late, along preferred fluid pathways. Tonga processes are somewhat different from Site 504 processes because at Site 504, initial black haloes formed due to interaction of Fe-rich solutions with the rock; this was then followed by alteration involving the movement of cold oxidizing seawater through fractures (Alt et al., 1996a,b). In Tonga, however, interaction of rocks with cold oxidizing seawater was first, and there are no significant black haloes around veins. Tonga forearc alteration processes, particularly at low temperatures, also appear to have been relatively similar to those at Site 786 in the IBM forearc. At Site 786, the pattern of phyllosilicate, then zeolite, then carbonate deposition in veins (Alt et al., 1998) is similar to what is observed in the Tonga forearc, suggesting that fluid compositional changes and progressive cooling of fluids with time are similar for the two settings.

Chapter 4. Bulk Rock Geochemistry

4.1 Introduction

Various methods may be used to evaluate how bulk rock compositions are affected by hydrothermal alteration. If a fresh rock is available or its composition can be determined with reasonable accuracy, elemental fluxes due to alteration (what was gained or lost) may be calculated. Where this is not possible (for example, when dealing with dredge samples whose fresh bulk compositions cannot be quantified), trends of depletion or enrichment of elements may still be qualitatively examined by comparing elemental concentrations to some indicator of the extent of alteration. For this study, elemental contents were compared to Loss-On-Ignition (LOI) of samples. (Details of LOI procedures are in Appendix I, under the description of ICP-AES procedures.) LOI tests measure the amount of volatile materials in samples (which are not measured by some other bulk chemical methods). In addition to plotting LOI versus elements of interest directly, samples were classed as "fresh" or "altered" based on LOI, in order to make alteration trends easier to recognize graphically. For tholeiites and arc tholeiites, samples with LOI<2 weight % are classed as fresh, and those with LOI>2 weight % are classed as altered. Due to the higher primary volatile content of boninites, these samples are classed as fresh if LOI<5.5 weight % and altered if LOI>5.5 weight %. "Fresh" and "altered" tholeiites, arc tholeiites, and boninites dredged from this transect yield similar ranges of TiO_2 and Zr concentrations (Figure 17), indicating that the fresh samples can reasonably be considered to represent initial compositional ranges for the altered samples. (These

two elements are generally considered to be immobile during hydrothermal alteration.) Apart from this very broad classification of samples as "fresh" or "altered", looking at how specific elements varied with LOI also allowed some qualification of chemical trends. It was not possible to compare geochemical trends between high temperature alteration, low temperature alteration, and seafloor weathering because of the very small number of high temperature samples identified, and because low temperature alteration and seafloor weathering commonly occur together (within the same sample).

Major and trace element analyses were performed at the Oregon State University Department of Oceanography, using Inductively-Coupled Plasma Atomic Emission Spectrometry (ICP-AES) (details are given in Appendix I). Additional bulk chemical data (including all analyses outside of transect 87-91) were provided by Trevor Falloon at the University of Tasmania. Comparison data are from the CY-1 drillcore of the Troodos Ophiolite (Gibson et al., 1991).

4.2 Major element trends

Major element trends may be due to variations in primary compositions of the rocks compared, as well as due to alteration. However, within each defined rock type (e.g. boninites), major element contents in fresh rocks should be similar within a certain range. Major element contents versus LOI (which should increase with extent of alteration) are shown in Figures 57a-k. These figures include data from the entire forearc, not just from transect 87-91, since the smaller number of analyses available with data only from this transect made it difficult to recognize meaningful trends due to alteration. The most

Figure 57. (Following pages) A-j show major element contents of Tonga forearc bulk rocks, plotted versus LOI to show extent of alteration. Some data from dredges 88-91 are from Trevor Falloon (unpublished data). Error bars are shown in the top left of each plot for each major element. If no error bar is shown, the error bar is smaller than the symbol. 57k shows CaO versus Na_2O for the same sample set. Symbols for Figure 57a-k are defined on Figure 57a.

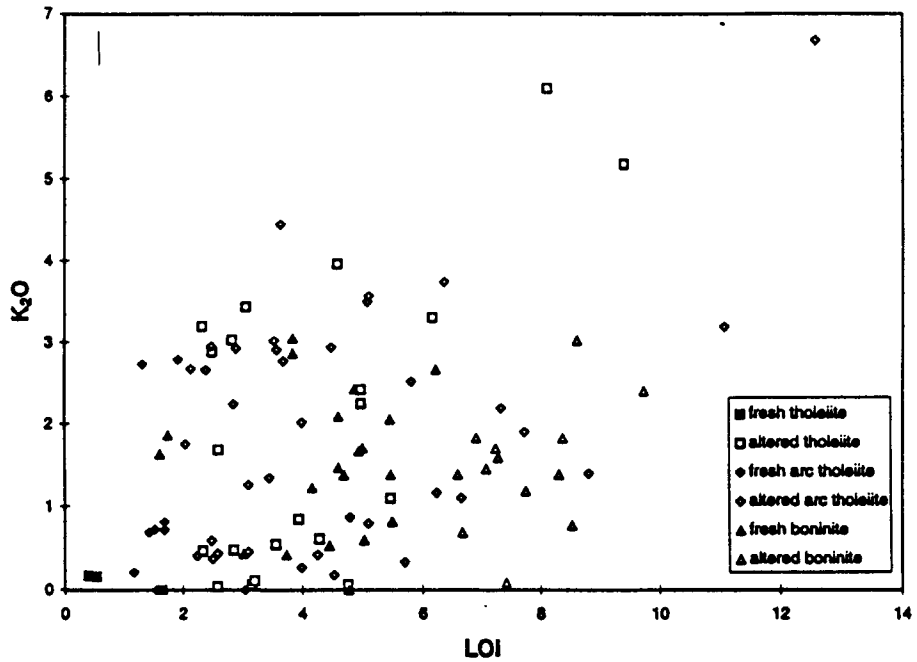
K2O
LOI
fresh tholeiite
altered tholeiite
fresh arc tholeiite
altered arc tholeiite
fresh boninite
altered boninite

57a.

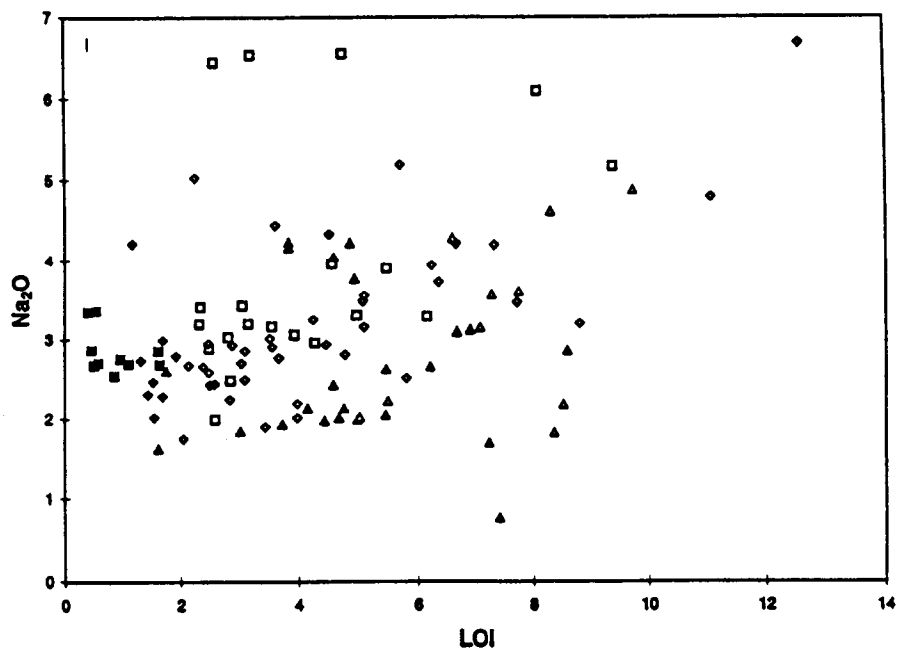
Na2O
LOI

57b.

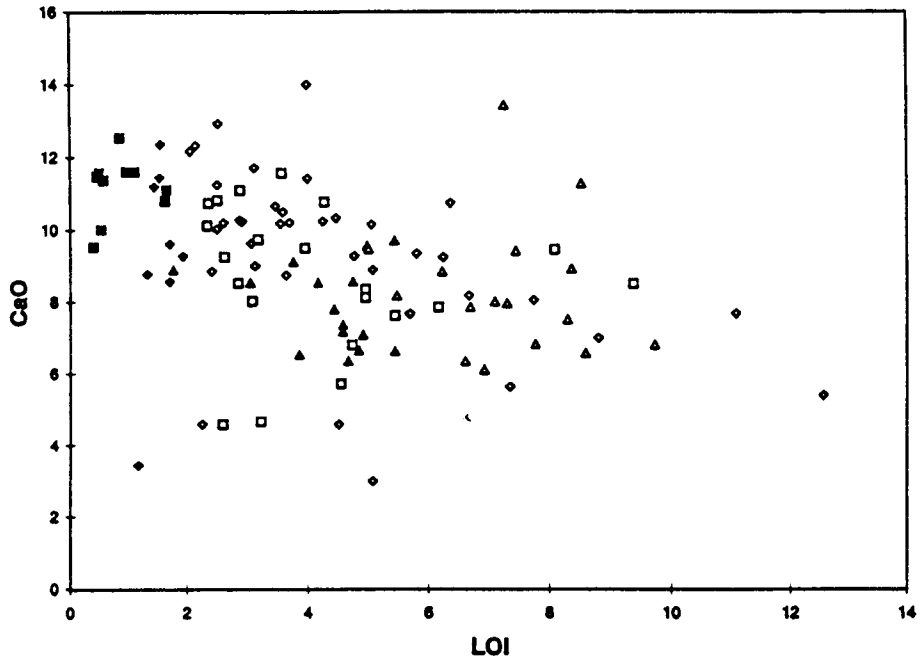

57c.

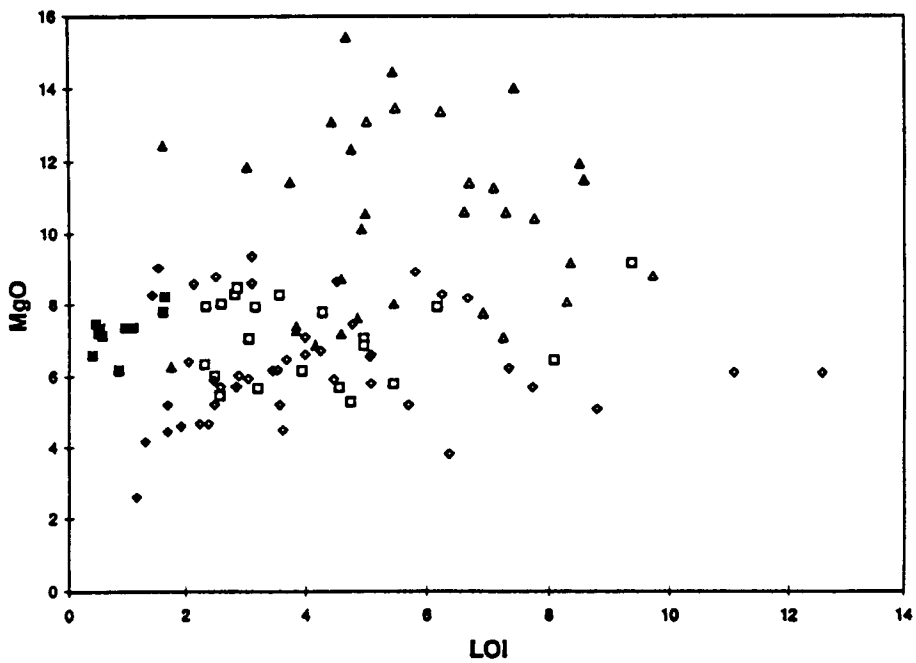

57d.

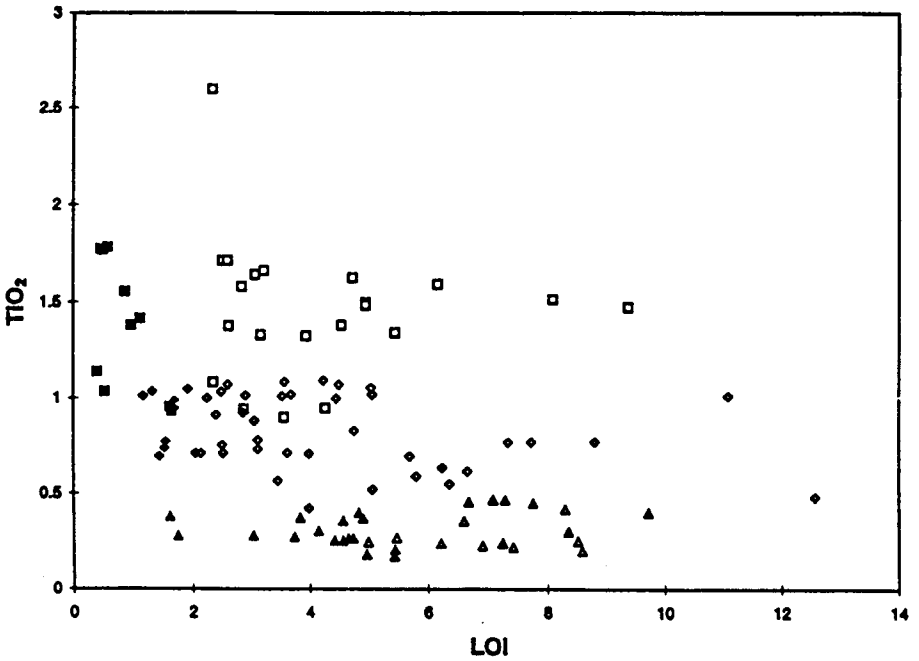
TiO2
LOI
0
0.5
1
1.5
2
2.5
3
0
2
4
6
8
10
12
14

57e.

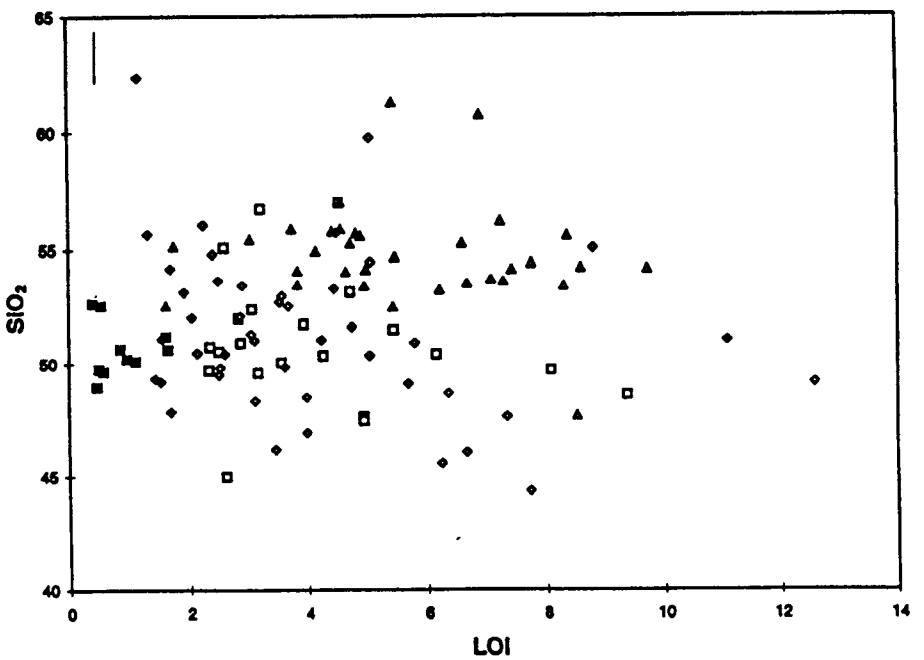
SiO2
LOI
40
45
50
55
60
65
0
2
4
6
8
10
12
14

57f.

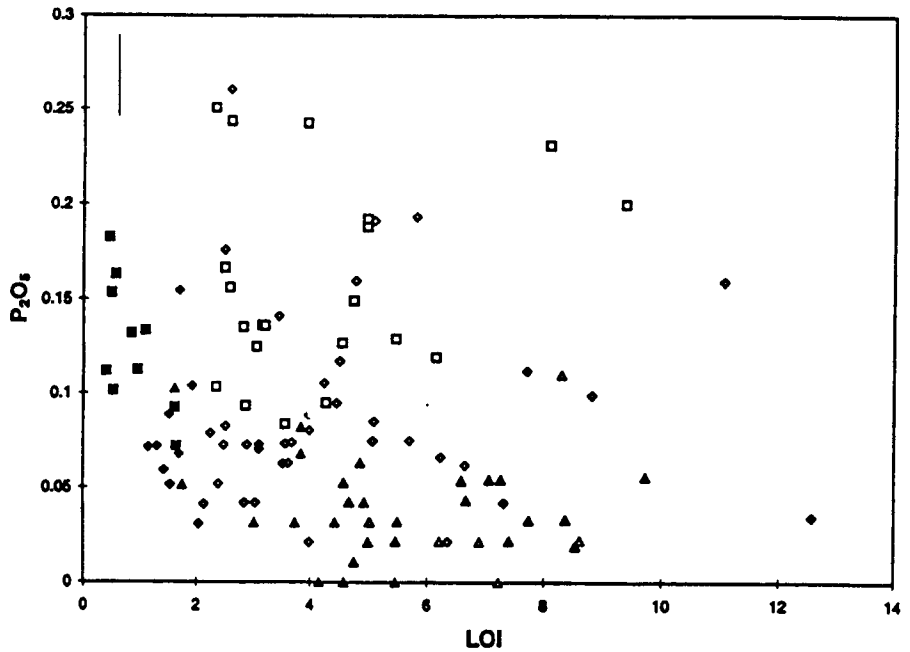
0.3
0.25
0.2
0.15
0.1
0.05
0
P_2O_5
0
2
4
6
8
10
12
14
LOI

57g.

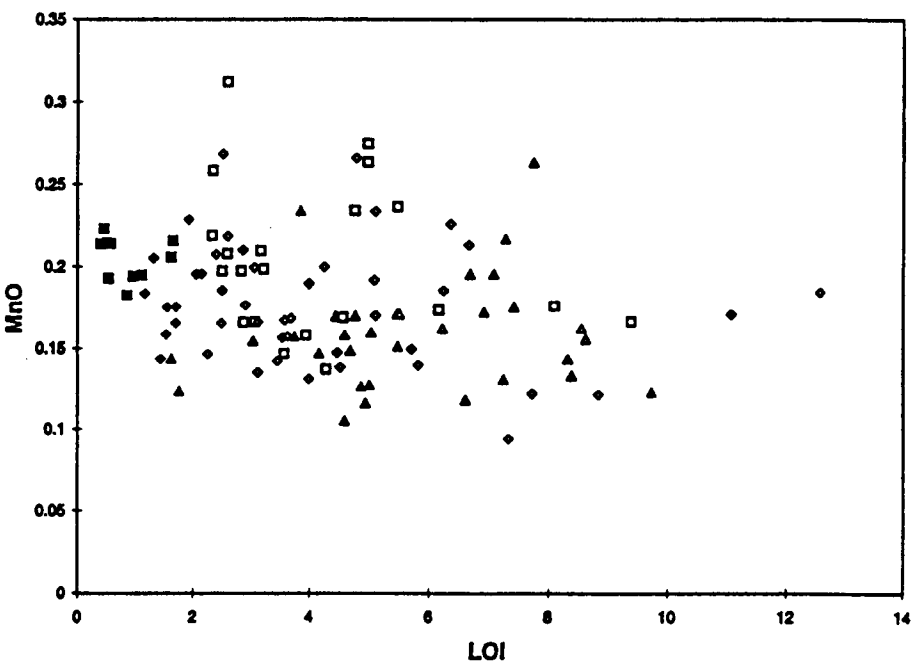
0.35
0.3
0.25
0.2
0.15
0.1
0.05
0
MnO
0
2
4
6
8
10
12
14
LOI

57h.

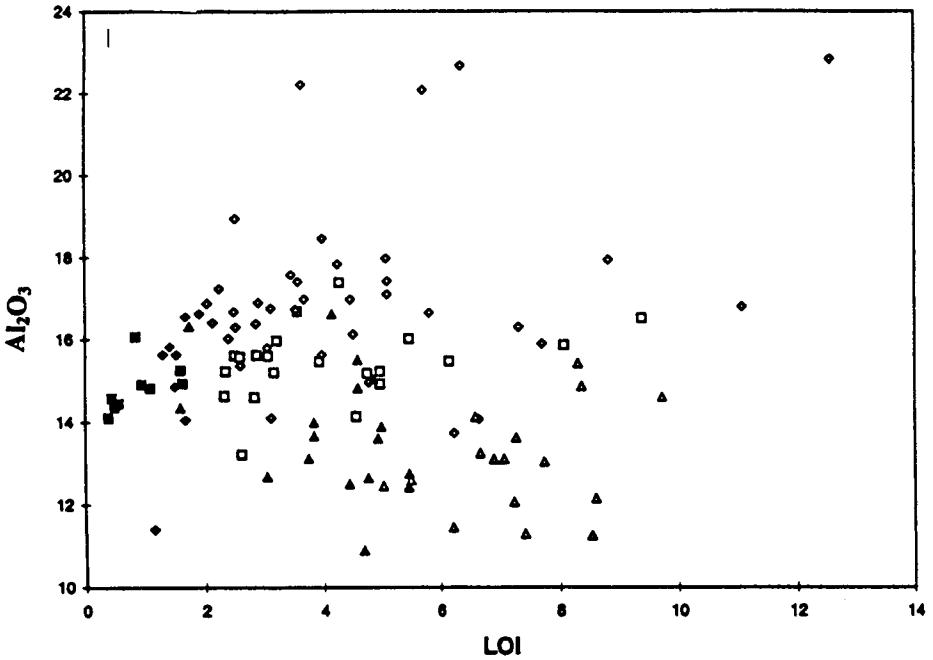
24
22
20
18
16
14
12
10
Al_2O_3
0
2
4
6
8
10
12
14
LOI

57i.

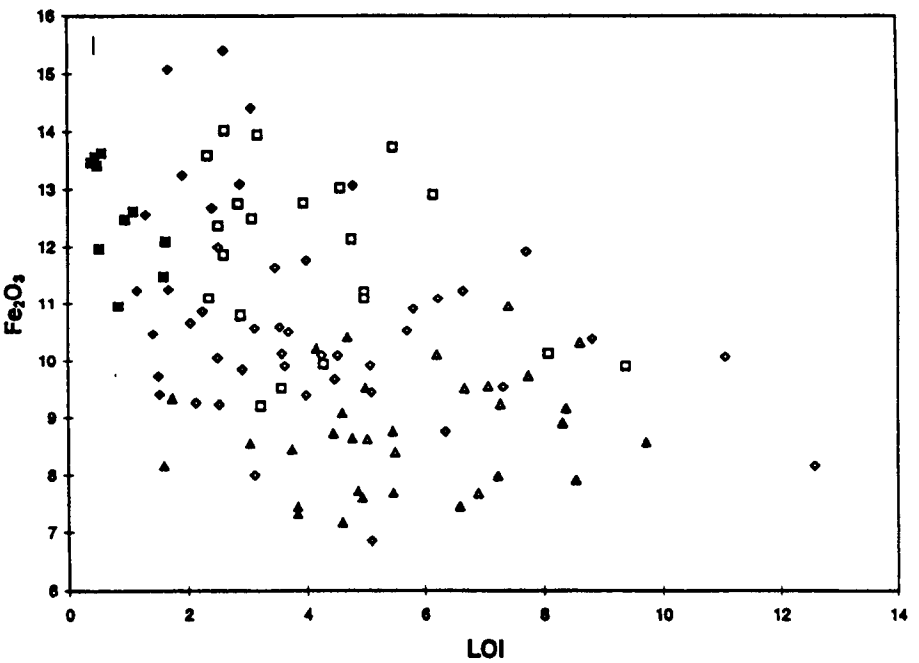
16
15
14
13
12
11
10
9
8
7
6
Fe_2O_3
0
2
4
6
8
10
12
14
LOI

57j.

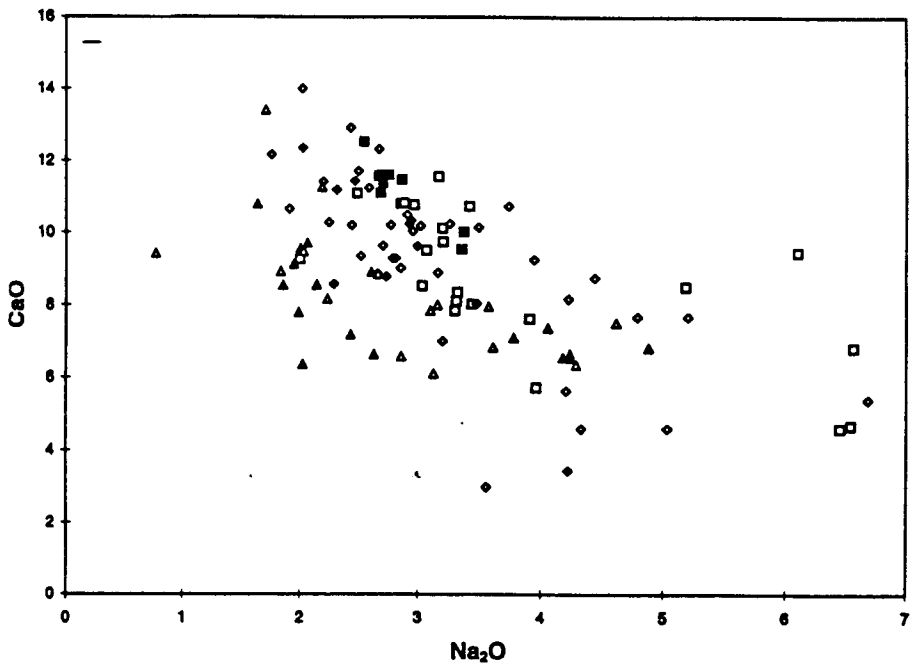

57k.

pronounced trend is the enrichment of K_2O in tholeiites and arc tholeiites (Figure 57a). Na_2O is enriched in tholeiites and in some arc tholeiites (Figure 57b). CaO is depleted in tholeiites and unchanged in arc tholeiites (Figure 57c). Alteration effects for Na_2O and CaO in transect 87-91 alone are similar but less pronounced to those for the entire forearc, while enrichments in K_2O are much stronger in transect 87-91 than in the rest of the forearc. MgO (Figure 57d) and TiO_2 (Figure 57e) are not significantly affected by alteration. SiO_2 (Figure 57f) may be mobilized in tholeiites, as altered samples show a wider range of SiO_2 values than do fresh samples. SiO_2 is unchanged in arc tholeiites. P_2O_5 (Figure 57g) is slightly enriched in arc tholeiites and in some tholeiites. MnO (Figure 57h) is enriched in tholeiites and unchanged in arc tholeiites. Al_2O_3 (Figure 57i) is enriched in arc tholeiites and unchanged in tholeiites; its apparent enrichment in arc tholeiites may be due to phenocryst accumulation. FeO (Figure 57j) is slightly depleted in tholeiites and is mobilized in arc tholeiites. A weak negative correlation exists between Ca and Na in the sample set as a whole (Figure 57k), which is may be due to partial albitization of plagioclase (at the upper end of the probable temperature range for low temperature alteration, since albite forms at >140°C [Munha et al., 1980; Honnorez et al., 1983]). Boninites do not show any recognizable major element trends due to alteration. This may be due to the fact that most boninites examined were not highly altered. Alternatively, it may be due to the inappropriateness of using LOI as an indicator of extent of alteration in boninites, since they contain larger amounts of volatiles than tholeiites and arc tholeiites to begin with. Trends in samples from transect 87-91

generally parallel those for the entire forearc (where trends within transect 87-91 alone are actually recognizable).

Ti, Zr, and MgO contents measured for the CY-1 drillcore of the Troodos Ophiolite suggest similar starting compositions to Tonga forearc arc tholeiites (Figure 58, Figure 59). A comparison of the portion of the CY-1 drillcore subjected to low-temperature alteration with Tonga arc tholeiites shows that K_2O contents in both are high, ranging up to 7-8 weight % (Figure 60a). In the CY-1 drillcore, the upper 300 m are enriched in K_2O with respect to the lower 200 m (Gillis, 1987). Without stratigraphic relationships, it cannot be determined if this is also true for Tonga forearc samples. Tonga volcanic samples tend to be higher in Na_2O than Troodos Ophiolite CY-1 samples (Figure 60b), in which the upper portion of the section is depleted with respect to the lower portion. High Na_2O in the Tonga samples as a whole (due to its common inclusion in clays and zeolites) suggests this may be a relevant difference between alteration at the two localities. As most Tonga forearc alteration occurred at low temperatures and no significant albitization of plagioclase has been observed, albitization is probably not responsible for the high Na_2O. Tonga samples generally contain higher Si than Troodos samples. These comparisons suggest that the Tonga volcanic sample suite is more analogous to the upper 300 m of the CY-1 drillcore than to the lower portion.

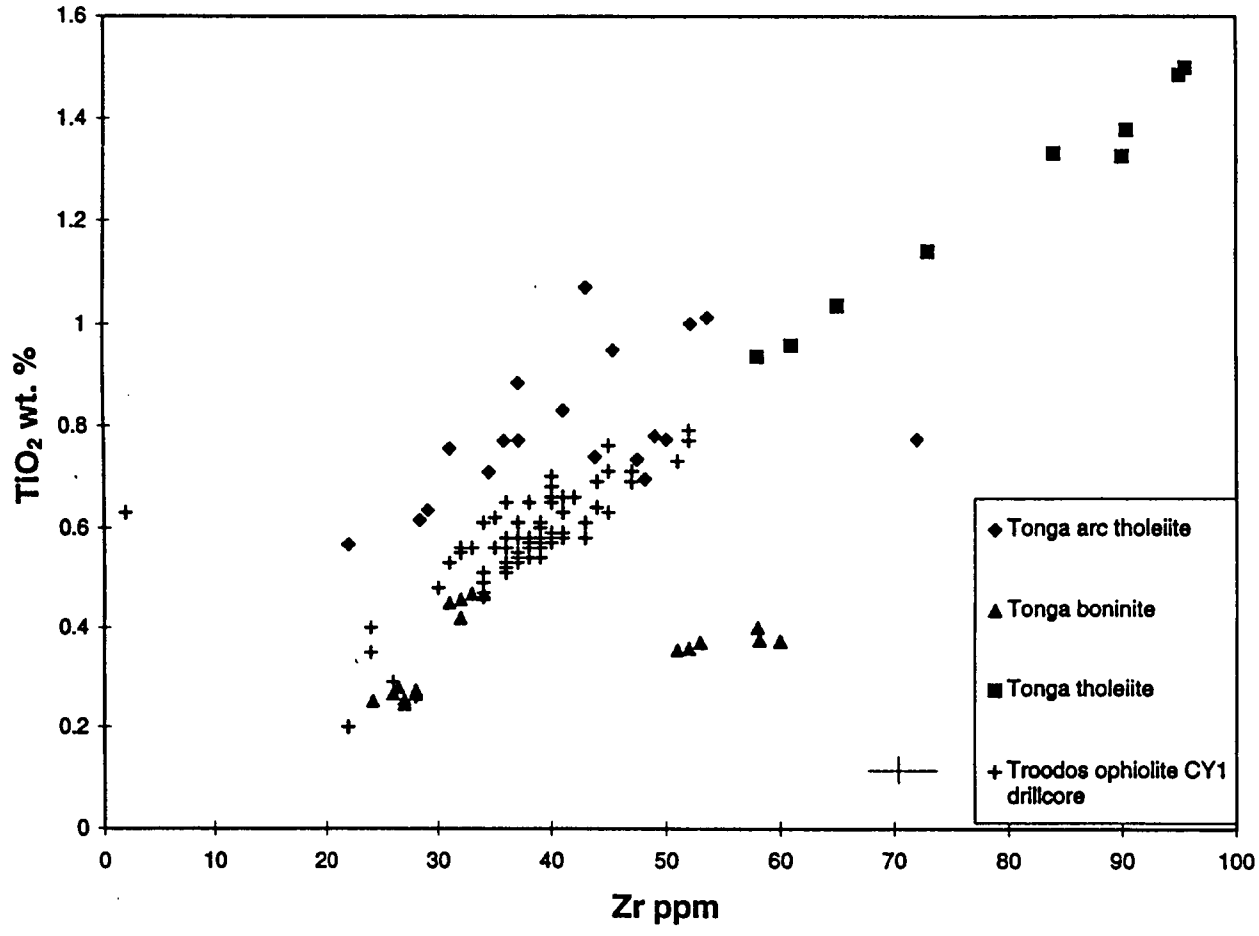

Figure 58. TiO_2 versus Zr for Tonga forearc volcanic samples (some data from dredges 88-91 are from Trevor Falloon [unpublished data]) and the CY-1 drillcore from the Troodos Ophiolite (Gibson et al., 1991).

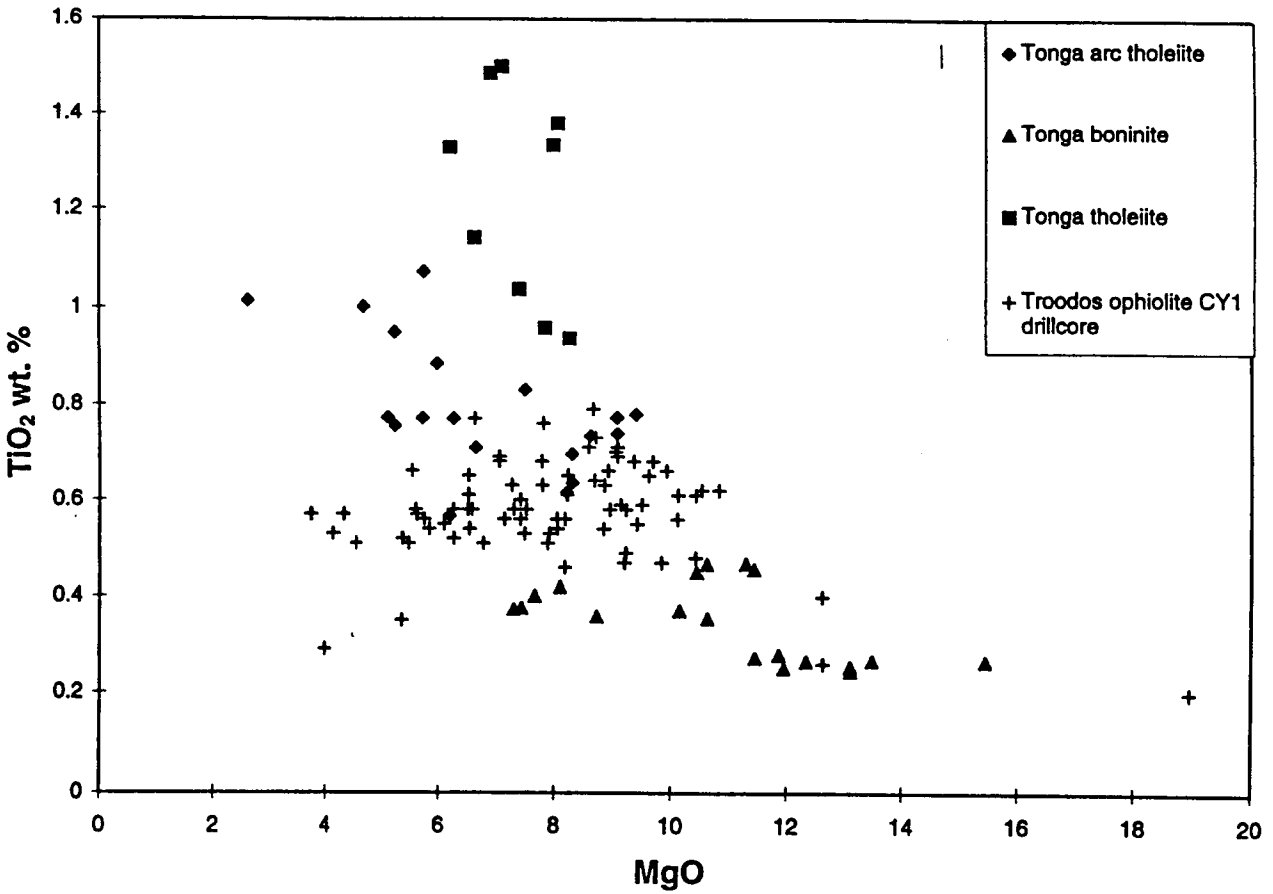

Figure 59. TiO_2 versus MgO for Tonga forearc volcanic samples (some data from dredges 88-91 are from Trevor Falloon [unpublished data]) and the CY-1 drillcore from the Troodos Ophiolite (Gibson et al., 1991).

Figure 60. (Following page) A-b show certain major elements versus Zr for Tonga forearc volcanic samples (some data from dredges 88-91 are from Trevor Falloon [unpublished data]) and the CY1 drillcore from the Troodos Ophiolite (Gibson et al., 1991). The upper and lower CY-1 drillcore are shown separately. Symbols for Figure 60a-b are defined on Figure 60a.

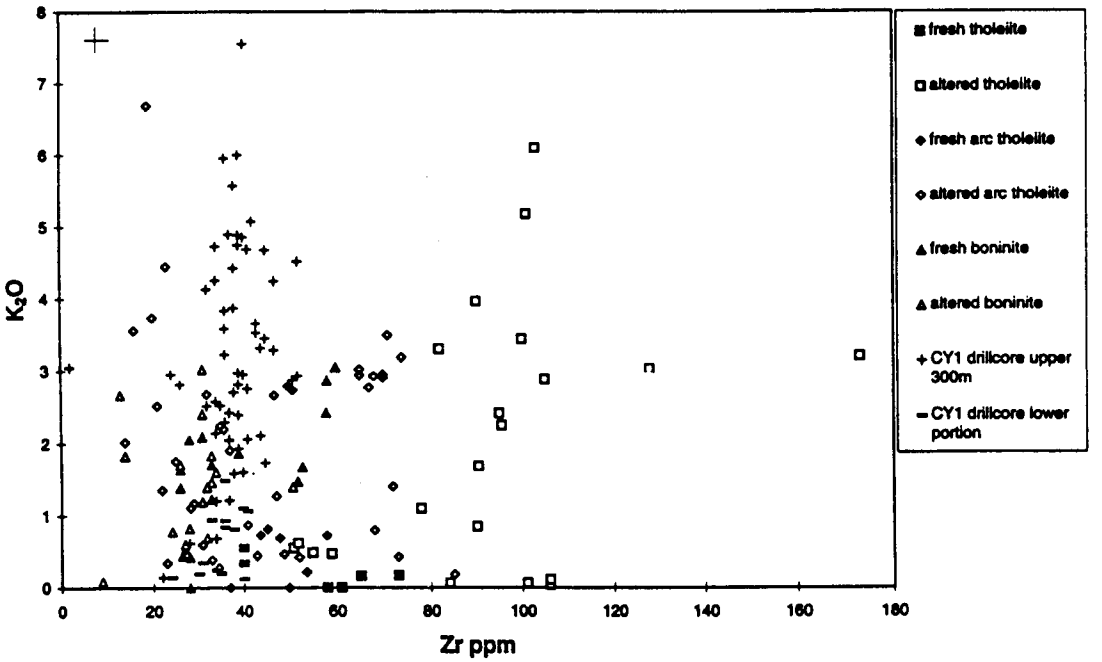
fresh tholeiite
altered tholeiite
fresh arc tholeiite
altered arc tholeiite
fresh boninite
altered boninite
CY1 drillcore upper 300m
CY1 drillcore lower portion
K2O
Zr ppm
0
1
2
3
4
5
6
7
8
0
20
40
60
80
100
120
140
160
180

60a.

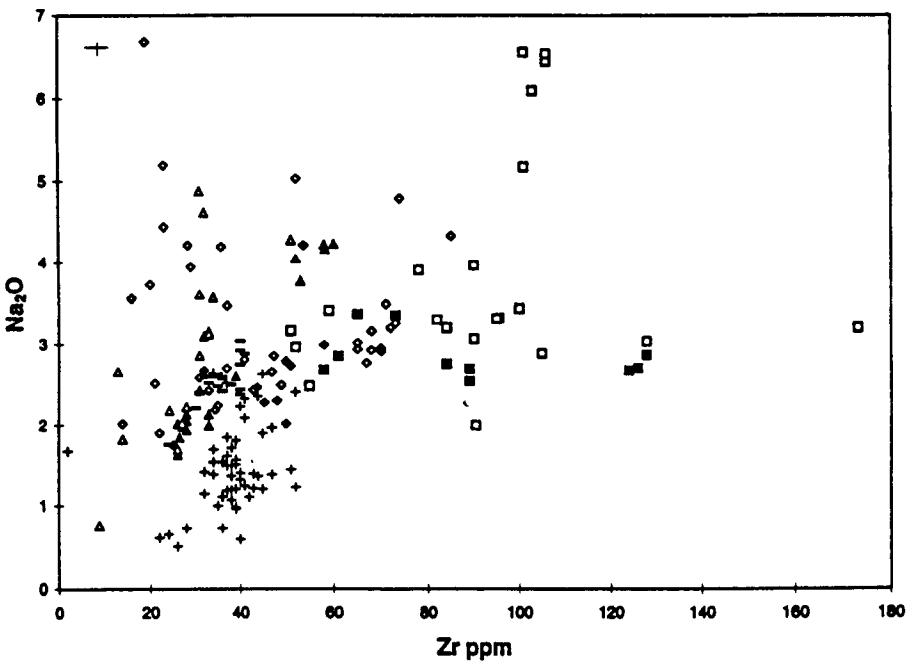
Na2O
Zr ppm
0
1
2
3
4
5
6
7
0
20
40
60
80
100
120
140
160
180

60b.

4.3 Trace element trends

Trace elements (those which are not essential in minerals but may be found in small quantities in their structures or adsorbed on their surfaces) show varying enrichments and depletions due to alteration, which are largely dependent on their mobilities in fluids under specific conditions. The element Zr is generally immobile during hydrothermal alteration, and so its quantity should not change due to alteration, although its concentration may change somewhat if there are net gains or losses of mass from the bulk rock. Here, it has been used as an indicator of primary igneous composition, along with Ti (which is also immobile, as shown in Figure 57e) and Mg. Mg is not generally immobile during alteration, although in this case there are no significant net changes in Mg content between fresh and altered rocks (Figure 57d). Trace elements which are mobile can be used to study alteration processes.

The trace element most affected by hydrothermal alteration is Ba, which is strongly enriched in tholeiites and, to a lesser degree, in arc tholeiites (Figure 61a). In boninites, Ba varies, so it may be mobilized slightly. All other trace elements show no trends due to alteration in boninite samples. Sr is slightly enriched in tholeiites and arc tholeiites (Figure 61b). Ni varies due to alteration in both tholeiites and arc tholeiites, suggesting some mobilization (Figure 61c). Cr is strongly enriched in arc tholeiites and slightly enriched in tholeiites (Figure 61d). Sc (Figure 61e), Y (Figure 61f), and V (Figure 61g) are relatively unchanged by alteration in all rock types. As with the major elements, boninites show no bulk chemical changes that correlate with LOI (except for Ba). Trace element trends are typically similar for samples from both the forearc and transect 87-91

Figure 61. (Following pages) A-g show trace element contents of Tonga forearc bulk rocks, plotted versus LOI to show extent of alteration. Some data from dredges 88-91 are from Trevor Falloon (unpublished data). Error bars are shown in the top left of each plot for each element. If no error bar is shown, the error bar is smaller than the symbol. Symbols for Figure 61a-g are defined on Figure 61a.

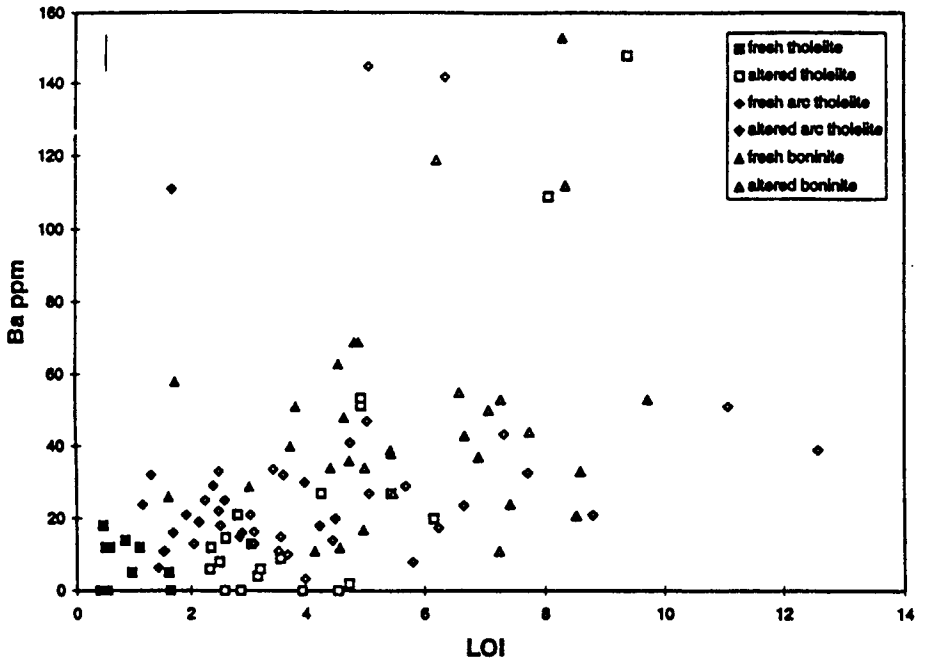
fresh tholeiite
altered tholeiite
fresh arc tholeiite
altered arc tholeiite
fresh boninite
altered boninite
Ba ppm
LOI
0
20
40
60
80
100
120
140
160
0
2
4
6
8
10
12
14

61a.

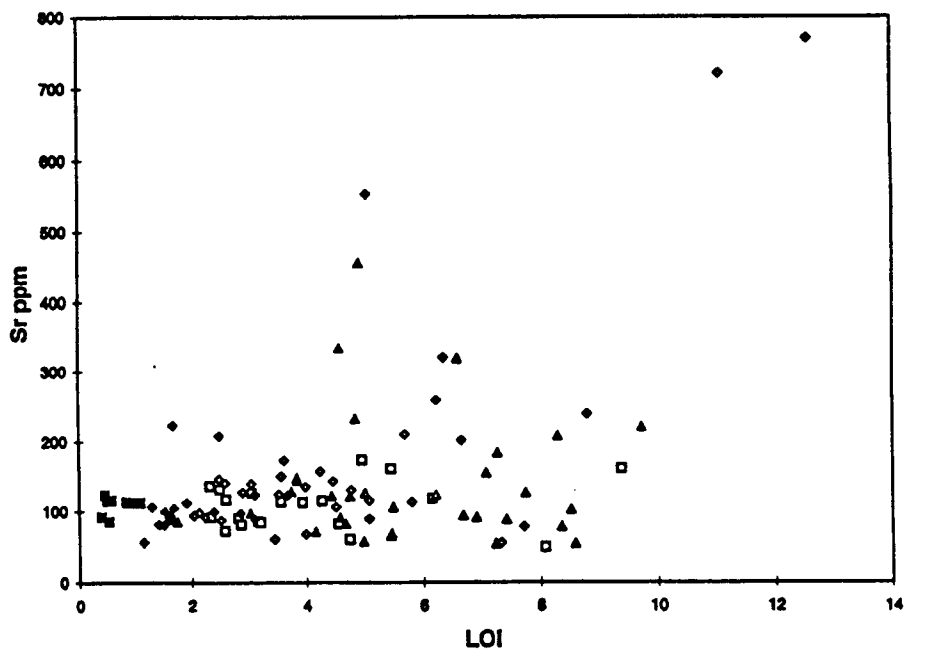
Sr ppm
LOI
0
100
200
300
400
500
600
700
800
0
2
4
6
8
10
12
14

61b.

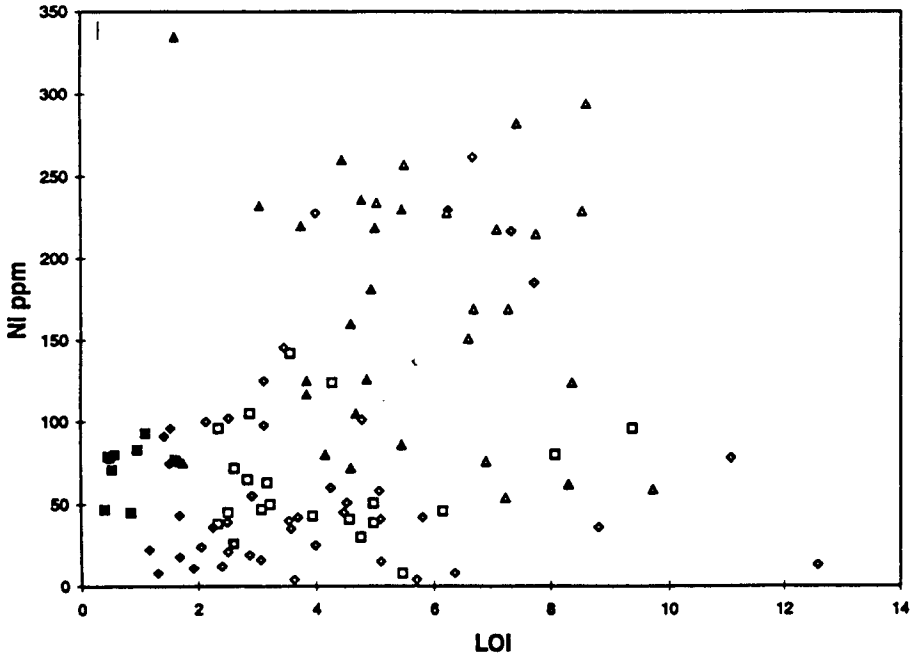
Ni ppm
LOI
0
50
100
150
200
250
300
350
0
2
4
6
8
10
12
14

61c.

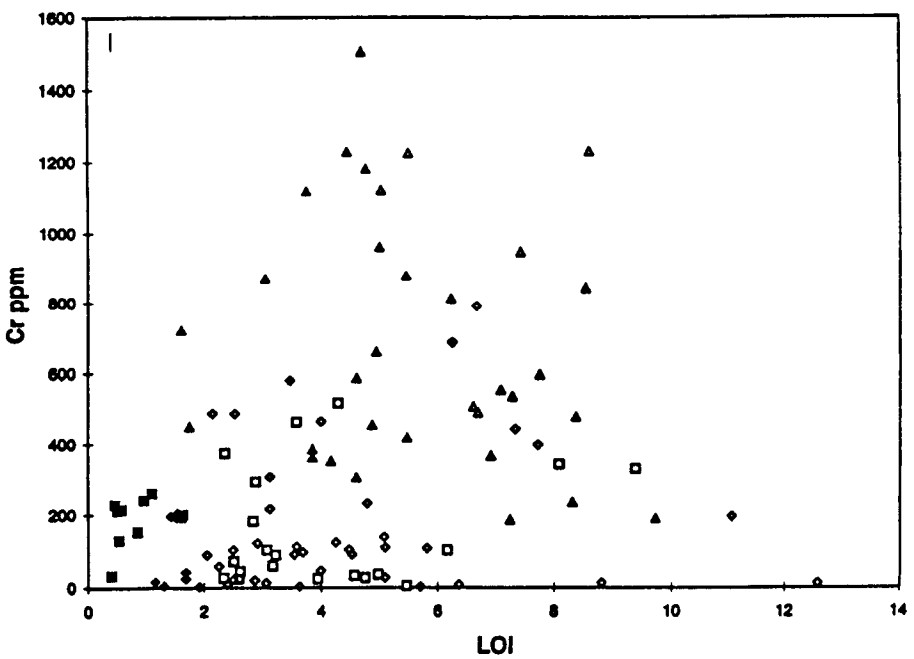
Cr ppm
LOI
0
200
400
600
800
1000
1200
1400
1600
0
2
4
6
8
10
12
14

61d.

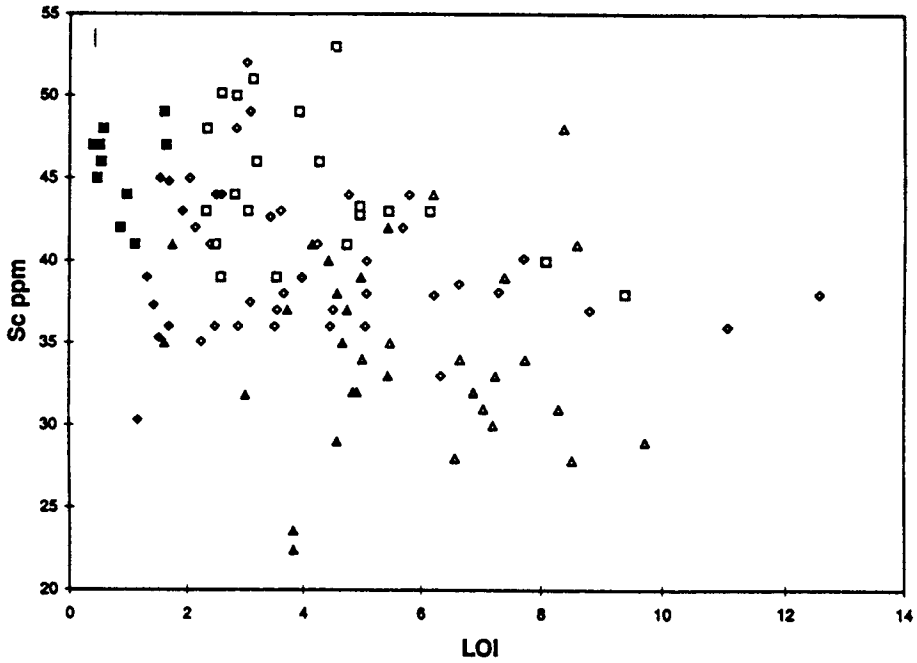
Sc ppm
LOI
55
50
45
40
35
30
25
20
0
2
4
6
8
10
12
14

61e.

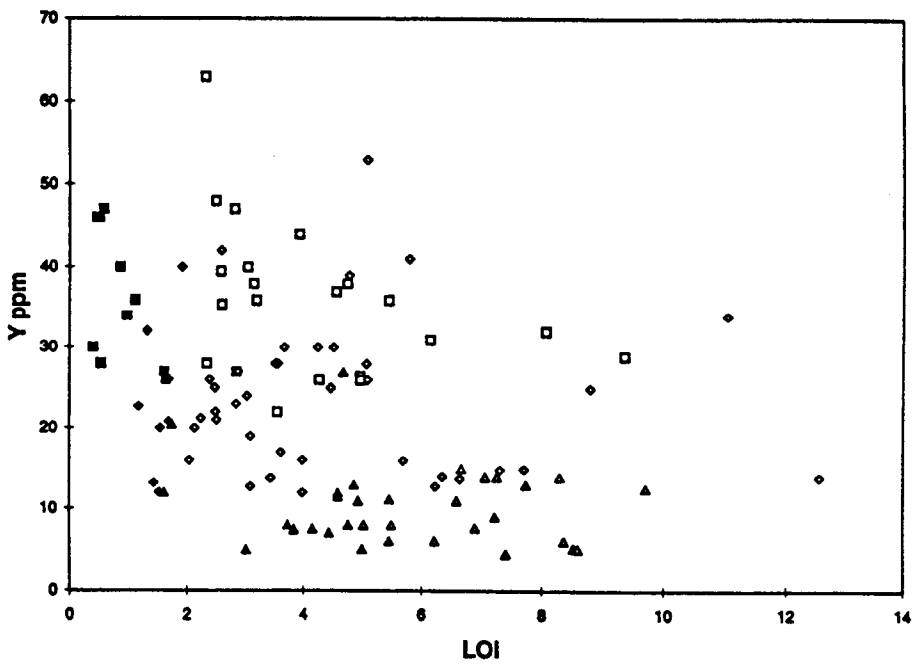
Y ppm
LOI
70
60
50
40
30
20
10
0
0
2
4
6
8
10
12
14

61f.

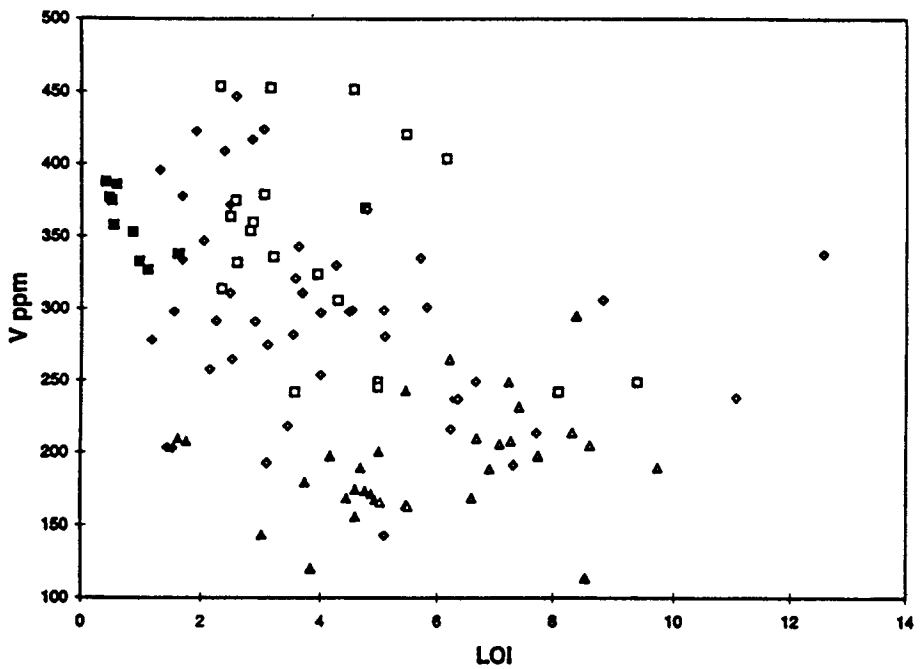

61g.

alone, although degrees of enrichments and depletions may vary, suggesting local variations in redistribution.

In comparison with the CY-1 drillcore of the Troodos ophiolite, Tonga forearc rocks show a similar range of Ba contents (Figure 62a) but are more variable and higher in Sr (Figure 62b). Within the CY-1 drillcore, Ba and Sr in the upper 300 m are enriched with respect to the lower 200 m (Gillis, 1987). If drillcores were available for Tonga, a similar comparison might be made.

4.4 Correlation of mineral chemistry and bulk compositional trends

4.4.1 Major elements and mineral chemistry

Clay minerals alone, despite their abundance, cannot account for the bulk K_2O enrichment in Tonga samples. Even assuming that 20 weight % of a sample consists of clays which (based on microprobe data) average approximately 5 weight % K_2O, this would still contribute only 1 weight % K_2O to the bulk rock. K_2O in some bulk samples is as high as 3.05 weight %; therefore, there must be another source for the K_2O enrichment, probably K-feldspar. Assuming the bulk rock contained 10 weight % K-feldspar which averaged 15 weight % K_2O, there would be a 1.5 weight % K_2O contribution to the bulk rock. Combined with the K_2O enrichments due to clay minerals (and not including the K in zeolites), this would be sufficient to produce the high bulk rock K_2O contents found in Tonga forearc samples (up to 3.05 weight %). K enrichment due to alteration thus correlates with the presence of secondary K-feldspar and, to a lesser

Figure 62. (Following page) A and b show Ba and Sr versus Zr for Tonga forearc volcanic samples (some data from dredges 88-91 are from Trevor Falloon [unpublished data]) and the CY1 drillcore from the Troodos Ophiolite (Gibson et al., 1991). The upper and lower CY-1 drillcore are shown separately. Symbols for Figure 62a-b are defined on Figure 62a.

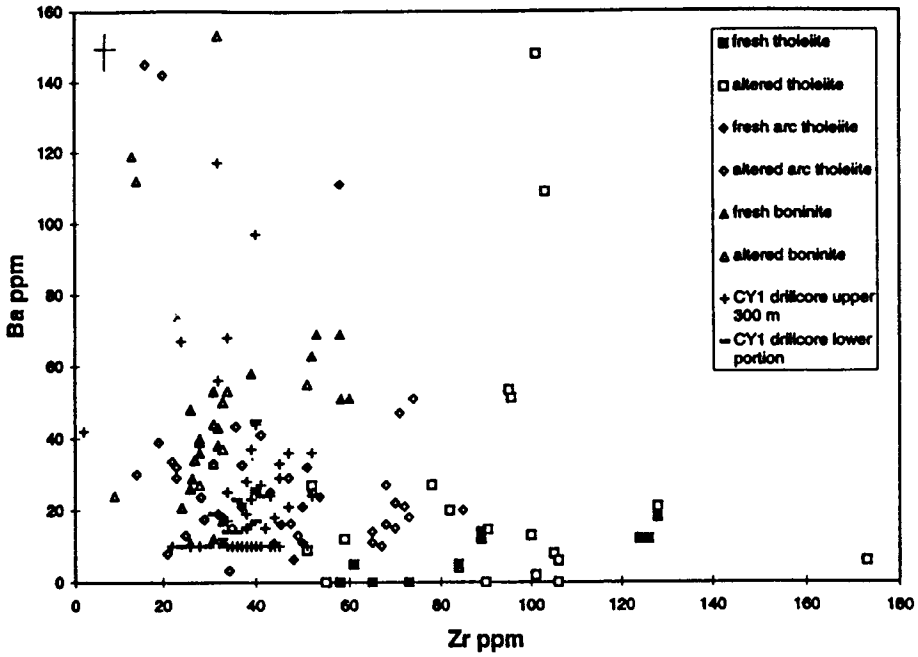
Ba ppm
Zr ppm
fresh tholeiite
altered tholeiite
fresh arc tholeiite
altered arc tholeiite
fresh boninite
altered boninite
CY1 drillcore upper 300 m
CY1 drillcore lower portion

62a.

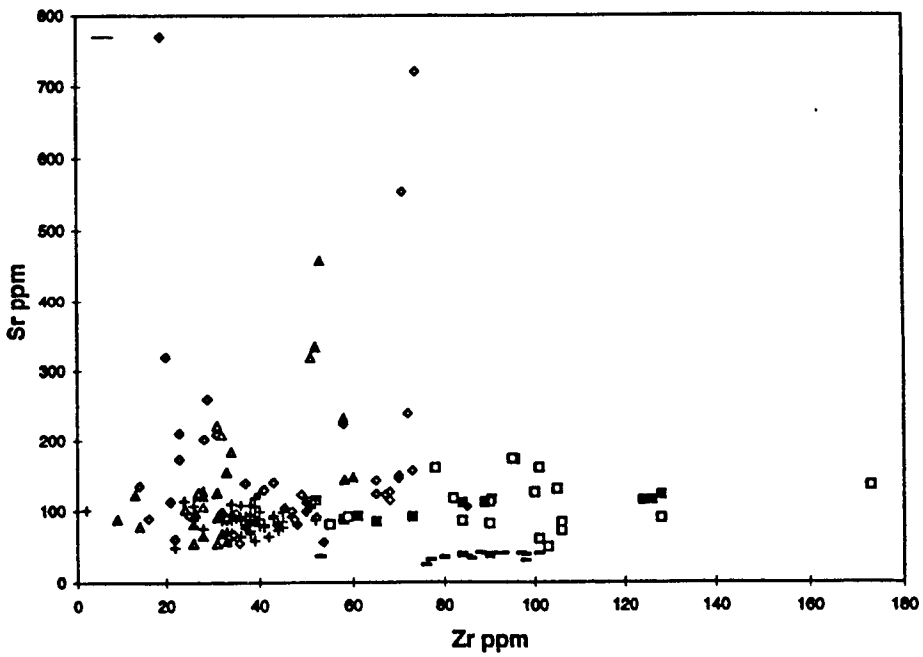
Sr ppm
Zr ppm

62b.

extent, with high K in clays and zeolites. Bulk K enrichment due to low temperature alteration in the Troodos Ophiolite is also due to the presence of abundant secondary K-feldspar. In Tonga, pure celadonite, mixtures of celadonite and smectite, or smectite in which K is the dominant interlayer cation (which includes most smectites analyzed from the forearc) are the sites in clays where the excess K is located. For example, Troodos Ophiolite celadonite may be >9 weight % K_2O (Gillis, 1986; Gallahan and Duncan, 1994), and K in Tonga celadonites may range from 6-9 weight %. K is also stored by the zeolite phillipsite. Lack of K enrichment in boninites is attributed to the rarity of plagioclase phenocrysts (which might be altered to K-feldspar) and to the relative scarcity of veins (in which adularia or K-bearing clays and zeolites could precipitate).

Excess Na and Ca are carried in clays as interlayer cations, or in zeolites. A few zeolites with an apparent phillipsite structure are rich in Na rather than the typical K, although Na-rich phillipsites are not unheard of (Deer et al., 1962). Na may be enriched through albitization of plagioclase at higher temperatures (>140°C; Munha et al., 1980; Honnorez et al., 1983), but the number of high temperature samples in this suite is too small to make any generalizations. Petrographic evidence in the few high temperature samples suggests there may be slight albitization of some plagioclase phenocrysts. Most Tonga clays are Ca-poor, and no calcic zeolites have been identified, which explains the lack of Ca enrichment in these rocks. Ca, Mg, Fe, and Mn may be deposited in carbonate minerals but the quantities of carbonates in Tonga samples are small. Ca and alkalis can also occur in minor amounts in chlorite as adsorbed surface cations (Deer et al., 1963). Fe

and Mg occur principally in clay minerals and celadonite, both of which are abundant; however, net gains and losses of these elements are insignificant for the bulk rocks, suggesting that redistribution is local.

4.4.2 Trace elements and mineral chemistry

Ba, the most significantly enriched trace element (in tholeiites and arc tholeiites) may be incorporated into various clays and zeolites, as well as into carbonates. In zeolites, it occurs as a major constituent of the mineral harmotome (not occurring here), which has a similar structure to phillipsite, and could substitute into phillipsite in the analogous position (in phillipsite, this position is occupied by K, 1/2Ca, and Na [Deer et al., 1962]). Phillipsite is common in the glassy rinds and fractures of both tholeiites and arc tholeiites. It is less common in boninites, perhaps due in part to the rarity of glassy rinds and fractures in most boninitic samples. Ba could also presumably substitute as an interlayer cation (for K, Na, and Ca) in clays (since it is of similar charge). To a lesser extent, Sr may also enter phillipsite (in the same structural position as Ba). Sr enrichment may be due to its inclusion as an interlayer cation in clays.

The strong Cr enrichment in arc tholeiites is due to its inclusion in clays (up to 118 ppm in electron microprobe analyses of smectites), most likely in the octahedral positions but possibly also in tetrahedral positions (Lapham, 1958). It correlates in some cases with high Mg content in clay. Ni may also occur in minor amounts in clay octahedral sites, and behaves similarly (though less strongly) to Cr in its enrichment in

arc tholeiites and depletion in tholeiites. Ni, Cr, and Ti may all occur in small quantities in chlorite and clays.

4.5 Summary

Tonga forearc major and trace element bulk rock chemical trends for tholeiites and arc tholeiites correlate fairly well with observed alteration mineralogies. Boninites are less altered than the other rock types, and no such correlation is identifiable. Principally, K is enriched in more altered samples due to its inclusion ion secondary K-feldspar and, to a lesser extent, its inclusion in clays and zeolites. Ba enrichment (and the slight Na enrichment in some samples) is due to the presence of clays and zeolites. Other major and trace elements may be variably mobilized, or may not change significantly in the bulk rock due to alteration, but are probably redistributed locally, based on mineralogy and mineral chemistry. Ti and Zr are not mobilized, although they may be passively accumulated in samples where there are significant changes in the bulk density due to alteration. K, Ba, and Sr enrichments are similar to those measured for the CY-1 drillcore of the Troodos Ophiolite (where they are also carried in K-feldspar, clays, and zeolites). In the CY-1 drillcore, however, Na is depleted (due to the presence of abundant K-feldspar) and Ca is enriched (due to pervasive carbonate mineralization) in the upper 300 m (relevant to the lower 200 m) (Gillis, 1987). Nonetheless, bulk chemistry suggests that the Tonga forearc volcanic sample suite is most similar to the upper 300 m of the CY-1 drillcore. More detailed comparisons would require analogous information for Tonga (i.e. drillcores, so that elemental concentrations might be plotted versus depth).

Chapter 5. Discussion and Summary of Conclusions

5.1 Temperature

Alteration mineral compositions and assemblages in Tonga forearc samples affected by "low temperature alteration" (most samples) indicate the temperature ranges at which alteration likely occurred. The extensive incorporation of K into secondary minerals (K-feldspars, clays, and zeolites) is common in low temperature alteration involving seawater (Richardson et al., 1980; Staudigel et al., 1981; Seyfried et al., 1984; Berndt and Seyfried, 1986). The temperature range for smectite and celadonite formation in MORBs and altered ophiolite volcanic rocks is 0-100°C (Alt, 1995). Celadonite, which is not common in Tonga forearc rocks, generally forms at temperatures of less than 40°C, while saponite, which is common in Tonga forearc volcanic rocks, forms at 50-200°C (Kristmannsdottir, 1975; Seyfried et al., 1978; Stakes and O'Neil, 1982; Honnorez et al., 1983; Bohlke et al., 1984). Phillipsite forms at <50°C (Bohlke et al., 1984; Honnorez, 1978). Based on this, it is hypothesized that the low temperature alteration in Tonga forearc volcanic rocks occurred at <50-200°C. There are a few samples probably altered at transitional temperatures (less than those for the high temperature alteration) which contain physical or structural mixtures of smectite and chlorite. The transition from saponite to mixed-layer smectite/chlorite in Icelandic geothermal fields occurs at 100-200°C (Kristmannsdottir, 1975). Finally, there are a few samples of high temperature alteration, which contain chlorite and epidote. The smectite/chlorite to chlorite transition in Icelandic geothermal fields occurs at 200-240°C (Kristmannsdottir, 1975), while

chlorite from the Troodos Ophiolite was determined to have been formed at 80-240°C (Gillis and Robinson, 1990). Epidote is stable at >200°C in geothermal systems (Kristmannsdottir, 1975; Bird et al., 1984; Liou et al., 1985). Thus, Tonga forearc samples with chlorite and epidote probably formed at a minimum temperature of 200°C, although temperatures could have been even higher; in some samples, amphibole was identified petrographically, and assemblages of calcic plagioclase + amphibole + chlorite should require at least 300°C (Mottl and Holland, 1978; Liou et al., 1985).

5.2 Water/rock ratios

Tonga forearc volcanic samples differ in the extent of their alteration within and between dredges and especially between rock types. Although no stratigraphy is available, some particularly weathered samples must have been in locations where seawater-rock interaction was extensive. There is commonly centimeter scale variability (i.e. within single dredge samples) in the degree of alteration. This suggests variable water/rock conditions on a small scale (within individual cooling units), and control of water/rock interaction by the distribution of fractures.

Water/rock ratios could be calculated using bulk rock compositions if the fresh rock compositions were known, and if it was assumed that differences between fresh and altered rock compositions reflected the amount of chemically unmodified seawater that interacted with the rocks. However, without better information on the correct fresh rock compositions (e.g. stratigraphic relationships might be needed), this is not possible. Generalizations may be made based on trends in bulk rock composition. The strong

enrichment of K in most samples probably came from extensive interaction with seawater, as large quantities of seawater circulated through the relatively cool volcanic section, until fractures were filled with secondary minerals. As boninites are relatively silicic with respect to basalts, they would be expected to show greater alteration effects, since silicic glass reacts more rapidly than basaltic glass (Dobson and O'Neil, 1987). However, this is not the case, as boninites from transect 87-91 of the Tonga forearc are typically less altered than tholeiites or arc tholeiites. This is likely due in part to the fact that boninite samples are less fractured than tholeiites and arc tholeiites, and their reduced surface area would slow reaction rates. A further consideration is that the boninite samples in transect 87-91 all come from Dredge 88 and thus may have all originated from a single location whose alteration was not necessarily typical.

5.3 Fluid composition and evolution

The seafloor weathering seen in Tonga forearc volcanic samples (characterized by red staining, especially of the groundmass) preceded the low temperature alteration, and must have occurred under oxidizing conditions. Precipitation of Fe-oxyhydroxides would produce H^+ and lower the fluid's pH (Seyfried et al., 1978; Alt and Honnorez, 1984). As seawater migrated downward into the volcanic pile and inward into cooling units, its oxygen content would have decreased while its pH increased, preventing further formation of Fe-oxyhydroxides. These conditions would instead favor saponite formation (Bass, 1976; Seyfried et al., 1978; Andrews, 1980). Although seafloor weathering and low temperature alteration may overlap, the seafloor weathering clearly occurred first,

based on petrography. This could have led (in samples where both are present) to closing of most fluid pathways, decreasing the intensity of fluid flow, therefore leading to more evolved fluids, which is why saponite veins always come after seafloor weathering. The few areas where celadonite is present in low temperature alteration would have required more oxidative conditions and lower pH (Wise and Eugster, 1964), but this is uncommon, and occurs in fractures and vesicles, not in the groundmass (where interaction with unmodified seawater would have been unlikely). More common are alkaline conditions, which favor zeolite precipitation. Zeolites generally follow clays in Tonga forearc rocks (although there may be several cycles of clays followed by zeolites), indicating a general trend of increasing alkalinity of fluids, consistent with the progressive evolution of seawater as it interacts with basic volcanic rocks. This is supported by the absence of zeolites in intensely weathered samples, where high fO_2 and low pH would have been maintained (e.g. Alt et al., 1996a). This is similar to patterns seen at Site 786 and in MORBs, where phyllosilicate precipitation is followed by zeolite, then carbonate formation, and a general decrease of Mg, increase of pH, and increase of Ca in solution occurs (Alt and Honnorez, 1984; Alt et al., 1986a; Teagle et al., 1996). In Tonga forearc samples, carbonates also come late or last in the sequence of precipitation.

Lack of Mg enrichment in Tonga forearc volcanic rocks is similar to that seen in the Troodos Ophiolite volcanic section (Gillis, 1987) and at Site 786 (Alt et al., 1998). This is probably due to only local redistribution of Mg from olivine into magnesian clays in fractures nearby; the Mg did not travel far. This is unlike Site 504, where Mg is gained by the volcanic section in breccias with smectite cements (Alt et al., 1996b). A more

extensive study of Tonga forearc rocks might allow for comparison of the bulk compositions of breccias and lavas to determine if there were similar chemical differences there, since the dredge samples studied did not include friable interpillow zones where smectite would be expected to be abundant. Such zones (in Tonga samples) might be enriched in Mg like those at Site 504. Alt et al. (1998) suggested that Site 786 fluids were closer (than is typical in oceanic hydrothermal systems) to equilibrating with the rocks, since there is evidence for significant isotopic exchange between the two, but no Mg-enrichment which would be expected to occur due to high fluid fluxes (as Mg was removed from seawater). It is not possible to tell if this occurs in Tonga forearc rocks, since no isotope work has yet been done.

5.4 Summary of conclusions

Tonga forearc volcanic rocks (collected as dredge samples during the 1996 Boomerang Leg 8 research cruise) are dominated by tholeiites, arc tholeiites, and boninites, which occur as pillow fragments, breccias, and as massive lava fragments of indeterminate igneous morphology. These rocks are altered to varying degrees, with boninites being notably less altered than the other two rock types. Brecciated lavas and glassy pillow rinds tend to be the most intensely altered morphologies.

There are three types of alteration documented in these volcanic samples, seafloor weathering, low temperature alteration, and high temperature alteration, which are analogous to alteration of oceanic crust at other locations. The generalized vertical and temporal relationships between these three types of alteration are shown in Figure 63.

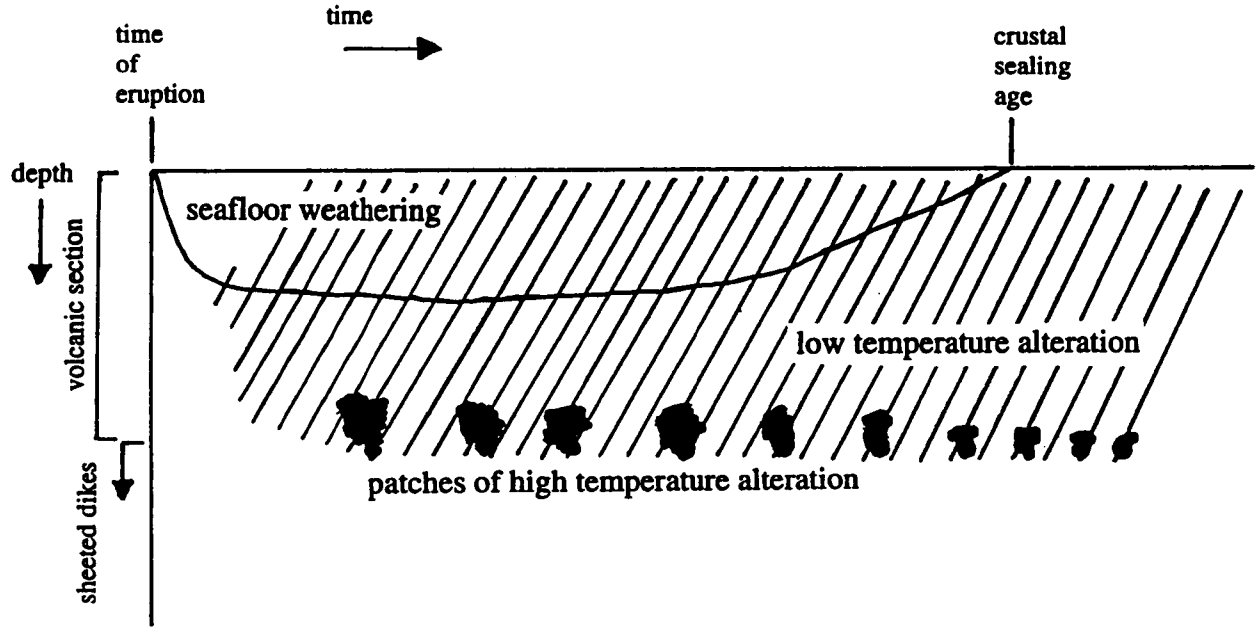

Figure 63. Temporal and depth relationships of seafloor weathering, low temperature alteration, and high temperature alteration.

Elemental fluxes for different rock types are shown in Table 8. Seafloor weathering (beginning at the time of eruption and continuing until sealing of the crust by secondary mineralization occurs) is due to extensive interaction of cold seawater with the rock, and occurs to some degree in many samples. It is characterized by a red staining of the groundmass of the rock, which is usually accompanied by alteration of olivine to Fe-oxyhydroxides, and locally by alteration of plagioclase and pyroxenes to smectite.

Low temperature alteration occurs at temperatures <50-200°C, with the latest phases being deposited at the lowest temperatures. Low temperature alteration begins at some time after the initiation of seafloor weathering, when seawater-derived fluids have had time to circulate through the volcanic section, and have been chemically modified. This alteration continues for some time after the sealing of the crust (although no fresh seawater can be added after this point), until the circulating fluids have equilibrated with the surrounding rocks. Low temperature alteration is characterized by alteration of olivine to Fe-oxyhydroxides and smectite ± calcite, alteration of plagioclase to K-feldspar, smectites, celadonite, or mixtures of clays, and slight alteration of pyroxenes to smectites. Groundmass is altered to smectites, smectite-celadonite, or chlorite-smectite, while glassy rinds are altered to smectite, smectite-celadonite mixtures, K-feldspar, calcite, phillipsite, and silica. Veins and vesicles are filled with smectites, smectite-celadonite mixtures, celadonite, chlorite-smectite, K-feldspar, phillipsite, silica, calcite, and Fe-oxyhydroxides in varying sequences. Vein sequences indicate a general trend of decreasing fO_2 and increasing pH (with the transition from Fe-oxyhydroxides to saponite), and increasing Mg with time, although variability of vein sequences is high. Low temperature alteration

	tholeiites	arc tholeiites	boninites
SiO_2	NC	NC	NC
Al_2O_3	NC	+	NC
Fe_2O_3	NC	NC	NC
MgO	NC	NC	NC
CaO	-	NC	NC
Na_2O	+	+	NC
K_2O	+++	++	NC
Sr	+	++	NC
Ba	+++	NC	+
Zr	+	-	-
Y	+	NC	NC
Ni	NC	++	NC
Sc	NC	NC	NC
V	NC	NC	+
Cr	NC	++	-

Table 8. Major and trace element fluxes for different rock types. Fluxes were determined by averaging the values for each element for those rocks classed as "fresh" (based on LOI, as in Figure 61) and doing the same for those rocks classed as "altered". Each average "altered" value was then divided by the average "fresh" value for each element and rock type, to obtain a ratio of altered/fresh composition for that element in that rock type. Symbols (showing relative enrichments and depletions) in the table are as follows:

altered/fresh ≥ 3	+++
altered/fresh = 1.5-3	++
altered/fresh = 1.1-1.5	+
altered/fresh = 0.9-1.1	NC (no change)
altered/fresh = 0.7-0.9	-

leads to K, Ba, and slight Na enrichment of the bulk rock. Differences between typical alteration at mid-oceanic ridges and in the Tonga forearc are seen in those volcanic rocks subjected to low temperature alteration. Specifically, Tonga forearc rocks contain Al-rich dioctahedral smectites (not common in mid-oceanic ridge crust), Tonga saponites are commonly higher in Al (similar to those of the Troodos Ophiolite) than those typically found in mid-oceanic ridge crust, and the interlayer cation in smectites is almost invariably K (this is not true for typical oceanic crust).

High temperature alteration begins contemporaneously with or later than low temperature alteration, at temperatures of at least 200°C (possibly >300°C). Although its depth distribution cannot be determined from the Tonga dredge data, analogies with ophiolites (e.g. Gillis, 1987) and Site 504 (Alt et al., 1996a,b) suggests that the high temperature alteration at Tonga probably occurs in patches close to the volcanic-dike transition. Within the dikes, the permeability contrast prevents extensive interaction of the rock with cooler, seawater-derived fluids, thus resulting in increased temperatures. Localized zones of hydrothermal upwelling allow these high temperature fluids to enter the lower volcanic section. Temperatures throughout the volcanic section then decrease with time as the system moves away from the axis and cools. High temperature alteration is characterized by alteration of the mesostasis and phenocrysts to chlorite + epidote + quartz ± opaques. Plagioclase specifically may be partially albitized or sericitized. Pyroxenes are altered to amphibole. Vesicles and veins may be filled with quartz, chlorite, epidote, and hematite. This high temperature alteration may be overprinted by

low temperature alteration, which would have lasted longer than the high temperature alteration, as fluids progressively cooled.

Based on the comparison of Tonga forearc hydrothermal alteration with that of the Troodos Ophiolite, that of mid-oceanic ridge crust from Sites 504 and 896 in the eastern equatorial Pacific, and that of Site 786 in the Izu-Bonin-Mariana forearc (a setting that is tectonically similar to the Tonga forearc), Tonga forearc alteration is more similar to that of ophiolites than to that of mid-oceanic ridge crust. Although alteration assemblages, the physical conditions which produced them (particularly temperature, fluid composition, and water:rock ratio), and the elemental fluxes due to alteration are superficially similar to those in other settings, there are some specific differences which probably reflect differences in hydrothermal fluid evolution with time. The most striking differences between Tonga forearc and mid-oceanic ridge alteration are seen in the secondary clay minerals and their distinctive chemistries, and these characteristics of Tonga forearc alteration bear a closer resemblance to what has been observed in the Troodos Ophiolite.

5.5 Recommendations for future work

Further detailed studies of hydrothermal alteration in the Tonga forearc would best be accomplished by drilling at various locations along the length of the forearc and at various positions on the forearc slope. This would provide the stratigraphic information necessary in order to have a clearer idea of fresh rock compositions, relationships between rock types and alteration types, spatial distribution of seafloor weathering and low and high temperature alteration, the relationship of alteration to faults and

topography, and the correlation of alteration with rock units of known age. Drilling would also increase the sample set available for study (and hopefully provide more examples of high temperature alteration, which is not well represented in the current sample set), although more importantly, the precise origin of samples would be known.

Useful work that could be done with or without drilling the forearc basement would be isotopic analyses of Sr and O to determine the extent of seawater contributions to alteration, and of S to determine the source of any secondary sulphides. Stable isotope studies could also provide information about fluid evolution with time. Also, geothermometry on specific minerals (e.g. calcite) would make the determination of the temperatures at which alteration occurred less speculative and would make it easier to understand the alteration processes which took place. Finally, if sufficient quantities of celadonite (a K-rich, Ar-retentive mica)were found, it could be K-Ar dated in order to obtain some absolute age constraints on the timing of secondary mineralization. All of this would permit more detailed comparisons between hydrothermal alteration in the Tonga forearc and that in other oceanic settings.

Bibliography

Abdenko GL, Bezrukov A, Murdmaa IV, Prokopchev NG (1972) New data on the composition of the volcanic rocks of the basement of the Tonga arc. Doklady, Academy of Sciences USSR 204: 1232-1235

Acland AS, Vysotsky SV, Pearce JA, Parson LM (1992) Geochemistry of a boninitic crustal section from the northern Tonga Trench. *In:* Back-arc development and crustal accretion in the Western Pacific [abs.]: Cambridge University Press, United Kingdom

Adamson AC, Richards HG (1990) Low-temperature alteration of very young basalts from Ocean Drilling Project Hole 648B: Serocki Volcano, Mid-Atlantic Ridge, pp.181-194. *In:* Detrick R, Honnorez J, Bryan WB, Juteau T, et al. (eds) Proceedings of the Ocean Drilling Program, Scientific Results 106/109, College Station, TX

Alt JC (1993) Low-temperature alteration of basalts from the Hawaiian Arch, ODP Leg 136, pp.133-146. *In:* Wilkens RH, Firth J, Bender J, et al. (eds) Proceedings of the Ocean Drilling Program, Scientific Results 136, College Station, TX

Alt JC (1995) Sulfur isotopic profile through the oceanic crust: sulfur mobility and seawater-crustal sulfur exchange during hydrothermal alteration. Geology 23: 585-588

Alt JC, Honnorez J (1984) Alteration of the upper oceanic crust DSDP Site 417: Mineralogy and chemistry. Contributions to Mineralogy and Petrology 87: 149-169

Alt JC, Honnorez J, Laverne C, Emmerman R (1986) Hydrothermal alteration of a 1 km section through the upper oceanic crust, DSDP Hole 504b: mineralogy, chemistry and evolution of seawater-basalt interactions. Journal of Geophysical Research 91 B10: 10309-10335

Alt JC, Kinoshita H, Stokking LB, et al. (1993) Proceedings of the Ocean Drilling Program, Initial Reports 148, College Station, TX

Alt JC, Lanord CF, Floyd PA, Castillo P, Galy A (1992) Low-temperature hydrothermal alteration of Jurassic oceanic crust, Site 801, pp.415-427. *In:* Larson RL, Lancelot Y, et al. (eds), Proceedings of the Ocean Drilling Program, Scientific Results 129, College Station, TX

Alt JC, Laverne C, Vanko DA, Tartarotti P, Teagle DAH, Bach W, Zuleger E, Erzinger J, Honnorez J, Pezard PA, Becker K, Salisbury MH, Wilkens RH (1996a) Hydrothermal alteration of a section of upper oceanic crust in the eastern equatorial Pacific: a synthesis of results from Site 504 (DSDP Legs 69, 70, and 83, and ODP Legs 111, 137, 140, and 148), pp. 417-434. *In:* Alt JC, Kinoshita H, Stokking LB (eds) Proceedings of the Ocean Drilling Program, Scientific Results 148, College Station, TX

Alt JC, Teagle DAH, Laverne C, Vanko DA, Bach W, Honnorez J, Becker K, Ayadi M, Pezard PA (1996b) Ridge-flank alteration of upper ocean crust in the eastern Pacific: Synthesis of results for volcanic rocks of Holes 504B and 896A, pp.435-452. *In:* Alt JC, Kinoshita H, Stokking LB (eds) Proceedings of the Ocean Drilling Program, Scientific Results 148, College Station, TX

Alt JC, Teagle DAH, Brewer T, Shanks WC, Halliday A (1998) Alteration and mineralization of an oceanic forearc and the ophiolite-ocean crust analogy. Journal of Geophysical Research (in press)

Anderson RN, Honnorez J, Becker K, Adamson AC, Alt JC, Emmerman R, Kempton PD, Kinoshita H, Laverne C, Mottl MJ, Newmark RL (1982) DSDP Hole 504B, the first reference section over 1 km through Layer 2 of the oceanic crust. Nature 300: 589-594

Andrews AJ (1980) Saponite and celadonite in Layer 2 basalts DSDP Leg 37. Contributions to Mineralogy and Petrology 73: 323-340

Anosov GI, Il'yev A, Survorov AA, Argentov VV, Neverov YA, Zhiltsov EG, and Patrikeyev VN (1983) Features of the geological structure of the juncture zone between the Tonga and the Kermadec trenches. Geotectonics 17 no.3: 252-261

Arculus RJ, Pearce JA, Murton B, van der Laan S (1992) Igneous stratigraphy and major element geochemistry of Holes 786A and 786B, pp.143-170. *In:* Fryer P, Coleman P, Pearce JA, Stokking LB (eds) Proceedings of the Ocean Drilling Program, Scientific Results 125, College Station, TX

Ballance PF, Scholl DW, Vallier TL, Stevenson AJ, Ryan H, Herzer LH (1989) Subduction of a Late Cretaceous Seamount of the Louisville Ridge at the Tonga Trench: A model of normal and accelerated tectonic erosion. Tectonics 8: 953-962

Baragar WRA, Lambert MB, Baglow N, Gibson IL (1987) The sheeted dyke zone in the Troodos ophiolite, pp.37-51. *In:* . Malpas J, Moores EM, Panayiotou A, Xenophontos C (eds.) Troodos 87: Ophiolites and Oceanic Lithosphere

Bass MN (1976) Secondary minerals in oceanic basalt, with special reference to Leg 134, DSDP, pp.393-432. *In:* Yeats RS, Hart SR, et al. (eds.) Initial Reports of the Deep Sea Drilling Project 34, U.S. Government Printing Office, Washington

Becker K (1996) Permeability measurements in Hole 896A and implications for the lateral variability of upper crustal permeability at Sites 504 and 896, pp.353-364. *In:* Alt JC, Kinoshita H, Stokking LB, Michael PJ (eds) Proceedings of the Ocean Drilling Program, Scientific Results 148, Ocean Drilling Program, College Station, TX

Becker K (1985) Large-scale electrical resistivity and bulk porosity of the oceanic crust, Deep Sea Drilling Project Hole 504B, Costa Rica rift, pp.419-427. *In:* Anderson RN, Honnorez J, Becker K, et al (eds) Initial Reports of the Deep Sea Drilling Project 83, U.S. Government Printing Office, Washington

Becker K, Foss G, et al. (1992) Proceedings of the Ocean Drilling Program, Initial Reports of the Deep Sea Drilling Project 137, U.S. Government Printing Office, Washington

Becker K, Sakai H, Adamson A, Alexandrovich J, Alt JC, Anderson RN, Bideau D, Gable R, Herzig P, Houghton S, Ishizuka H, Kawahata H, Kinoshita H, Langseth MG, Lovell MA, Malpas J, Masuda H, Merril RB, Morin RH, Mottl MJ, Pariso JE, Pezard P, Phillips J, Sparks J, Uhlig S (1989) Drilling deep into young oceanic crust, Hole 504B, Costa Rica Rift. Reviews of Geophysics 27: 79-102

Berndt ME, Seyfried WE (1986) B, Li, and associated trace element chemistry of alteration minerals, Holes 597B and 597C. Initial Reports of the Deep Sea Drilling Project 92: 491-497

Berndt ME, Seyfried WE, Beck JW (1988) Hydrothermal alteration processes at mid-ocean ridges: Experimental and theoretical constraints from Ca and Sr exchange reactions and Sr isotopic ratios. Journal of Geophysical Research 93: 4573-4583

Bettison-Varga L, Varga RJ, Schiffman P (1992) Relation between ore-forming hydrothermal systems and extensional deformation in the Solea graben spreading center, Troodos Ophiolite. Geology 20: 987-990

Bevis M, Taylor FW, Schutz BE, Recy J, Isacks BL, Helu S, Singh R, Kendrick E, Stowell J, Taylor B, Calmant S (1995) Geodetic observations of very rapid convergence and back-arc extension at the Tonga arc. Nature 374: 249-251

Bickle MJ, Teagle DAH (1992) Strontium alteration in the Troodos ophiolite: implications for fluid fluxes and geochemical transport in mid-ocean ridge hydrothermal systems: Earth and Planetary Science Letters 113: 219-237

Bird DK, Schiffman PS, Elders WA, Williams AE, McDowell SD (1984) Calc-silicate mineralization in active geothermal systems. Economic Geology 79: 671-695

Bloomer SH (1987) Geochemical characteristics of boninite- and tholeiite-series volcanic rocks from the Mariana forearc and the role of an incompatible element-enriched fluid in arc petrogenesis. Geological Society of America Special Paper 215: 151-164

Bloomer SH, Fisher RL (1987) Petrology and geochemistry of igneous rocks from the Tonga Trench: implications for its structure. Journal of Geology 95: 469-495

Bloomer SH, Hawkins JW (1983) Gabbroic and ultramafic rocks from the Mariana trench: An island arc ophiolite, pp.294-317. *In:* Hayes DE (ed) The Tectonic and Geologic Evolution of Southeast Asian Seas and Islands (Part II). Geophysical Monograph Series 27, American Geophysical Union, Washington, D.C.

Bloomer SH, Taylor B, MacLeod CJ, Stern RJ, Fryer P, Johnson L (1995) Early arc volcanism and the ophiolite problem: a perspective from drilling in the western Pacific. *In:* Taylor B, Natland JH (eds) Active Margins and Marginal Basins: A Synthesis of Ocean Drilling in the Western Pacific. AGU Monograph Series, Washington, D.C.

Bloomer SH, Wright D, MacLeod CJ, Tappin D, Clift P, Falloon T, Fisher RL, Gillis K, Ishii T, Kelman MC, Mafi K, Sato H, Winowitch M (1996) Geology of the Tonga forearc: a supra-subduction zone ophiolite. EOS Transactions 77 (46) F325, American Geophysical Union

Bohlke JK, Alt JC, Muehlenbachs K (1984) Oxygen isotope-water relations in altered deep-sea basalts: low-temperature mineralogical controls. Canadian Journal of Earth Science 21: 67-77

Brindley GW, Brown G (1980) Crystal Structures of Clay Minerals and their XRD Identification. Mineralogical Society of London, 495 pp.

Burns RE, Andrews JE, et al. (1973) Initial Reports of the Deep Sea Drilling Project 21, U.S. Government Printing Office, Washington

Cande SC, Kent DV (1995) Revised calibration of the geomagnetic polarity timescale for the Late Cretaceous and Cenozoic. Journal of Geophysical Research 100: 6093-6095

Cann JR, Langseth MG, Honnorez J, Von Herzen RP, White SM, et al. (1983) Initial Reports of the Deep Sea Drilling Project 69, U.S. Government Printing Office, Washington

Cawood PA (1994) Volcaniclastic debris from the southern Tonga forearc: Petrology and phase chemistry, pp.219-233. *In:* Herzer RH, Ballance PF, Stevenson AJ (eds) Geology and resources of island arcs-Tonga-Lau-Fiji region. SOPAC Technical Bulletin 8: 219-233

Chase TE (1985) Submarine topography of the Tonga-Fiji region and the southern Tonga platform area, pp.21-24. *In:* Scholl DW, Vallier TL (eds) Geology and offshore resources of Pacific island arcs - Tonga region. Circum-Pacific Council for Energy and Resources, Earth Science Series 2

Clift PD (1995) Volcaniclastic sedimentation and volcanism during the rifting of western Pacific backarc basins, pp.67-96. *In:* Taylor B, Natland JH (eds) Active Margins and Marginal Basins of the Western Pacific, AGU Monograph Series 88, Washington, D.C.

Clift PD, MacLeod CJ, Tappin DR, Wright DJ, Bloomer SH (1998) Tectonic controls on sedimentation and diagenesis in the Tonga Trench and forearc, southwest Pacific. Geological Society of America Bulletin 110 no.4: 483-496

Cole JW, Gill JB, Woodhall D (1985) Petrologic history of the Lau Ridhe, Fiji, pp.379-414. *In:* Scholl DW, Vallier TL (eds) Geology and offshore resources of Pacific island arcs--Tonga region. Circum-Pacific Council for Energy and Resources, Earth Science Series 2

Cole JW, Graham IJ, Gibson IL (1990) Magmatic evolution of Late Cenozoic volcanic rocks of the Lau Ridge, Fiji. Contributions to Mineralogy and Petrology 104: 540-554

Cunningham JK, Anscombe KJ (1985) Geology of 'Eua and other islands, Kingdom of Tonga, pp.221-258. *In:* Scholl DW, Vallier TL (eds) Geology and offshore resources of Pacific island arcs--Tonga region. Circum-Pacific Council for Energy and Resources, Earth Science Series 2

Deer WA, Howie RA, Zussman J (1962) Rock-Forming Minerals, Volume 3: Sheet Silicates, Longman Group, Hong Kong, 270 pp.

Deer WA, Howie RA, Zussman J (1992) An Introduction to the Rock-Forming Minerals, Longman Group, Hong Kong, 696 pp.

Dobson PF, O'Neil JR (1987) Stable isotope compositions and water contents of boninite series volcanic rocks from Chichi-jima, Bonin Islands, Japan. Earth and Planetary Science Letters 82: 75-86

Duncan RA, Vallier TL, Falvey DA (1985) Volcanic episodes at 'Eua, Tonga islands, pp.281-289. *In:* Geology and offshore resources of Pacific island arcs--Tonga region. Circum-Pacific Council for Energy and Resources, Earth Science Series, 2

Dupont J, Herzer RH (1985) Effects of subduction of the Louisville Ridge on the structure and morphology of the Tonga Arc, pp.323-332. *In:* Scholl DW, Vallier TL (eds) Geology and offshore resources of Pacific island arcs - Tonga region. Circum-Pacific Council for Energy and Resources, Earth Science Series 2

Evarts RC, Schiffman P (1983) Submarine hydrothermal metamorphism of the Del Puerto ophiolite, California. American Journal of Science 283: 289-340

Ewart A, Brothers RN, Mateen A (1977) An outline of the geology and geochemistry, and the possible petrogenetic evolution of the volcanic rocks of the Tonga-Kermadec-New Zealand island arc. Journal of Volcanology and Geothermal Research 2: 205-250

Ewart A, Bryan WB (1972) Petrography and geochemistry of the igneous rocks from 'Eua, Tongan islands. Geological Society of America Bulletin 83: 3281-3298

Fisher AT, Becker K, Narasimhan TN (1994) Off-axis hydrothermal circulation: parametric tests of a refined model of processes at DSDP/ODP Site 504. Journal of Geophysical Research 99: 3097-3123

Fisher RL (1974) Pacific-type continental margins, pp.25-41. *In:* Burk CA, Drake CL (eds) The Geology of Continental Margins, Springer-Verlag, New York

Fisher RL, Engel CG (1969) Ultramafic and basaltic rocks dredged from the nearshore flank of the Tonga Trench. Geological Society of America Bulletin 80: 1373-1378

Friedrichsen H (1985) Strontium, oxygen, and hydrogen isotopic studies on primary and secondary minerals in basalts from the Costa Rica Rift, DSDP Hole 504B, pp.289-296. *In:* Cann JR, Langseth MG, Honnorez J, Von Herzen RP, White SM, et al (eds) Initial Reports of the Deep Sea Drilling Project 69, U.S. Government Printing Office, Washington

Fryer P, Pearce, JA, Stokking LB, et al. (1990) Proceedings of the Ocean Drilling Program, Initial Reports 125, College Station, TX

Gallahan WE, Duncan RA (1994) Spatial and temporal variability in crystallization of celadonites within the Troodos ophiolite, Cyprus: implications for low-temperature alteration of the oceanic crust. Journal of Geophysical Research 99: 3147-3162

Gass I, Smewing JD (1973) Intrusion, extrusion, and metamorphism at constructive margins: Evidence from the Troodos Massif, Cyprus. Nature 242: 26-29

Gibson IL, Malpas J, Robinson PT, Xenophontos X (1991) Cyprus Crustal Study Project: Initial Reports, Holes CY1 and CY-1A, Geological Survey of Canada: 264-283

Gillis KM, Robinson PT (1990) Patterns and processes of alteration in the lavas and dikes of the Troodos ophiolite, Cyprus. Journal of Geophysical Research 95: 21 523-21 548

Gillis KM (1987) Multistage alteration of the extrusive sequence, Troodos ophiolite, Cyprus, Doctoral thesis, Dalhousie University, Halifax, Nova Scotia, 368 pp

Gillis KM, Robinson PT (1987) Multistage alteration in the extrusive sequence of the Troodos Ophiolite, Cyprus, pp.655-664. *In:* Malpas J, Moores EM, Panayiotou A, Xenophontos C (eds) Troodos 87: Ophiolites and Oceanic Lithosphere

Gillis KM, Thompson G (1993) Metabasalts from the Mid-Atlantic Ridge: new insights into hydrothermal systems in slow-spreading crust. Contributions to Mineralogy and Petrology 113: 502-523

Gnibidenko HS, Anosov GI, Argentov VV, Pushchin IK (1985) Tectonics of the Tonga-Kermadec Trench and Ozbourn Seamount junction area. Tectonophysics 112: 357-383

Greene HG, Wong PL (1983) Hydrocarbon resource studies of the southwestern Pacific. USGS Open-File Report 82-293, 24 pp.

Hartland WB, Cox AV, Llewellyn PG, Pickton CAG, Smith AG, Walters R (1982) A geologic timescale: Cambridge University Press, Cambridge, England, 131 pp.

Hawkins JW (1974) Geology of the Lau Basin, a marginal sea behind the Tonga arc, pp.505-520. *In:* Burk CA, Drake CL (eds) The geology of continental margins. Springer-Verlag, New York

Hawkins JW, Falvey DA (1985) Petrology of andesitic dikes and flows from 'Eua, Tonga, pp..269-279. *In:* Scholl DW, Vallier TL (eds) Geology and Offshore Resources of Pacific Island Arcs-Tonga Region. Earth Science Series 2 Circum-Pacific Council for Energy and Mineral Resources, Houston, TX

Herzer RH, Exon N (1985) Structure and basin analysis of the southern Tonga forearc, pp.55-74. *In:* Scholl DW, Vallier TL (eds) Geology and Offshore Resources of Pacific Island Arcs-Tonga Region. Earth Science Series 2, Circum-Pacific Council for Energy and Mineral Resources, Houston, TX

Hey MH (1954) A new review of the chlorites. Mineralogical Magazine 30: 277-292

Hilde TWC (1983) Sediment subduction versus accretion around the Pacific. Tectonophysics 99: 381-397

Hilde TWC, Fisher RL (1979) Graben structure and axial zone tectonics of the Tonga Trench, southwestern Pacific [abs] *In:* ICG Symposium No. 5, Tectonics of the Southwestern Pacific Margins, XVII General Assembly of IUGG, Canberra

Honnorez J (1978) Generation of phillipsites by palagonitization of basaltic glass in seawater and the origin of K-rich deep-sea sediments, pp.245-258. *In:* Sand LB, Mumpton FA (eds) Natural Zeolites: Occurrence, Properties, Use, Permagon Press, New York

Honnorez J, Laverne C, Hubberten H-W, Emmerman R, Muehlenbachs K (1983) Alteration processes in layer 2 basalts from DSDP Hole 504B, Costa Rica Rift, pp.509-542. *In:* Cann JR, Langseth MG, Honnorez J, Von Herzen RP, White SM, et al. (eds) Initial Reports of the Deep Sea Drilling Project 69, U.S. Government Printing Office, Washington

Iijima A, Utada M (1971) Present-day zeolitic diagenesis of the Neogene geosynclinal deposits in the Niigata oil field, Japan. Molecular Sieve Zeolites - Advances in Chemistry Serial 101: 342-349

Ishii T (1985) Dredged samples from the Ogasawara forearc seamount of "Ogasawara Paleoland" - forearc ophiolite, pp.307-342. *In:* Nasu N (ed) Formation of Active Ocean Margins. Terrapub., Tokyo

Kastner M, Gieskes JM (1976) Interstitial water profiles and sites of diagenetic reactions, DSDP Leg 135, Bellingshausen Abyssal Plain. Earth and Planetary Science Letters 33: 11-20

Kristmannsdottir H (1975) Hydrothermal alteration of basaltic rocks in Icelandic geothermal areas, Proceedings, 2nd U.N. Symposium on the development and use of geothermal resources, San Francisco, California: 441-445
Liou JG, Maruyama S, Cho M (1985) Phase equilibria and mineral parageneses of metabasalts in low-grade metamorphism. Mineralogical Magazine 49: 321-333

Lonsdale P (1986) A multibeam reconnaissance of the Tonga Trench axis and its intersection with the Louisville guyot chain. Marine Geophysical Research 8: 295-327

Lonsdale P (1988) Geography and history of the Louisville hotspot chain in the southwest Pacific. Journal of Geophysical Research 93: 3078-3104

Larson RL, Fisher AT, Jarrard RD, Becker K (1993) Highly permeable and layered Jurassic oceanic crust in the western Pacific. Earth and Planetary Science Letters 119: 71-83

Laverne C, Belarouchi A, Honnorez J (1996) Alteration mineralogy and chemistry of the upper oceanic crust from Hole 896A, Costa Rica Rift, pp.151-170. *In:* Alt JC, Kinoshita H, Stokking LB, et al. (eds) Proceedings of the Ocean Drilling Program, Scientific Results 148, College Station, TX

MacLeod CJ (1994) Structure of the outer Tonga forearc at Site 841, pp.313-329. *In:* Hawkins JW, Parson LM, Allan JF, et al. (eds) Proceedings of the Ocean Drilling Program, Scientific Results 135, College Station, TX

MacLeod CJ, Lothian A (1994) Comparison of GLORIA sidescan sonar and core-derived structural data from Site 841, Tonga Trench, pp.373-382. *In:* Hawkins JW, Parson LM, Allan JF, et al. (eds) Proceedings of the Ocean Drilling Program, Scientific Results 135, College Station, TX

Malahoff A, Feden RH, Fleming HS (1982) Magnetic anomalies and tectonic fabric of marginal basins north of New Zealand. Journal of Geophysical Research 87: 4109-4125

McDougall I (1994) Dating of rhyolitic glass in the Tonga forearc (Hole 841B). *In:* Hawkins JW, Parson LM, Allan JF, et al. (eds) Proceedings of the Ocean Drilling Program, Scientific Results 135, College Station, TX

McMurtry GM, Wang C-H, Yeh H-W (1983) Chemical and isotopic investigations into the origin of clay minerals from the Galapagos hydrothermal mounds. Geochimica et Cosmochimica Acta 47: 475-489

Mehegan J, Robinson P (1985) Lava compositions of the Troodos ophiolite, Cyprus. EOS 66: 1123

Mitchell JG, Peate DW, Murton BJ, Pearce JA, Arculus RJ, van der Laan S (1992) K-Ar dating of samples from Sites 782 and 786 (Leg 125): the Izu-Bonin forearc region, pp.203-210. *In:* Fryer P, Coleman P, Pearce JA, Stokking LB (eds) Proceedings of the Ocean Drilling Program, Scientific Results 125, College Station, TX
Moores EM, Varga EJ (1984) Extensional tectonics and possible abandoned axial valley, Troodos ophiolite, Cyprus. EOS 65: 1115

Moores EM, Vine FJ (1971) The Troodos Massif, Cyprus, and other ophiolites as oceanic crust: Evaluation and implications: Philosophical Transactions of the Royal Society of London, v.268, p.443-466.

Mottl MJ (1989) Hydrothermal convection, reaction, and diffusion in sediments on the Costa Rica Rift flank: pore-water evidence from Ocean Drilling Program Sites 677 and 678, pp.195-213. *In:* Becker K, Sakai H, et al. (eds) Proceedings of the Ocean Drilling Program, Scientific Results 111, College Station, TX

Mottl MJ, Holland HD (1978) Chemical exchange during hydrothermal alteration of basalt by seawater - 1. Experimental results for major and minor components of seawater. Geochimica et Cosmochimica Acta 42: 1103-1115

Mottl MJ, Wheat CG (1994) Hydrothermal circulation through mid-ocean ridge flanks: fluxes of heat and magmatism. Geochimica et Cosmochimica Acta 58: 2225-2238

Munha J, Fyfe WS, Kerrich R (1980) Adularia, the characteristic mineral of felsic spilites: Contributions to Mineralogy and Petrology 75:15-19

Natland JH, Hekinian R (1981) Hydrothermal alteration of basalts and sediments at DSDP Site 456, Mariana Trough, pp.759-769. *In:* Hussong D, Ueda S (eds) Initial Reports of the Deep Sea Drilling Project 60, U.S. Government Printing Office, Washington

Natland JH, Mahoney JJ (1981) Alteration of igneous rocks at DSDP Sites 458 and 459, Mariana forearc region: Relationship to basement structure, pp.769-788. *In:* Hussong D, Ueda S (eds) Initial Reports of the Deep Sea Drilling Project 60, U.S. Government Printing Office, Washington

Natland JH, Tarney J (1981) Petrologic evolution of the Mariana arc and back-arc system: a synthesis of drilling results in the southern Philippine Sea,pp.681-708. *In:* Hussong D,

Ueda S (eds) Initial reports of the Deep Sea Drilling Project, 60, U.S. Government Printing Office, Washington

Nehlig P, Juteau T (1988) Flow porosities, permeabilities, and preliminary data on fluid inclusions and fossil thermal gradients in the crustal sequence of the Semail ophiolite (Oman). Tectonophysics 151: 199-221

Newmark RL, Anderson RN, Moos D, Zoback MD (1985) Sonic and ultrasonic logging of Hole 504B and its implications for the structure, porosity, and stress regime of the upper 1 km of the oceanic crust, pp.479-510. *In:* Anderson RN, Honnorez J, Becker K, et al. (eds) Initial Reports of the Deep Sea Drilling Project 83, U.S. Government Printing Office, Washington

Packham GH (1985) Vertical tectonics on the Tonga Ridge from Tongatapu oil exploration wells, pp.291-300. *In:* Scholl DW, Vallier TL (eds) Geology and offshore resources of Pacific island arcs - Tonga region. Circum-Pacific Council for Energy and Resources, Earth Science Series 2

Parson LM, Hawkins JW, Allan JF, et al. (1992) Proceedings of the Ocean Drilling Program, Initial Reports 135, College Station, TX

Petelin VP (1964) Hard rock in the deep-water trenches of the southwestern Pacific Ocean, pp. 78-86. *In:* International Geological Congress, 22nd Session, Reports of Soviet Geologists: Geology of the Oceans and Seas 16

Pezard PA (1990) Electrical properties of mid-ocean ridge basalt and implications for the structure of the upper oceanic crust in Hole 504B Journal of Geophysical Research 95: 9237-9264

Pezard PA, Anderson RN, Ryan WBF, Becker K, Alt JC, Gente P (1992) Accretion, structure, and hydrology of intermediate spreading-rate oceanic crust from drillhole experiments and seafloor observations. Marine Geophysical Research 14: 93-123

Pflumio C (1991) Evidences for polyphased oceanic alteration of the extrusive sequence of the Semail Ophiolite from the Salahi Block (northern Oman). *In:* Ophiolite Genesis and Evolution of the Oceanic Lithosphere, Kluwer Academic Publishers

Rautenschlein MG, Jenner GA, Herfogen J, Hoffman A, Kerrich R, Schmincke H-U, White WM (1985) Isotopic and trace element composition of volcanic glasses from Akaki Canyon, Cyprus: implications for the origin of the Troodos ophiolite. Earth and Planetray Science Letters 75: 369-383

Richardson SH, Hart SR, Staudigel H (1980) Vein mineral ages of old ocean crust. Journal of Geophysical Research 85: 7195-7200

Richardson CJ, Cann JR, Richards HG, Cowan JG (1987) Metal-depleted root zones of the Troodos ore-forming hydrothermal systems, Cyprus. Earth and Planetary Science Letters 84: 243-253

Robinson PT, Melson W, Schmincke H-U (1983) Volcanic glass compositions of the troodos ophiolite, Cyprus. Geology 11: 400-404

Schiffman P, Evarts RC, Williams AE, Pickthorn WP (1991) Hydrothermal metamorphism in oceanic crust from the Coast Range ophiolite of California: Fluid-rock interaction in a rifted arc, pp.399-426. *In:* Peters TJ, Nicolas A, Coleman RG (eds) Ophiolite genesis and evolution of oceanic lithosphere, Kluwer Academic Publishers

Schiffman P, Smith BM, Varga RJ, Moores EM (1987) Geometry, conditions, and timing of off-axis hydrothermal metamorphism and ore deposition in the Solea Graben. Nature 325: 423-425

Scholl DW, Vallier TL, Maung TU (1985) Introduction, pp.379-414. *In:* Scholl DW, Vallier TL (eds) Geology and offshore resources of Pacific island arcs - Tonga region: Circum-Pacfic Council for Energy and Resources, Earth Science Series 2

Schöps D, Herzig PM (1994a) Hydrothermally altered felsic rocks of the Tonga forearc, pp.653-663. *In:* Hawkins JW, Parson LM, Allan JF, et al. (eds) Proceedings of the Ocean Drilling Program, Scientific Results 135, College Station, TX

Schöps D, Herzig PM (1994b) Thaumasite in Lau Basin basaltic andesite, Hole 841B, pp.647-652. *In:* Hawkins JW, Parson, LM, Allan JF, et al. (eds) Proceedings of the Ocean Drilling Program, Scientific Results 135, College Station, TX

Serri G (1981) The petrochemistry of ophiolitic gabbroic complexes: a key for the classification of ophiolites into low-Ti and high-Ti types. Earth and Planetary Science Letters 52: 203-212

Seyfried WE Jr., Shanks III WC, Dibble WE Jr. (1978) Clay mineral formation in DSDP Leg 134 basalt. Earth and Planetary Science Letters 41: 265-276

Seyfried WE (1987) Experimental and theoretical constraints on hydrothermal processes at mid-ocean ridges. Annual Review of Earth and Planetary Science 15: 317-335

Seyfried WE, Ding K (1993) The effect of redox on the relative solubilities of copper and iron in Cl-bearing aqueous fluids at elevated temperatures and pressures: an experimental study with application to seafloor hydrothermal systems. Geochimica et Cosmochimica Acta 57: 1905-1918

Seyfried WE Jr., Janecky DR, Mottl M (1984) Alteration of the oceanic crust: Implications for geochemical cycles of lithium and boron. Geochimica et Cosmochimica Acta 48: 557-569

Sharaskin A, Pushchin IK, Zlobin SK, Kolesov GM (1984) Two ophiolite sequences from the basement of the northern Tonga arc: Ofioliti 8: 411-430

Stakes DS, O'Neil JR (1982) Mineralogy and stable isotope geochemistry of hydrothermally altered oceanic rocks. Earth and Planetary Science Letters 57: 285-304

Staudigel H, Hart SR, Richardson SH (1981) Alteration of the oceanic crust: processes and timing. Earth and Planetary Science Letters 52: 311-327

Stein CA, Stein S (1994) Constraints on hydrothermal heat flux through the oceanic lithosphere from global heat flow. Journal of Geophysical Research 99: 3081-3095

Tagudin JE, Scholl DW (1994) The westward migration of the Tofua Volcanic Arc towards the Lau Basin, pp.121-130. *In:* Herzer RH, Ballance PF, Stevenson AJ (eds) Geology and resources of island arcs - Tonga-Lau-Fiji region. SOPAC Technical Bulletin 8

Tappin DR (1994) The Tonga Frontal-Arc Basin, pp.157-176. *In:* Ballance PF (ed) South Pacific Sedimentary Basins, Sedimentary Basins of the World 2, Elsevier

Tappin DR, Ballance PF (1994), Contributions to the sedimentary geology of 'Eua Island, Kingdom of Tonga: reworking in an oceanic forearc, pp.1-20. *In:* Stevenson AJ, Herzer RH, Ballance PF (eds) Geology and resources of island arcs - Tonga-Lau-Fiji region. SOPAC Technical Bulletin 8

Taylor B, Fujioka K, et al. (1990) Proceedings of the Ocean Drilling Program, Initial Reports 126, College Station, TX

Taylor B (1992) Rifting and the volcanic-tectonic evolution of the Izu-Bonin-Mariana arc, pp.627-653. *In:* Proceedings of the Ocean Drilling Program, Scientific Results 126, College Station, TX

Teagle DAH, Alt JC, Bach W, Halliday AN, Erzinger J (1996) Alteration of upper ocean crust in a ridge-flank hydrothermal upflow zone: mineral, chemical, and isotopic constraints from Hole 896A, pp.119-150. *In:* Alt JC, Kinoshita H, Stokking LB, et al. (eds) Proceedings of the Ocean Drilling Program, Scientific Results 148, College Station, TX

Udintsev GR, Dmitriyev LV (1974) New data on trench-faults in the southwestern Pacific. AGU translation series, Geotectonics 2: 65-69

Vallier TL, O'Connor RM, Scholl DW, Stevenson AJ, Quinterno PJ (1985) Petrology of rocks dredged from the landward slope of the Tonga Trench: implications for middle Miocene volcanism and subsidence of the Tonga Ridge, pp.109-120. *In:* Scholl D, Vallier TL (eds) Geology and Offshore Resources of Pacific Island Arcs-Tonga Region. Circum-Pacific Council for Energy and Mineral Resources, Earth Science Series 2

von Huene R, Scholl DW (1991) Observations at convergent margins concerning sediment subduction, subduction erosion, and the growth of continental crust. Reviews in Geophysics 29: 279-316

Watts AB, Weissel JK, Duncan RA, Larson RL (1988) Origin of the Louisville Ridge and its relationship to the Eltanin Fracture Zone. Journal of Geophysical Research 97: 3051-3077

Zuleger E, Alt JC, Erzinger JA (1995) Primary and secondary variations in major and trace element geochemistry of the lower sheeted dike complex: Hole 504B, Leg 140, pp.65-80. *In:* Erzinger J, Becker K, Dick HJB, Stokking LB (eds) Proceedings of the Ocean Drilling Program, Scientific Results 137/140, College Station, TX

Appendix I. Analytical Methods

A. ICP-AES

Samples analyzed by ICP-AES (inductively-coupled plasma atomic emission spectrometry) were sawed into pieces that were small enough to fit into the jaw mill. The amount of rock cut was increased for more coarsely crystalline or less homogeneous samples. The cut surfaces were polished to remove saw blade contamination, rinsed in distilled water, cleaned in a sonic bath for approximately 2-4 minutes, and air-dried. The pieces were crushed in a tungsten carbide jaw mill, then in a tungsten carbide ball mill, until a fine powdered consistency was reached. Powders were dried for at least three hours in a 60°C oven. Loss On Ignition (LOI) was determined for each rock powder by weighing, then heating, approximately 1 g (measured to the ten-thousandth of a gram) of powder at 1050 K in a Thermolyne F1500 muffle furnace for 30 minutes, after which it was cooled in a desiccator, then weighed again to determine the mass lost.

Approximately 0.25 g (measured to the ten-thousandth of a gram) of each rock powder was placed in a carbon crucible containing 0.75 g of lithium metaborate flux. The crucibles were then heated at 1050 K in the furnace for 20 minutes. Immediately after removal from the furnace, each sample of molten rock and flux was poured into a polyethylene vial containing 50 ml of a 1.5 N solution of trace metal grade nitric acid in ultrapure distilled water, with 10 ppm Ge, in a polyethylene vial. The Ge was added so that it might be used to recalculate the working curves for the elements, if drift in the results made this necessary. The solutions were stirred until dissolution was as complete

as possible (approximately 20 minutes). In some vials, minor glass particles or carbon dust from the crucible remained. For five of the samples, two separate solutions were prepared in order to check for reproducibility of measurements. These solutions were used for trace element analysis. Major element solutions were prepared by adding 1 g of each of the trace element solutions to 25 ml of a 1.5 N solution of nitric acid in ultrapure distilled water, with 10 ppm Ge and 2100 ppm lithium carbonate, in a polyethylene vial. Incomplete dissolutions of rock and dilution errors in the major element solutions led to all elements being analyzed from the trace element solutions.

Five USGS rock standards (W2, RGM-1, BCR-1, G-2, AGV-1) were prepared as above. Additionally, two splits each of three previously analyzed samples from Sherman Bloomer (EPR, EPR Panur, Panum Dome) were used as additional standards.

Liquid standards were prepared as successive dilutions of separate major and trace element standard solutions. The five major element liquid standards thus produced all contained 10 ppm Ge and 2100 ppm lithium carbonate in 1.5 N nitric acid in ultrapure distilled water. These standards contained, respectively, 90, 50, 10, 1, and 0.1 ppm of each of the elements Al, Fe, Mg, Ti, Na, Ca, K, P, Mn, and Si. The four trace element liquid standards all contained 10 ppm Ge in 1.5 N trace metal grade nitric acid in ultrapure distilled water. These standards contained, respectively, 10, 2, 0.1, and 0.05 ppm of each of the elements Rb, Ba, Sr, Zr, Ni, Cr, V, Cu, Zn, La, Sc, and Y; however, the elements Rb and La were not analyzed from these solutions. All solutions were mixed by volume but checked by weight due to the possibility of significant errors in pipetting small amounts of liquids.

ICP-AES analysis was performed using the Liberty 150 inductively-coupled plasma spectrometer at Oregon State University's College of Oceanic and Atmospheric Science. All liquid standards were analyzed first, followed by two blank solutions, the unknowns, the rock standards, and lastly another blank solution. The 2 ppm trace element liquid standard was used as a drift monitor and was reanalyzed after every five samples and at the end of the run. The elements Al, Fe, Mg, Ti, Ca, P, Mn, and Si were analyzed under the following conditions: 1.0 kW power, 15 s stabilization time, 40 s rinse time, and 20 s sample delay time. Na and K were analyzed in a separate run under these conditions: 0.80 kW power, 15 s stabilization time, 40 s rinse time, and 20 s sample delay time. Ba, Sr, Zr, Ni, Cr, V, Cu, Zn, Sc, and Y were analyzed under the same conditions as the major elements.

It was necessary to manually recalculate the Si, Na, and K working curves from the raw intensities of these elements and from their machine-calculated concentrations in the drift monitors due to a systematic error of unknown cause. The trace element data for all elements except Zr tended to be systematically low, and were corrected by calculating the factors necessary for the analyzed standards to yield the correct known concentrations of those elements, averaging these factors, and multiplying the measured concentrations (in ppm) of these elements by the appropriate factors to get the corrected concentrations. The Zr working curve was recalculated using the raw intensities measured for Zr, and the Zr concentrations measured for the drift standard.

B. Electron microprobe

Electron microprobe analyses were performed on 14 carbon-coated polished thin sections using the Cameca SX-50 electron microprobe at Oregon State University. Beam conditions were set at 30 nA current and 15.1 keV accelerating voltage. Na, Mg, Al, Si, Cl, K, and Mn were counted for 10 s on peak, while F, Ti, and Fe were counted for 20 s on peak. Background counts were taken on either side of the peak for half the peak counting time. Due to the difficulties in obtaining a high quality polish on soft altered phases, data reproducibility was difficult to assess. The validity of data was determined by calculating structural formulas for the analyzed minerals using the oxide analyses. If formulas were not stoichiometric within appropriate compositional boundaries for clays and zeolites, or the oxide totals were too low, the analyses were discarded (approximately 20-30% of analyses).

C. X-ray diffraction

Samples were prepared for x-ray diffraction by crushing sawed rock fragments in the tungsten carbide jaw crusher followed by the tungsten carbide ball mill. Non-oriented dry powder mounts were made using these powders. The <2μ clay fraction was separated from the powders by flocculation and multiple instances of centrifuging. This fraction was then used to make oriented mounts by smearing the wet material onto glass slides. Those slides for which ethylene glycol treatment was desired were heated at 60°C and then placed in the glycolator for overnight or longer. X-ray diffraction was performed at

Oregon State University with the Phillips x-ray diffractometer, scanning from 2-34° with a step size of 0.02, and counting for 1 s.

Appendix II. Electron Microprobe Data

Label	mineral	Ox%(Na	Ox%(Mg	Ox%(Al)	Ox%(Si)	Ox%(K)	Ox%(Ca	Ox%(Ti)	Ox%(Mn	Ox%(Fe)	Total
ana1	sap-cel	0.15	8.33	4.09	47.36	7.49	0.12	0.32	0.05	12.39	80.62
ana2	sap-cel	0.06	7.42	7.41	47.90	6.18	0.20	0.19	0.02	13.86	83.51
ana3	sap-cel	0.08	6.92	6.48	53.42	8.14	0.28	0.13	0.03	15.58	91.30
ana4	sap-cel	0.07	6.90	7.18	50.57	7.53	0.22	0.14	0.06	13.85	86.76
ana5	sap-cel	0.11	6.58	6.45	53.06	7.84	0.15	0.04	0.01	17.27	91.66
ana6	sap-cel	0.09	8.21	7.11	50.96	7.01	0.27	0.07	0.07	14.24	88.31
ana7	sap-cel	0.07	5.59	7.62	49.16	7.42	0.18	0.12	0.14	20.99	91.39
ana8	sap-cel	0.10	4.90	8.06	48.68	7.73	0.21	0.08	0.03	22.94	92.80
ana9	sap-cel	0.21	4.37	8.06	49.70	6.38	1.48	0.34	0.07	22.51	93.23
ana10	sap-cel	0.13	3.88	7.98	47.78	6.93	0.20	0.16	0.11	23.51	90.73
ana11	sap-cel	0.15	5.05	8.12	49.24	7.79	0.19	0.08	0.07	22.77	93.49
ana12	sap-cel	0.14	4.92	8.68	49.93	7.60	0.26	0.10	0.06	21.44	93.20
ana13	sap-cel	0.11	6.52	7.25	50.44	7.62	0.24	0.17	0.09	20.14	92.77
ana14	sap-cel	0.12	5.34	6.30	50.34	7.91	0.17	0.15	0.08	21.49	91.96
ana15	sap-cel	0.06	6.10	7.28	51.85	7.27	0.19	0.13	0.05	19.90	92.99
ana16	sap-cel	0.06	6.24	7.14	51.10	7.32	0.18	0.10	0.09	20.72	93.07
ana17	sap-cel	0.13	3.78	8.08	47.62	6.77	0.23	0.14	0.09	23.83	90.73
ana18	sap-cel	0.17	4.24	7.07	47.37	7.34	0.30	0.60	0.27	24.81	92.19
ana19	sap-cel	0.15	4.42	7.35	48.60	7.33	0.24	0.11	0.10	24.63	92.99
ana20	sap-cel	0.19	4.48	7.19	48.42	7.34	0.23	0.11	0.08	24.68	92.74
ana21	sap-cel	0.21	4.11	8.17	48.26	7.12	0.22	0.17	0.07	24.66	93.01
ana22	sap-cel	0.10	4.94	7.87	47.85	7.28	0.18	0.03	0.08	23.06	91.43
ana23	sap-cel	0.15	5.09	8.01	48.66	6.97	0.28	0.09	0.08	23.45	92.81
ana24	sap-cel	0.19	9.05	8.66	49.98	6.19	0.17	0.24	0.14	16.09	90.93
ana25	sap-cel	0.11	4.12	6.60	48.35	7.14	0.21	0.07	0.06	25.82	92.53
ana26	sap-cel	0.19	4.92	7.74	47.83	7.06	0.26	0.10	0.07	23.94	92.19
ana27	sap-cel	0.16	4.67	7.49	46.67	6.88	0.24	0.09	0.11	23.72	90.11
ana28	sap-cel	0.14	8.32	8.25	49.02	6.73	0.25	0.11	0.12	18.19	91.27
ana29	sap-cel	0.12	4.58	6.19	48.38	7.13	0.25	0.09	0.09	25.70	92.60
ana30	sap-cel	0.18	4.62	6.23	48.33	7.25	0.23	0.07	0.08	25.94	93.01
ana31	sap-cel	0.08	5.21	7.40	47.21	6.73	0.30	0.09	0.12	23.40	90.60
ana32	sap-cel	0.16	4.71	6.13	47.83	7.27	0.25	0.04	0.09	26.02	92.54
ana33	sap-cel	0.16	6.13	7.98	48.45	6.88	0.25	0.13	0.19	22.94	93.16
ana34	sap-cel	0.11	4.63	6.19	47.92	7.19	0.25	0.05	0.05	26.08	92.53
ana35	sap-cel	0.14	5.02	6.29	48.01	7.13	0.22	0.06	0.10	25.47	92.48
ana36	sap-cel	0.12	4.69	6.23	47.76	7.29	0.26	0.06	0.03	26.08	92.58
ana37	sap-cel	0.09	5.36	7.76	47.73	6.76	0.36	0.09	0.09	24.18	92.53
ana38	sap-cel	0.14	4.89	6.14	47.97	7.10	0.26	0.03	0.09	26.04	92.69
ana39	sap-cel	0.20	4.20	7.69	46.69	6.72	0.29	0.17	0.07	25.85	91.93
ana40	sap-cel	0.15	4.05	7.59	46.76	6.82	0.26	0.20	0.06	26.46	92.40
ana41	sap-cel	0.11	4.78	5.52	46.92	6.87	0.24	0.23	0.16	26.93	91.80
ana42	sap-cel	0.20	6.76	9.50	46.40	5.80	0.32	0.13	0.16	23.50	92.82
ana43	sap-cel	0.10	5.80	8.37	45.47	5.87	0.39	0.15	0.17	25.85	92.27
ana44	sap-cel	0.08	9.75	4.64	49.38	5.55	0.61	0.21	0.02	15.39	86.43
ana45	sap-cel	0.30	10.79	4.73	47.18	6.00	0.07	0.19	0.05	12.51	82.05
ana46	sap-cel	0.08	10.52	4.42	49.29	6.04	0.29	0.25	0.06	14.52	86.17
ana47	sap-cel	0.24	4.53	7.16	46.29	6.93	0.30	0.10	0.06	23.99	89.77
ana48	sap-cel	0.20	4.43	9.43	45.50	6.30	0.30	0.08	0.09	23.30	89.79
ana49	sap-cel	0.15	4.45	9.77	45.07	5.88	0.30	0.11	0.15	23.04	89.02
ana50	sap-cel	0.17	4.73	11.07	45.34	5.90	0.36	0.14	0.11	22.75	90.69
ana51	sap-cel	0.25	4.11	8.04	45.69	6.48	0.38	0.08	0.09	26.00	91.26

Label	mineral	Ox%(Na)	Ox%(Mg	Ox%(Al)	Ox%(Si)	Ox%(K)	Ox%(Ca)	Ox%(Ti)	Ox%(Mn	Ox%(Fe)	Total
ana52	sap-cel	0.25	4.39	12.31	44.87	5.25	0.35	0.00	0.09	22.31	89.86
ana53	sap-cel	0.27	4.90	14.08	44.74	5.03	0.45	0.11	0.13	21.26	91.05
ana54	sap-cel	0.25	4.67	12.84	44.31	5.11	0.35	0.00	0.13	22.45	90.16
ana55	sap-cel	0.54	12.36	9.29	48.81	4.35	0.29	0.14	0.14	12.91	88.97
ana56	sap-cel	0.22	4.27	7.80	42.70	6.12	0.41	0.12	0.13	28.41	90.34
ana57	sap-cel	0.39	12.83	13.49	46.83	3.16	0.61	0.06	0.26	11.76	89.48
ana58	sap-cel	0.47	13.06	14.39	46.79	3.26	0.64	0.06	0.30	11.91	90.98
ana59	sap-cel	0.45	11.68	5.18	49.25	5.37	0.32	0.09	0.05	17.39	89.97
ana60	sap-cel	0.49	11.68	5.24	49.50	5.21	0.13	0.04	0.01	17.21	89.72
ana61	sap-cel	0.46	11.86	5.81	44.49	3.65	0.53	0.11	0.06	14.91	82.11
ana62	sap-cel	0.13	12.56	7.53	48.83	3.45	0.59	0.05	0.05	14.44	87.81
ana63	sap-cel	0.16	9.07	16.75	49.95	3.20	0.31	0.63	0.02	15.92	96.08
ana64	sap-cel	0.15	9.35	16.20	48.99	3.22	0.30	0.63	0.11	15.65	94.74
ana65	sap-cel	0.11	9.47	11.22	46.61	2.09	0.61	1.00	0.07	9.78	81.16
ana66	sap-cel	0.16	7.37	4.17	48.17	7.70	0.30	0.37	0.06	13.09	81.45
ana67	sap-cel	0.05	7.88	3.20	48.11	7.80	0.16	0.32	0.05	13.40	81.00
ana68	sap-cel	0.30	8.20	3.73	51.42	7.93	0.09	0.31	0.01	14.46	86.64
ana69	sap-cel	0.30	7.59	4.20	48.96	7.67	0.11	0.33	0.07	13.43	82.84
ana70	sap-cel	0.25	8.06	3.69	48.94	7.80	0.18	0.33	0.07	13.61	83.01
ana71	sap-cel	1.22	7.84	10.87	48.70	6.15	1.10	0.07	0.05	11.65	87.66
ana72	sap-cel	0.05	7.21	5.05	53.12	9.08	0.50	0.02	0.00	17.87	93.15
ana73	sap-cel	0.08	6.91	5.00	53.28	8.91	0.38	0.00	0.08	18.28	93.06
ana74	sap-cel	0.11	8.29	3.76	50.04	7.23	0.16	0.33	0.02	14.21	84.40
ana75	sap-cel	0.08	6.68	4.39	47.84	7.96	0.20	0.26	0.06	15.70	83.25
ana76	sap-cel	0.03	6.59	6.68	48.88	7.32	0.12	0.21	0.04	14.51	84.38
ana77	sap-cel	0.27	7.85	3.81	48.92	7.29	0.50	0.71	0.07	14.85	84.69
ana78	sap-cel	0.15	6.68	7.88	46.28	6.79	0.14	0.04	0.03	12.42	80.46
ana79	sap-cel	0.05	8.60	3.97	53.71	7.22	0.60	0.28	0.06	16.34	91.15
ana80	sap-cel	0.23	8.49	3.83	47.49	6.74	1.31	0.39	0.14	14.17	82.85
ana81	sap-cel	0.09	6.86	6.24	52.58	7.70	0.26	0.05	0.01	16.99	90.78
ana82	sap-cel	0.06	6.94	5.89	52.16	8.07	0.30	0.03	0.06	17.63	91.19
ana83	sap-cel	0.17	8.83	4.06	48.33	7.29	0.35	0.40	0.09	13.29	82.85
ana84	sap-cel	0.24	9.14	4.11	48.96	7.46	0.35	0.36	0.05	13.36	84.09
ana85	sap-cel	0.15	7.29	6.71	48.10	7.44	0.13	0.15	0.02	14.58	84.59
ana86	sap-cel	0.33	8.65	4.44	46.60	6.79	0.09	0.30	0.05	12.77	80.18
ana87	sap-cel	0.11	5.18	5.06	53.43	7.66	0.38	0.01	0.03	23.64	95.52
ana88	sap-cel	0.12	6.61	5.05	53.02	7.64	0.44	0.03	0.02	21.04	94.00
ana89	sap-cel	0.13	6.45	6.15	51.13	7.29	0.19	0.00	0.03	19.17	90.57
ana90	sap-cel	0.11	6.07	5.32	52.81	7.55	0.32	0.00	0.00	21.58	93.76
ana91	sap-cel	0.10	5.19	4.92	53.33	7.80	0.33	0.03	0.00	24.01	95.76
ana92	sap-cel	0.16	6.26	5.03	52.12	7.51	0.40	0.01	0.02	21.51	93.04
ana93	sap-cel	0.11	6.63	4.79	52.40	7.96	0.35	0.00	0.05	21.45	93.76
ana94	sap-cel	0.07	5.37	4.74	53.32	7.95	0.26	0.03	0.02	24.04	95.81
ana95	sap-cel	0.13	6.44	5.33	51.79	7.83	0.50	0.03	0.01	21.60	93.69
ana96	sap-cel	0.12	5.39	4.43	51.55	8.03	0.32	0.04	0.03	23.64	93.54
ana97	sap-cel	0.09	5.58	4.50	51.77	7.84	0.26	0.01	0.01	23.05	93.10
ana98	sap-cel	0.12	7.06	4.65	52.50	7.38	0.40	0.04	0.00	20.97	93.14
ana99	sap-cel	0.16	6.60	5.42	51.29	7.50	0.39	0.04	0.02	21.19	92.66
ana100	sap-cel	0.10	5.32	4.48	51.01	7.67	0.49	0.01	0.02	23.97	93.09
ana101	sap-cel	0.12	5.47	4.56	51.73	7.98	0.30	0.03	0.06	24.21	94.46
ana102	sap-cel	0.10	6.03	5.21	49.92	6.76	0.32	0.01	0.00	20.84	89.19

Label	mineral	Ox%(Na	Ox%(Mg	Ox%(Al)	Ox%(Si)	O:%(K)	Ox%(Ca	Ox%(Ti)	Ox%(Mn	Ox%(Fe)	Total
ana103	sap-cel	0.08	5.54	4.49	51.11	7.78	0.49	0.00	0.05	24.16	93.72
ana104	sap-cel	0.18	7.56	6.99	50.82	6.69	0.61	0.05	0.03	18.65	91.60
ana105	sap-cel	1.28	9.57	10.85	47.37	5.09	0.33	0.14	0.10	11.46	86.24
ana106	sap-cel	0.11	5.66	4.69	50.81	7.85	0.32	0.00	0.04	23.82	93.33
ana107	sap-cel	0.19	9.18	4.02	53.39	7.22	0.33	0.17	0.07	18.95	93.61
ana108	sap-cel	0.16	6.56	5.70	50.99	7.40	0.40	0.00	0.05	22.13	93.44
ana109	sap-cel	0.14	6.30	5.08	51.74	7.64	0.34	0.03	0.03	23.38	94.67
ana110	sap-cel	0.18	5.90	5.92	50.44	6.87	0.44	0.04	0.04	22.51	92.37
ana111	sap-cel	0.08	5.77	5.14	49.94	7.69	0.20	0.08	0.07	23.21	92.21
ana112	sap-cel	0.18	5.91	5.51	51.21	7.75	0.14	0.02	0.06	23.73	94.52
ana113	sap-cel	0.10	8.20	5.32	51.83	6.78	0.35	0.08	0.01	19.84	92.52
ana114	sap-cel	0.08	5.41	5.67	49.12	7.25	0.32	0.07	0.06	23.71	91.71
ana115	sap-cel	0.09	5.61	4.73	49.63	7.50	0.26	0.04	0.00	24.59	92.49
ana116	sap-cel	0.08	4.68	5.98	48.06	7.17	0.34	0.05	0.10	25.17	91.70
ana117	sap-cel	0.16	3.94	6.96	47.49	7.26	0.22	0.07	0.07	26.00	92.20
ana118	sap-cel	0.13	3.83	7.29	47.42	7.06	0.25	0.13	0.02	25.94	92.12
ana119	sap-cel	0.16	9.49	7.19	50.80	6.32	0.39	0.08	0.05	17.46	91.98
ana120	sap-cel	0.16	3.87	7.09	47.30	7.31	0.25	0.10	0.03	26.40	92.52
ana121	sap-cel	0.17	4.17	6.58	47.64	7.10	0.21	0.03	0.11	26.18	92.26
ana122	sap-cel	0.15	4.13	6.75	47.16	7.26	0.24	0.05	0.07	26.55	92.38
ana123	sap-cel	0.09	4.67	5.02	47.19	7.41	0.23	0.03	0.06	26.44	91.15
ana124	sap-cel	0.20	6.01	5.50	48.66	7.41	0.15	0.07	0.09	24.99	93.10
ana125	sap-cel	0.13	5.62	4.65	48.91	7.52	0.28	0.03	0.03	26.52	93.70
ana126	sap-cel	0.06	4.66	5.40	47.27	6.60	0.31	0.08	0.08	26.27	90.76
ana127	sap-cel	0.09	9.65	5.46	49.37	5.78	0.39	0.03	0.05	17.85	88.68
ana128	sap-cel	0.09	4.62	4.61	46.51	7.50	0.20	0.16	0.05	27.19	90.94
ana129	sap-cel	0.07	6.09	6.43	47.32	5.95	0.37	0.02	0.08	23.03	89.38
ana130	sap-cel	0.18	6.34	5.54	48.72	7.26	0.11	0.04	0.12	25.17	93.51
ana131	sap-cel	0.15	4.58	6.49	46.77	6.89	0.26	0.02	0.10	26.62	91.87
ana132	sap-cel	0.14	10.62	5.88	48.58	5.42	0.34	0.06	0.06	16.15	87.32
ana133	sap-cel	0.16	6.02	5.12	47.50	7.27	0.08	0.05	0.08	26.22	92.56
ana134	sap-cel	0.37	11.64	5.32	51.76	1.34	0.24	0.04	0.05	12.69	83.45
ana135	sap-cel	0.18	4.89	8.32	45.50	5.94	0.41	0.05	0.15	25.51	91.02
ana136	sap-cel	0.15	10.79	6.58	47.52	4.96	0.89	0.11	0.09	16.56	87.70
ana137	sap-cel	0.17	11.53	8.96	47.86	5.55	0.63	0.08	0.06	14.99	89.87
ana138	sap-cel	0.13	5.92	6.43	46.59	5.79	0.34	0.03	0.05	24.61	89.92
ana139	sap-cel	0.18	5.10	8.57	46.28	5.82	0.37	0.01	0.12	25.98	92.50
ana140	sap-cel	0.20	5.63	5.04	47.64	6.94	0.10	0.04	0.09	28.00	93.70
ana141	sap-cel	1.19	13.12	13.86	46.73	4.13	0.85	0.04	0.09	11.54	91.55
ana142	sap-cel	0.22	14.08	7.21	49.21	4.03	0.96	0.09	0.06	13.15	89.03
ana143	sap-cel	0.26	13.32	8.53	48.24	5.37	0.16	0.03	0.09	14.98	91.01
ana144	sap-cel	0.23	14.46	11.79	46.74	4.61	0.66	0.06	0.11	11.04	89.75
ana145	sap	0.12	12.60	7.25	48.30	3.49	0.42	0.05	0.05	15.00	87.44
ana146	sap	0.20	10.11	18.64	42.12	2.12	0.57	0.18	0.34	11.74	86.14
ana147	sap	0.44	13.15	14.40	46.06	2.79	0.67	0.06	0.30	12.03	90.07
ana148	sap	0.45	12.74	13.48	43.84	2.77	0.64	0.05	0.35	11.64	86.18
ana149	sap	0.11	10.81	18.39	41.24	1.60	0.76	0.24	0.40	11.17	84.94
ana150	sap	0.19	11.04	18.69	41.89	2.21	0.61	0.18	0.42	12.55	87.94
ana151	sap	0.39	17.66	5.62	46.85	2.52	0.46	0.97	0.06	8.69	83.63
ana152	sap	0.57	17.71	5.11	46.14	2.81	0.32	0.60	0.05	8.61	82.30
ana153	sap	0.15	11.44	18.49	40.89	1.41	0.71	0.30	0.38	11.14	85.09

Label	mineral	Ox%(Na)	Ox%(Mg)	Ox%(Al)	Ox%(Si)	Ox%(K)	Ox%(Ca)	Ox%(Ti)	Ox%(Mn)	Ox%(Fe)	Total
ana154	sap	0.75	14.44	5.85	46.51	3.35	0.11	0.05	0.01	15.44	86.79
ana155	sap	0.26	11.14	17.60	40.60	1.51	0.77	0.09	0.51	13.41	86.04
ana156	sap	0.24	10.94	17.64	39.27	1.56	0.65	0.21	0.40	12.41	83.42
ana157	sap	0.52	18.27	5.27	45.11	2.74	0.63	0.42	0.03	8.71	82.29
ana158	sap	0.47	17.99	5.45	45.22	2.55	0.44	0.60	0.01	9.58	82.74
ana159	sap	0.24	13.04	19.91	41.96	1.68	0.80	0.01	0.36	12.53	90.59
ana160	sap	1.10	15.59	5.85	43.79	2.45	0.17	0.03	0.06	13.83	83.18
ana161	sap	0.25	13.71	18.97	42.59	1.71	0.77	0.07	0.28	12.53	90.93
ana162	sap	0.15	11.76	17.73	39.32	1.40	0.67	0.23	0.42	13.20	85.00
ana163	sap	0.19	12.50	19.31	40.27	1.32	0.91	0.07	0.31	12.73	87.70
ana164	sap	0.35	17.40	14.19	45.89	2.91	0.42	0.11	0.37	11.37	93.06
ana165	sap	0.20	13.27	20.33	42.00	1.61	0.76	0.04	0.42	13.05	91.73
ana166	sap	0.11	18.92	7.28	44.94	0.58	1.21	0.05	0.04	7.50	80.85
ana167	sap	0.30	13.35	19.80	41.11	1.41	0.98	0.09	0.42	13.50	91.08
ana168	sap	0.10	17.60	7.08	43.74	1.29	1.11	0.04	0.09	9.83	81.14
ana169	sap	0.31	13.50	19.61	40.52	1.43	0.94	0.26	0.49	13.45	90.67
ana170	sap	0.30	13.57	19.61	40.54	1.36	0.93	0.47	0.47	13.52	90.90
ana171	sap	0.35	16.13	12.85	42.21	2.46	0.42	0.46	0.37	12.01	87.39
ana172	sap	0.11	19.25	8.22	43.66	0.18	1.40	0.00	0.03	6.53	79.63
ana173	sap	0.97	13.75	5.41	45.31	4.13	0.31	0.04	0.05	14.34	84.33
ana174	sap	0.10	11.63	7.10	46.32	4.98	0.34	0.14	0.08	18.04	88.77
ana175	sap	0.53	13.53	10.67	44.60	4.20	0.28	0.12	0.14	12.85	86.97
ana176	sap	0.19	13.80	6.97	46.90	4.41	0.42	0.06	0.01	14.80	87.62
ana177	sap	0.14	5.52	7.99	43.95	4.66	0.46	0.15	0.16	28.36	91.42
ana178	sap	0.19	5.52	5.19	44.53	6.27	0.15	0.06	0.14	31.10	93.23
ana179	sap	0.12	14.96	6.31	46.89	3.21	0.73	0.07	0.04	13.13	85.51
ana180	sap	0.10	14.22	6.45	42.58	3.15	1.45	0.09	0.10	12.75	80.93
ana181	sap	0.62	15.15	5.68	46.80	1.40	0.34	0.01	0.05	11.85	81.90
ana182	sap	0.23	13.18	7.22	41.77	2.69	2.69	0.30	0.23	17.65	86.01
ana183	sap	0.12	16.67	6.47	45.94	2.72	0.79	0.13	0.03	12.03	84.93
ana184	sap	0.73	17.55	12.24	42.25	2.96	0.60	0.13	0.11	7.85	84.44
ana185	sap	0.15	17.23	6.24	45.84	2.41	0.82	0.11	0.01	11.14	83.95
ana186	sap	0.13	5.17	7.13	40.90	4.35	0.41	0.00	0.23	31.63	89.99
ana187	sap	0.10	16.19	9.80	43.33	3.75	0.44	0.06	0.08	13.07	86.85
ana188	sap	1.69	17.30	5.87	43.93	1.69	0.16	0.10	0.05	12.58	83.42
ana189	ds-sap	0.29	7.11	17.97	52.26	3.45	0.58	0.41	0.10	6.10	88.40
ana190	ds-sap	0.39	7.47	18.72	52.66	3.81	0.50	0.33	0.08	5.18	89.52
ana191	ds-sap	0.26	7.44	17.98	51.97	3.26	0.58	0.36	0.11	5.74	87.84
ana192	ds-sap	0.23	6.01	19.69	51.53	4.27	0.58	0.21	0.09	10.68	93.38
ana193	ds-sap	0.27	6.86	17.36	47.43	3.26	0.63	0.44	0.10	6.48	82.96
ana194	ds-sap	0.26	7.51	18.09	51.67	3.37	0.57	0.50	0.08	7.17	89.36
ana195	ds-sap	0.21	5.76	21.09	51.51	3.68	0.51	0.45	0.14	11.28	94.71
ana196	ds-sap	0.20	7.42	19.10	50.86	3.32	0.37	0.38	0.11	6.34	88.29
ana197	ds-sap	0.36	6.97	21.14	50.46	3.38	1.56	0.47	0.14	10.54	95.16
ana198	ds-sap	0.21	6.22	21.34	51.04	3.69	0.55	0.42	0.09	10.68	94.34
ana199	ds-sap	0.22	6.40	19.43	50.75	3.99	0.50	0.17	0.15	12.15	93.91
ana200	ds-sap	0.20	6.09	18.79	49.01	4.01	0.50	0.19	0.08	12.50	91.49
ana201	ds-sap	0.24	7.61	17.87	50.20	3.36	0.46	0.39	0.18	8.77	89.20
ana202	ds-sap	0.24	7.88	18.34	47.48	3.48	2.29	0.30	0.14	12.39	92.70
ana203	ds-sap	0.29	7.72	17.04	47.39	2.89	0.60	0.32	0.19	9.33	85.92
ana204	di smec	1.06	2.28	19.56	51.67	4.23	1.09	0.18	0.14	6.80	87.07

Label	mineral	Ox%(Na)	Ox%(Mg)	Ox%(Al)	Ox%(Si)	Ox%(K)	Ox%(Ca)	Ox%(Ti)	Ox%(Mn)	Ox%(Fe)	Total
ana205	di smec	0.89	6.39	15.14	52.16	3.99	3.20	1.74	0.15	11.10	94.94
ana206	di smec	0.59	3.16	15.71	52.74	2.88	1.07	1.04	0.05	13.90	91.80
ana207	di smec	1.18	2.65	14.67	52.10	3.57	1.09	2.00	0.06	15.99	93.72
ana208	di smec	0.85	3.06	14.86	51.70	2.95	0.75	1.53	0.02	14.54	90.79
ana209	di smec	0.80	3.65	13.32	53.31	3.76	0.95	1.25	0.07	15.91	93.22
ana210	di smec	0.82	2.95	14.79	48.74	3.09	1.18	3.61	0.11	12.50	88.02
ana211	di smec	1.06	2.98	15.33	55.40	2.92	1.04	1.04	0.10	14.38	94.85
ana212	di smec	0.55	3.28	14.68	51.68	3.19	0.94	1.04	0.06	14.01	89.89
ana213	di smec	0.96	3.83	13.37	48.75	2.74	2.32	1.04	0.06	13.63	87.16
ana214	di smec	0.84	3.23	14.32	49.22	3.03	1.56	1.07	0.07	14.26	88.01
ana215	di smec	0.74	3.42	14.34	50.52	3.30	0.94	1.12	0.04	14.14	89.03
ana216	di smec	0.54	3.27	14.77	51.66	2.96	0.77	1.18	0.07	13.82	89.38
ana217	di smec	0.92	3.98	13.49	54.39	3.12	0.99	0.92	0.07	14.62	92.68
ana218	di smec	0.13	3.69	9.56	51.98	4.00	0.57	1.90	0.01	19.37	91.26
ana219	di smec	0.25	2.48	14.96	49.99	2.97	0.87	1.24	0.02	16.65	89.59
ana220	di smec	0.14	3.69	11.39	53.74	3.71	0.61	1.44	0.06	17.34	92.20
ana221	di smec	0.09	3.40	9.19	49.83	3.60	0.64	1.61	0.08	17.82	86.43
ana222	di smec	0.65	3.74	13.16	56.27	2.79	0.95	0.18	0.08	14.21	92.16
ana223	di smec	0.30	2.41	15.22	50.98	2.89	0.97	1.51	0.05	15.41	89.88
ana224	di smec	0.26	2.76	14.52	51.52	3.03	0.79	1.48	0.06	16.32	90.85
ana225	di smec	0.29	3.39	12.22	53.66	1.66	0.30	0.52	0.04	17.20	89.36
ana226	di smec	0.68	2.86	17.32	53.92	3.50	0.81	0.42	0.04	13.22	92.92
ana227	di smec	0.44	2.60	15.34	51.74	1.26	0.35	0.68	0.03	15.73	88.31
ana228	di smec	0.42	2.95	14.10	52.00	3.23	0.60	1.41	0.06	15.97	90.85
ana229	di smec	0.91	2.67	14.98	51.58	3.62	0.83	1.47	0.06	15.70	91.91
ana230	di smec	0.46	2.95	13.92	51.83	3.39	0.52	1.44	0.03	17.15	91.75
ana231	di smec	0.44	3.91	10.04	53.73	4.23	0.44	1.38	0.03	19.38	93.65
ana232	di smec	0.38	3.59	9.17	52.57	4.16	0.45	1.69	0.06	20.96	93.10
ana233	di smec	0.60	3.06	13.59	50.32	3.78	0.70	1.44	0.05	15.67	89.40
ana234	di smec	0.62	2.74	19.46	53.21	2.36	1.10	1.71	0.05	8.76	90.19
ana235	di smec	0.53	3.59	11.61	53.51	3.97	0.59	1.38	0.05	17.76	93.05
ana236	di smec	0.62	5.04	8.69	48.45	3.41	0.53	0.77	0.07	18.04	85.73
ana237	di smec	0.70	2.60	15.05	49.06	3.56	0.84	1.44	0.13	14.89	88.39
ana238	di smec	0.37	3.48	10.66	52.88	2.04	1.07	1.27	0.00	13.14	85.00
ana239	di smec	0.22	3.43	10.04	50.87	3.67	0.51	1.34	0.00	15.76	85.91
ana240	di smec	0.30	3.00	12.66	51.81	2.91	0.54	0.95	0.07	14.84	87.21
ana241	di smec	0.32	3.48	9.06	51.04	4.51	0.38	1.01	0.06	16.62	86.57
ana242	di smec	0.50	2.84	14.33	50.04	3.30	0.61	1.29	0.05	16.10	89.15
ana243	di smec	0.46	2.92	14.32	50.09	3.67	0.61	1.33	0.04	15.75	89.27
ana244	di smec	0.49	4.37	9.17	53.26	4.45	0.48	1.26	0.05	18.19	91.82
ana245	di smec	0.50	4.19	9.34	52.86	4.38	0.54	1.54	0.00	18.01	91.42
ana246	di smec	0.47	3.91	11.18	53.27	4.29	0.46	1.05	0.03	17.03	91.80
ana247	di smec	0.41	3.13	14.26	51.77	3.40	0.73	1.37	0.11	15.83	91.13
ana248	di smec	0.45	3.31	13.80	51.09	3.76	0.68	1.28	0.08	15.87	90.47
ana249	di smec	0.92	2.66	14.60	50.47	3.71	0.56	1.32	0.10	16.07	90.57
ana250	di smec	0.95	2.77	14.09	51.03	3.81	0.55	1.20	0.10	16.63	91.25
ana251	di smec	0.93	2.83	13.38	51.46	4.31	0.66	1.21	0.08	16.92	91.88
ana252	di smec	0.47	3.95	11.04	53.75	4.04	0.51	0.95	0.05	17.06	91.90
ana253	di smec	0.80	2.97	14.68	51.36	3.47	0.79	1.47	0.04	15.61	91.31
ana254	di smec	0.71	2.80	15.42	50.25	3.86	0.78	1.63	0.09	16.15	91.82
ana255	di smec	0.53	3.86	11.66	53.35	4.36	0.51	1.16	0.04	17.42	92.97

Label	mineral	Ox%(Na)	Ox%(Mg)	Ox%(Al)	Ox%(Si)	Ox%(K)	Ox%(Ca)	Ox%(Ti)	Ox%(Mn)	Ox%(Fe)	Total
ana256	di smec	0.68	2.54	15.33	49.50	2.40	1.14	1.15	0.07	13.67	86.76
ana257	di smec	0.83	2.23	15.02	46.95	3.16	0.86	1.03	0.02	13.15	83.56
ana258	cel	1.19	4.42	9.48	49.05	9.00	0.51	0.27	0.03	8.98	82.95
ana259	cel	1.56	5.39	6.44	50.27	6.97	0.27	0.25	0.01	10.90	82.14
ana260	cel	0.59	5.82	4.55	50.36	8.06	0.15	0.34	0.08	13.22	83.24
ana261	cel	0.27	5.29	6.00	47.97	8.68	0.12	0.36	0.04	11.42	80.16
ana262	cel	0.13	6.15	3.97	48.23	8.50	0.07	0.30	0.09	12.83	80.30
ana263	cel	0.24	6.71	3.55	48.08	8.24	0.09	0.34	0.09	13.49	80.88
ana264	cel	0.07	6.77	2.87	49.70	8.63	0.24	0.23	0.00	15.41	84.00
ana265	cel	0.10	7.08	3.45	50.66	8.31	0.10	0.39	0.04	14.61	84.80
ana266	cel	0.15	6.90	3.05	47.94	8.21	0.20	0.37	0.06	13.92	80.87
ana267	cel	0.22	7.15	4.03	49.92	8.26	0.11	0.36	0.06	13.67	83.80
ana268	cel	0.22	6.95	3.47	48.51	7.47	0.38	0.32	0.05	13.90	81.35
ana269	cel	1.08	6.94	6.47	48.69	6.21	0.69	0.27	0.06	10.93	81.39
ana270	chlorite	0.00	18.18	19.91	28.20	0.02	0.09	0.0703	0.2898	21.3271	88.11
ana271	chlorite	0.02	18.70	20.37	28.25	0.03	0.02	0.0257	0.3015	21.354	89.08
ana272	chlorite	0.01	18.69	19.65	28.53	0.01	0.05	0.0067	0.322	21.5272	88.8
ana273	chlorite	0.03	18.77	19.69	28.34	0.03	0.05	0.0049	0.3197	21.3589	88.62
ana274	chlorite	0.03	18.38	19.71	28.15	0.01	0.05	0.0098	0.3451	21.4593	88.21
ana275	chlorite	0.03	18.69	19.73	27.70	0.01	0.00	0.0042	0.3693	21.5659	88.12
ana276	chlorite	0.02	18.19	20.31	27.73	0.00	0.00	0.0183	0.2667	21.1981	87.76
ana277	chlorite	0.03	18.60	20.31	28.02	0.01	0.08	0.0116	0.2661	21.2613	88.64
ana278	chlorite	0.01	17.95	20.70	27.45	0.02	0.08	0.0183	0.3182	21.4676	88.07
ana279	chlorite	0.02	18.09	20.35	28.06	0.01	0.06	0.0129	0.4256	21.3482	88.46
ana280	chlorite	0.02	18.73	19.89	28.53	0.00	0.00	0.036	0.3878	21.7935	89.44
ana281	chlorite	0.04	18.23	20.47	27.20	0.01	0.00	0.0256	0.3225	21.2902	87.62
ana282	chlorite	0.02	17.74	20.60	27.04	0.00	0.07	0.0299	0.3073	21.2379	87.07
ana283	chlorite	0.01	18.42	20.37	27.20	0.01	0.03	0.0311	0.3961	21.3531	87.84
ana284	chlorite	0.00	16.82	21.36	26.73	0.03	0.03	0.0286	0.5709	22.6737	88.27
ana285	chlorite	0.01	17.94	20.72	27.81	0.02	0.06	0.022	0.3153	21.382	88.31
ana286	chlorite	0.01	18.60	19.29	27.88	0.00	0.06	0.0208	0.3261	21.4472	87.7
ana287	chlorite	0.03	18.25	19.39	27.42	0.02	0.02	0.0372	0.2944	21.4685	86.99
ana288	chlorite	0.04	18.51	19.28	27.73	0.02	0.03	0.0147	0.3167	21.09	87.06
ana289	chlorite	0.03	18.61	19.66	28.30	0.01	0.04	0.0147	0.3768	21.434	88.49
ana290	chlorite	0.03	18.50	19.86	28.45	0.00	0.05	0.0019	0.3373	21.386	88.63
ana291	chlorite	0.02	18.43	19.17	28.43	0.00	0.00	0.0033	0.2735	21.0866	87.41
ana292	chlorite	0.03	18.28	19.32	28.41	0.00	0.00	0.0019	0.3282	21.0549	87.44
ana293	chl/sm	0.13	19.49	6.95	45.00	0.12	1.28	0.0079	0.0144	8.7794	81.97
ana294	chl/sm	0.15	18.20	7.53	43.71	1.12	1.47	0.0395	0.1182	11.015	83.53
ana295	chl/sm	0.14	27.56	11.61	35.64	0.26	0.31	0.0566	0.2619	9.1247	85.02
ana296	chl/sm	0.09	19.54	7.14	44.08	0.58	0.91	0.0669	0.094	7.4167	80.21
ana297	chl/sm	0.13	18.86	7.85	43.96	0.83	1.31	0.0182	0.0818	9.1538	82.45
ana298	chl/sm	0.12	18.42	10.20	43.23	1.90	0.48	0.0422	0.149	14.4607	89.06
ana299	chl/sm	0.12	17.96	10.14	36.31	0.99	0.71	0.1876	0.2269	20.0112	86.72
ana300	chl/sm	0.13	21.38	10.42	41.58	0.86	0.58	0.0125	0.1785	11.3842	86.59
ana301	chl/sm	0.11	18.61	10.66	42.38	1.71	0.46	0.0412	0.1515	14.0199	88.21
ana302	chl/sm	0.21	20.25	17.83	38.54	0.83	0.50	0.0192	0.5527	11.0214	89.82
ana303	chl/sm	0.21	20.72	17.43	38.09	0.81	0.46	0.0186	0.386	11.1465	89.32
ana304	chl/sm	0.28	17.15	15.65	38.88	1.20	0.60	0.0781	0.6787	11.4777	86.15
ana305	chl/sm	0.24	14.01	19.69	40.49	1.41	0.70	0.0213	0.3988	13.2954	90.28
ana306	chl/sm	0.26	14.41	19.94	40.88	1.32	0.68	0.0672	0.4001	13.6225	91.65

Label	mineral	Ox%(Na)	Ox%(Mg)	Ox%(Al)	Ox%(Si)	Ox%(K)	Ox%(Ca)	Ox%(Ti)	Ox%(Mn	Ox%(Fe)	Total
ana307	chl/sm	0.24	17.14	14.67	38.80	1.36	0.59	0.0523	0.5441	11.1701	84.77
ana308	chl/sm	0.21	20.30	15.60	35.70	0.54	0.36	0.0376	0.667	14.305	87.77
ana309	chl/sm	0.18	20.00	16.48	35.17	0.44	0.44	0.0587	0.5756	14.0591	87.46
ana310	zeolite	1.79	0.84	19.01	51.40	5.53	0.73	0.0358	0.0016	0.9385	80.53
ana311	zeolite	1.64	0.31	18.69	51.46	8.40	0.96	0.0092	0.0042	0.3185	81.99
ana312	zeolite	5.21	0.04	16.62	60.25	0.98	0.16	0.0021		0.0937	83.36
ana313	zeolite	5.10	0.09	24.94	49.14	5.06	1.32	0.003	0.0405	0.1088	85.83
ana314	zeolite	3.38	0.13	21.93	56.87	3.33	0.27	0.0021	0.0341	0.0946	86.07
ana315	zeolite	4.20	0.06	20.29	57.00	4.61	0.55	0.0223	0.0256	0.2366	87.07
ana316	zeolite	4.90	0.12	24.93	50.72	4.96	1.30	0.0218	0.0104	0.1729	87.2
ana317	zeolite	4.53	0.08	22.35	54.28	6.07	0.36	0.0021	0.0016	0.0174	87.72
ana318	zeolite	5.52	0.08	24.11	51.55	5.68	1.15	0.0152	0.0069	0.0885	88.21
ana319	zeolite	3.77	0.38	20.71	55.30	7.87	0.57	0.0079	0.0016	0.1964	88.82
ana320	zeolite	4.67	0.21	24.04	53.94	4.11	1.70	0.0132	0.0111	0.2727	88.98
ana321	zeolite	4.45	0.07	22.90	57.64	3.66	0.41	0.003	0.0039	0.0019	89.16
ana322	zeolite	3.77	0.00	21.50	57.85	5.91	0.11	0.0066	0.026	0.031	89.21
ana323	zeolite	4.84	0.12	23.40	55.68	4.72	0.40	0.0086	0.0261	0.0912	89.33
ana324	zeolite	6.23	0.00	19.39	61.62	2.22	0.03	0.0021	0.0151	0.0362	89.55
ana325	zeolite	4.38	0.12	22.85	57.80	3.92	0.47	0.0152	0.014	0.0126	89.63
ana326	zeolite	4.50	0.15	25.53	55.47	2.68	1.28	0.0125	0.0098	0.148	89.82
ana327	zeolite	4.45	0.17	24.72	54.18	4.69	1.39	0.0155	0.015	0.1896	89.85
ana328	zeolite	3.32	0.58	22.47	54.40	8.10	0.60	0.0157	0.0016	0.3525	89.86
ana329	zeolite	5.35	0.14	25.36	52.17	5.37	1.44	0.0046	0.0118	0.1422	90.01
ana330	zeolite	2.25	0.58	22.18	57.34	6.34	1.01	0.0316	0.0016	0.3927	90.15
ana331	zeolite	5.52	0.08	25.43	52.61	5.04	1.34	0.0021	0.0118	0.1052	90.16
ana332	zeolite	9.60	0.00	17.93	55.74	6.79	0.04	0.0021	0.0016	0.0773	90.21
ana333	zeolite	0.37	0.34	21.15	62.71	4.66	0.76	0.0169	0.0247	0.1891	90.26
ana334	zeolite	3.52	0.44	20.24	59.19	6.39	0.36	0.0357	0.0253	0.0568	90.28
ana335	zeolite	4.84	0.18	25.48	53.84	4.28	1.43	0.0021	0.0108	0.1993	90.29
ana336	zeolite	5.22	0.11	25.09	53.80	4.58	1.28	0.0138	0.0016	0.1888	90.31
ana337	zeolite	5.84	0.13	21.08	55.62	7.10	0.55	0.0043	0.0016	0.0649	90.44
ana338	zeolite	4.44	0.22	25.22	54.96	3.93	1.49	0.0021	0.0016	0.2153	90.48
ana339	zeolite	5.24	0.09	24.46	51.91	7.50	1.22	0.0021	0.0016	0.1446	90.64
ana340	zeolite	6.65	0.02	19.27	63.85	0.54	0.13	0.0162	0	0.1821	90.65
ana341	zeolite	1.22	0.34	20.86	60.63	6.86	0.65	0.0027	0.0071	0.1523	90.73
ana342	zeolite	4.35	0.44	19.19	59.93	6.38	0.37	0.0175	0.0016	0.0609	90.76
ana343	zeolite	4.67	0.20	25.49	54.57	4.29	1.39	0.0149	0.0016	0.186	90.84
ana344	zeolite	5.17	0.10	25.43	52.47	6.26	1.23	0.006	0.0288	0.1528	90.86
ana345	zeolite	5.29	0.08	25.38	53.92	4.65	1.56	0.0109	0.0016	0.1179	91.03
ana346	zeolite	4.00	0.75	22.50	52.97	9.39	0.68	0.0183	0.0439	0.6148	91.03
ana347	zeolite	2.75	0.00	18.85	63.98	5.42	0.01	0.0021	0.0085	0.0136	91.06
ana348	zeolite	5.24	0.15	25.51	54.39	3.96	1.57	0.0083	0.0137	0.1793	91.06
ana349	zeolite	2.40	0.26	19.91	61.06	7.17	0.31	0.0021	0.0016	0.0264	91.15
ana350	zeolite	4.47	0.19	22.43	52.84	10.29	0.73	0.0309	0.0016	0.1861	91.18
ana351	zeolite	4.53	0.09	25.01	52.09	8.56	0.90	0.0099	0.0016	0.0146	91.24
ana352	zeolite	4.09	0.12	24.98	54.47	6.60	0.87	0.0021	0.0196	0.0721	91.24
ana353	zeolite	4.87	0.08	23.56	55.28	6.92	0.49	0.0023	0.0016	0.0321	91.26
ana354	zeolite	3.34	0.03	19.63	63.34	4.79	0.10	0.0132	0.013	0.0339	91.34
ana355	zeolite	3.48	0.00	20.83	62.07	4.81	0.09	0.0021	0.0306	0.0016	91.35
ana356	zeolite	3.61	0.00	20.86	64.87	1.64	0.06	0.0176	0.0016	0.3042	91.42
ana357	zeolite	3.83	0.44	22.39	55.35	8.37	0.53	0.1278	0.0016	0.2434	91.43

Label	mineral	Ox%(Na	Ox%(Mg	Ox%(Al)	Ox%(Si)	Ox%(K)	Ox%(Ca	Ox%(Ti)	Ox%(Mn	Ox%(Fe)	Total
ana358	zeolite	5.46	0.08	24.83	52.45	7.38	1.12	0.0021	0.0186	0.103	91.49
ana359	zeolite	5.34	0.13	25.35	55.53	3.63	1.32	0.0021	0.0016	0.1586	91.49
ana360	zeolite	1.18	0.50	20.49	60.51	7.43	0.94	0.0021	0.0168	0.4159	91.53
ana361	zeolite	3.44	0.45	20.85	58.86	7.28	0.46	0.0357	0.0016	0.1359	91.58
ana362	zeolite	3.81	0.42	20.23	58.10	8.55	0.37	0.0714	0.0058	0.1449	91.76
ana363	zeolite	5.23	0.07	24.83	55.43	4.79	1.33	0.0021	0.0173	0.1178	91.84
ana364	zeolite	4.98	0.05	23.08	58.59	4.24	0.42	0.0344	0.0016	0.3765	91.87
ana365	zeolite	1.09	0.19	20.94	59.94	7.68	1.91	0.0021	0.0016	0.1319	91.93
ana366	zeolite	3.20	0.04	21.28	61.68	5.50	0.15	0.0021	0.0016	0.0783	91.96
ana367	zeolite	3.93	0.23	22.24	56.04	8.03	1.34	0.0202	0.0186	0.0609	91.96
ana368	zeolite	4.59	0.02	18.62	65.25	3.14	0.04	0.1078	0.0496	0.1812	92.02
ana369	zeolite	2.57	0.96	19.48	61.21	7.06	0.59	0.0027	0.0016	0.1441	92.05
ana370	zeolite	2.51	0.61	21.75	57.68	7.34	1.07	0.108	0.0016	0.9173	92.06
ana371	zeolite	5.08	0.11	23.61	57.28	5.51	0.47	0.0235	0.0128	0.04	92.15
ana372	zeolite	3.84	0.15	22.97	55.71	8.69	0.45	0.0169	0.0016	0.2953	92.17
ana373	zeolite	4.46	0.12	23.39	56.77	6.81	0.43	0.0021	0.0245	0.218	92.24
ana374	zeolite	2.62	0.02	19.22	64.69	5.40	0.09	0.0089	0.0039	0.1337	92.26
ana375	zeolite	3.16	0.12	26.45	56.70	4.03	1.53	0.0109	0.0108	0.2426	92.29
ana376	zeolite	3.08	0.01	20.10	64.88	4.10	0.06	0.0021	0.0016	0.0349	92.3
ana377	zeolite	1.01	0.34	20.98	61.61	7.52	0.80	0.0054	0.0016	0.2243	92.55
ana378	zeolite	3.73	0.20	21.29	57.76	8.64	0.42	0.351	0.0016	0.0212	92.55
ana379	zeolite	2.79	0.82	20.38	61.83	5.72	0.83	0.0465	0.0194	0.1726	92.64
ana380	zeolite	4.51	0.29	22.16	56.92	7.85	0.86	0.0028	0.0016	0.1324	92.75
ana381	zeolite	9.59	0.02	23.56	59.25	0.06	0.21	0.003	0.0016	0.0233	92.78
ana382	zeolite	0.85	0.14	20.59	60.72	9.85	0.51	0.0021	0.0016	0.0902	92.78
ana383	zeolite	4.06	0.56	24.44	54.75	6.67	1.20	0.0021	0.0016	1.0818	92.81
ana384	zeolite	4.96	0.10	24.17	57.54	5.35	0.64	0.0021	0.0016	0.0458	92.87
ana385	zeolite	4.40	0.88	22.15	55.39	8.87	0.86	0.0027	0.0038	0.4367	93.03
ana386	zeolite	1.05	0.31	21.29	63.46	6.26	0.41	0.0303	0.0253	0.1351	93.07
ana387	zeolite	4.54	0.08	25.25	54.82	7.45	0.84	0.0021	0.0128	0.0769	93.1
ana388	zeolite	5.45	0.09	24.48	54.17	7.61	1.19	0.0021	0.0016	0.0516	93.13
ana389	zeolite	3.12	0.88	20.01	61.46	6.79	0.63	0.0115	0.0175	0.1827	93.13
ana390	zeolite	5.53	0.10	25.80	55.11	5.22	1.43	0.0021	0.0016	0.1032	93.33
ana391	zeolite	4.29	0.25	22.25	56.17	9.35	0.82	0.0112	0.0365	0.1152	93.34
ana392	zeolite	3.71	0.35	21.28	58.94	8.44	0.44	0.037	0.0016	0.1652	93.39
ana393	zeolite	2.16	0.14	20.87	60.66	6.79	2.24	0.1429	0.0563	0.2657	93.41
ana394	zeolite	11.18	0.02	23.65	58.17	0.06	0.23	0.0131	0.0068	0.0408	93.43
ana395	zeolite	2.39	0.17	22.73	57.02	10.67	0.31	0.0088	0.0016	0.094	93.43
ana396	zeolite	4.36	0.17	23.52	57.58	6.92	0.57	0.0021	0.0091	0.3305	93.48
ana397	zeolite	5.35	0.08	25.66	55.42	5.46	1.33	0.0021	0.0046	0.1598	93.49
ana398	zeolite	3.70	0.18	22.96	57.04	8.91	0.54	0.015	0.0051	0.1152	93.5
ana399	zeolite	3.14	0.00	20.63	68.63	1.01	0.03	0.0146	0.0115	0.0647	93.54
ana400	zeolite	2.64	0.16	23.19	59.01	7.80	0.61	0.0225	0.0199	0.0573	93.55
ana401	zeolite	3.94	0.21	22.95	58.04	7.99	0.29	0.0199	0.0016	0.0934	93.56
ana402	zeolite	3.11	0.09	23.26	54.20	11.96	0.69	0.02	0.0127	0.1782	93.59
ana403	zeolite	4.15	0.62	19.95	61.47	7.20	0.22	0.0021	0.0016	0.0016	93.65
ana404	zeolite	3.91	0.06	19.95	63.62	5.76	0.09	0.0021	0.0426	0.2196	93.71
ana405	zeolite	7.16	0.92	23.09	60.27	0.06	1.46	0.0851	0.0414	0.6045	93.73
ana406	zeolite	5.05	0.10	24.52	59.13	4.25	0.61	0.0116	0.0016	0.0029	93.74
ana407	zeolite	4.34	0.14	26.01	55.80	5.84	1.36	0.0026	0.0016	0.2457	93.77
ana408	zeolite	10.82	0.03	23.64	59.07	0.10	0.18	0.02	0.0016	0.0825	93.99

Appendix III. ICP-AES Data

Label	rock type	SiO2	TiO2	Al2O3	Fe2O3	MnO	MgO	CaO	Na2O	K2O	P2O5	LOI	SUM
e96-1-2	arc thol	62.34	1.01	11.39	11.25	0.18	2.61	3.45	4.22	0.21	0.07	1.16	97.91
90-1-5	arc thol	49.34	0.69	15.81	10.47	0.14	8.28	11.19	2.31	0.69	0.06	1.43	100.41
90-2-16(fre)a	arc thol	49.20	0.74	14.85	9.73	0.16	9.06	11.44	2.46	0.73	0.09	1.52	99.97
91-3-5	arc thol	47.87	0.95	14.05	15.08	0.17	5.21	8.58	2.28	0.81	0.07	1.69	96.75
e96-1-12	arc thol	56.05	1.00	17.23	10.85	0.15	4.68	4.60	5.03	0.41	0.08	2.25	102.33
90-2-16(alt)	arc thol	48.35	0.73	14.10	10.57	0.17	8.60	9.01	2.85	1.27	0.07	3.11	98.83
87-2-9(alt)	arc thol	46.18	0.57	17.57	11.64	0.14	6.17	10.65	1.90	1.35	0.14	3.45	99.76
87-3-3	arc thol	46.94	0.71	15.62	11.76	0.13	6.62	11.41	2.19	0.27	0.08	3.99	99.73
87-2-3(fre)	arc thol	45.57	0.63	13.73	11.10	0.19	8.29	9.24	3.94	1.17	0.07	6.24	100.16
87-2-3(alt)	arc thol	46.06	0.62	14.06	11.24	0.21	8.19	8.17	4.22	1.10	0.06	6.66	100.60
87-2-1	arc thol	47.66	0.77	16.29	9.54	0.09	6.24	5.63	4.21	2.19	0.04	7.33	100.00
87-2-2	arc thol	44.34	0.77	15.89	11.92	0.12	5.70	8.05	3.47	1.90	0.11	7.72	100.00
88-1-9	boninite	55.45	0.28	12.67	8.56	0.15	11.85	8.55	1.85	0.44	0.03	3.03	102.87
88-1-23a	boninite	53.47	0.38	13.66	7.32	0.23	7.41	6.55	4.18	2.86	0.08	3.84	99.98
88-1-23b	boninite	54.12	0.37	13.99	7.45	0.23	7.28	6.54	4.24	3.05	0.07	3.84	101.18
88-1-10(alt)	boninite	47.72	0.25	11.26	7.92	0.16	11.94	11.27	2.18	0.78	0.02	8.52	102.02
89-3-3(fre)	tholeiite	45.00	1.38	13.21	14.02	0.31	8.03	9.26	1.99	1.68	0.24	2.61	97.75
89-3-3(alt)a	tholeiite	47.66	1.50	15.22	11.22	0.27	7.06	8.36	3.32	2.25	0.19	4.97	102.02
89-3-3(alt)b	tholeiite	47.48	1.49	14.92	11.10	0.26	6.88	8.12	3.31	2.42	0.19	4.97	101.13